



UNIVERSITAT DE  
BARCELONA

## Energy Harvesting Solutions for Self-Powered Devices: From Structural Health Monitoring to Biomedical Applications

Albert Álvarez-Carulla

**ADVERTIMENT.** La consulta d'aquesta tesi queda condicionada a l'acceptació de les següents condicions d'ús: La difusió d'aquesta tesi per mitjà del servei TDX ([www.tdx.cat](http://www.tdx.cat)) i a través del Dipòsit Digital de la UB ([diposit.ub.edu](http://diposit.ub.edu)) ha estat autoritzada pels titulars dels drets de propietat intel·lectual únicament per a usos privats emmarcats en activitats d'investigació i docència. No s'autoritza la seva reproducció amb finalitats de lucre ni la seva difusió i posada a disposició des d'un lloc aliè al servei TDX ni al Dipòsit Digital de la UB. No s'autoritza la presentació del seu contingut en una finestra o marc aliè a TDX o al Dipòsit Digital de la UB (framing). Aquesta reserva de drets afecta tant al resum de presentació de la tesi com als seus continguts. En la utilització o cita de parts de la tesi és obligat indicar el nom de la persona autora.

**ADVERTENCIA.** La consulta de esta tesis queda condicionada a la aceptación de las siguientes condiciones de uso: La difusión de esta tesis por medio del servicio TDR ([www.tdx.cat](http://www.tdx.cat)) y a través del Repositorio Digital de la UB ([diposit.ub.edu](http://diposit.ub.edu)) ha sido autorizada por los titulares de los derechos de propiedad intelectual únicamente para usos privados enmarcados en actividades de investigación y docencia. No se autoriza su reproducción con finalidades de lucro ni su difusión y puesta a disposición desde un sitio ajeno al servicio TDR o al Repositorio Digital de la UB. No se autoriza la presentación de su contenido en una ventana o marco ajeno a TDR o al Repositorio Digital de la UB (framing). Esta reserva de derechos afecta tanto al resumen de presentación de la tesis como a sus contenidos. En la utilización o cita de partes de la tesis es obligado indicar el nombre de la persona autora.

**WARNING.** On having consulted this thesis you're accepting the following use conditions: Spreading this thesis by the TDX ([www.tdx.cat](http://www.tdx.cat)) service and by the UB Digital Repository ([diposit.ub.edu](http://diposit.ub.edu)) has been authorized by the titular of the intellectual property rights only for private uses placed in investigation and teaching activities. Reproduction with lucrative aims is not authorized nor its spreading and availability from a site foreign to the TDX service or to the UB Digital Repository. Introducing its content in a window or frame foreign to the TDX service or to the UB Digital Repository is not authorized (framing). Those rights affect to the presentation summary of the thesis as well as to its contents. In the using or citation of parts of the thesis it's obliged to indicate the name of the author.

PhD Thesis

Energy Harvesting Solutions for  
Self-Powered Devices:  
From Structural Health Monitoring to  
Biomedical Applications

Albert Álvarez-Carulla



UNIVERSITAT<sub>DE</sub>  
BARCELONA



# Energy Harvesting Solutions for Self-Powered Devices: From Structural Health Monitoring to Biomedical Applications

Programa de doctorat en  
Enginyeria i Ciències Aplicades

Autor/a:           Albert Álvarez Carulla  
Directors/es:     Dr. Pere Ll. Miribel Català  
                          Dr. Jordi Colomer Farrarons  
Tutor/a:            Dr. Jordi Colomer Farrarons



UNIVERSITAT DE  
BARCELONA

A handwritten signature in blue ink, consisting of a large, stylized initial 'A' followed by a series of loops and a long horizontal stroke extending to the right.



*Albert Alvarez Carulla*

---

***Energy Harvesting  
Solutions for Self-Powered  
Devices: From Structural  
Health Monitoring to  
Biomedical Applications***



*Per a l'Olga i l'Aina.*







---

# *Contents*

---

<b>Acknowledgments</b>	<b>xi</b>
<b>List of Figures</b>	<b>xiii</b>
<b>List of Tables</b>	<b>xvii</b>
<b>1 Introduction</b>	<b>1</b>
1.1 Energy Harvesting Sources . . . . .	2
1.2 Maximum Power Point Tracking Algorithms . . . . .	5
1.3 Applications: From SHM to PoC Devices . . . . .	11
1.4 Contributions and Outlook of this Thesis . . . . .	14
Acronyms . . . . .	18
References . . . . .	21
<b>2 Self-Powered Nodes for Structural Health Monitoring Applications</b>	<b>29</b>
2.1 WSNs for Aerospace Applications . . . . .	30
2.2 The SMARTER Project . . . . .	33
2.3 Adaptative Self Powered Circuit for SHM . . . . .	33
2.3.1 Prototype Implementation . . . . .	36
2.3.1.1 Piezoelectric Generator . . . . .	37
2.3.1.2 Power Management . . . . .	38
2.3.1.3 Analog Control Unit . . . . .	38
2.3.1.4 Wireless End Point . . . . .	40
2.3.2 Validation Methods . . . . .	40
2.3.3 Results and Discussion . . . . .	42
2.4 Energy Aware Adaptative Super capacitor Storage System . . . . .	46
2.4.1 The Prototype . . . . .	46
2.4.2 Results and Discussion . . . . .	48
2.5 CMOS Integrated Circuit for SHM . . . . .	48
2.5.0.1 Low Power Successive approximation ADC . . . . .	48
2.5.1 The Prototype . . . . .	51
2.5.2 Results and Discussion . . . . .	53
2.6 Chapter Conclusions . . . . .	57
Acronyms . . . . .	57
References . . . . .	59

**3 Dual-Galvanic-Cell-based Self-Powered Devices 63**

- 3.1 Self Powered Point of Care Devices . . . . . 64
- 3.2 'Plug and Power' Point of Care Device . . . . . 65
  - 3.2.1 The Test Strip . . . . . 67
  - 3.2.2 The Electronic Reader . . . . . 69
    - 3.2.2.1 Power Management Unit . . . . . 69
    - 3.2.2.2 Front end Module . . . . . 72
    - 3.2.2.3 Back end Module . . . . . 73
    - 3.2.2.4 User Interface Module . . . . . 73
- 3.3 Results and Discussion . . . . . 75
  - 3.3.1 Test strip characterization . . . . . 75
  - 3.3.2 Electronic reader characterization . . . . . 78
- 3.4 Chapter Conclusions . . . . . 80
- Acronyms . . . . . 81
- References . . . . . 83

**4 Single-Galvanic-Cell-based Self-Powered Devices 87**

- 4.1 [REDACTED] . . . . . 88
- 4.2 [REDACTED] . . . . . 90
  - 4.2.1 The Galvanic Cell . . . . . 90
  - 4.2.2 The Electronic Reader . . . . . 95
    - 4.2.2.1 [REDACTED] . . . . . 95
    - 4.2.2.2 [REDACTED] . . . . . 97
    - 4.2.2.3 [REDACTED] . . . . . 97
  - 4.2.3 Results and Discussion . . . . . 98
- 4.3 Chapter Conclusions . . . . . 102
- Acronyms . . . . . 104
- References . . . . . 105

**5 Ubiquitous Self-Powered Architecture for Galvanic Cell-based Applications 109**

- 5.1 Exploiting the Galvanic Cell's Role as Sensor and Power Source Simultaneously . . . . . 110
- 5.2 The Galvanic Cell as a Sensor . . . . . 112
- 5.3 The Galvanic Cell as a Power Source . . . . . 113
- 5.4 Ubiquitous Self Powered Architecture . . . . . 113
  - 5.4.1 Architecture Concept and Operation . . . . . 115
  - 5.4.2 Prototype Implementation . . . . . 116
    - 5.4.2.1 Galvanic cell selection and characterization . . . . . 116
    - 5.4.2.2 Architecture implementation . . . . . 119
  - 5.4.3 Results and Discussion . . . . . 123
- 5.5 Chapter Conclusions . . . . . 130
- Acronyms . . . . . 131
- References . . . . . 132

<b>6</b>	<b>Conclusions and Future Work</b>	<b>137</b>
6.1	Conclusions . . . . .	137
6.2	Future Work . . . . .	139
	Acronyms . . . . .	140
	References . . . . .	142
<b>A</b>	<b>Resum</b>	<b>145</b>
<b>B</b>	<b>Certificat de Procés de Protecció</b>	<b>147</b>
<b>C</b>	<b>List of Patents &amp; Publications</b>	<b>149</b>
C.1	Patents . . . . .	149
C.2	Journals . . . . .	150
C.3	Books Chapters . . . . .	152
C.4	Conferences proceedings . . . . .	152
<b>D</b>	<b>Patent &amp; Journal Publications</b>	<b>155</b>
D.1	European Patent Office: Self Powered System and Method for Power Extraction and Measurement of Eenergy Generator Units . . . . .	156
D.2	Ubiquitous Self Powered Architecture for Fuel Cell based Point of Care Applications . . . . .	184
D.3	Self Powered Point of Care Device for Galvanic Cell based Sample Concentration Measurement . . . . .	194
D.4	Biosensors & Bioelectronics: 'Plug and Power' Point of Care Diagnostics: A Novel Approach for Self Powered Electronic Reader based Portable Analytical Devices . . . . .	202
D.5	Sensors: Self Powered Portable Electronic Reader for Point of Care Amperometric Measurements . . . . .	212
D.6	IOPscience (PowerMEMS): Self Powered Adaptive Switched Architecture Storage . . . . .	228
D.7	IOPscience (PowerMEMS): Self Powered Energy Harvester Strain Sensing Device for Structural Health Monitoring . . .	232



---

## Acknowledgments

The author would like to thank the support of the SMARTER Project (PCIN 2013 069), Ministerio de Economía y Competitividad, and the MINAUTO Project (TEC2016 78284 C3 3 R), Ministerio de Economía, Industria y Competitividad Agencia Estatal de Investigación, and Fondo Europeo de Desarrollo Regional (AEI/FEDER, UE).



UNIVERSITAT DE  
BARCELONA



GOBIERNO  
DE ESPAÑA

MINISTERIO  
DE ECONOMÍA  
Y COMPETITIVIDAD



**Unión Europea**

Fondo Europeo  
de Desarrollo Regional  
"Una manera de hacer Europa"



# List of Figures

1.1	Energy Harvesting Sources types . . . . .	2
1.2	Output characteristics of a TGM 127 1.0 2.5 Thermoelectric Generator for different gradients of temperature . . . . .	5
1.3	Common self powered device block diagram . . . . .	12
1.4	Prototypes developed in this research . . . . .	16
2.1	In service fleet and average age. . . . .	31
2.2	First implemented Wireless Sensor Network. . . . .	32
2.3	Application example of a WSN for SHM application in an air craft. . . . .	34
2.4	Schematic of a bridge rectifier based AC/DC converter without and with adaptation. . . . .	35
2.5	Simulated efficiency for a PEG without and with adaptation. . . . .	36
2.6	Block diagram and picture of a self powered wireless sensor node. . . . .	37
2.7	Schematic of a self powered SHM device. . . . .	38
2.8	Experimental setup for PEG and prototype characterizations. . . . .	39
2.9	MCU's flow diagram. . . . .	41
2.10	Experimental efficiency for a PEG without and with adaptation. . . . .	42
2.11	Oscilloscope capture of the real time monitoring of $V_{OC}/2$ for different amplitudes of $V_{OC}$ . . . . .	43
2.12	Power extracted from a PEG with adaptation and different amplitudes and frequencies of oscillation. . . . .	43
2.13	Strain to voltage transfer function and corresponding digital code. . . . .	44
2.14	Current consumption of the microcontroller. . . . .	45
2.15	Voltage at the super capacitor during prototype initialization and steady state operation. . . . .	45
2.16	Schematic of the super capacitor based matrix . . . . .	47
2.17	Schematic of the Dynamic Adaptative Load Controller (DALC) . . . . .	47
2.18	Control signals and voltage from the super capacitor based storage system during charging . . . . .	49
2.19	Control signals and voltage from the super capacitor based storage system during discharging . . . . .	50



2.20 Block diagram of the Successive Approximation Register (SAR) Analog to Digital Converter (ADC) . . . . . 52

2.21 CADENCE Schematic of the SAR ADC . . . . . 53

2.22 Layout of the CMOS integrated circuit for SHM. . . . . 54

2.23 CADENCE Transient waveforms during a single analog to digital conversion . . . . . 55

2.24 CADENCE Transient waveforms during multiple analog to digital conversions . . . . . 56

3.1 User steps with the 'plug and power' prototype. . . . . 66

3.2 Block diagram of the 'plug and power' prototype. . . . . 67

3.3 Picture and exploded view of paper based test strip and its main components. . . . . 68

3.4 Exploded view and picture of the 'plug and power' prototype. 70

3.5 Schematic of the 'plug and power' prototype. . . . . 71

3.6 Application flow diagram of the 'plug and power' prototype. . 74

3.7 Test strip performance as a power source with serum. . . . . 75

3.8 Start up current and voltage waveforms for the test strip with serum. . . . . 76

3.9 Current and voltage waveforms for a current step load at the LDO regulator's output. . . . . 77

3.10 Current and voltage waveforms for a current step load at the DC/DC converter's output. . . . . 78

3.11 'Plug and power' prototype's power consumption. . . . . 79

3.12 Chronoamperometry and transfer function of the 'plug and power' reader. . . . . 80

4.1 Polarization curves for a general purpose galvanic cell . . . . . 88

4.2 [REDACTED] . . . . . 91

4.3 Picture of the NaCl galvanic cell . . . . . 92

4.4 Characteristics of the NaCl galvanic cell . . . . . 93

4.5 [REDACTED] . . . . . 94

4.6 [REDACTED] . . . . . 95

4.7 [REDACTED] . . . . . 96

4.8 Transient waveforms during device's operation for under threshold concentration . . . . . 99

4.9 Transient waveforms during device's operation for over threshold concentration . . . . . 100

4.10 [REDACTED] . . . . . 101

5.1 Polarization curves for a general purpose galvanic cell . . . . . 112

5.2	Common potentiostat architectures used for fuel cell characterization . . . . .	114
5.3	Block diagram of the ubiquitous self powered architecture . .	115
5.4	Direct Methanol Fuel Cell used to validate the ubiquitous self powered architecture . . . . .	117
5.5	Ethanol and lactate based fuel cell's emulated polarization and power curves . . . . .	118
5.6	Methanol based fuel cell's measured and later emulated polarization and power curves . . . . .	119
5.7	Schematic and picture of the ubiquitous self powered architecture implementation . . . . .	121
5.8	Transient waveforms during device's start up . . . . .	125
5.9	Prototype characterization for the ethanol based fuel cell . . .	127
5.10	Prototype characterization for the lactate based fuel cell . . .	128
5.11	Prototype characterization for the methanol based fuel cell . .	129



---

# *List of Tables*

---

1.1	Power ranges for different state of the art Energy Harvesting Sources. . . . .	3
1.2	Main Maximum Power Point Tracking (MPPT) algorithms used in off grid applications. . . . .	7
2.1	SAR ADC characterisation results . . . . .	56
3.1	'Plug and power' prototype's characterization results . . . . .	80
4.1	Prototype's characterization results . . . . .	102
5.1	Open Circuit Potentials and power densities provided by state of the art fuel cells . . . . .	111
5.2	Prototype's characterization results . . . . .	126



# 1

---

## *Introduction*

---

### CONTENTS

1.1	Energy Harvesting Sources .....	1
1.2	Maximum Power Point Tracking Algorithms .....	4
1.3	Applications: From SHM to PoC Devices .....	11
1.4	Contributions and Outlook of this Thesis .....	14
	Acronyms .....	18
	References .....	21

Energy autonomy is one of the most requested functionalities in the explosion of off grid applications that the digital evolution, due to paradigms such as the Internet of Things (IoT), Wireless Sensor Networks (WSNs) or Trillion Sensors (TSensors), carries [1]. The most common solution is to use batteries. However, there are scenarios where the use of batteries is not practical, such as in remote locations or hazardous environments. In addition, among the disadvantages of using batteries, we must add the economic impact of their replacement and maintenance due to direct, logistical and environmental costs that will become unbearable if the number of sensor nodes really multiplies exponentially as the revisions point out [2, 3]. It is therefore appropriate to research and develop other alternatives to achieve energy autonomy, both for applications that require it for a short time and for a long time.

These alternatives fall within the field of Energy Harvesting (EH) research. In this field, transducers are used to convert the energy available in the environment in different forms, such as thermal, mechanical, Radio Frequency (RF), light or fuel source energies, into electrical energy. Despite being able to extract energy from the environment using different transducers, we are currently facing the challenge of extracting this energy in the most efficient way in order to extract the maximum power and energy (in such a way that it can be increased either the complexity of the electronics or its autonomy) under extreme operating conditions (such as power levels that can range from mW to  $\mu$ W).

### 1.1 Energy Harvesting Sources

While there are a huge number of Energy Harvesting Sources (EHSs) available to recover energy from the environment, a typical classification [4] refers to up to four main types of EHSs as function of the physical phenomena in which are based on (Fig. 1.1): kinetic, solar, thermal and inductive. In recent years, a fifth type of EHS has flourished based on the chemical reactions that take place in a Galvanic Cell (GC). Because most of research is focused in Fuell Cell (FC), a specific type of GC, these type of EHSs are commonly referred as FC based EHSs. The power levels that these EHSs provide vary over a very wide range of values as function of their intrinsic characteristics (materials, geometry, size, construction, etc.) and the environmental conditions (temperature, wind, weather, time of day, etc.). Table 1.1 shows power ranges for different state of the art EHSs . Obviously, all the EHSs provide an Operating Point (OP) where no power is delivered. The power ranges indicated correspond to the maximum power delivered by different EHSs.

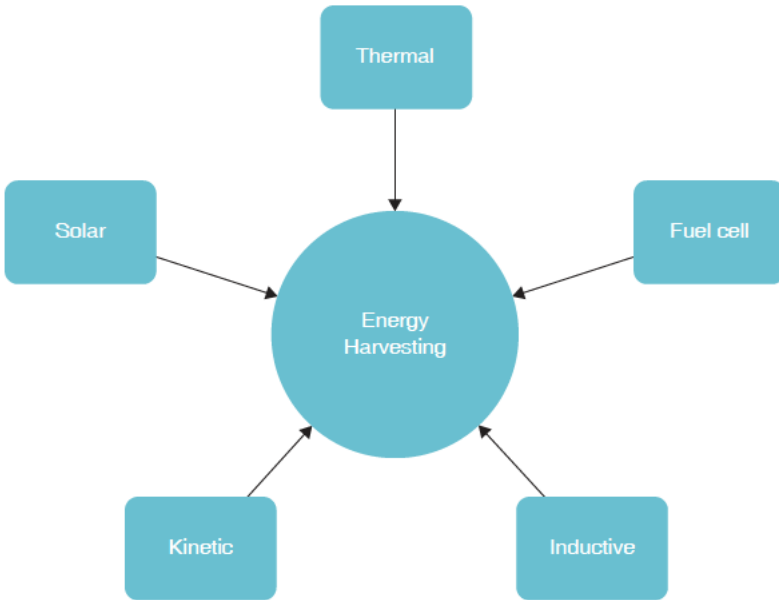


Figure 1.1: EHS types.

---

<sup>1</sup>The exposed data are from those EHSs that, due to their form factor and their off-grid operation, can be considered indoor-scaled EHSs in order to exclude macro-EHSs used in power plants.

Table 1.1: Power ranges for different state of the art EHS .

EHS	Transductor	Power range
Kinetic	Wind turbine [5–8]	1 mW to 60 W
	Piezoelectric generator [9, 10]	100 $\mu$ W to 8 mW
	Triboelectric generator [11–14]	25 $\mu$ W to 2 mW
Solar	Photovoltaic cell [15–17]	40 $\mu$ W to 12 mW
Thermal	Thermoelectric generator [18, 19]	10 $\mu$ W to 25 mW
Inductive	Radio Frequency [20, 21]	1 $\mu$ W to 1 mW
Fuel Cell	Microbial FC [22, 23]	<120 $\mu$ W
	Glucose FC [24, 25]	<5 $\mu$ W
	Direct Methanol Fuel Cell (DMFC) [26, 27]	<50 mW

The kinetic based EHSs transduce mechanical movement into electrical power. The kind of movement and the application condition the transducer to use: piezoelectric, electrostatic or electromagnetic generators [28]. Piezoelectric Generators (PEGs) consist of electrically polarized materials that provide electric charge when they are subjected to a mechanical strain. Because Lead Zirconate Titanate  $\text{Pb}[\text{Zr}_x\text{Ti}_{1-x}]\text{O}_3$  is one of the most common and widely used material, sometimes, PEGs are also referred as PZT. Another common used materials are Barium Titanate and Zinc Oxide. PEGs provide relatively high voltage levels and a good power density per unit of volume. On the other hand, PEGs suffer a poor coupling characteristic that requires relatively large load impedances to operate efficiently. The other type of kinetic based EHS, the electrostatic generator, bases its operation in the variation of the dielectric gap or the overlap surface of the electrodes of a capacitor. This is achieved suspending at least one of the electrodes of a capacitor. Thus, the capacitance of the capacitor varies in front of a movement. The variation of the capacitance causes a variation in the number of electric charges at the electrodes in order to hold the bias voltage of the capacitor. This variation in electric charges generates a current across the load attached to the capacitor to close the circuit. This kind of generator provides a poor power density compared to the other kinetic based EHSs and suffers an important disadvantage: it needs an external voltage source to initially charge the capacitor. The last kinetic based EHS, the electromagnetic generator, is based on current generated through a coil due to a variable magnetic field originated by a permanent magnet in relative movement to the coil. They provide a higher power density than PEGs and better performance is achieved for low load impedances and in low frequency applications.



Indoor solar cells or indoor Photovoltaic Cells (PVCs) generate electrical energy from solar radiation. A sub classification of this type of EHS is based on the material being used to build the PVC: monocrystalline, polycrystalline and thin film. They have an important presence in macro scale energy harvesting applications like electric generation in power plants, but also exist some applications in the micro scale where usual power densities delivered by PVC in embedded systems are  $15 \text{ mW cm}^{-3}$  [29].

The thermal based EHS transforms a gradient temperature into electrical power. The transducers used to perform this conversion are known as Thermoelectric Generators (TEGs). TEGs consist of one or more pairs of p type and n type semiconductors connected thermally in parallel and electrically in series. Based on the Seebeck effect, these generators generate an Open Circuit Potential (OCP) proportional to the gradient temperature present between the cold and hot sides of the TEG. They provide a good power density, however extra effort is needed to design a heatsink for the cold side in order to guarantee a constant minimum temperature gradient across the TEG. Other thermal based EHS is the pyroelectric generator that bases its operation in fluctuations of a gradient temperature.

In inductive based EHSs, RF energy harvesting system is the responsible to harvest energy from electromagnetic waves to convert it into electrical power. Usually, the basic RF energy harvesting system consists on a receiving antenna, a matching circuit, a peak detector and a voltage elevator. The receiving antenna can be designed to harvest energy from electromagnetic waves with different frequencies like broadcast TV signal (Ultra High Frequency (UHF)), mobile phones (900 to 950 MHz) or Local Area Network (LAN) (2.4 GHz/5.8 GHz), among others. RF based EHSs provide the lowest power density from all EHSs, which has a direct impact in the complexity and performance of the electronic circuits that use them.

The last type of EHS is the Galvanic Cell (GC) or Fuel Cell (FC) based. They base their operation on the chemical reactions that take place in an electrochemical cell. Batteries and FC are specific cases of a GC. While the term "battery" can originate a some sort of rejection when we talk about energy harvesting, in this context, the term "battery" refers strictly to its technical definition where it is defined as an electrochemical cell that provides electrical energy by means of internal redox reaction that degrades its electrodes. A battery used in context of energy harvesting uses an electrolyte provided by the environment or by the applications *per se*. For example, a salt based battery can be used to harvest energy from seawater in an underwater node [30] or the same salt based battery can be used to perform a conductivity test in a Point of Care (PoC) application for cystic fibrosis screening [31, 32]. Alternatively, FC extracts the energy from its fuel. Due to this, it can provide electrical energy as long as fuel is provided.

## 1.2 Maximum Power Point Tracking Algorithms

All EHSs have their unique output characteristics with an Operating Point (OP) where the power delivered by the EHS is maximum. This point is referred as Maximum Power Point (MPP). The output characteristic of a EHS is influenced by the environmental conditions where the EHS operates and its intrinsic characteristics. Examples of environmental conditions that can influence the output characteristics of a EHS are the wind speed for wind turbine, the vibration of a mechanical part where a PEG is attached, the weather conditions for a PVC or, as shown in Fig. 1.2, the temperature gradient for a TEG. On the other hand, examples of intrinsic characteristics of a EHS that influence its output characteristics are the electrode size for a FC, the Seebeck coefficient for a TEG, the internal output impedance for a PEG or the materials used for a PVC. All conditions interfere in where the MPP is set. Thus, the MPP becomes a dynamic OP that depends on the environmental and intrinsic conditions of the EHS.

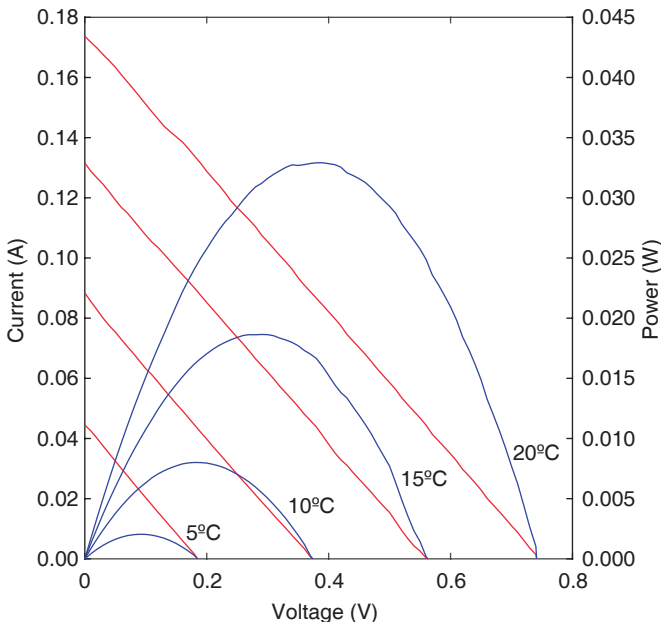


Figure 1.2: Output characteristics of a TGM 127 1.0 2.5 TEG for different gradients of temperature. Image: "Energy Aware Adaptive Supercapacitor Storage System for Multi Harvesting Solutions" by Albert Álvarez Carulla *et al.* © 2018 IEEE.

This dynamic behavior of the MPP plays a critical role in the technical and economic feasibility of applications based on EHSs. Macro scale on grid EH applications are also known as Renewable Energy Systems (RESs). With PVCs and wind turbines as some of the more representative flagships of RESs, these solutions provide a way to generate electrical power from unlimited renewable sources like the sun or wind. They have as direct benefit their clean and eco friendly operation that directly impacts on the protection of the environment and the public health. As a counterpart, they are less cost effective and efficient than other sources of energy based on fossil fuels or nuclear energy. As consequence, the energy extracted from RES has a higher cost. Because of this, in RESs is crucial to operate the EHS in its MPP in order to extract energy efficiently to make them economically feasible [33, 34]. Here, efficiency  $\eta$  is defined as the ratio between the current power extracted from the EHS and the maximum power that the EHS can deliver in its MPP for a given operating conditions. Thus, an efficiency of 100 % is achieved when the EHS is operated at its MPP.

Due to the high energy and power levels available in macro scale scenarios, is common to use mechanical based algorithms to search the MPP. These techniques are referred as Maximum Power Point Tracking (MPPT) algorithms. For example, the authors in [35] increase the conversion efficiency up to a 90 % of PVCs controlling their temperature using air cooled heat sinks. This efficiency can be improved even further tracking the sun position in order to ensure that PVCs face the sun as long as possible, as the authors of [36] review in their work reporting an efficiency increase of 30 p.p.. This type of mechanical based MPPT algorithms is also found in other types of EHSs like wind turbines. In [37], the authors describe how the power generated by a wind turbine can be maximized ensuring that the rotor faces the wind using yaw mechanisms. Another mechanical adaptation is to control the pitch of the blades in order to maximize the power when low speed wind is present, as author of [38] describe in their work. This last approach also provides a way to secure the generator itself when high speed wind is present.

For micro scale EHSs, commonly used in off grid applications, the use of MPPT algorithms is crucial for the technical feasibility of the application. In these scenarios, the power levels provided by the EHS are in the order of mW to some  $\mu$ W. Thus, to guarantee that maximum power is extracted from the EHS is crucial in order to power the associated electronics. Due to the low power levels available in these scenarios, all the efforts are mainly focused on electrical MPPT algorithms, putting aside all those MPPT algorithms based on mechanical actions. Table 1.2 shows some of the most used electrical based MPPT algorithms.

One of the most used MPPT algorithm is the P&O. This consists in shifting the Operating Point while the power outputted by the EHS is monitored. If the power increases, the OP is shifted in the same direction. On the contrary, if the power decreases, the OP is shifted to the opposite direction. Thus, this algorithm is continuously tracking the gradient of the generated power.

Table 1.2: Main MPPT algorithms used in off grid applications.

Technique	Based principle	Benefits	Drawback
Derived from [39]. Perturb and Observation (P&O) [40]	Comparison of prior power outputted by the EHS with the current one after OP perturbation.	<ul style="list-style-type: none"> <li>Ease of implementation.</li> </ul>	<ul style="list-style-type: none"> <li>Oscillation around MPP.</li> <li>Efficiency greatly affected by circuit noise.</li> <li>Slow speed MPP setting.</li> </ul>
Fractional Open Circuit Voltage (FOCV) [41]	Measurement of the open circuit voltage of the EHS to calculate and set the proper output voltage for MPP achievement.	<ul style="list-style-type: none"> <li>Simple and easy to implement.</li> </ul>	<ul style="list-style-type: none"> <li>Unable to track short term changes of the MPP without constantly interrupting the EHS operation for open circuit measurement reducing the power extracted.</li> </ul>
Fractional Short Circuit Current (FSCC) [42]	Measurement of the short circuit current of the EHS to calculate and set the proper output current for the MPP achievement.	<ul style="list-style-type: none"> <li>Simple and easy to implement.</li> </ul>	<ul style="list-style-type: none"> <li>Unable to track short term changes of MPP without constantly interrupting the EHS operation for short circuit measurement reducing the power extracted.</li> </ul>

Table 1.2: Main MPPT algorithm used in off grid applications (continued).

Derived from [39]. Technique	Based principle	Benefits	Drawback
Incremental Conductance (InC) algorithm [43]	Based on $\partial P/\partial V = 0$ , aims to equalize the current conductance with incremental conductance.	<ul style="list-style-type: none"> <li>• Higher tracking accuracy compared to methods that are more complex.</li> </ul>	<ul style="list-style-type: none"> <li>• More complex and computationally demanding compared to other techniques.</li> </ul>
Incremental Impedance (InI) algorithm [43]	Same principle than InC but based on $\partial P/\partial I = 0$ and equalizing the current impedance with incremental impedance.	<ul style="list-style-type: none"> <li>• Higher tracking accuracy compared to methods that are more complex.</li> </ul>	<ul style="list-style-type: none"> <li>• More complex and computationally demanding compared to other techniques.</li> </ul>
Extremum Seeking Control (ESC) [44]	Feedback control loop is used to apply a perturbation to the duty cycle of a converter, observe the power outputted by the generator and derive from it the next duty cycle perturbation to move OP towards MPP.	<ul style="list-style-type: none"> <li>• Does not oscillate around MPP.</li> <li>• Does not require system model.</li> </ul>	<ul style="list-style-type: none"> <li>• More complex and computationally demanding compared to other techniques.</li> <li>• The existence of various parameters for the control loop increases the chances of malfunctions if no proper adjustment is performed.</li> </ul>

Table 1.2: Main MPPT algorithm used in off grid applications (continued).

Technique	Based principle	Benefits	Drawback
Derived from [39].		<ul style="list-style-type: none"> <li>Efficiency issues present at Impedance Matching (ImpM) method due to accuracy setting the value of the inductance and switching frequency are overcome.</li> </ul>	<ul style="list-style-type: none"> <li>Efficiency affected by the mismatch between the targeted input impedance and the variability of the internal output impedance of the generator due to environmental conditions.</li> </ul>
Paraskevas' method [45]	The input impedance of a DC/DC converter is tuned by the MPPT module itself varying the duty cycle.	<ul style="list-style-type: none"> <li>Fast speed MPP setting.</li> </ul>	<ul style="list-style-type: none"> <li>Bulk storage memory proportional to the number of stored operational conditions.</li> <li>LUT specific for a given EHS.</li> </ul>
Look Up Table (LUT) method [45]	Comparison of the generator's voltage and current with stored values of the into LUT at MPP for different environmental conditions.	<ul style="list-style-type: none"> <li>Fast speed MPP setting.</li> </ul>	<ul style="list-style-type: none"> <li>Bulk storage memory proportional to the number of stored operational conditions.</li> <li>LUT specific for a given EHS.</li> </ul>

Table 1.2: Main MPPT algorithm used in off grid applications (continued).

Derived from [39]. Technique	Based principle	Benefits	Drawback
ImpM [45, 46]	<p>The input impedance of a DC/DC converter is tuned selecting the switching frequency, the duty cycle and the value of the converter's inductance to equalize it to the EHS internal output impedance.</p>	<ul style="list-style-type: none"> <li>• Simple and easy to implement.</li> <li>• Does not oscillate around the MPP.</li> </ul>	<ul style="list-style-type: none"> <li>• Efficiency related to accuracy of setting the value of the inductance to the desired value.</li> <li>• Fixed switching frequency and inductance's value during design stage. Not possible to optimize the converter performance once it is implemented.</li> <li>• Discontinuous conduction mode. At higher power levels, high current rating semiconductors are needed.</li> </ul>

An usage example of this algorithm can be found in [44], where the authors show how the energy harvested from biomass stoves by a TEG can be extracted with an efficiency of 99%. Another work based on a different type of EHS [47], an RF energy harvesting system, shows how, with a reconfigurable Dickson rectifier [48], WLAN 2.4 GHz RF energy can be converted to a DC voltage with a peak conversion efficiency of 38.4%. In [49], the authors use a different MPPT algorithm: the FOCV algorithm. They use this algorithm to extract energy from a PVC achieving a power of 112 mW instead of the 16 mW achieved without the MPPT. In this example, the MPPT sets the operating voltage of the EHS to an 80% of its OCP. I have applied the same algorithm in a completely different field with a different type of EHS. This implementation, which is described in detail in Chapter 2, can be found in [10, 50, 51]. In this example, the type of EHS is a PEG and is applied in the field of aerospace. The PEG is operated with a voltage equal to one half of its OCP in order to maximize the power extracted from it. Thus, an efficiency close to 100% is achieved.

---

### 1.3 Applications: From SHM to PoC Devices

The range of applications where EHSs are used is wide. From Structural Health Monitoring (SHM) applications to monitor the strain suffered by a wing of an aircraft [10, 50–52], to PoC devices where the blood glucose concentration is measured [25, 53]. In this wide spectrum of applications, the types of EHSs used are different, as well as the power levels available from them, and the goal of the application. However, all have a common architecture present in major part of self powered devices. Figure 1.3 shows a block diagram of the common architecture of a self powered device.

A self powered system or device usually consists of an EHS, a Power Management Unit (PMU), an energy storage, a front end and a back end modules. The EHS is the responsible to transduce the energy available in the environment to electrical power in order to power the system. While the most common approach uses a single EHS, new developments are focused in developing systems based on multiple single type or multiple multi type EHSs [54]. Thus, the system is able to extract energy from different sources ensuring a continuous source of power even when one or more of the EHSs are not able to harvest energy from the environment. If, by contrast, all the EHSs are operating, the system harvest higher levels of energy than in the common single EHS approach. There are a wide range of applications based on energy harvesting where the application itself conditions the type of EHS used. From SHM applications where one of the most used EHS is the PEG [55], to PoC devices where the state of the art flagship EHS is the FC [56]. While both types of EHSs are flagships of their respective field of applications, other types are



also present in state of the art like TEG in both SHM [57] and PoC applications [58–60], solar energy in PoC applications [61], or inductive EHSs in SHM applications [62].

On the other hand, the PMU manages the power extraction from the EHSs and provide the regulated voltage sources required by the system. The first task that the PMU must face is to operate the EHS at its MPP. To do this, it has to apply some of the MPPT algorithms shown in Table 1.2. Furthermore, if there is more than one EHS, it has to deal with the power extraction from all of them, simultaneously if possible, at the same time that it applies a MPPT algorithm per each EHS. If that was not enough, it has to provide the required regulated voltage sources from the energy extracted. Normally, this is done using switching regulators in order to perform the conversion efficiently. In this case, the efficiency is defined as the ratio between the output and the input power of the converter. Due to the low power levels in micro scale applications, all this must be done with minimum power consumption in order to make feasible the system operation. However, some of state of the art solutions use simple PMU without MPPT algorithms. This is the case shown in [24] where a charge pump is used to generate a signal whose frequency serves as indicator of the glucose concentration of the sample deposited in a FC. Even simpler is the PMU used with a glucose FC in [63] which consists on an linear regulator to provide an under OCP regulated voltage. Instead, a PMU based on a BQ25504 [64] from Texas Instruments, presented in [65], is used to extract energy from a FC of lactate. The extraction is performed efficiently by means of a MPPT algorithm and the output voltage is boosted to power a microcontroller based back end. Easier is to find more complex PMUs in SHM applications where higher energy and power levels are available. In [66], two DC/DC converters in series are used to apply a FOCV algorithm to a piezoelectric and to provide a regulated voltage source. The first DC/DC converter is in charge of the MPPT algorithm and the second one of the

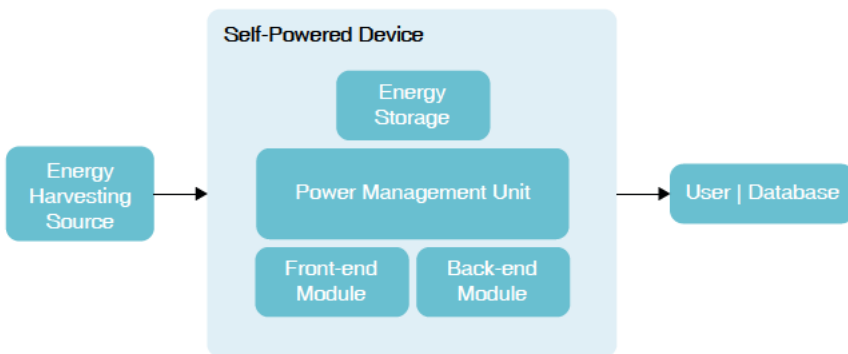


Figure 1.3: Common self powered device block diagram.

output voltage regulation. Another example based on PEGs, can be found in [67] where a DC/DC boost buck converter that applies a P&O algorithm is presented.

One more task that can be delegated to the PMU is to store energy not used into an energy storage module. Thus, the system is able to attend a punctual high power demand required by one module of the electronic circuit, e.g., a wireless transmission, or to power the system during the absence of energy to harvest, e.g., during night for PVC based applications. Examples of usage of super capacitor go from a single super capacitor to attend the punctual high power requirement of a wireless transmission [50], to a matrix of super capacitors to provide and adaptative equivalent impedance to allow the system start up [68].

The front end and back end modules are the electronic circuits of the device specific of the application itself. The front end is usually an analog circuit dedicated to the interface with sensors. Meanwhile, the back end is usually a digital circuit dedicated to processing and transmission of the signals provided by the front end. While is very common to find examples of low and ultra low power front ends in state of the art solutions, is not so common to find implementation of back end modules due to its relative high power consumption compared to the power levels provided by the EHS. Due to this, an important part of state of the art self proclaimed self powered devices are not really self powered because they need external instrumentation to operate, e.g, oscilloscopes, multimeters, Data Acquisition (DAQ) hardware, etc., due to the lack of a back end module to process and transmit the data to a user interface or database. One example is the glucose sensor presented in [69]. The authors describe the sensor as quantitative and self powered. The reality is that the sensor itself provides a colorimetric result subjected to the subjectivity of the user and illumination conditions of the environment. The author purpose to use a smartphone to retrieve a quantitative result from the color obtained by means of image processing. So, in order to get a quantitative result we need a non self powered third party device. Quantitative and self powered are not compatible in this example. Another example is the glucose or lactate sensors presented in [24, 70]. These authors also define the sensor as self powered, however the sensor provides an analog signal, whose frequency is indicator of the concentration of the agent, that needs to be read by an external non self powered device. In this case, an oscilloscope. In a last example, presented in [71], a 3D paper based fuel cell for self powered sensors is presented. The solution is able to measure different glucose concentrations and the transducer used to output the measurement is a resistor. Again, a non self powered third party device, a multimeter, is needed to get the measurement invalidating the qualifier of self powered. However, there are some interesting truly self powered solutions that are able to output a quantitative result, like the solution presented in [32], where a self powered device for fibrosis cystic screening is presented and outputs the test result in a discreti

zed by levels electrochromic display, or the solutions developed in this thesis [10, 25, 31, 50 53, 72, 73].

---

## 1.4 Contributions and Outlook of this Thesis

While most state of the art solutions are defined as self powered devices, the reality is that these devices are slaves to third party devices that are powered by batteries or directly from the electrical grid. Without them, these solutions are not capable of outputting the data measured making their implementation useless. On the other hand, we have seen a series of devices that do offer information to the user. Due to the low power available in the scenarios in which these types of solutions operate, their implementations are extremely simple. To the extent that the type of result they offer is qualitative and usually falls under the umbrella of subjectivity. This makes them unfeasible for fields of application as demanding as biomedical or SHM. Even so, some solutions propose the use of third party devices to achieve a quantitative and objective result. Here, once again, we fall back into the need for non self powered third party devices that invalidates the self powered device definition of the proposed solutions.

New approaches and innovations are needed to allow truly self powered devices to be developed and to deliver a quantitative and objective result. The field in which the implementation of these approaches must take place has as its main candidate the field of electronics. Its long history in the development of precision devices has been proving to be the best option in areas as demanding as biomedical, for example, being the glucometer, born in 1971 [74], a clear example of one of its flagships.

The goal of this work is to explore and develop these new ways of implementing self powered devices in such a way that these are truly self powered without the need for third party devices, and that they offer a quantitative and objective result. The new approaches proposed in this research are based on the same principle or aim at the same goal: to use the same transducer that collects energy from the environment as a sensor, so that energy harvesting and measurement take place simultaneously, and, in addition, that energy extraction takes place efficiently from the EHS point of view. In this way, this goal seeks to be able to obtain a greater energy levels allowing either to increase the complexity of the system (add signal processing, wireless transmissions, etc.) or to increase the autonomy of the device. But all this without sacrificing the ultimate objective: to offer a quantitative and objective result in a truly self powered way.

This thesis reflects the process that I have carried out in my research to achieve this goal. This process has consisted of different developments that have allowed me to evolve this concept from an initial self powered device

based on a single piezoelectric for SHM applications where energy extraction and measurement did not take place simultaneously, to a self powered device based in galvanic cells for PoC devices where efficient energy extraction and amperometric measurement take place simultaneously. This last development is where the objective of this research is achieved. The results therefrom open the door to a new and innovative paradigm in the development of self powered devices, as witnessed by the patent that protects the novelty [75] and a second process of intellectual property protection that takes place at the time of writing this thesis.

This thesis is divided into six chapters. Four of them dedicated to the four main developments made during my research, shown in Fig. 1.4.

In this first chapter we have seen an introduction to the concept of energy harvesting, what is and which are the main types of EHSs. Along with the different types of EHSs, we have seen the different power densities that they can deliver according to the state of the art. This determines their scenarios and strategies used for them. Related to the power density, we have seen that all the EHSs have different output characteristics that vary depending on the environmental conditions and the intrinsic characteristics of the EHS. For this reason, we have seen the use of MPPT algorithms to operate EHSs at the OP where they are capable of delivering their maximum power. Next, we have analyzed, in the state of the art, different applications of EHSs in the development of self powered devices. We have been able to verify how today the results they offer are mainly qualitative and are subjected to the subjectivity of the user. Some solve it by using third party devices to achieve a quantitative and objective measurement. These third party devices usually operate using batteries or directly connected to the electrical network. In this chapter we were able to identify a critical need: the development of a truly self powered device that outputs a quantitative and objective result. From this need, the goal of this research which is included in this section is born.

In Chapter 2, we will see the development of a self powered device based on a single piezoelectric such as EHS for SHM applications in the aerospace field [10, 39, 50–52, 68, 76]. The EHS is attached to the wing of an aircraft and its use is intended to collect energy from the vibrations of the wing caused by the air flow, and to monitor the mechanical stress to which the wing is subjected. We will see the use of a MPPT algorithm, specifically the FOCV, to efficiently extract energy from a piezoelectric while using the OCP measurement of the piezoelectric to obtain an indicator of the mechanical stress of the mechanical part where it is attached. This measurement, once taken, is sent to a host using a wireless transmission. In this case, the extraction of energy from the piezoelectric and the monitoring of mechanical stress do not take place simultaneously. It takes place multiplexed in time.

In the second development, presented in Chapter 3, we will look at the development of a PoC device for blood glucose measurement [25, 53, 72]. This device extracts energy efficiently from a biological sample while simultaneously performing an amperometric measurement. While this development allows

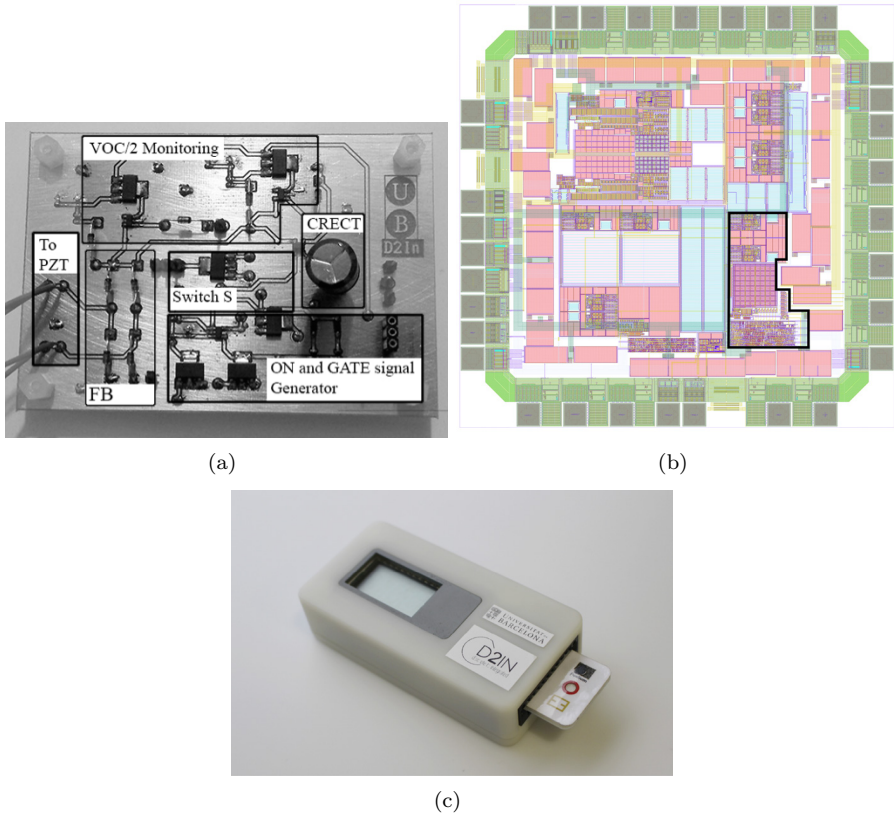
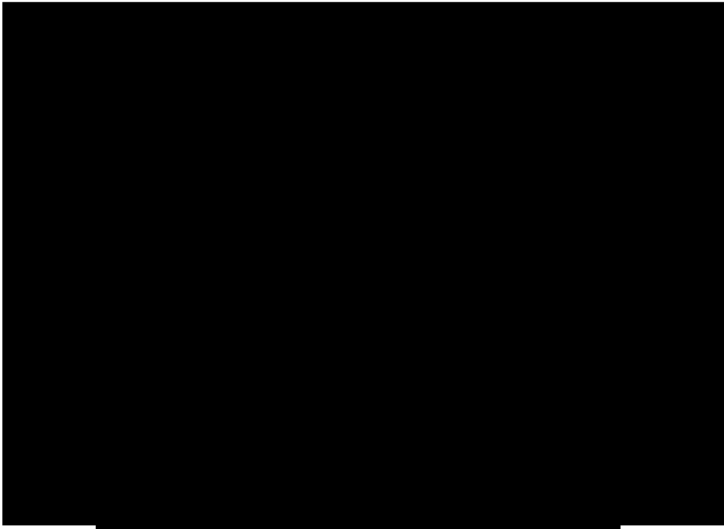
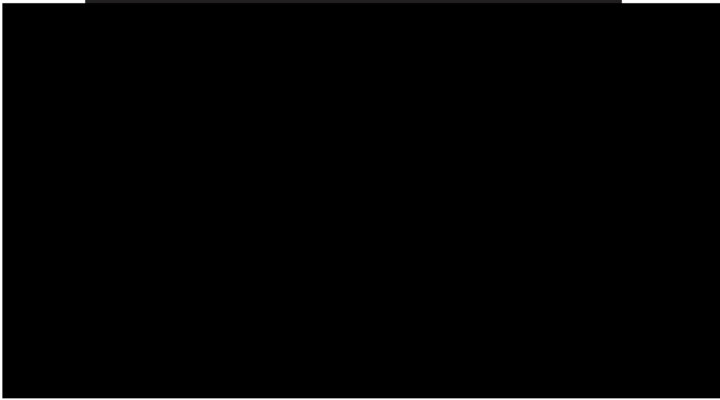


Figure 1.4a: Prototypes developed in this research: (a) discrete and (b) integrated piezoelectric based self powered device for SHM applications, and (c) dual galvanic cell based self powered device for PoC applications. Image (a): "Piezoelectric Harvester based Structural Health Monitoring that uses a Self Powered Adaptive Circuit" by Albert Álvarez Carulla *et al.* © 2015 IEEE. Image (b): "Self Powered Energy Harvester Strain Sensing Device for Structural Health Monitoring" by Albert Álvarez Carulla *et al.* is licensed under CC BY 3.0. Image (c): "Plug and Power' Point of Care Diagnostics: A Novel Approach for Self Powered Electronic Reader based Portable Analytical Devices" by Yaiza Montes Cebrián *et al.* © 2018 Elsevier, with permission.



(d)



(e)

Figure 1.4b: Prototypes developed in this research: (d) galvanic cell based self powered device for PoC applications, and (e) ubiquitous self powered architecture for galvanic cell based applications. Images (d) and (e): submitted and under review for publication.

exploring a first approach to the use of MPPT algorithms for the extraction of energy from galvanic cells efficiently, and the same sample is used for the operation of the system, in this device two different elements are used for power and measurement. In this case, a battery and a fuel cell, respectively.

The third chapter includes the development of a solution based on a single galvanic cell that, for the first time in this research, manages to extract energy and perform an amperometric measurement simultaneously with a single cell and, in addition, offering a quantitative and objective result based on levels [31]. Despite the innovation of this proposal, which is currently under intellectual property protection process, the objective of efficient energy extraction has not yet been achieved.

It is in Chapter 5 where the objective of this research is achieved: to achieve a device that uses a single EHS to extract energy and to measure, that both actions take place simultaneously, that the extraction of energy is efficient and that the device offers a quantitative and objective result [73, 75]. The prototype developed to validate this new architecture is a galvanic cell based PoC device designed to perform amperometric measurements with different samples; such as, in this case, ethanol, lactate and methanol. This new architecture, which can be adapted to different EHSs, as indicated by the patent that protects it [75], allows us to go one step further in the realization of self powered devices, initiating a new paradigm in which all the energy and power that the EHS can give is available. Power will always be extracted efficiently (use of MPPT algorithms) and continuously (use of the same EHS as a power supply and sensor, simultaneously) offering to the developers, thanks to the new levels of power and energy available, the possibility to extend the functionalities of their devices (wireless transmissions, signal processing, on field self calibration,...), increase their autonomy or, directly, operate as a truly self powered device without needing third party devices.

Finally, in Chapter 6, I collect the main conclusions of my research as well as future lines of work that can exploit the results obtained in this research in the development of a new generation of truly self powered devices.

---

## Acronyms

<b>DAQ</b>	Data Acquisition
<b>DALC</b>	Dynamic Adaptative Load Controller
<b>DMFC</b>	Direct Methanol Fuel Cell
<b>DNL</b>	Differential Nonlinearity
<b>EH</b>	Energy Harvesting

<b>EHS</b>	Energy Harvesting Source
<b>ENOB</b>	Effective Number Of Bits
<b>ESC</b>	Extremum Seeking Control
<b>FC</b>	Fuell Cell
<b>FOCV</b>	Fractional Open Circuit Voltage
<b>FSCC</b>	Fractional Short Circuit Current
<b>GC</b>	Galvanic Cell
<b>LAN</b>	Local Area Network
<b>LUT</b>	Lookup Table
<b>ImpM</b>	Impedance Matching
<b>InC</b>	Incremental Conductance
<b>InI</b>	Incremental Impedance
<b>INL</b>	Integral Nonlinearity
<b>IoT</b>	Internet of Things
<b>MPP</b>	Maximum Power Point
<b>MPPT</b>	Maximum Power Point Tracking
<b>OCP</b>	Open Circuit Potential
<b>OP</b>	Operating Point
<b>PEG</b>	Piezoelectric Generator
<b>PVC</b>	Photovoltaic Cell
<b>PZT</b>	Lead Zirconate Titanate
<b>P&amp;O</b>	Perturb and Observation
<b>PoC</b>	Point of Care
<b>PMU</b>	Power Management Unit
<b>RES</b>	Renewable Energy System
<b>RF</b>	Radio Frequency
<b>SFDR</b>	Spurious Free Dynamic Range
<b>SHM</b>	Structural Health Monitoring



<b>SNR</b>	Signal to Noise Ratio
<b>SOSUS</b>	SOund SURveillance System
<b>TEG</b>	Thermoelectric Generator
<b>TSensors</b>	Trillion Sensors
<b>UHF</b>	Ultra High Frequency
<b>WSN</b>	Wireless Sensor Network

---

## References

- [1] Y. D. Marinakis, S. T. Walsh, and V. A. Chavez, “Here there be dragons: The TSensors systems technology roadmap,” in *PICMET 2016 Portland International Conference on Management of Engineering and Technology: Technology Management For Social Innovation, Proceedings*. Institute of Electrical and Electronics Engineers Inc., jan 2017, pp. 2736–2750.
- [2] R. Kanan, “IoT devices: The quest for energy security,” in *Midwest Symposium on Circuits and Systems*, vol. 0. Institute of Electrical and Electronics Engineers Inc., jul 2016.
- [3] EnOcean, “The True Cost of Batteries why energy harvesting is the best power solution for wireless sensors,” Tech. Rep., 2015.
- [4] M. Prauzek, J. Konecny, M. Borova, K. Janosova, J. Hlavica, and P. Musilek, “Energy Harvesting Sources, Storage Devices and System Topologies for Environmental Wireless Sensor Networks: A Review,” *Sensors*, vol. 18, no. 8, p. 2446, jul 2018.
- [5] A. Jushi, A. Pegatoquet, and T. N. Le, “Wind Energy Harvesting for Autonomous Wireless Sensor Networks,” in *Proceedings 19th Euromicro Conference on Digital System Design, DSD 2016*. Institute of Electrical and Electronics Engineers Inc., oct 2016, pp. 301–308.
- [6] Y. K. Tan and S. K. Panda, “Optimized wind energy harvesting system using resistance emulator and active rectifier for wireless sensor nodes,” *IEEE Transactions on Power Electronics*, vol. 26, no. 1, pp. 38–50, 2011.
- [7] D. Carli, D. Brunelli, D. Bertozzi, and L. Benini, “A high efficiency wind flow energy harvester using micro turbine,” in *SPEEDAM 2010 International Symposium on Power Electronics, Electrical Drives, Automation and Motion*, 2010, pp. 778–783.
- [8] I. Fagarasan, I. Stamatescu, C. Nichiforov, G. Stamatescu, N. Arghira, and S. S. Iliescu, “Laboratory scale wind energy harvester,” in *Proceedings of the 2017 IEEE 9th International Conference on Intelligent Data Acquisition and Advanced Computing Systems: Technology and Applications, IDAACS 2017*, vol. 2. Institute of Electrical and Electronics Engineers Inc., nov 2017, pp. 674–678.
- [9] L. Beker, H. Külah, and A. Muhtarolu, “Piezoelectric cantilever prototype for energy harvesting in computing applications,” *2011 International Conference on Energy Aware Computing, ICEAC 2011*, 2011.
- [10] A. Álvarez Carulla, J. Colomer Farrarons, J. Lopez Sanchez, and

- P. Miribel Catala, "Piezoelectric Harvester based structural health monitoring that uses a self powered adaptive circuit," in *2nd IEEE International Workshop on Metrology for Aerospace*. Institute of Electrical and Electronics Engineers Inc., aug 2015, pp. 531 535.
- [11] A. Bertacchini, L. Larcher, M. Lasagni, and P. Pavan, "Ultra low cost triboelectric energy harvesting solutions for embedded sensor systems," in *IEEE NANO 2015 15th International Conference on Nanotechnology*. Institute of Electrical and Electronics Engineers Inc., 2015, pp. 1151 1154.
- [12] X. S. Zhang, Y. B. Guo, Y. Wang, H. Zhang, and J. Brugger, "A transparent silk fibroin based triboelectric microgenerator for airflow energy harvesting," in *2017 IEEE 12th International Conference on Nano/Micro Engineered and Molecular Systems, NEMS 2017*. Institute of Electrical and Electronics Engineers Inc., aug 2017, pp. 65 68.
- [13] U. T. Jurado, S. H. Pu, and N. M. White, "A contact separation mode triboelectric nanogenerator for ocean wave impact energy harvesting," in *Proceedings of IEEE Sensors*, vol. 2017 Decem. Institute of Electrical and Electronics Engineers Inc., dec 2017, pp. 1 3.
- [14] Y. Wang, Y. Yang, and Z. L. Wang, "Triboelectric nanogenerators as flexible power sources," *npj Flexible Electronics*, vol. 1, no. 1, pp. 1 10, dec 2017.
- [15] X. Ma, S. Bader, and B. Oelmann, "Power Estimation for Indoor Light Energy Harvesting Systems," *IEEE Transactions on Instrumentation and Measurement*, pp. 1 1, mar 2020.
- [16] H. Y. Huang, C. O. Mocorro, J. Pinaso, and K. H. Cheng, "Indoor energy harvesting using photovoltaic cell for battery recharging," in *Proceedings of the 2013 IEEE 16th International Symposium on Design and Diagnostics of Electronic Circuits and Systems, DDECS 2013*. IEEE Computer Society, 2013, pp. 224 227.
- [17] M. S. Costa, L. T. Manera, and H. S. Moreira, "Study of the light energy harvesting capacity in indoor environments," in *INSCIT 2019 4th International Symposium on Instrumentation Systems, Circuits and Transducers*. Institute of Electrical and Electronics Engineers Inc., aug 2019.
- [18] D. Enescu, "Thermoelectric Energy Harvesting: Basic Principles and Applications," in *Green Energy Advances*. IntechOpen, feb 2019.
- [19] H. P. Wong and Z. Dahari, "Human body parts heat energy harvesting using thermoelectric module," in *2015 IEEE Conference on Energy Conversion, CENCON 2015*. Institute of Electrical and Electronics Engineers Inc., 2015, pp. 211 214.

- [20] S. Carrara, A. Cavallini, S. Ghoreishizadeh, J. Olivo, and G. De Micheli, "Developing highly integrated subcutaneous biochips for remote monitoring of human metabolism," in *Proceedings of IEEE Sensors*, 2012.
- [21] J. P. Curty, N. Joehl, C. Dehollain, and M. J. Declercq, "Remotely powered addressable UHF RFID integrated system," *IEEE Journal of Solid State Circuits*, vol. 40, no. 11, pp. 2193–2202, nov 2005.
- [22] C. P. B. Siu and Mu Chiao, "A Microfabricated PDMS Microbial Fuel Cell," *Journal of Microelectromechanical Systems*, vol. 17, no. 6, pp. 1329–1341, dec 2008.
- [23] M. Alaraj and J. D. Park, "Net power positive maximum power point tracking energy harvesting system for microbial fuel cell," *Journal of Power Sources*, pp. 225–232, apr 2019.
- [24] G. Slaughter and T. Kulkarni, "A self powered glucose biosensing system," *Biosensors and Bioelectronics*, vol. 78, pp. 45–50, 2016.
- [25] Y. Montes Cebrián, L. del Torno de Román, A. Álvarez Carulla, J. Colomer Farrarons, S. D. Minter, N. Sabaté, P. L. Miribel Català, and J. P. Esquivel, "Plug and Power' Point of Care diagnostics: A novel approach for self powered electronic reader based portable analytical devices," *Biosensors and Bioelectronics*, vol. 118, pp. 88–96, 2018.
- [26] L. Wang, M. He, Y. Hu, Y. Zhang, X. Liu, and G. Wang, "A "4 cell" modular passive DMFC (direct methanol fuel cell) stack for portable applications," *Energy*, vol. 82, pp. 229–235, mar 2015.
- [27] N. Hashim, S. K. Kamarudin, and W. R. Daud, "Design, fabrication and testing of a PMMA based passive single cell and a multi cell stack micro DMFC," *International Journal of Hydrogen Energy*, vol. 34, no. 19, pp. 8263–8269, oct 2009.
- [28] H. Vocca and F. Cottone, "Kinetic Energy Harvesting," in *ICT Energy Concepts Towards Zero Power Information and Communication Technology*. InTech, feb 2014.
- [29] V. Raghunathan, A. Kansal, J. Hsu, J. Friedman, and M. Srivastava, "Design considerations for solar energy harvesting wireless embedded systems," in *2005 4th International Symposium on Information Processing in Sensor Networks, IPSN 2005*, vol. 2005, 2005, pp. 457–462.
- [30] S. T. Senthilkumar, W. Go, J. Han, L. Pham Thi Thuy, K. Kishor, Y. Kim, and Y. Kim, "Emergence of rechargeable seawater batteries," pp. 22803–22825, oct 2019.
- [31] A. Álvarez Carulla, Y. Montes Cebrián, M. Puig Vidal, J. Colomer Farrarons, and P. L. Miribel Català, "Self Powered Point of Care Device

- for Galvanic Cell based Sample Concentration Measurement,” *IEEE Transactions on Biomedical Circuits and Systems*, under embargo.
- [32] L. Ortega, A. Llorella, J. P. Esquivel, and N. Sabaté, “Self powered smart patch for sweat conductivity monitoring,” *Microsystems & Nanoengineering*, vol. 5, no. 1, p. 3, dec 2019.
- [33] International Energy Agency (IEA), Nuclear Energy Agency (NEA), and Organization for Economic Co operation and Development (OECD), “Projected Costs of Generating Electricity 2015 Edition,” Paris, France, Tech. Rep., 2015.
- [34] A. K. Gupta and R. Saxena, “Review on widely used MPPT techniques for PV applications,” in *2016 International Conference on Innovation and Challenges in Cyber Security (ICICCS INBUSH)*. IEEE, feb 2016, pp. 270–273.
- [35] C. G. Popovici, S. V. Huditeanu, T. D. Mateescu, and N. C. Chereche, “Efficiency Improvement of Photovoltaic Panels by Using Air Cooled Heat Sinks,” *Energy Procedia*, vol. 85, pp. 425–432, jan 2016.
- [36] V. Sumathi, R. Jayapragash, A. Bakshi, and P. Kumar Akella, “Solar tracking methods to maximize PV system output A review of the methods adopted in recent decade,” *Renewable and Sustainable Energy Reviews*, vol. 74, pp. 130–138, jul 2017.
- [37] J. G. Njiri and D. Söffker, “State of the art in wind turbine control: Trends and challenges,” *Renewable and Sustainable Energy Reviews*, vol. 60, pp. 377–393, jul 2016.
- [38] R. Tiwari and N. R. Babu, “Recent developments of control strategies for wind energy conversion system,” *Renewable and Sustainable Energy Reviews*, vol. 66, pp. 268–285, dec 2016.
- [39] A. Álvarez Carulla, J. Colomer Farrarons, and P. L. Miribel, “Low Power Energy Harvesting Solutions for Smart Self Powered Sensors,” in *Sensors for Diagnostics and Monitoring*. CRC Press, 2018, pp. 217–250.
- [40] I. Laird and D. D. C. Lu, “Steady state reliability of maximum power point tracking algorithms used with a thermoelectric generator,” in *2013 IEEE International Symposium on Circuits and Systems (ISCAS2013)*. IEEE, may 2013, pp. 1316–1319.
- [41] Y. K. Ramadass and A. P. Chandrakasan, “A Battery Less Thermoelectric Energy Harvesting Interface Circuit With 35 mV Startup Voltage,” *IEEE Journal of Solid State Circuits*, vol. 46, no. 1, pp. 333–341, jan 2011.

- [42] N. Phillip, O. Maganga, K. J. Burnham, M. A. Ellis, S. Robinson, J. Dunn, and C. Rouaud, "Investigation of Maximum Power Point Tracking for Thermoelectric Generators," *Journal of Electronic Materials*, vol. 42, no. 7, pp. 1900–1906, jul 2013.
- [43] S. Bandyopadhyay and A. P. Chandrakasan, "Platform Architecture for Solar, Thermal, and Vibration Energy Combining With MPPT and Single Inductor," *IEEE Journal of Solid State Circuits*, vol. 47, no. 9, pp. 2199–2215, sep 2012.
- [44] D. Champier, C. Favarel, J. P. Bédécarrats, T. Kousksou, and J. F. Rozis, "Prototype Combined Heater/Thermoelectric Power Generator for Remote Applications," *Journal of Electronic Materials*, vol. 42, no. 7, pp. 1888–1899, jul 2013.
- [45] A. Paraskevas and E. Koutroulis, "A simple maximum power point tracker for thermoelectric generators," *Energy Conversion and Management*, vol. 108, pp. 355–365, jan 2016.
- [46] H. P. Desai and H. K. Patel, "Maximum Power Point Algorithm in PV Generation: An Overview," in *2007 7th International Conference on Power Electronics and Drive Systems*. IEEE, nov 2007, pp. 624–630.
- [47] Z. Zeng, X. Li, A. Bermak, C. Y. Tsui, and W. H. Ki, "A WLAN 2.4 GHz RF energy harvesting system with reconfigurable rectifier for wireless sensor network," in *2016 IEEE International Symposium on Circuits and Systems (ISCAS)*. IEEE, may 2016, pp. 2362–2365.
- [48] J. Dickson, "On chip high voltage generation in MNOS integrated circuits using an improved voltage multiplier technique," *IEEE Journal of Solid State Circuits*, vol. 11, no. 3, pp. 374–378, jun 1976.
- [49] J. H. Hyun, D. S. Ha, D. Daeick Han, and C. M. Kyung, "A solar energy harvesting system for a portable compact LED lamp," in *IECON 2015 41st Annual Conference of the IEEE Industrial Electronics Society*. IEEE, nov 2015, pp. 001 616–001 621.
- [50] A. Álvarez Carulla, J. Colomer Farrarons, J. Lopez Sanchez, P. Miribel Catala, A. Alvarez Carulla, J. Colomer Farrarons, J. Lopez Sanchez, and P. Miribel Catala, "PiezoElectric Harvester Based Self Powered Adaptive Circuit with Wireless Data Transmission Capability for Structural Health Monitoring," in *2015 Conference on Design of Circuits and Integrated Systems, DCIS 2015*. Institute of Electrical and Electronics Engineers Inc., jan 2016.
- [51] A. Álvarez Carulla, J. Colomer Farrarons, J. López Sánchez, and P. Miribel Català, "An adaptive self powered energy harvester strain sensing device based on mechanical vibrations for structural health monitoring applications," in *2016 IEEE 25th International Symposium on*

- Industrial Electronics (ISIE)*, vol. 2016 Novem. IEEE, nov 2016, pp. 638–644.
- [52] A. Álvarez, M. Baffleur, J. M. M. Dilhac, J. Colomer, D. Dragomirescu, J. Lopez, M. Zhu, and P. Miribel, “Self Powered energy harvester strain sensing device for structural health monitoring,” dec 2016.
- [53] Y. Montes Cebrián, A. Álvarez Carulla, J. Colomer Farrarons, M. Puig Vidal, and P. L. Miribel Català, “Self Powered Portable Electronic Reader for Point of Care Amperometric Measurements,” *Sensors*, vol. 19, no. 17, p. 3715, aug 2019.
- [54] J. Colomer Farrarons, P. Miribel Català, A. Saiz Vela, and J. Samitier, “A multiharvested self powered system in a low voltage low power technology,” *IEEE Transactions on Industrial Electronics*, vol. 58, no. 9, pp. 4250–4263, 2011.
- [55] E. Sazonov, P. Pillay, H. Li, and D. Curry, “Self Powered Sensors for Monitoring of Highway Bridges,” *IEEE Sensors Journal*, vol. 9, no. 11, pp. 1422–1429, 2009.
- [56] S. Choi, “Powering point of care diagnostic devices,” *Biotechnology Advances*, vol. 34, no. 3, pp. 321–330, may 2016.
- [57] C. Mo and J. Davidson, “Energy harvesting technologies for structural health monitoring applications,” in *2013 1st IEEE Conference on Technologies for Sustainability, SusTech 2013*, 2013, pp. 192–198.
- [58] J. Su, V. Leonov, M. Goedbloed, Y. van Andel, M. C. de Nooijer, R. Elfrink, Z. Wang, and R. J. M. Vullers, “A batch process micromachined thermoelectric energy harvester: fabrication and characterization,” *Journal of Micromechanics and Microengineering*, vol. 20, no. 10, p. 104005, oct 2010.
- [59] J. Olivo, S. Carrara, and G. De Micheli, “Energy Harvesting and Remote Powering for Implantable Biosensors,” *IEEE Sensors Journal*, vol. 11, no. 7, pp. 1573–1586, oct 2010.
- [60] V. Leonov, “Thermoelectric energy harvesting of human body heat for wearable sensors,” in *IEEE Sensors Journal*, vol. 13, no. 6, jun 2013, pp. 2284–2291.
- [61] L. Jiang, M. Mancuso, and D. Erickson, “Light Driven Microfluidics Towards Solar Powered Point Of Care Diagnostics,” 2012.
- [62] M. Q. Le, J. F. Capsal, M. Lallart, Y. Hebrard, A. Van Der Ham, N. Reffe, L. Geynet, and P. J. Cottinet, “Review on energy harvesting for structural health monitoring in aeronautical applications,” pp. 147–157, nov 2015.

- [63] Y. T. Liao, H. Yao, B. Parviz, and B. Otis, "A  $3\mu\text{W}$  wirelessly powered CMOS glucose sensor for an active contact lens," in *2011 IEEE International Solid State Circuits Conference*. IEEE, feb 2011, pp. 38–40.
- [64] Texas Instruments, "BQ25504 Ultra Low Power Boost Converter With Battery Management for Energy (Datasheet)," [Online]. Available: <http://ti.com/lit/ds/symlink/bq25504.pdf>. [Accessed September 12, 2019].
- [65] A. J. Bandodkar, J. M. You, N. H. Kim, Y. Gu, R. Kumar, A. M. V. Mohan, J. Kurniawan, S. Imani, T. Nakagawa, B. Parish, M. Parthasarathy, P. P. Mercier, S. Xu, and J. Wang, "Soft, stretchable, high power density electronic skin based biofuel cells for scavenging energy from human sweat," *Energy & Environmental Science*, vol. 10, no. 7, pp. 1581–1589, jul 2017.
- [66] X. D. Do, S. K. Han, and S. G. Lee, "Optimization of piezoelectric energy harvesting systems by using a MPPT method," in *2014 IEEE 5th International Conference on Communications and Electronics, IEEE ICCE 2014*. Institute of Electrical and Electronics Engineers Inc., oct 2014, pp. 309–312.
- [67] S. Li, A. Roy, and B. H. Calhoun, "A Piezoelectric Energy Harvesting System with Parallel SSHI Rectifier and Integrated Maximum Power Point Tracking," *IEEE Solid State Circuits Letters*, vol. 2, no. 12, pp. 301–304, dec 2019.
- [68] A. Alvarez Carulla, Y. Montes Cebrian, M. Puig Vidal, J. Lopez Sanchez, J. Colomer Farrarons, and P. Miribel Catala, "Energy Aware Adaptive Supercapacitor Storage System for Multi Harvesting Solutions," in *Proceedings 33rd Conference on Design of Circuits and Integrated Systems, DCIS 2018*. Institute of Electrical and Electronics Engineers Inc., apr 2019.
- [69] M. A. Pellitero, A. Guimerà, M. Kitsara, R. Villa, C. Rubio, B. Lakard, M. L. Doche, J. Y. Hihn, and F. Javier del Campo, "Quantitative self powered electrochromic biosensors," *Chemical Science*, vol. 8, no. 3, pp. 1995–2002, feb 2017.
- [70] A. Baingane and G. Slaughter, "Self powered electrochemical lactate biosensing," *Energies*, vol. 10, no. 10, oct 2017.
- [71] C. Fischer, A. Fraiwan, and S. Choi, "A 3D paper based enzymatic fuel cell for self powered, low cost glucose monitoring," *Biosensors and Bioelectronics*, vol. 79, pp. 193–197, may 2016.
- [72] Y. Montes Cebrian, A. Álvarez Carulla, J. Colomer Farrarons, M. Puig Vidal, J. Lopez Sanchez, and P. Miribel Catala, "A Fuel Cell based adaptable Self Powered Event Detection platform enhanced for biosampling



- applications,” in *2018 Conference on Design of Circuits and Integrated Systems (DCIS)*. IEEE, nov 2018, pp. 1–6.
- [73] A. Álvarez Carulla, Y. Montes Cebrián, M. Puig Vidal, J. Colomer Farrarons, and P. L. Miribel Català, “Ubiquitous Self Powered Architecture for FuelCell based Point of Care Applications,” *IEEE Transactions on Industrial Electronics*, submitted for publication.
- [74] A. H. Clemens, “United States Patent,” Tech. Rep., apr 1968.
- [75] A. Álvarez Carulla, P. L. Miribel Català, Y. Montes Cebrián, and J. Colomer Farrarons, “Self Powered System and Method for Power Extraction and Measurement of Energy Generator Units,” European Patent Office Patent Request EP19382604.7, July 17, 2019.
- [76] F. E. Mahboubi, M. Baffleur, V. Boitier, A. Alvarez, J. Colomer, P. Miribel, and J. M. Dilhac, “Self Powered Adaptive Switched Architecture Storage,” in *Journal of Physics: Conference Series*, vol. 773, no. 1. Institute of Physics Publishing, dec 2016.

# 2

---

## *Self-Powered Nodes for Structural Health Monitoring Applications*

---

### CONTENTS

2.1	WSNs for Aerospace Applications .....	30
2.2	The SMARTER Project .....	33
2.3	Adaptative Self Powered Circuit for SHM .....	33
2.3.1	Prototype Implementation .....	36
2.3.1.1	Piezoelectric Generator .....	37
2.3.1.2	Power Management .....	38
2.3.1.3	Analog Control Unit .....	38
2.3.1.4	Wireless End Point .....	40
2.3.2	Validation Methods .....	40
2.3.3	Results and Discussion .....	42
2.4	Energy Aware Adaptative Super capacitor Storage System .....	44
2.4.1	The Prototype .....	46
2.4.2	Results and Discussion .....	47
2.5	CMOS Integrated Circuit for SHM .....	48
2.5.0.1	Low Power Successive approximation ADC ..	48
2.5.1	The Prototype .....	51
2.5.2	Results and Discussion .....	53
2.6	Chapter Conclusions .....	57
	Acronyms .....	57
	References .....	59

In this Chapter, a self powered device for Wireless Sensor Networks (WSNs) for Structural Health Monitoring (SHM) applications is presented. The device, framed in the research project Smart Multifunctional ARchitecture & Tech nology for Energy aware wireless sensoR (SMARTER), is based on a Piezo electric Generator (PEG) and is designed to monitor the strain suffered by an aircraft's wing where the device is attached. The PEG is used both for harvest energy from the mechanical vibrations of the wing and for measure its mechan ical strain. A discrete prototype is presented with a Maximum Power Point Tracking (MPPT) functionality and a super capacitor based energy storage. Then, the prototype is translated to an Application Specific Integrated Cir cuit (ASIC) that outputs the strain measurement to a second ASIC developed

by Laboratoire d'Analyse et d'Architecture des Systèmes (LAAS) that will send the data wirelessly to a host.

---

## 2.1 WSNs for Aerospace Applications

In order to guarantee the structural integrity of an aircraft and, therefore, to guarantee its safe use, monitoring techniques are used during its operation. This type of monitoring techniques are included in the scope known as SHM. In the aerospace field, the structural health of an aircraft is closely linked to the ability of the structure to perform its work, so it must be guaranteed to maximize the safety of the aircraft. This is especially important in passenger transport vehicles, in both the civil and military fields. In turn, the SHM allows not only to see the capacity of the structure to carry out its work, but with which efficiency or under which conditions it is doing it. In this aspect, the objective is to minimize the costs of the aircraft, whether direct (corrective and preventive maintenance) or indirect (opportunity cost due to having the aircraft under repair, leasing of another aircraft, cost of operator training, etc.).

In addition to the objective of increasing aircraft safety (a goal whose need for achievement is more than obvious), the aviation industry seeks to minimize costs. A clear example is the aging of the current air park shown in Fig. 2.1. In the last two decades the average age has been between 10 and 12 years of service, but the number of aircraft with an average age of more than 20 years is increasing considerably [1]. Currently, the industry seeks to extend the useful life of aircrafts in order to reduce costs, but this in turn leads to a decrease in safety, as well as an increase in repair and maintenance costs. That is why increasingly the SHM in the field of aviation is becoming one of the first lines of research in the R&D departments of the different companies within the aerospace industry.

As a solution to the needs mentioned above, WSNs appear. A WSN is a wireless network of autonomous sensors distributed throughout a structure or space that offer information about its environment. Its applications are multiple; from environmental monitoring to structural monitoring, through industrial monitoring, process monitoring and asset monitoring, among many others. With structural monitoring it is possible to have a history of the mechanical stress suffered by the aircraft.

An important aspect of WSNs is their wireless nature. Thanks to this, their incorporation into the aircraft does not imply a substantial increase in weight, it is possible to reduce the costs associated with rewiring and safety re certification in the case of incorporating or replacing a sensor, and it is possible to reduce damage; i.e., costs, due to cuts, breaks or degradation in

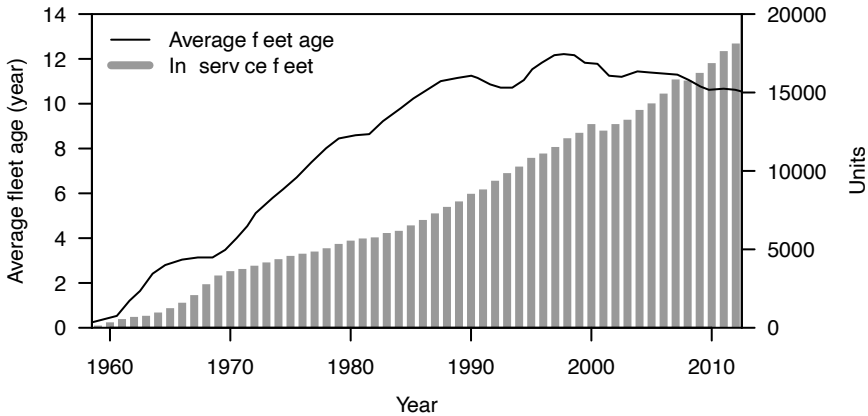


Figure 2.1: In service fleet and average age. Data from [1].

the wiring. To quantitatively assess the importance of this wireless feature of the WSN, the following data is available:

- An Airbus 380 carries about 500 km of cables (98,000 cables and 40,000 connectors) [2].
- The US Army has lost 6 aircraft in 10 years due to electrical failure [3].
- The US Army has 78 inoperative aircrafts per year to carry out missions due to incidents in the wiring [3].
- About 1,000 missions per year are aborted due to wiring errors [3].
- The use of wireless networks for the control system of a Cessna 310R can reduce its total weight by 41 kg, a reduction in weight that would increase its flight range by 10 % [4].
- A 50 % reduction in the wiring of an SH60 would reduce its weight by 121 kg [4].

It can be seen how using wireless networks instead of cabling can provide multiple advantages at a functional level, as well as reducing costs, whether direct or indirect.

Due to the wireless nature of a WSN, ideally, the different nodes should be powered locally. For this, batteries can be used, but this would increase the cost due to the acquisition of a battery, at least, for each node plus the cost associated with its replacement or recharging. Therefore, a solution that does not use batteries is preferable. It is here where WSNs and Energy Harvesting intersect. What is proposed is to collect energy available in the environment

to transform it into electrical energy that allows the different nodes of a WSN to be powered locally.

Like many other technological advances, the first known WSN implementation, shown in Fig. 2.2 was carried out by the US Navy in 1949 when they installed a network of underwater acoustic sensors along the Atlantic and Pacific oceans for the detection of Russian submarines during the Cold War [5]. The system, called SOund SURveillance System (SOSUS), was made up of underwater acoustic sensors that transmitted information from the environment to stations (hosts) called NAVFACs (Naval Facilities) so that they would look for the trace of the presence of enemy submarines in the signal spectrum received.

Nowadays, WSNs have crossed the borders of military enforcement to be in high demand from the civilian market. Applications ranging from environmental control [7], structural health monitoring [8], industrial monitoring [9] or in biomedical applications [10]. Each of these applications have their own objectives and requirements, but they have in common a tendency towards miniaturization, the search for cost reduction and the search for harvesting energy from the environment to eliminate dependence on an external source as it can be a battery. This involves an effort in four key technological areas: sensors, integration capacity, communication protocols and the ability to col

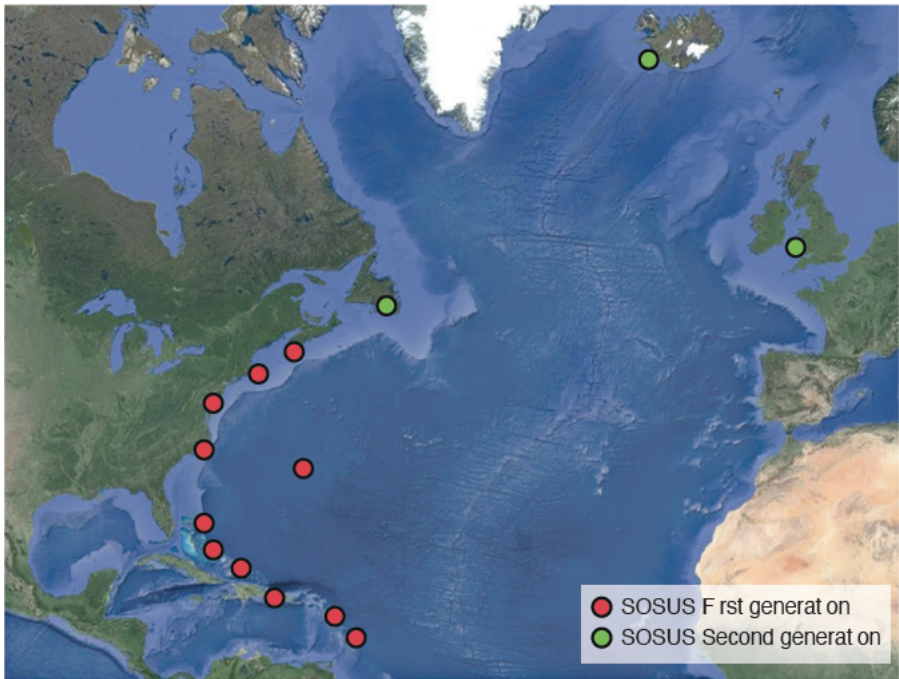


Figure 2.2: First implemented WSN. Data from [6].

lect and store energy. The aim of evolving these four areas is to achieve the emerging concept Internet of Things (IoT) [11].

---

## 2.2 The SMARTER Project

The SMARTER project [12] works on a node for a WSN that, by means of a PEG, monitors the structural health of the wing of an aircraft while collecting mechanical energy from their vibrations to locally power the node. Fig. 2.3 depicts an illustration example of the application. The solution must extract electrical energy from a PEG that will collect energy from the mechanical vibrations. It will also monitor the structural health of the wing by monitoring the Open Circuit Potential (OCP) of the PEG, which is a direct indication of the mechanical stress on the structure where the piezoelectric is attached. Finally, the measured value will be converted to a 6 bit digital signal that will be sent to an ASIC designed by LAAS [13], which is responsible of wirelessly transmitting the information to a host.

---

## 2.3 Adaptative Self-Powered Circuit for SHM

Maximum power can be extracted from a PEG when the polarization voltage  $V_{PEG}$  across its output terminal is one half of the OCP regardless the frequency or amplitude of oscillation of the PEG [14]. The equation that describes this condition is

$$V_{PEG} \Big|_{P=P_{MAX}} = \frac{V_{OCP}}{2} \quad (2.1)$$

A PEG provides power in AC mode and the voltage, current and power levels provided depend on characteristics of oscillation of the PEG. Due to this, an AC/DC converter is needed in order to power an electronic circuit. In Fig. 2.4(a), we can see a common diode based full bridge rectifier with a filter capacitor  $C_{DD}$  and a resistor load  $R_{LOAD}$  intended to modelize an electronic circuit to be powered. Thus, the AC/DC converter provides a DC output voltage supply  $V_{DD}$ . Fig. 2.5(a) shows the efficiency achieved during the simulation of the circuit for different load conditions. This efficiency, from the PEG point of view, is defined as

$$\eta_{PEG} = \frac{P_P}{P_{P_{MAX}}} \quad (2.2)$$

where  $P_P$  is the power outputted by the PEG at given Operating Point (OP)

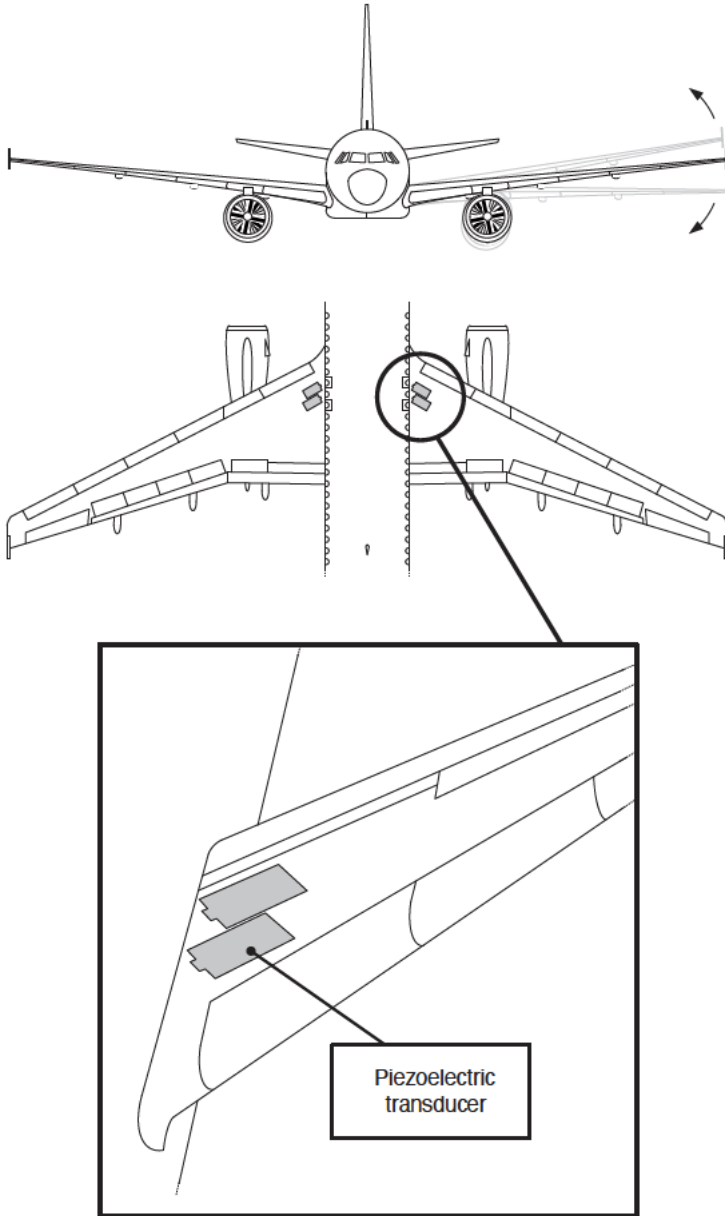


Figure 2.3: Application example of a WSN for SHM application in an aircraft. Image: "An adaptative self powered energy harvester strain sensing device based of mechanical vibrations for structural health monitoring applications" by Albert Álvarez Carulla *et al.* © 2016 IEEE.

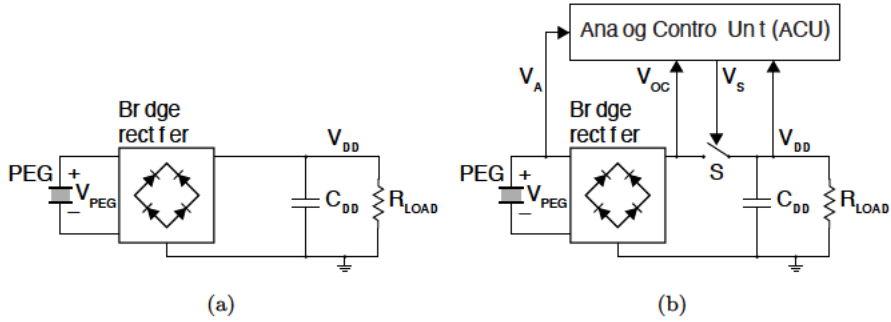


Figure 2.4: Schematic of a bridge rectifier based AC/DC converter (a) without and (b) with adaptation.

Images (a) and (b): "Piezoelectric Harvester based structural health monitoring that uses a self powered adaptive circuit" by Albert Álvarez Carulla *et al.* © 2015 IEEE.

and  $P_{P_{MAX}}$  the maximum power that the PEG can provide in optimal OP. As can be seen, the circuit exhibits a maximum efficiency peak for a given load. The load is normalized and expressed as the ratio between the given load and the load where maximum efficiency is achieved (annotated as  $R_{P_{MAX}}$ ). For a short circuit condition, the circuit exhibits a 0% efficiency. Then efficiency starts to increase rapidly until 100% for a normalized load of  $1 \Omega \Omega$ . Then, the efficiency starts to drop as load increases. Thus, with this circuit, maximum efficiency is achieved only for specific load condition.

In order to maximize the efficiency for a broader load range, a MPPT algorithm can be applied. In this case, in the SMARTER project, and as shown in [15 17], we have implemented a Fractional Open Circuit Voltage (FOCV) MPPT algorithm using an Analog Control Unit (ACU). The block schematic of the proposed circuit is shown in Fig. 2.4(b). The ACU, which implementation is detailed in Section 2.3.1, opens a switch  $S$  placed between the diode based full bridge rectifier and the capacitor  $C_{DD}$  and the load. This way, the PEG is let to open circuit state and PEG OCP is sampled by the ACU. The ACU switches  $S$  in order to regulate  $V_{DD}$  to one half of OCP adapting the output impedance of the PEG with the impedance of the load. Thus, we achieve maximum efficiency from PEG point of view regardless of the load condition.

The results of the simulation of this circuit, presented in Fig. 2.5(b), exhibits an efficiency near to 100% sustained along a wider load range. As in the circuit without the adaptation, efficiency starts to increase from 0% for a short circuit condition. The efficiency starts to increase and, for a load condition equal to, the previously annotated,  $R_{P_{MAX}}$ , an efficiency of 90% is



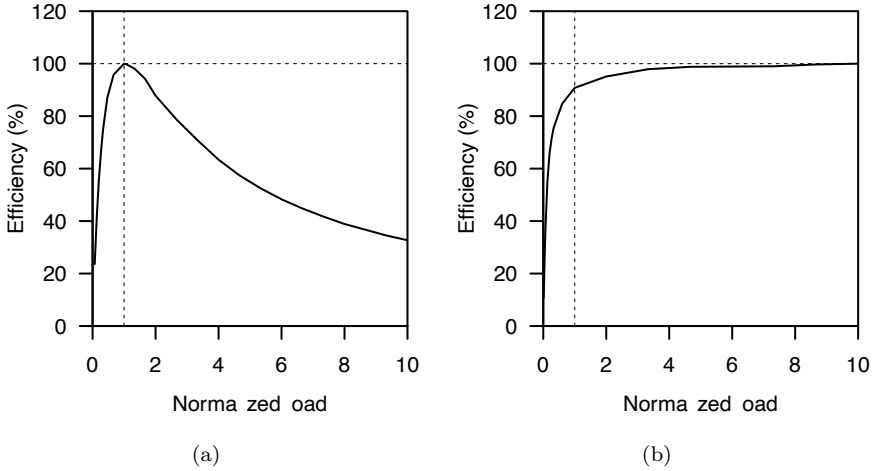


Figure 2.5: Simulated efficiency for a PEG and different load conditions (a) without and (b) with adaptation [16].

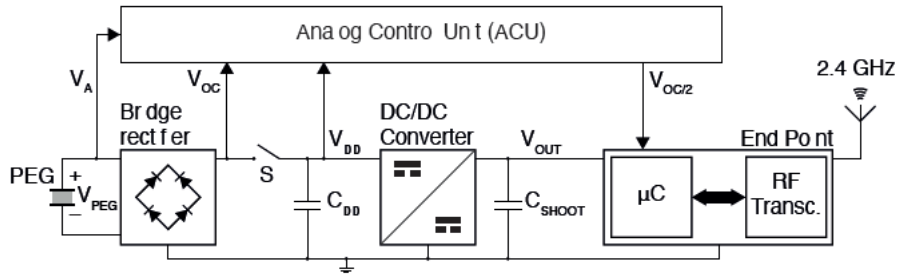
Images (a) and (b): "Piezoelectric Harvester based structural health monitoring that uses a self powered adaptive circuit" by Albert Álvarez Carulla *et al.* © 2015 IEEE.

achieved. From there on forward, we achieve an efficiency near to 100% regardless the load condition.

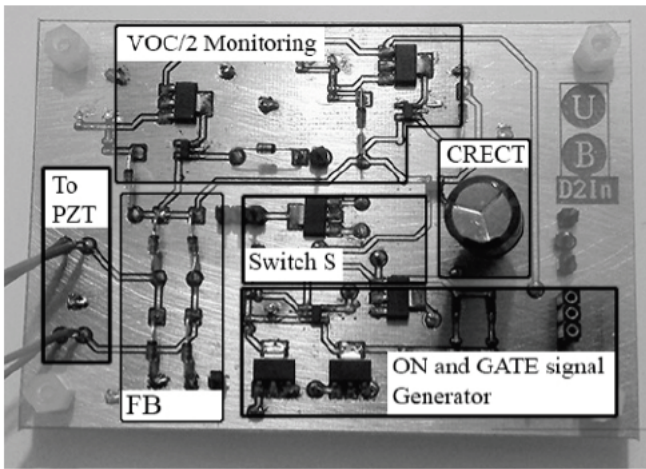
### 2.3.1 Prototype Implementation

The block diagram and a picture of the discrete implemented prototype are shown in Fig. 2.6. We have implemented the prototype on a 80 mm x 100 mm double sided Printed Circuit Board (PCB) using Commercial off the Shelf (COTS) parts. The system consists of an AC/DC converter, a DC/DC converter, the ACU and a Microcontroller Unit (MCU) based end point module with wireless data transmitter.

As described in the previous Section, the AC/DC converter rectifies the voltage from the PEG to generate an output voltage supply  $V_{DD}$ . This voltage depends on characteristics of oscillation of the PEG. In the AC/DC converter, a switch  $S$  is placed to disconnect the PEG from the circuit for its OCP sampling and to regulate  $V_{DD}$  to one half of the PEG OCP. The ACU is the responsible to control the switch  $S$  and of PEG OCP sampling. Due to  $V_{DD}$  is also dependent on PEG characteristics of oscillation, a DC/DC converter is placed to provide a constant output voltage supply, annotated as  $V_{OUT}$  in Fig. 2.6(a). This voltage supply is used to charge a super capacitor  $C_{SHOOT}$  and to power an end point module. This module consists of a MCU



(a)



(b)

Figure 2.6: (a) Block diagram and (b) picture of a self powered wireless sensor node.

Images (a) and (b): "Piezoelectric Harvester Based Self Powered Adaptive Circuit with Wireless Data Transmission Capability for Structural Health Monitoring" by Albert Álvarez Carulla *et al.* © 2016 IEEE.

that converts the  $V_{OC}/2$  to a digital value and sends it to a wireless transmitter which will deliver the data to a host wirelessly. The schematic of the implemented prototype is shown in Fig. 2.7.

### 2.3.1.1 Piezoelectric Generator

For the validation of the prototype, we have used a Quick Pack®QP40W double layered piezoelectric generator from Mid Technology Corp. [18]. The PEG is operated as a cantilever on  $d_3$  mode [19]. One of the ends of the PEG is clamped to a ET 132 2 shaker from Labworks Inc. while the other

end remains free to allow its oscillation. Amplitude and frequency oscillations of 3 to 5 mm and 20 to 30 Hz, respectively, are used during experiments. The PEG can be seen in the picture of the setup used for the validation of the prototype shown in Fig. 2.8.

### 2.3.1.2 Power Management

To generate  $V_{DD}$ , the AC/DC converter is implemented using four 1N4148 diodes for the full bridge rectifier and a 220  $\mu\text{F}$  filter capacitor. The switch  $S$  is implemented using two P channel Metal Oxide Semiconductor Field Effect Transistor (PMOS) transistors in back to back configuration in order to block current in both directions. The voltage supply  $V_{DD}$  is then regulated to 2 V,  $V_{OUT}$ , using a LT1761 Low Dropout (LDO) regulator from Linear Technology [20]. The power management also has a super capacitor intended to attend the current peak required by the end point module during a wireless transmission. The end point current requirements are detailed in Section 2.3.1.4.

### 2.3.1.3 Analog Control Unit

The ACU consists of three major sub circuits: 1) PEG OCP monitor, 2)  $V_{DD}$  vs.  $V_{OCP}/2$  amplifier, and 3) switch control signal generator.

The PEG OCP monitor uses a high impedance resistor based voltage divider connected to the output of the diode based full bridge rectifier  $V_{OCP}$ . The output of the voltage divider, which is configured to provide an output ratio of 1/2, is connected to a TS1005IG5T Operational Amplifier (OpAmp), from Silicon Labs [21], configured as voltage follower. The output of the vol

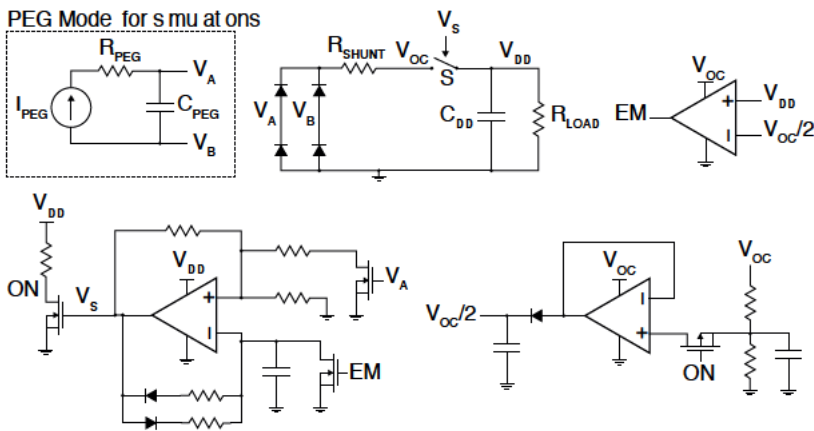


Figure 2.7: Schematic of a self powered SHM device.

Image: "Piezoelectric Harvester based structural health monitoring that uses a self powered adaptive circuit" by Albert Álvarez Carulla *et al.* © 2015 IEEE.

tage followed is connected to an output capacitor through a diode placed in series. Thus, one half of the envelope of the PEG OCP is captured providing an output signal  $V_{OCP}/2$ . This signal has two purposes: 1) to provide a signal reference to control the voltage level of  $V_{DD}$  for maximum efficiency, and 2) indicate the strain suffered by the mechanical part where the PEG is attached. Finally, a switch is placed in series between the output of the voltage divider and the input of the voltage divider in order to disable the monitoring when the PEG is not in open circuit state.

The  $V_{DD}$  vs.  $V_{OCP}/2$  amplifier is implemented using one TS1005IG5T OpAmp from Silicon Labs [21]. The amplifier is used to control the voltage at  $V_{DD}$  regulating it to  $V_{OCP}/2$  enabling/disabling the switch control signal generator.

The last sub circuit, the switch control signal generator, is an astable multivibrator OpAmp based circuit. We have used another TS1005IG5T OpAmp from Silicon Labs [21] to implement it. The sub circuit provides a rectangular waveform with fixed duty cycle which is enabled/disabled by the  $V_{DD}$  vs.  $V_{OCP}/2$  amplifier. A common source amplifier is placed at the output to gen

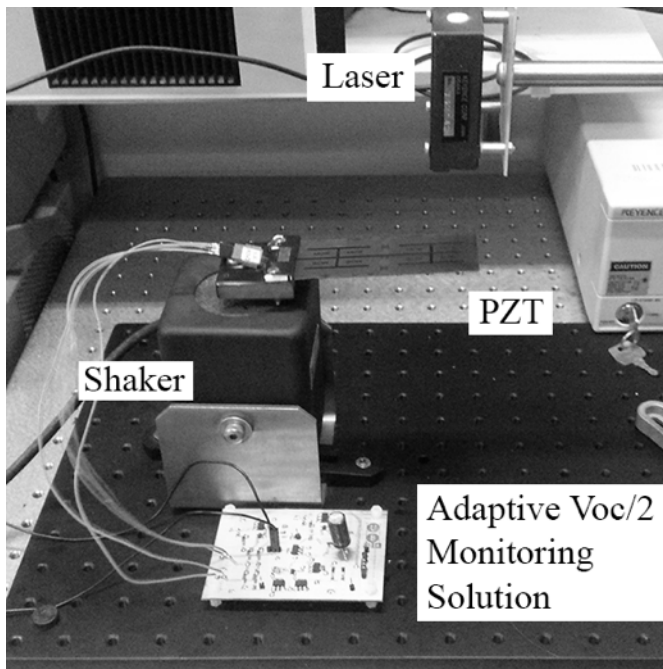


Figure 2.8: Experimental setup for PEG and prototype characterizations. Image: "Piezoelectric Harvester based structural health monitoring that uses a self powered adaptive circuit" by Albert Álvarez Carulla *et al.* © 2015 IEEE.

erate a complementary signal. Thus, the switch  $S$  can be open/closed and the PEG OCP monitor sub circuit enabled/disabled properly.

### 2.3.1.4 Wireless End-Point

We have used an ez430 RF2500 Development Board from Texas Instruments [22]. This development board provides a MSP430F2274 MCU [23], a 16 bit ultra low power MCU, and a CC2500 RF transceiver [24], a low power 2.4 GHz RF transceiver, from Texas Instruments. The MCU uses its Analog to Digital Converter (ADC) to digitalize the signal  $V_{OCP}/2$  and send it to the RF transceiver which sends the data to a host, in this case, a PC.

In order to attend the current peaks needed by the RF transceiver, a super capacitor was placed in the power management module. The MCU will monitor the voltage across the super capacitor and will only allow a RF transmission when enough energy is available. For this, we have characterized the power consumption of the end point module during connection pairing and data transmission with a Keysight B2962A Source Meter Unit (SMU). The end point module needs a minimum operating voltage supply of 1.8 V, but connection pairing and RF transmission will be allowed only when the voltage across the super capacitor reaches 2 V. Thus, we ensure that the voltage supply does not decrease under the minimum operating of 1.8 V due to the voltage drop occasioned by the punctual current peak demand of the RF transceiver.

The flow diagram of the firmware is shown in Fig. 2.9. Once enough energy is harvested from the PEG and the end point is powered, the MCU performs the initialization of all the peripherals used during its operation: timers, ADCs, interruptions, Serial Peripheral Interface (SPI), etc. Then the MCU enters in Low Power Mode (LPM) and monitors the voltage across the super capacitor. When the voltages reaches 2 V, the MCU wakes up and starts the connection pairing with the host. Then, MCU enters again in LPM while  $V_{OCP}/2$  is continuously captured. The maximum transmission rate of  $V_{OCP}/2$  is configured to 1 Sps, i.e., the MCU wakes up very 1 s and sends the data. This data transmission is conditioned to the energy available for the transmission, i.e., voltage across the super capacitor must reach 2 V before data is transmitted.

## 2.3.2 Validation Methods

We have validated the prototype in terms of capability of  $V_{OCP}/2$  monitoring, efficiency,  $V_{OCP}$  to strain transfer function, data digitalization and transmission, current consumption of the end point module during connection pairing and transmission, and overall power consumption of the device. The capability of the prototype to monitor  $V_{OCP}/2$  capturing  $V_{OCP}$  at the output of the full bridge rectifier and  $V_{OCP}/2$  at the output of the ACU simultaneously has been validated using a Keysight MSOX3034A oscilloscope for different conditions of oscillation. The efficiency has been measured using a Keysight B2962A

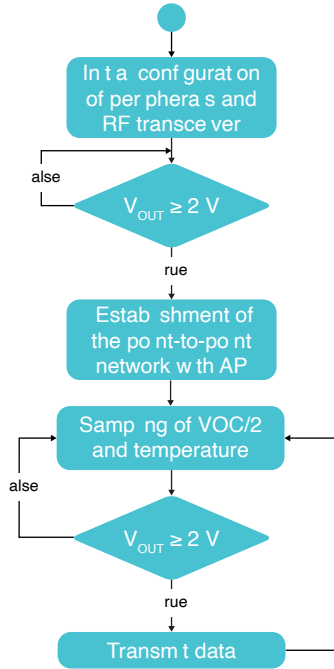


Figure 2.9: MCU's flow diagram.

Image: "Piezoelectric Harvester Based Self Powered Adaptive Circuit with Wireless Data Transmission Capability for Structural Health Monitoring" by Albert Álvarez Carulla *et al.* © 2016 IEEE.

SMU for different load conditions using a potentiometer as a variable resistor load. We have extracted the  $V_{OCP}$  to strain transfer function simultaneously capturing, with the Keysight MSOX3034A oscilloscope,  $V_{OCP}$  and  $V_\varepsilon$ . The signal  $V_\varepsilon$  is captured from the output of an external circuit intended to measure the strain suffered by the mechanical part where the PEG is attached. The circuit consists in full bridge strain gauge based on four N11MA212011 strain gauges from RS [25]. Thus, maximum sensitivity, low variation with temperature, linear response and only to bend strain response are achieved. For the data digitalization and transmission, we have captured  $V_{OCP}$  using the Keysight MSOX3034A oscilloscope while the digital transmitted data is registered in the host. The voltage across the super capacitor has been logged in order to measure the time needed by the system to harvest enough energy for connection pairing and time between consecutive transmissions. Finally, we have measured the current consumption of the end point module during

connection pairing and transmission, and the overall power consumption with the Keysight B2962A SMU.

### 2.3.3 Results and Discussion

Fig. 2.10(a) shows the experimental efficiency measured for different load conditions without the ACU, i.e., without adaptation. The simulated results from Fig. 2.5(a) are overlaid. As in simulations, the prototype, for the used PEG, exhibits a maximum efficiency peak for a load of  $55\text{ k}\Omega$ . The same measurements with the ACU enabled are shown in Fig. 2.10(b). With the ACU enabled, the prototype exhibits the same efficiency levels than in simulations. The prototype performs an adaptation and near 100 % efficiency is achieved for loads from  $55\text{ k}\Omega$  on. This efficiency, as described in Section 2.3, is achieved regulating  $V_{DD}$  to  $V_{OCP}/2$  that, in turn, is a direct indicator of the strain suffered by the mechanical part. Fig. 2.11 shows the capability of the system to monitor the envelope of one half of  $V_{OCP}$ .

Fig. 2.12(a) shows power extracted for different amplitudes and a fixed frequency of 25 Hz, while Fig. 2.12(b) shows power extracted for different frequencies and a fixed amplitude of 4 mm.

The  $V_{OCP}$  to strain transfer function is shown in Fig. 2.13(a). The PEG shows a linear response between its OCP and the strain suffered by the mechanical part. The ADC of the MCU is configured to read strain measurements

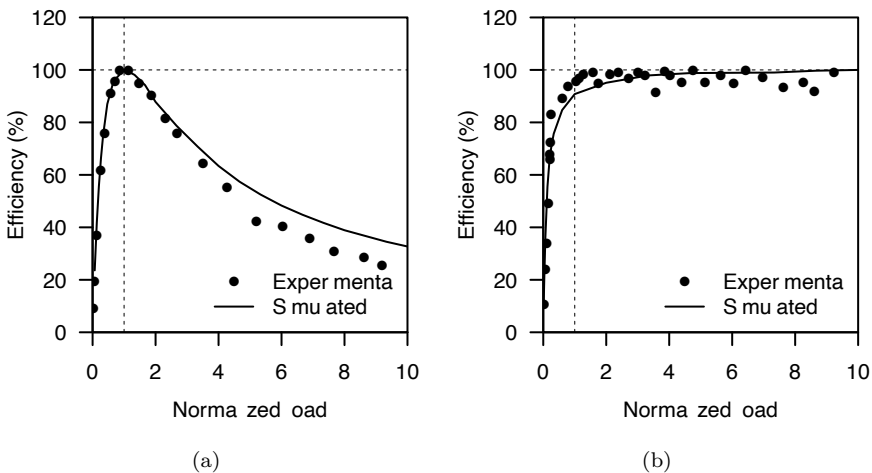


Figure 2.10: Experimental efficiency for a PEG and different load conditions (a) without, (b) with adaptation and with the simulated data overlaid.

Image: "Piezoelectric Harvester based structural health monitoring that uses a self powered adaptive circuit" by Albert Álvarez Carulla *et al.* © 2015 IEEE.

up to  $0.8\mu\epsilon$ . The corresponding digital conversion a 6 bit value is shown in Fig. 2.13(b).

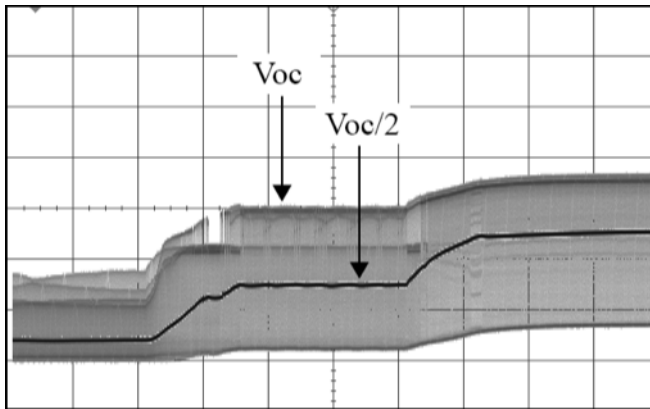


Figure 2.11: Oscilloscope capture of the real time monitoring of  $V_{OC}/2$  for different amplitudes of  $V_{OC}$  (1 V/div, 5 s/div).

Image: "Piezoelectric Harvester based structural health monitoring that uses a self powered adaptive circuit" by Albert Álvarez Carulla *et al.* © 2015 IEEE.

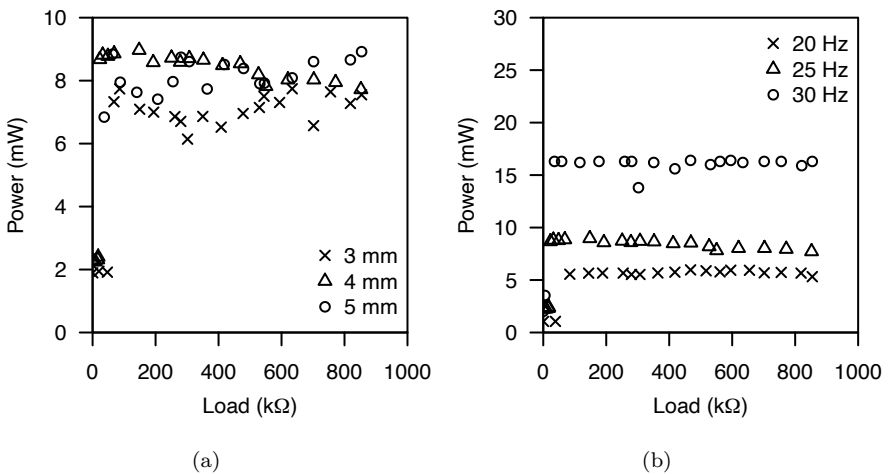


Figure 2.12: Power extracted from a PEG with adaptation and different (a) amplitudes and (b) frequencies of oscillation.

Images (a) and (b): "Piezoelectric Harvester based structural health monitoring that uses a self powered adaptive circuit" by Albert Álvarez Carulla *et al.* © 2015 IEEE.



Once converted, the value is wirelessly transmitted to a host. The current consumption of the initial connection pairing is shown in Fig. 2.14(a). The end point module needs a total charge of  $197.2\mu\text{C}$  with a maximum current peak of  $22.8\text{mA}$ . This step lasts  $15.5\text{ms}$  and only takes place once at the beginning of the transmitter operation. On the other hand, the charge needed by the transmitter to send data is  $31.6\mu\text{C}$  with a maximum current peak of  $22.7\text{mA}$  during a process that lasts  $2.8\text{ms}$ . The connection pairing is the most demanding process in terms of charge. Thus, connection pairing is the process that determines the super capacitor’s capacitance value.

When the end point is not transmitting, it remains in LPM most of the time exhibiting an average current consumption of  $2.5\mu\text{A}$ . Fig. 2.15(a) show the voltage at the super capacitor during the initialization of the prototype and its steady state operation. The prototype needs up to  $25\text{s}$  to harvest enough energy for connection pairing. Meanwhile, from Fig. 2.15(b), we can observe that the prototype sends data every second performing a data transmission with a transmission rate of  $1\text{Sps}$ .

All this is achieved with an overall power consumption of  $150\mu\text{W}$  with power consumption peaks of  $45.6\text{mW}$  during wireless transmissions.

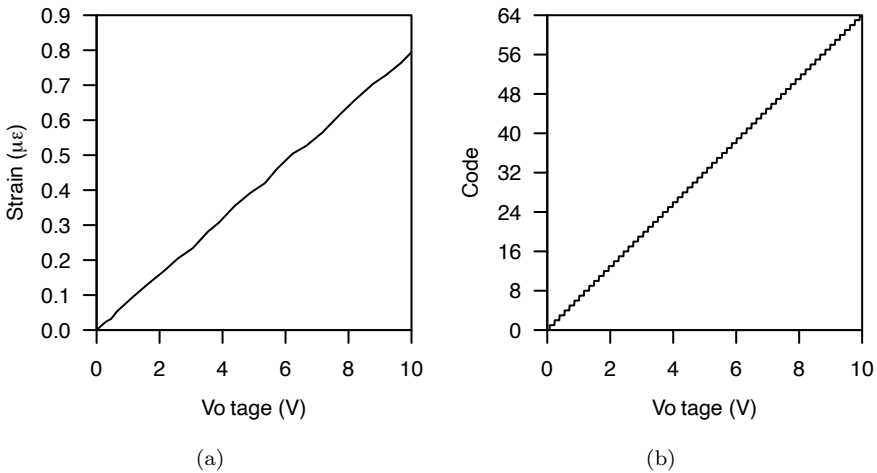


Figure 2.13: (a) Strain to voltage transfer function and (b) corresponding 6 bit digital code.

Images (a) and (b): "An adaptative self powered energy harvester strain sensing device based of mechanical vibrations for structural health monitoring applications" by Albert Álvarez Carulla *et al.* © 2016 IEEE.

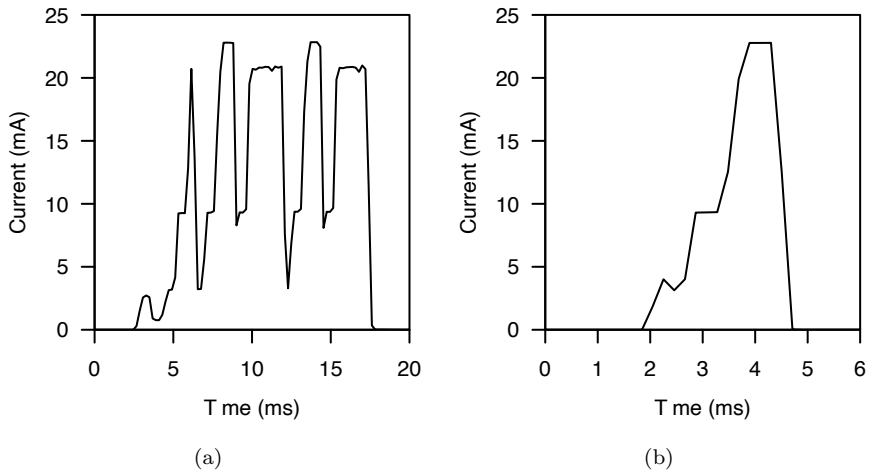


Figure 2.14: Current consumption of the microcontroller during (a) initial pairing and (b) data transmission [15].

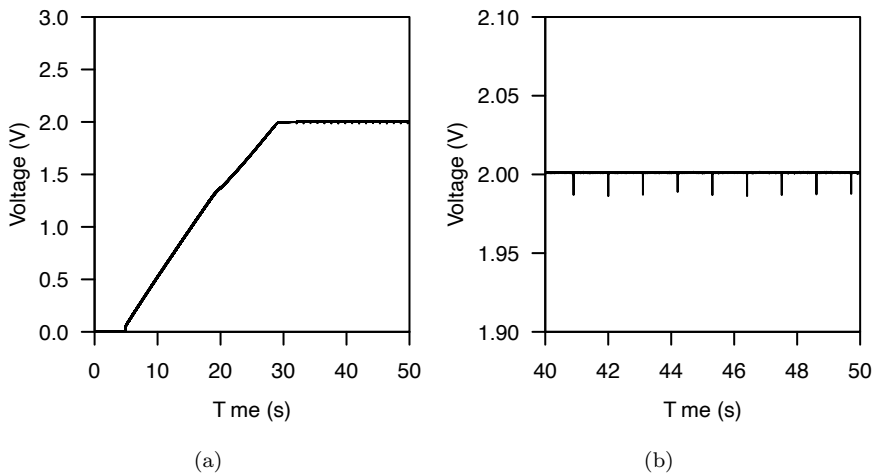


Figure 2.15: Voltage at the super capacitor during prototype (a) initialization and (b) steady state operation.

Images (a) and (b): "An adaptative self powered energy harvester strain sensing device based of mechanical vibrations for structural health monitoring applications" by Albert Álvarez Carulla *et al.* © 2016 IEEE.

## 2.4 Energy-Aware Adaptative Super-capacitor Storage System

It is essential to store surplus of energy in order to operate during periods in which energy cannot be collected from the environment. For this, there are mainly two possibilities: batteries or super capacitors. In this section, the development of a super capacitor based storage system is presented. The advantages of super capacitors compared to batteries are a much longer life time, especially in low temperature conditions (such as in aircraft), and the ability to offer higher power peaks. But they also have some drawbacks. The two biggest drawbacks are: 1) the voltage of a super capacitor varies with its charge level, and 2) an empty super capacitor will need an initial charge time that will be greater for larger capacitances. This leads us to desire a super capacitor with a low capacitance during the startup of the system, and a large capacitance once the system is in a steady state to store as much energy as possible. Therefore, we propose the development of an energy storage system based on a matrix of super capacitors that varies its equivalent capacitance depending on the level of energy stored [26, 27].

### 2.4.1 The Prototype

Fig. 2.16 shows the implemented matrix of super capacitors. The capacitance of each super capacitor  $C_i$  is 100 mF. The matrix can be configured in four different states. Each state is referenced following the  $C(X, Y)$  nomenclature where  $X$  is the number super capacitors in series that make up a stack and  $Y$  is the number stacks in parallel [28]. To configure the matrix with the minimum capacitance and thus obtain a shorter starting time, the configuration  $C(4, 1)$  must be set. On the other hand, the  $C(1, 4)$  configuration is the one that offers a higher capacitance and, therefore, maximizes the capacity of the matrix to store energy. Configuration  $C(2, 2)$  serves as an intermediate configuration.

To setup the matrix configuration, nine normally open analog switches have been used. To control these switches, a control module called Dynamic Adaptative Load Controller (DALC) has been implemented. The DALC, shown in Fig. 2.17 monitors the energy stored in the matrix by the voltage of one of the super capacitors. In order to carry out a single ended measurement, the super capacitor  $C_4$  is monitored, which will always have one of its terminals grounded. The relationship between the polarization voltage of the super capacitor  $V_{CELL}$  and the energy stored in the matrix  $U_T$  is

$$U_T = 2C_i V_{CELL}^2 \tag{2.3}$$

Through a resistor ladder, different voltage levels are generated from  $V_{CELL}$ . These voltage levels are compared to a reference voltage such that different energy levels are defined for which the configuration of the mat

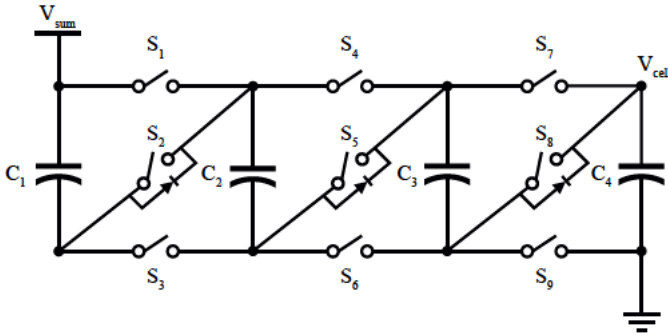


Figure 2.16: Schematic of the super capacitor based matrix.  
 Image: "Energy Aware Adaptative Supercapacitor Storage System for Multi Harvesting Solutions" by Albert Álvarez Carulla *et al.* © 2018 IEEE.

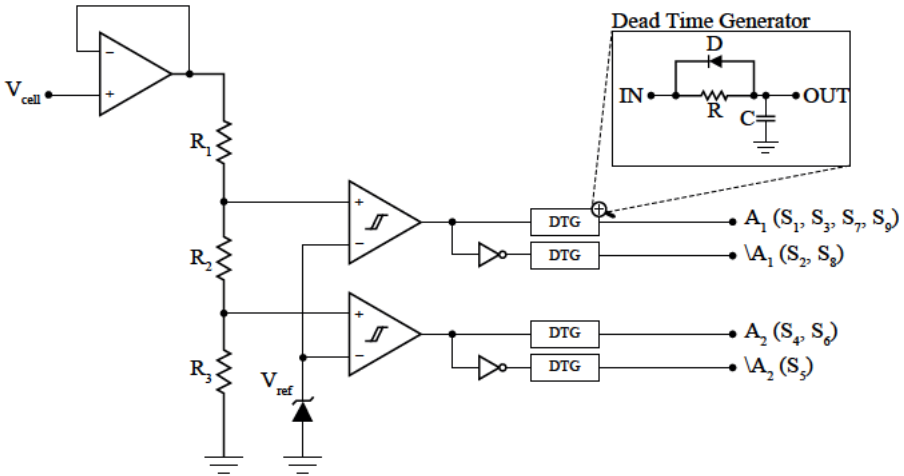


Figure 2.17: Schematic of the DALC.  
 Image: "Energy Aware Adaptative Supercapacitor Storage System for Multi Harvesting Solutions" by Albert Álvarez Carulla *et al.* © 2018 IEEE.

rix changes. The comparison has a hysteresis configured to avoid oscillations between configurations. Furthermore, at the output of the generated control signals, a simple dead time generator circuit is added in order to avoid short circuiting the super capacities during configuration changes.

## 2.4.2 Results and Discussion

Fig. 2.18 and 2.18 show the control signals generated by the DALC as well as the voltage in the matrix. The voltage of storage systems with a fixed configuration are also overlaid for performance comparison. As can be seen, at the start of the charge, the system offers the lowest equivalent capacitance possible using a  $C(4, 1)$  configuration. A substantial improvement can be seen with respect to other configurations such as  $C(2, 2)$  and  $C(1, 4)$ . Considering the startup time as the time it takes to reach a voltage of 2.6 V, which is the minimum voltage needed by the TPS62740 DC/DC converter from Texas Instruments connected to the matrix in this prototype [26]. The system achieves a startup time that is 94% shorter than the  $C(1, 4)$  configuration. On the other hand, during the discharge, we see how the capacity matrix is able to extend the autonomy of the system up to 2000% compared to a fixed configuration of  $C(4, 1)$ . Autonomy time is considered the time it takes for the voltage of the matrix to drop below 2.6 V. All is achieved with a maximum current consumption of 9.5  $\mu$ A.

---

## 2.5 CMOS Integrated Circuit for SHM

Once the architecture is validated for the SHM application in aerospace field, its translation from discrete to integrated approximation is straightforward in terms of correspondence part per part except for the analog to digital conversion. Until now, we have used an external microcontroller to perform the analog to digital conversion. In the integrated approximation the conversion must be taken in the ASIC itself. Due to this, an ADC must be incorporated to the architecture. The development of this ADC is presented in this Section.

### 2.5.0.1 Low-Power Successive approximation ADC

An example of ADC used in a wireless node, in this case, for biomedical applications, is the one shown in [29]. This node is used to monitor small amplitude biomedical signals such as an Electrocardiogram (ECG) or an Electroencephalography (EEG). This solution works with an external battery, so in this type of application it is important to have a very low consumption in order to carry out long term patient monitoring without the patient or the doctor being aware of the remaining battery level. To do this, it uses a very low power conditioning and signal conversion circuit. The ADC used is a Successive Approximation Register (SAR) type differential ADC based on load redistribution. The authors argue that this ADC has been chosen because a simple, reliable and very low consumption architecture is necessary in medical applications. The ADC of this solution has a precision of 8 bits operating at a sampling frequency of 10 kSps and works with a minimum supply voltage of

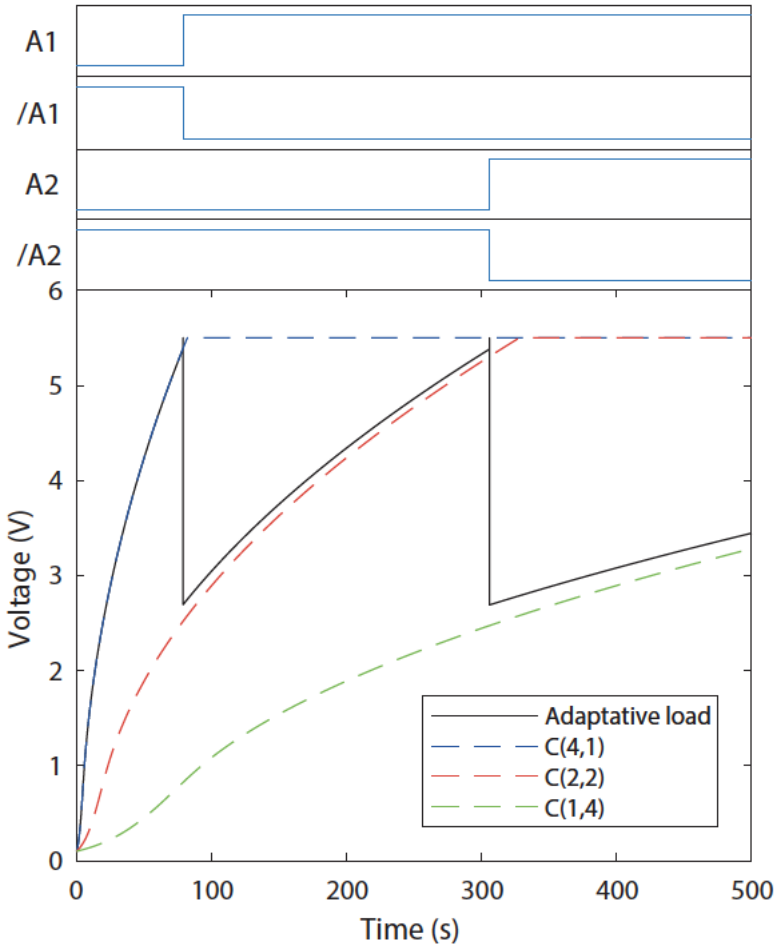


Figure 2.18: Control signals and voltage from the super capacitor based storage system during charging.

Image: "Energy Aware Adaptative Supercapacitor Storage System for Multi Harvesting Solutions" by Albert Álvarez Carulla *et al.* © 2018 IEEE.

0.5 V with a consumption of  $0.6 \mu\text{A}$ . The integrated circuit has been developed with a  $0.13 \mu\text{m}$  Complementary Metal Oxide Semiconductor (CMOS) technology.

Another example is shown in [30]. In this case it is a wireless master node for monitoring acoustic signals. The author proposes a  $\Delta\Sigma$  converter with non differential output with a design focused on reducing consumption and the area of the converter. One way to achieve these objectives is to replace the conventional Operational Transconductance Amplifiers (OTAs) of the con

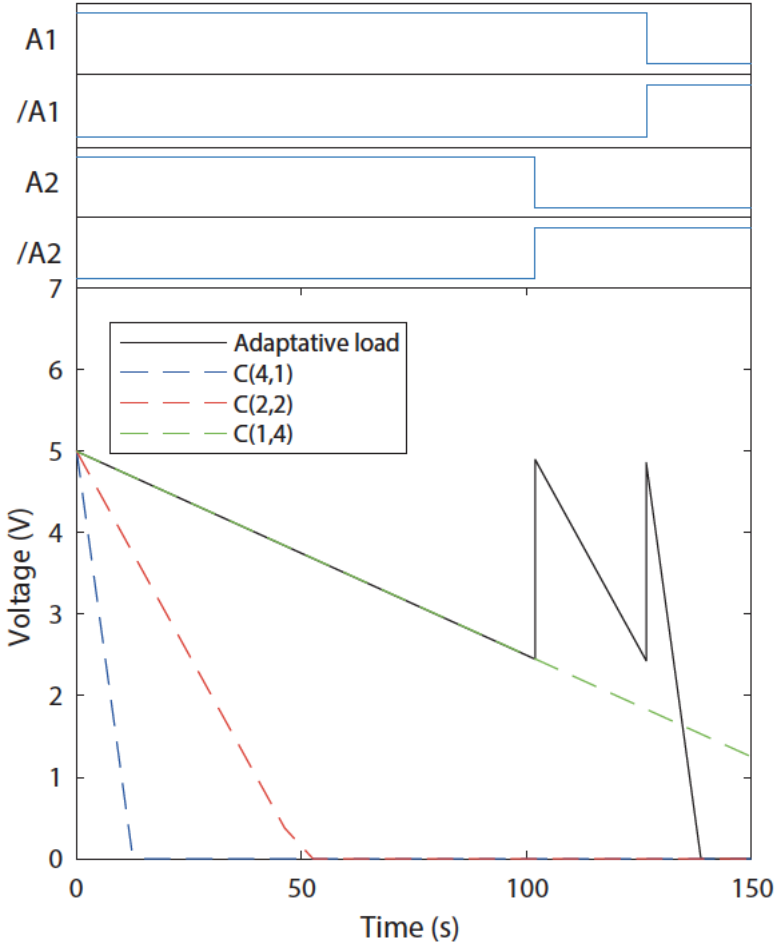


Figure 2.19: Control signals and voltage from the super capacitor based storage system during discharging.

Image: "Energy Aware Adaptative Supercapacitor Storage System for Multi Harvesting Solutions" by Albert Álvarez Carulla *et al.* © 2018 IEEE.

verter by CMOS inverters accompanied by auxiliary circuitry to control their output in common mode. With this, he manages to design a third order  $\Delta\Sigma$  converter with a consumption of 7.5  $\mu\text{W}$ , a minimum voltage supply of 0.7 V, a sampling frequency of 4 MHz and a resolution of 8.9 bits.

Although a  $\Delta\Sigma$  converter has been used in the above case, the most widely used converter in WSN applications is the SAR ADC. In [31] a SAR ADC for WSN applications is presented. In this work, a converter is designed that modifies the design of the capacity matrix and uses a Digital to Analog Con

verter (DAC) capacity matrix switching algorithm called Set and Down. The authors manage to reduce the average consumption using commutations by 80%. With this, they achieve a converter with a resolution of 7 bits with a sampling rate of 26 MSps. The authors indicate a consumption of 1.66 mW at the maximum sampling frequency, but do not indicate the consumption at lower frequencies that are closer to our frequencies of interest.

Another application of the SAR ADC in WSN is presented in [32]. In this work, the authors propose reducing consumption by reducing the voltage at which the converter's DAC operates using a step down converter. With this, they achieve an ADC that consumes 1.79  $\mu$ W with a minimum power of 1 V while sampling at a frequency of 1 MSps with a resolution of 9.34 bits.

Finally, in [33] a SAR ADC is once again implemented. This time, two different configurations are used for the DAC at the same time. A first stage formed by capacities in following a C 2C ladder architecture [34, 35] and a second stage formed by a matrix of binary weighted capacities. With this configuration, the authors seek to minimize both area and consumption. With this converter they achieve a consumption of 1.93  $\mu$ W for a 1 V supply at a maximum sampling frequency of 100 kSps with a resolution of 10 bits. All this they achieve with an area of 600 x 300  $\mu$ m.

In a review of the current state of the art in ADC converters for WSN applications, consumption ranges (from  $\mu$ W to a few mW), supply voltage ranges (equal to or below 1 V) and resolution and frequency ranges can be obtained sampling rate (10 or less bits of resolution at a sampling rate of less than 10 MSps). The SAR ADC appears in the current literature as the predominant option when choosing an ADC for WSN applications due to its good performance/consumption ratio.

### 2.5.1 The Prototype

The SAR ADC is a derivative of the digital ramp converter. In a digital ramp converter the analog input signal is sampled and routed to a comparator. A DAC controlled by a counter register is placed in the other comparator input. When the conversion starts, the counter initializes to 0 and starts increasing its value. This causes the output of the DAC also increase. When the DAC output exceeds the value of the analog input signal, the comparator indicates the end of the conversion, the counter stops, and its value becomes the result of the conversion. A great disadvantage of this type of converters is that the time required to perform a conversion varies depending on the magnitude of the analog input signal. The greater the magnitude, the longer it will take for the counter to reach a value that outputs a value of equal magnitude to the analog input signal on the DAC. Conversely, a low input analog signal value will take less time for the conversion to take place [36].

The successive approximation converter uses a different search algorithm to obtain an optimized and constant conversion time regardless of the value of



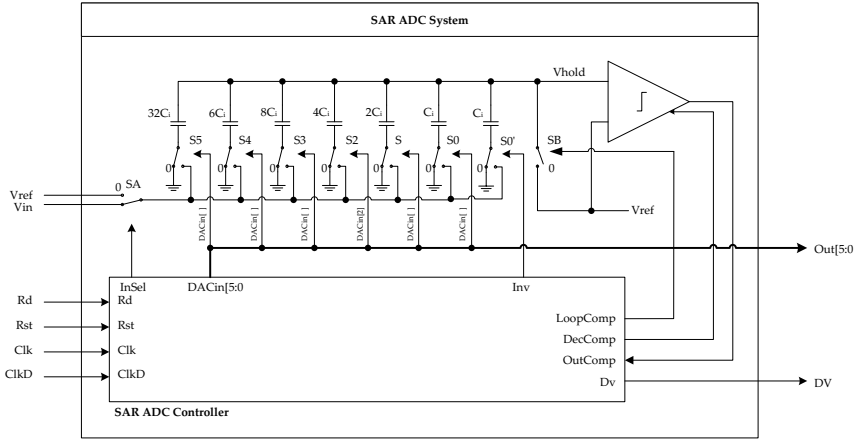


Figure 2.20: Block diagram of the SAR ADC.

the analog input signal. Fig. 2.20 shows the block diagram of the implemented SAR converter.

A search is performed in this converter using a binary algorithm. At the start of the conversion, the analog input signal is sampled. Then an  $N$  bit register is set to its average value. That is, its most significant bit is set to 1 while the rest of the register bits are set to 0. Thus, a voltage equal to half the used reference voltage is obtained at the output of the DAC controlled by the register. The comparison is then made between the DAC output voltage and the analog input signal. If the value of the analog input signal is greater than the DAC output voltage, the most significant bit of the register is left at 1, while if the value is less, the bit is set to 0. Then control of the register passes to the next most significant bit by setting it to '1' and performs the same process. The sequence continues until it reaches the least significant bit. After conversion is complete, the registry value is the result of the conversion [37, 38].

This type of converters, without reaching the speed of flash converters, are fast and have a very low consumption. Because they only have a single comparator, which can be dynamic, and digital logic circuits, the static consumption is minimized to the maximum, with most of the consumption of the converter being the dynamic consumption. Also, due to the low number of necessary components, it is a converter that does not require a lot of area. On the contrary, it has a more complex design than the digital ramp converter and, despite having a more than remarkable resolution, it does not offer a high resolution like that a  $\Delta\Sigma$  converter can offer.

The schematic of the implemented SAR ADC is shown in Fig. 2.21. The

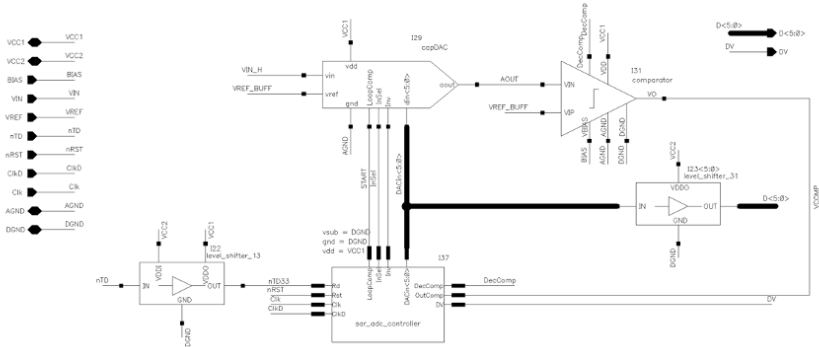


Figure 2.21: CADENCE Schematic of the SAR ADC.

6 bit converter has been designed using the 0.35  $\mu\text{m}$  CMOS technology from ams AG [39].

### 2.5.2 Results and Discussion

Fig. 2.22 shows the layout of the implemented ASIC. The area inside the box corresponds to the implemented SAR ADC.

Fig. 2.23 shows the waveforms taken by the different signals involved in a conversion cycle, while Fig. 2.24 shows the conversion of two cycles of a 25 Hz sinusoidal signal. These simulations have served to verify the functionality of the converter by seeing how the different signals follow the desired waveform and how the SAR ADC performs the appropriate successive approximations until the conversion process is complete. A consumption for the converter of 20  $\mu\text{W}$  has also been obtained.

Linearity errors, both integral and differential, have been obtained using the histogram based test [40]. This test consisted of converting a ramp type signal with a slope that would allow 16 points for each ADC digital code, and the deviation of the ADC’s output with respect to the actual expected output was recorded. The results obtained for the Differential Nonlinearity (DNL) and Integral Nonlinearity (INL) errors are below 0.5 LSB.

Then, a spectral analysis of the converter output was carried out with the intention of obtaining its Signal to Noise Ratio (SNR), Spurious Free Dynamic Range (SFDR) and Effective Number Of Bits (ENOB). The analysis was carried out using as input a sinusoidal signal of amplitude equal to the dynamic range of the ADC input at a frequency of 25 Hz (which is the typical frequency with which it will be found in real operating conditions) that has been converted to a frequency of 750 Sps which will be the typical sampling frequency with which it will operate in real conditions. From the spectral anal

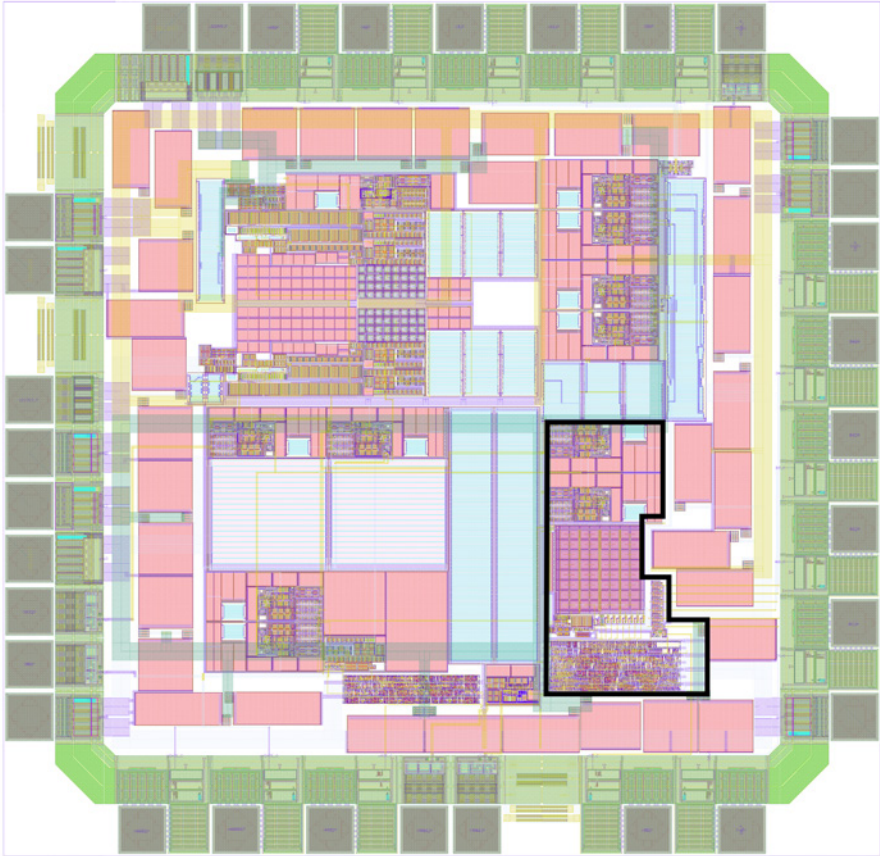


Figure 2.22: Layout of the CMOS integrated circuit for SHM (area of  $1790 \times 1740 \mu\text{m}$ ).

Image (b): "Self Powered Energy Harvester Strain Sensing Device for Structural Health Monitoring" by Albert Álvarez Carulla *et al.* is licensed under CC BY 3.0.

ysis, it is extracted that the converter has an ENOB of 5.3 bits, an SNR of 33.2 dB and a SFDR of 42.1 dB.

Table 2.1 shows a summary with the specifications of the implemented ADC.

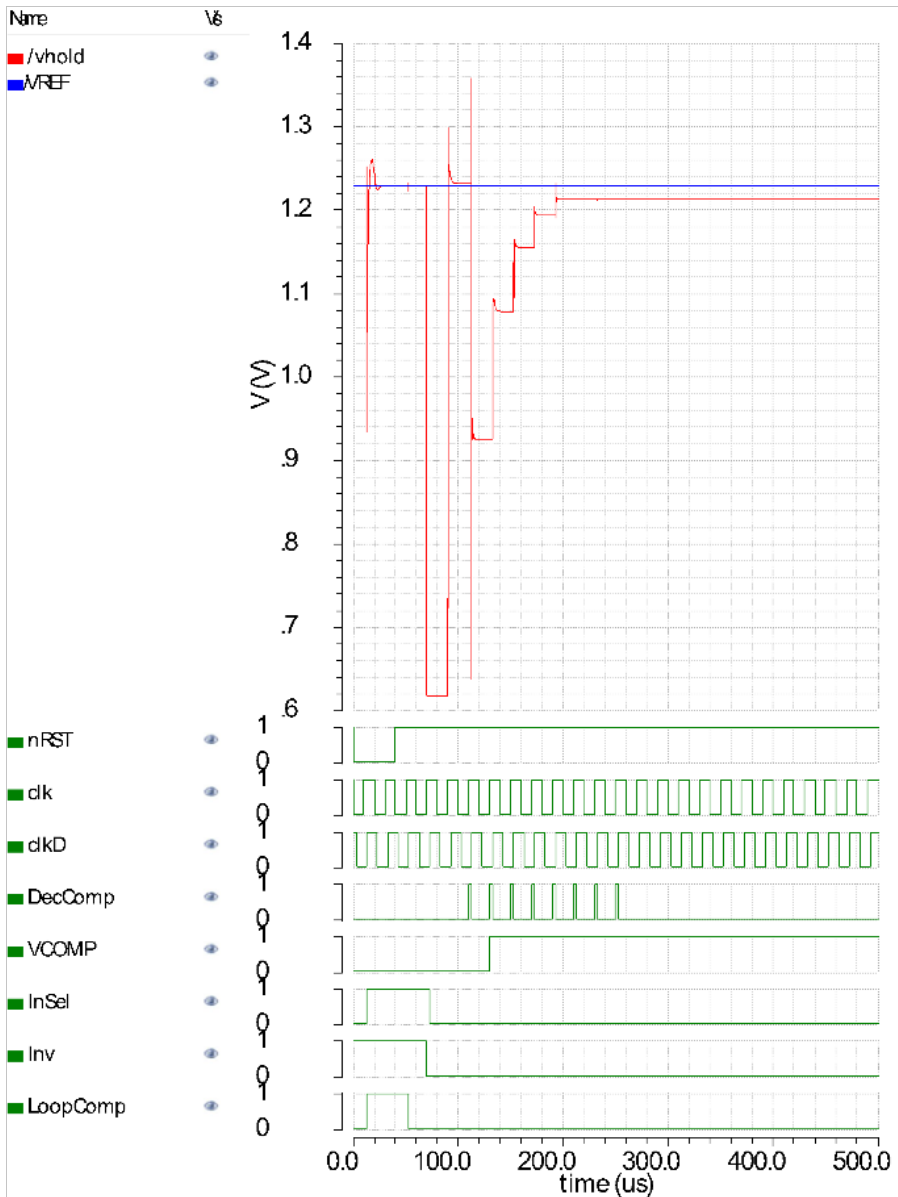


Figure 2.23: CADENCE Transient waveforms during a single analog to digital conversion.

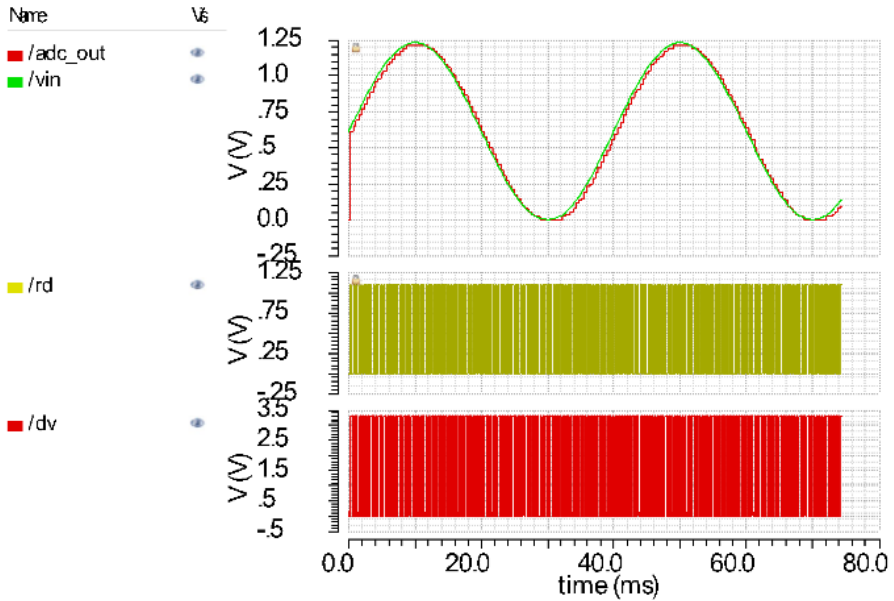


Figure 2.24: CADENCE Transient waveforms during multiple analog to digital conversions.

Table 2.1: SAR ADC characterisation results.

Parameter	Value
Resolution	6 bits
Sampling frequency	750 Sps
Voltage supply	3.3 V
Voltage reference	1.23 V
Differential nonlinearity	$<0.5\text{LSB}$
Integral nonlinearity	$<1\text{LSB}$
Effective number of bits	5.3 bits
Signal to Noise Ratio	33.3 dB
Spurious Free Dynamic Range	42.1 dB
Area	$550 \times 250 \mu\text{m}$
Power consumption	$20 \mu\text{W}$

---

## 2.6 Chapter Conclusions

In this Chapter, we have seen a first prototype of self powered device. In this case, a self powered device for WSN to be used in SHM applications in aerospace field. The urgency to reduce costs associated with the maintenance of an increasingly old aeronautical park makes the implementation of WSNs essential.

A self powered device is designed to be attached to the wing of an aircraft and monitor its mechanical strain. The sensor used to measure mechanical strain is an PEG which, in turn, is used to harvest energy from the vibrations to which the aircraft wing is subjected. The power extraction is performed efficiently applying a MPPT algorithm. In this case, the FOCV algorithm. Setting the PEG voltage equal to one half of its OCP allows us to achieve efficiencies close to 100 % regardless of the electronic load. All this is achieved with a maximum consumption of 150  $\mu$ W.

In addition, a super capacitor based energy storage system has been implemented that allows the storage of excess of unused energy. This way, the autonomy of the system is extended in case that energy cannot be collected from the environment. This system consists in a matrix of super capacitors that modifies its configuration based on the stored energy. When there is low energy stored, the matrix is configured to offer the minimum equivalent capacitive load and thus favor a startup time up to a 94 % shorter than in the worst case. On the other hand, during the operation of the system in steady state, the matrix offers a maximum equivalent capacitance in order to maximize energy storage and provide the system with an autonomy time of up to 2000 % greater than in the worst case. The consumption of the super capacitor matrix controller does not exceed 9.5  $\mu$ A.

Finally, the entire system has been integrated into an ASIC, requiring the design and implementation of an ADC. Until now, the analog to digital conversion has been done with an external microcontroller. Therefore, a 6 bit SAR ADC has been implemented using a CMOS technology of 0.35  $\mu$ m. This type of ADC is one of the most widely used in low power applications. The implemented ADC has a maximum consumption of 20  $\mu$ W with an area of 550 x 250  $\mu$ m.

---

## Acronyms

AC	Alternating Current
ACU	Analog Control Unit
ADC	Analog to Digital Converter

<b>ASIC</b>	Application Specific Integrated Circuit
<b>CMOS</b>	Complementary Metal Oxide Semiconductor
<b>DAC</b>	Digital to Analog Converter
<b>DC</b>	Direct Current
<b>ECG</b>	Electrocardiogram
<b>EEG</b>	Electroencephalography
<b>FOCV</b>	Fractional Open Circuit Voltage
<b>LAAS</b>	Laboratoire d'Analyse et d'Architecture des Systemes
<b>LPM</b>	Low Power Mode
<b>MCU</b>	Microcontroller Unit
<b>MPPT</b>	Maximum Power Point Tracking
<b>OCP</b>	Open Circuit Potential
<b>OP</b>	Operating Point
<b>OpAmp</b>	Operational Amplifier
<b>OTA</b>	Operational Transconductance Amplifier
<b>PEG</b>	Piezoelectric Generator
<b>PMOS</b>	P channel Metal Oxide Semiconductor
<b>SAR</b>	Successive Approximation Register
<b>SHM</b>	Structural Health Monitoring
<b>SMARTER</b>	Smart Multifunctional ARchitecture & Technology for Energy aware wireless sensoR
<b>SMU</b>	Source Meter Unit
<b>SPI</b>	Serial Peripheral Interface
<b>WSN</b>	Wireless Sensors Network

---

## References

- [1] H. J. Hansman, "Analysis of Impact of Aircraft Age on Safety for Air Transport Jet Airplanes," *International Center for Air Transportation (ICAT), Massachusetts Institute of Technology: Cambridge, MA, USA*, 2014.
- [2] M. Heinen, "The A380 program," in *Global Investor Forum*. EADS, 2006.
- [3] J. Collins, "The challenges facing US navy aircraft electrical wiring systems," in *Proceedings of the 9th annual aging aircraft conference*, 2006.
- [4] K. Kiefer, "Real world experience in wireless instrumentation and control systems," in *Proceedings of the CANEUS Fly by Wireless Workshop*, 2007.
- [5] M. Gonzalez Gutierrez, "A VANETs Routing Protocol Adaptation to WSNs," *Embedded Systems and Wireless Technology: Theory and Practical Applications*, p. 407, 2012.
- [6] E. C. Whitman, "Sosus: The secret weapon of undersea surveillance," *Undersea Warfare*, vol. 7, no. 2, p. 256, 2005.
- [7] P. Corke, T. Wark, R. Jurdak, W. Hu, P. Valencia, and D. Moore, "Environmental wireless sensor networks," in *Proceedings of the IEEE*, vol. 98, no. 11. Institute of Electrical and Electronics Engineers Inc., 2010, pp. 1903–1917.
- [8] Y. Lee, D. Blaauw, and D. Sylvester, "Ultralow Power Circuit Design for Wireless Sensor Nodes for Structural Health Monitoring," *Proceedings of the IEEE*, vol. 104, no. 8, pp. 1529–1546, aug 2016.
- [9] K. S. Low, W. N. N. Win, and M. J. Er, "Wireless sensor networks for industrial environments," in *Proceedings International Conference on Computational Intelligence for Modelling, Control and Automation, CIMCA 2005 and International Conference on Intelligent Agents, Web Technologies and Internet*, vol. 2, 2005, pp. 271–276.
- [10] R. Jafari, A. Encarnacao, A. Zahoory, F. Dabiri, H. Noshadi, and M. Sarrafzadeh, "Wireless sensor networks for health monitoring," in *MobiQuitous 2005: Second Annual International Conference on Mobile and Ubiquitous Systems Networking and Services*, 2005, pp. 479–481.
- [11] S. Labs, "The Evolution of Wireless Sensor Networks," *Silicon Labs*, 2013.



- [12] CHIST ERA, “SMARTER CHIST ERA,” [Online]. Available: <http://www.chistera.eu/projects/smarter>. [Accessed November 21, 2019]., 2016.
- [13] “Laboratoire d’analyse et d’architecture des systèmes LAAS CNRS.”
- [14] G. K. Ottman, H. F. Hofmann, and G. A. Lesieutre, “Optimized piezo electric energy harvesting circuit using step down converter in discontinuous conduction mode,” *IEEE Transactions on Power Electronics*, vol. 18, no. 2, pp. 696–703, mar 2003.
- [15] A. Álvarez Carulla, J. Colomer Farrarons, J. Lopez Sanchez, P. Miribel Catala, A. Alvarez Carulla, J. Colomer Farrarons, J. Lopez Sanchez, and P. Miribel Catala, “PiezoElectric Harvester Based Self Powered Adaptive Circuit with Wireless Data Transmission Capability for Structural Health Monitoring,” in *2015 Conference on Design of Circuits and Integrated Systems, DCIS 2015*. Institute of Electrical and Electronics Engineers Inc., jan 2016.
- [16] A. Álvarez Carulla, J. Colomer Farrarons, J. Lopez Sanchez, and P. Miribel Catala, “Piezoelectric Harvester based structural health monitoring that uses a self powered adaptive circuit,” in *2nd IEEE International Workshop on Metrology for Aerospace*. Institute of Electrical and Electronics Engineers Inc., aug 2015, pp. 531–535.
- [17] A. Álvarez, M. Baffleur, J. M. M. Dilhac, J. Colomer, D. Dragomirescu, J. Lopez, M. Zhu, and P. Miribel, “Self Powered energy harvester strain sensing device for structural health monitoring,” dec 2016.
- [18] Midé Technology Corp., “Midé Engineering Smart Technologies,” [Online]. Available: <http://www.mide.com/>. [Accessed May 3, 2015]., 2015.
- [19] B. K. Ling, T. Li, H. H. Hng, F. Boey, T. Zhang, and S. Li, “Waste Energy Harvesting: Mechanical and Thermal Energies. 24,” 2014.
- [20] Linear Technology Corporation, “LT1761 100mA, Low Noise, LDO Micropower Regulators in TSOT 23 (Datasheet),” [Online]. Available: [https://www.analog.com/media/en/technical\\_documentation/data\\_sheets/1761sff.pdf](https://www.analog.com/media/en/technical_documentation/data_sheets/1761sff.pdf). [Accessed October 5, 2019].
- [21] Silicon Labs, “TS1005 A 0.8V to 5.5V, 1.3uA, 20kHz Rail to Rail Single Op Amp (Datasheet),” [Online]. Available: [https://www.silabs.com/documents/public/data\\_sheets/TS1005.pdf](https://www.silabs.com/documents/public/data_sheets/TS1005.pdf). [Accessed August 17, 2019].
- [22] Texas Instruments, “eZ430 RF2500 Wireless Development Tool (User’s Guide),” [Online]. Available: <http://www.ti.com/lit/ug/slau227f/slau227f.pdf>. [Accessed August 31, 2019].

- [23] Texas Instruments, “MSP430F2274 16 bit Ultra Low Power Microcontroller (Datasheet),” [Online]. Available: <http://www.ti.com/lit/ds/symlink/msp430f2274.pdf>. [Accessed October 2, 2019].
- [24] Texas Instruments, “CC2500 Low Cost, Low Power 2.4 GHz RF Transceiver Designed for Low Power Wireless Apps in the 2.4 GHz ISM (Datasheet),” [Online]. Available: <http://www.ti.com/lit/ds/symlink/cc2500.pdf>. [Accessed October 2, 2019].
- [25] RS Pro, “N11MA212011 RS Pro Foil Strain Gauges (Datasheet),” [Online]. Available: <https://docs.rs-online.com/86d4/0900766b8153b58e.pdf>. [Accessed October 2, 2019].
- [26] A. Alvarez Carulla, Y. Montes Cebrian, M. Puig Vidal, J. Lopez Sanchez, J. Colomer Farrarons, and P. Miribel Catala, “Energy Aware Adaptive Supercapacitor Storage System for Multi Harvesting Solutions,” in *Proceedings 33rd Conference on Design of Circuits and Integrated Systems, DCIS 2018*. Institute of Electrical and Electronics Engineers Inc., apr 2019.
- [27] F. E. Mahboubi, M. Baffleur, V. Boitier, A. Alvarez, J. Colomer, P. Miribel, and J. M. Dilhac, “Self Powered Adaptive Switched Architecture Storage,” in *Journal of Physics: Conference Series*, vol. 773, no. 1. Institute of Physics Publishing, dec 2016.
- [28] Y. Kim, S. Park, Y. Wang, Q. Xie, N. Chang, M. Poncino, and M. Pedram, “Balanced reconfiguration of storage banks in a hybrid electrical energy storage system,” in *IEEE/ACM International Conference on Computer Aided Design, Digest of Technical Papers, ICCAD*, 2011, pp. 624–631.
- [29] Y. P. Hsu, Z. Liu, and M. M. Hella, “An ultra low power front end IC for wearable health monitoring system,” in *Proceedings of the Annual International Conference of the IEEE Engineering in Medicine and Biology Society, EMBS*, vol. 2016 Octob. Institute of Electrical and Electronics Engineers Inc., oct 2016, pp. 1906–1909.
- [30] Q. Duan, Z. Wang, and J. Roh, “A 7.5  $\mu$ W 0.08 mm<sup>2</sup> single ended SC delta sigma ADC for acoustic sensor applications,” *International Journal of Circuit Theory and Applications*, vol. 44, no. 5, pp. 1173–1185, may 2016.
- [31] T. Yang and Z. Li, “A 7 bit 26 MS/s SAR ADC in 0.18  $\mu$ m CMOS process for WSN application,” in *2012 4th International High Speed Intelligent Communication Forum, HSIC 2012, Proceeding*, 2012, pp. 96–99.

- [32] T. Rabuske, J. Fernandes, F. Rabuske, C. Rodrigues, and M. B. Dos Santos, "A self calibrated 10 bit 1 MSps SAR ADC with reduced voltage charge sharing DAC," in *Proceedings IEEE International Symposium on Circuits and Systems*, 2013, pp. 2452–2455.
- [33] A. Rodríguez Pérez, M. Delgado Restituto, J. Ruiz Amaya, and F. Medeiro, "An ultra low power consumption 1 V, 10 bit successive approximation ADC," in *Proceedings of the 15th IEEE International Conference on Electronics, Circuits and Systems, ICECS 2008*, 2008, pp. 634–635.
- [34] Sang Hyun Cho, Chang Kyo Lee, and Jong In Song, "Design of a 1 Volt and u power SARADC for Sensor Network Application," in *2007 IEEE International Symposium on Circuits and Systems*. IEEE, may 2007, pp. 3852–3855.
- [35] Y. M. Liao and T. C. Lee, "A 6 b 1.3Gs/s A/D converter with C<sub>2</sub>C switch capacitor technique," in *2006 International Symposium on VLSI Design, Automation and Test, VLSI DAT 2006 Proceedings of Technical Papers*, 2007, pp. 109–112.
- [36] O. Q. J. Al Thahab, "Design and Simulation of Moore Logic Circuit based SAR Analog to Digital Converter," *INTERNATIONAL JOURNAL OF LOGIC AND COMPUTATION (IJLP)*, p. 14.
- [37] I. C. Maxim, "Understanding sar adcs: Their architecture and comparison with other adcs," *Dallas Semiconductor Maxim IC*, 2001.
- [38] W. Kester, "ADC architectures II: successive approximation ADCs," *MT 021 Tutorial, Analog Devices*, 2009.
- [39] "ams AG."
- [40] W. Kester and A. D. I. Engineeri, *Data conversion handbook*. Newnes, 2005.

# 3

---

## *Dual-Galvanic-Cell-based Self-Powered Devices*

---

### CONTENTS

3.1	Self Powered Point of Care Devices .....	63
3.2	'Plug and Power' Point of Care Device .....	65
3.2.1	The Test Strip .....	67
3.2.2	The Electronic Reader .....	69
3.2.2.1	Power Management Unit .....	69
3.2.2.2	Front end Module .....	72
3.2.2.3	Back end Module .....	73
3.2.2.4	User Interface Module .....	73
3.3	Results and Discussion .....	73
3.3.1	Test strip characterization .....	75
3.3.2	Electronic reader characterization .....	77
3.4	Chapter Conclusions .....	79
	Acronyms .....	81
	References .....	83

While in Chapter 2 we have seen the development of self powered devices for Structural Health Monitoring (SHM), in this third Chapter we jump to self powered devices for applications focused on people health. A novel self powered Point of Care (PoC) device for blood glucose concentration measurement will be presented. The solution is based on two galvanic cells integrated in a single test strip: 1) a battery to supply the electronics and 2) a fuel cell for the measurement. Both cells share the biological sample as electrolyte. The device is able to generating energy and making a measurement (using a chronoamperometry) simultaneously from the same sample. All this with maximum efficiency thanks to a Power Management Unit (PMU) that applies a Maximum Power Point Tracking (MPPT) algorithm.

### 3.1 Self-Powered Point-of-Care Devices

A PoC or Point of Care Testing (PoCT) device is a device designed to perform tests in the same place where the patient is located [1]. These types of solutions aim to eliminate the common process of collecting biological samples in a medical center and then send them to a laboratory for analysis. Normally, this type of process requires trained and qualified personnel and a response time that can range from hours to days or even weeks. Furthermore, as mentioned previously, when the samples are taken in a medical center, it requires the patient to move there. This entails serious inconveniences such as the difficulty faced by a patient when their mobility is reduced or the saturation of the medical center for patients who do not require emergency care. The latter has taken a particularly relevant role in the current coronavirus (COVID 19) pandemic where the displacement to medical centers causes, not only its saturation, but the increased probability of contagion and spread of new infectious outbreaks [2]. PoC devices provide a way to perform those same tests without going to the medical center. In addition, they offer two other advantages: 1) a shorter time to obtain a result, and 2) a lower cost since they do not require specialized laboratory equipment. The latter makes PoC also a solution for those scenarios where few resources are available [3].

Some characteristics that any PoC device must meet are those defined by the World Health Organization in the acronym ASSURED (Affordable, Sensitive, Specific, User friendly, Rapid and robust, Equipment free, and Deliverable to users) [4]. The development of PoC devices based on electronic readers with a disposable test strip [5, 6] facilitates compliance with these characteristics. At least, when the power of the device is based on a battery or the electrical network. However, nowadays progress is being made in the investigation of new PoC devices that can operate in a self powered way [7]. That is, they extract energy either from the environment or from the biological sample itself. The latter case corresponds to the use of fuel cells as a power source and as a sensor. It is there where, due to the low energy available for the operation of the device, great difficulties are encountered in meeting the ASSURED criterion. This can be seen in the self powered devices based on colorimetric techniques [8] which, some of them [9], fail to offer a quantitative and objective result. Not at least without requiring a non self powered external device that would invalidate its "self powered" label as discussed in Chapter 1. Other solutions, such as those presented in [10 12], offer the result by means of a periodic signal whose frequency is linked to the concentration of the agent to be measured. Excluding the fact of needing external non self powered devices to obtain the result, the procedure to follow cannot be carried out by a user without technical training.

For all this, it is essential to find new ways in the development of self powered PoC devices, through new system architectures and new low

voltage and low power electronic technologies, which enable these devices with ASSURED characteristics.

---

### 3.2 'Plug-and-Power' Point-of-Care Device

In the present chapter, we will focus our attention to the electronic reader and, particularly, to the PMU and electronics architecture of the novel self powered PoC device presented in [13]. The approach is used to implement a solution intended for the measurement of glucose concentration in a blood sample. It provides an easy to use measurement proceeding that allows to a user without an specific formation to perform a glucose concentration measurement. The proceeding followed by the user is depicted in Fig. 3.1 and it consists of three steps:

1. The user plugs a disposable test strip in the electronic reader.
2. Then, the user adds the blood sample in the disposable test strip.
3. The device, powered by the paper based battery embedded in the test strip, performs the measurement and displays the result to the user.

The device consists of a disposable paper based test strip formed by two galvanic cells and an electronic reader with four major modules: 1) a PMU, 2) a front end module, 3) a back end or microcontroller module, and 4) a Liquid Cristal Display (LCD) based user interface module. The block diagram of the proposed PoC device is shown in Fig. 3.2.

In the proposed solution, the test strip is a disposable element while the electronic reader is reusable. Due to that, the test strip is based on paper in order to minimize the environmental impact of its usage and disposal. The test strip consists of a fuel cell and a battery embedded in the same paper and share the same sample as electrolyte. In this case, a blood sample. The fuel cell provides a current voltage output characteristic related to the glucose concentration of the sample. The voltage and current provided by the fuel cell are annotated as  $V_{FC}$  and  $I_{FC}$ , respectively. Meanwhile, the battery delivers a power level  $P_{BATT}$  independent of the glucose concentration of the sample. The voltage and current provided by the battery are annotated as  $V_{BATT}$  and  $I_{BATT}$ , respectively.

The power  $P_{SUPP}$  delivered by the battery is supplied to the PMU of the electronic reader, while the output of the fuel cell is connected to the front end module. The PMU maximizes the power delivered by the battery by means of a MPPT algorithm. Thus, maximum efficiency, from the battery point of view, is achieved. The PMU delivers a voltage source  $V_{DVCC}$  of 3.0 V, a typical operative voltage supply for digital parts like microcontrollers or Analog to

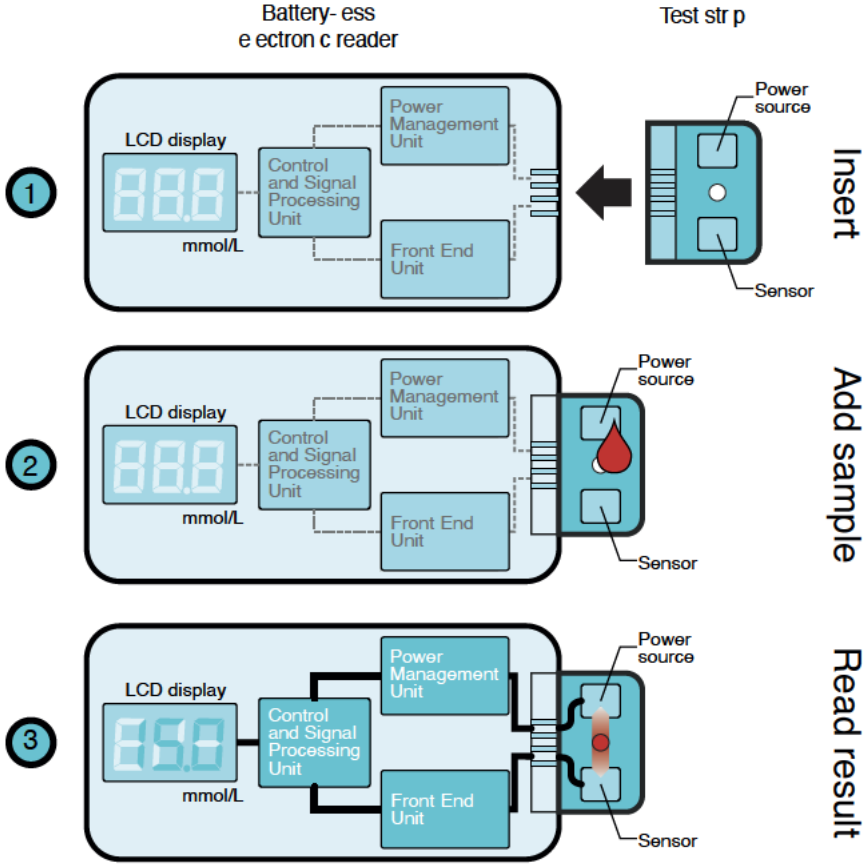


Figure 3.1: User steps with the 'plug and power' prototype.  
Image: "Plug and Power' Point of Care Diagnostics: A Novel Approach for Self Powered Electronic Reader based Portable Analytical Devices" by Yaiza Montes Cebrián *et al.* © 2018 Elsevier, with permission.

Digital Converters (ADCs), for the digital section of the electronic reader (formed by the back end or microcontroller module, and the LCD based user interface). Once enough energy is harvested from the paper based battery, the microcontroller activates in the PMU a secondary voltage source  $V_{AVCC}$  of 1.8V, the minimum operative voltage supply for Commercial off the Shelf (COTS) analog parts used.  $V_{AVCC}$  powers the analog section of the electronic reader (formed by the front end module) and an amperometric measurement is performed using the fuel cell of the test strip. Once the measurement has finished, the concentration measurement result is displayed to the user using a LCD.

The operation and construction details of each element of the device are described in the next subsections with a particular attention to the power management of the device. A detailed description of the device as measurement instrument can be found in [13–15].

### 3.2.1 The Test Strip

The disposable paper based test strip consists of two galvanic cells intended for different goals that share the same blood sample as electrolyte. This blood sample flows by capillary action through the paper towards both galvanic cells. The dimensions of the test strip are 5 x 20 mm and a picture with an exploded view of it are shown in Fig. 3.3(a) [13].

One of the galvanic cells is a LF55 paper based battery developed by Fuelium, S.L. [16] that is intended to power the electronic reader. The battery is fully implemented in paper except for the proprietary electrode technology used which does not contain heavy metals or other toxic components. Thus, the environmental impact of its usage and disposal is minimized. The battery starts its operation when an aqueous sample is added. This way, the battery does not suffer from self discharge during its storage. The aqueous sample can be deionized water or any other biomedical sample like physiological fluid such as sweat, urine or serum, among others. The battery has been adjusted

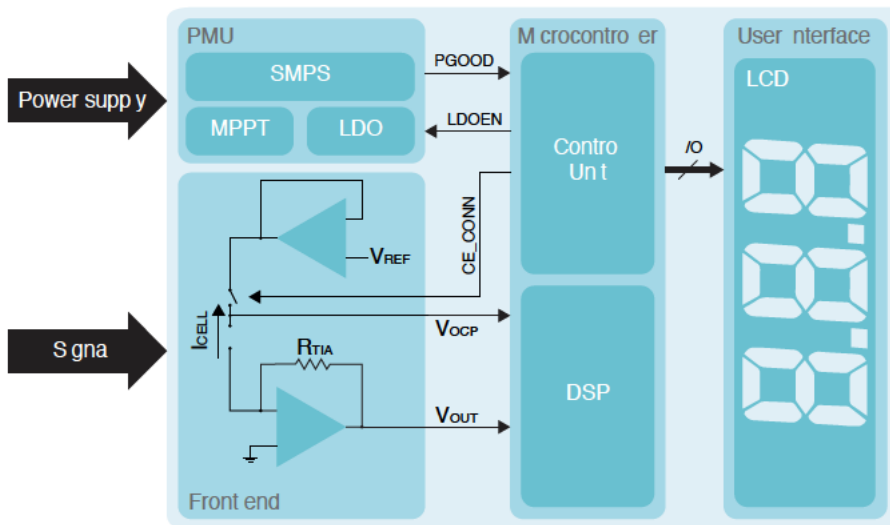


Figure 3.2: Block diagram of the 'plug and power' prototype.

Image: "'Plug and Power' Point of Care Diagnostics: A Novel Approach for Self Powered Electronic Reader based Portable Analytical Devices" by Yaiza Montes Cebrián *et al.* © 2018 Elsevier, with permission.



to provide an Open Circuit Potential (OCP) of 1.5 V and a maximum output power of 10 mW with a serum sample with a volume of 12.5  $\mu$ L. The experimental battery performance finally achieved is shown in Subsection 3.3.1.

The other galvanic cell consists in a bio fuel cell to sense glucose. The use of fuel cells as sensor instead of typical three electrode electrochemical cell is a well established and proven technique [17, 18] used, for example, in many commercial breath alcoholmeters or breathalysers [19 22]. Dehydrogenase (GDH) is used as anode and Bilirubin Oxidase (BOX) as cathode. The fuel cell provides an output power level dependent on glucose concentration. The technique applied to the fuel cell is an amperometry which consists in setting a fixed polarization voltage across the fuel cell's output terminals while the outputted current is measured [23 25]. The selection of the optimal polarization voltage for the amperometric technique depends on the output

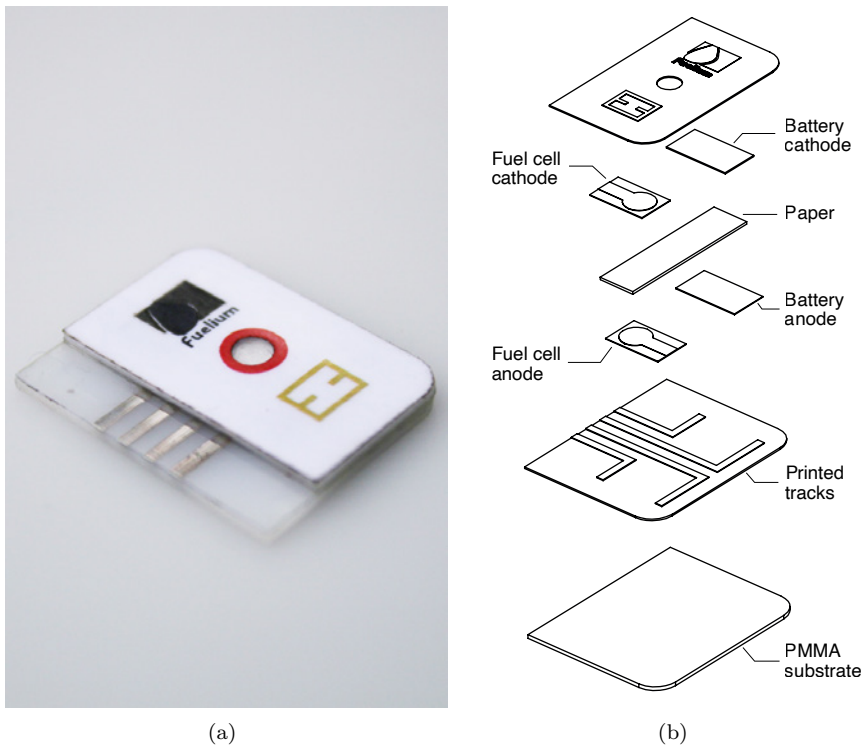


Figure 3.3: (a) Picture and (b) exploded view of paper based test strip and its main components.

Images (a) and (b): "Plug and Power' Point of Care Diagnostics: A Novel Approach for Self Powered Electronic Reader based Portable Analytical Devices" by Yaiza Montes Cebrián *et al.* © 2018 Elsevier, with permission.

characteristics of the fuel cell for different glucose concentrations. The characterization of the fuel cell is shown in Subsection 3.3.1. All the subjects related with the disposable and materials and methods related to the device concept are fully explained in the reference [13].

### 3.2.2 The Electronic Reader

The electronics reader has been implemented using COTS parts. We have implemented it in a double layer 77 x 32 mm Printed Circuit Board (PCB) and packaged it in a full custom 3D printed 85 x 42 x 21 mm case. A picture and exploded view of the electronic reader [13, 15] are shown in Fig. 3.4. The schematics of the PMU and the front end module are shown in Fig. 3.5.

#### 3.2.2.1 Power Management Unit

The PMU is responsible of the management of the power extracted from the embedded paper based battery in the test strip. It extracts the power efficiently, from the battery point of view; while it provides two regulated output voltages sources to the analog and digital sections of the electronic reader, as it has been pointed out before. The PMU consists of a DC/DC boost converter with a Low Dropout (LDO) regulator in series. As a DC/DC converter, it has been selected a BQ25504 boost converter from Texas Instruments [26] to implement the PMU. For the LDO, a LP5910 LDO regulator from Texas Instruments [27] has been used.

The efficiency from the point of view of the battery is defined as

$$\eta_{CELL} = \frac{P_P}{P_{P_{MAX}}} \quad (3.1)$$

where  $P_P$  is the power outputted by the battery at given Operating Point (OP) and  $P_{P_{MAX}}$  the maximum power that the battery can provide at the optimal OP. As can be seen in Section 3.3.1, the battery has a voltage dependent output power characteristic  $P_P$  with a maximum output power peak  $P_{P_{MAX}}$  for a given optimal OP defined by the battery output voltage  $V_{P_{MAX}}$ . Due to this, the PMU is able to extract the power from the battery efficiently using a MPPT algorithm that sets the battery polarization voltage to  $V_{P_{MAX}}$ . The MPPT algorithm used is a variation of the Open Circuit Fractional Voltage (OCFV) algorithm [28–31] described in Chapters 1 and 2. The PMU applies the MPPT algorithm setting the polarization voltage of the battery by means of the equivalent input impedance of the PMU. In this case, the battery output is connected to a Switched Mode Power Supply (SMPS) or DC/DC boost converter. The DC/DC converter can vary its equivalent input impedance by means of a Pulse Width Modulation (PWM) or a Pulse Frequency Modulation (PFM). Neither the OCP of the battery nor its output power characteristic changes with the glucose concentration of the sample; therefore, the Fractional Open Circuit Voltage (FOCV) algorithm step of disconnecting

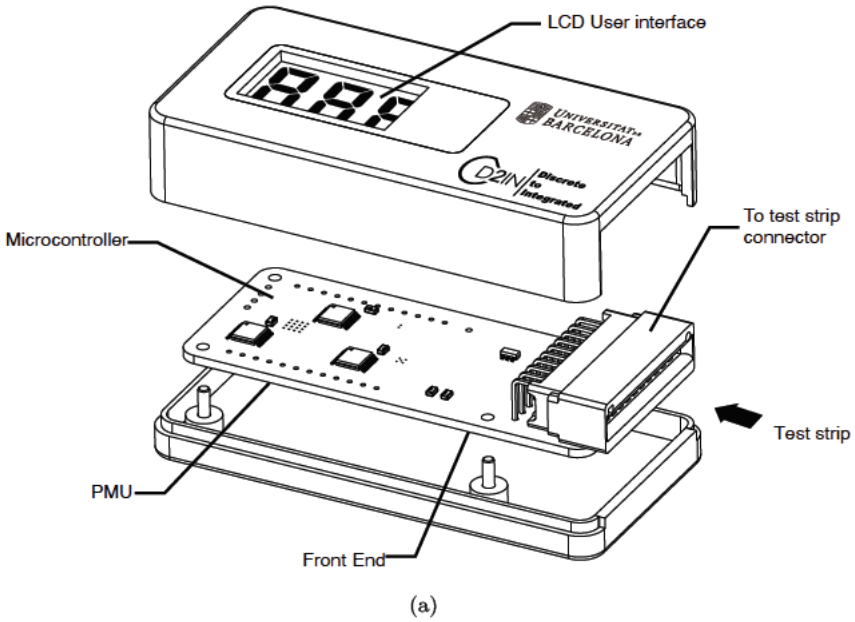


Figure 3.4: (a) Exploded view and (b) picture of the 'plug and power' proto type.  
Images (a) and (b): "'Plug and Power' Point of Care Diagnostics: A Novel Approach for Self Powered Electronic Reader based Portable Analytical Devices" by Yaiza Montes Cebrián *et al.* © 2018 Elsevier, with permission.

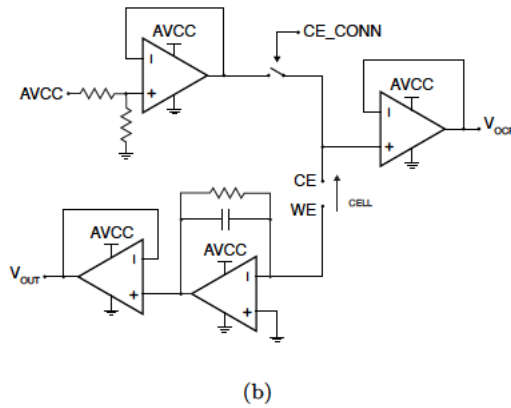
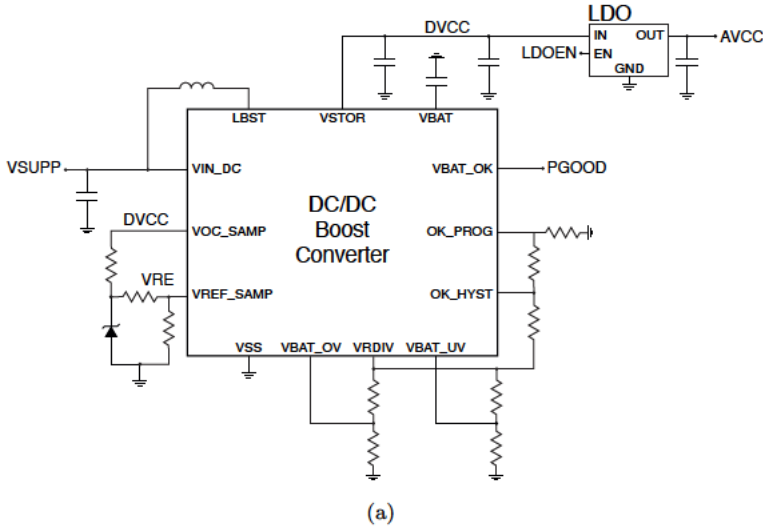


Figure 3.5: Schematic of (a) the PMU and (b) the front end of the 'plug and power' prototype.  
 Images (a) and (b): "Self Powered Portable Electronic Reader for Point of Care Amperometric Measurements" by Yaiza Montes Cebrián *et al.* is licensed under CC BY 4.0.

the PMU from the battery to sense its OCP is not necessary and continuous power extraction from the battery with maximum efficiency is achieved setting its polarization voltage to  $V_{P_{MAX}}$ . The achieved efficiency allows to attend punctual high power requirements coming from the different modules and to shorten the required start up time. A voltage reference  $V_{REF}$ , generated with a REF1004 1.2 voltage reference from Texas Instruments [32] and a high im

pedance resistor based voltage divider, is used to set the desired polarization voltage of the paper based battery.

While the PMU extracts energy from the battery efficiently, it regulates two output voltage supplies. The DC/DC converter provides a 3.0 V voltage supply, annotated as  $V_{DVCC}$ , that is used to power the digital section of the electronic reader. I.e., the back end or microcontroller module, and the user interface module, where all the COTS parts used have a recommended operating voltage supply range from 1.8 to 3.6 V. The second voltage supply, annotated as  $V_{AVCC}$ , is used to power the analog sections of the electronic reader. I.e., the front end module. This second voltage supply is provided by the LDO due to the required stable and high noise rejection voltage regulation required by the analog COTS parts. They have a recommended operating voltage supply range from 1.6 to 5.5 V; therefore,  $V_{AVCC}$  is regulated to 1.8 V.

The PMU also provides a low by default  $PGOOD$  signal that goes high when  $V_{DVCC}$  reaches a voltage of 2.9 V and goes low when  $V_{DVCC}$  drops under 2.4 V. Thus, the PMU can notify to the Microcontroller Unit (MCU) the state of the voltage source in order to manage the operation of the device as function of the available power. For example, the MCU starts the measurement of the glucose concentration enabling perviously the LDO when enough energy is harvested from the battery and  $PGOOD$  goes high.

To validate the operation of the PMU, a Keysight B2926A Source Meter Unit (SMU) was used to capture the current and voltage waveforms during the start up operation. We have used a Keysight B2962A SMU to capture current waveforms. For voltage waveforms capturing, we have used a Keysight MSOX3034A oscilloscope. Both have been operated in common triggered configuration. The caption of the current and voltage waveforms were also captured to study the system response during load step variations. For the analog voltage supply  $V_{AVCC}$ , it has been applied a current load step of 1.5 mA. For the digital voltage supply  $V_{DVCC}$ , a current load step of 2.5 mA has been applied. The current load step applied to  $V_{DVCC}$  is higher than the current load step applies to  $V_{AVCC}$  due to  $V_{DVCC}$  must supply power to the digital section and to the LDO that supplies the analog section. The current load steps applied are considerably higher than expected during the operation of the device to validate the performance of the paper based battery embedded in the test strip and PMU in conditions with high power requirements.

### **3.2.2.2 Front-end Module**

The front end module consists in a potentiostat with its current sensing circuit based on a Transimpedance Amplifier (TIA). The Operational Amplifiers (OpAmps) used to implement it are LPV521 from Texas Instruments [33]. The potentiostat also has a SN74AUC1G66 analog switch from Texas Instruments [34] placed between the output of the Control Amplifier (CA) and the Counter Electrode (CE) in order to be able to (dis)connect the fuel cell from the potentiostat and take full control of the measurement process. Thus, when

the MCU enables the LDO, the potentiostat do not polarize the fuel cell to a given voltage level  $V_{SENSOR}$  until the analog switch is closed. When the analog switch is closed and the fuel cell is polarized to  $V_{SENSOR}$ , the current outputted by the fuel cell is transduced to  $V_{OUT}$  through the TIA following the expression

$$V_{OUT} = R_{TIA}I_{FC} \quad (3.2)$$

where  $R_{TIA}$  is the feedback resistor used in the TIA.

### 3.2.2.3 Back-end Module

The back end module is based on a MSP430FR5969 MCU from Texas Instruments [35]. The MCU has been chosen due to its low power and low voltage operation, and because it already offers several integrated peripherals, like timers, ADCs or General Purpose Input/Outputs (GPIOs), among others. The firmware loaded in the MCU is designed to let the MCU the control of the full measurement process. The flow diagram of the firmware is shown in Fig. 3.6 [15].

Once the sample is deposited in the test strip and reaches the embedded paper based battery, the PMU starts to harvest energy from the battery and provides a regulated voltage source  $V_{DVCC}$ . When  $V_{DVCC}$  reaches 1.8 V, the minimum operative voltage supply of the MCU, it configures an interrupt for the GPIO where the signal  $PGOOD$  is connected and goes to a Low Power Mode (LPM). It is also configured to wake up when  $PGOOD$  goes high indicating that enough energy is harvested from the paper based battery in order to perform the glucose concentration measurement. Then, the MCU initializes the different peripherals needed during the measurement. These peripherals are: a) the timer (to measure the measurement time), b) the GPIOs (to enable/disable the LDO and to close/open the analog switch) and c) ADCs (to capture  $V_{OCP}$  and  $V_{OUT}$ ). As soon as these modules are initialized, the MCU enables the LDO through the signal  $LDOEN$  and waits for then fuel cell's OCP  $V_{OCP}$  stabilization. When stabilized, the MCU starts the timer and closes the analog switch (through the  $CE_{CONN}$  signal) to start the chronoamperometry. When the desired measurement time is reached, the MCU stops the measurement, i.e., captures the last value of  $V_{OUT}$ , stops the timer, opens the analog switch and disables the LDO. Finally, converts the  $V_{OUT}$  readout to a glucose concentration by means of a Look Up Table (LUT) [36] and displays the result to the user through the LCD.

### 3.2.2.4 User Interface Module

To display the glucose concentration measurement result to the user, it has been selected a commercial 3 digit 7 segments LCD. It has been chosen a VI 321 LCD from Varitronix as display and three CD4055B Binary Coded Decimal (BCD) to 7 segment LCD drivers from Texas Instruments [37] to reduce the number of pins needed in the MCU to drive the LCD.

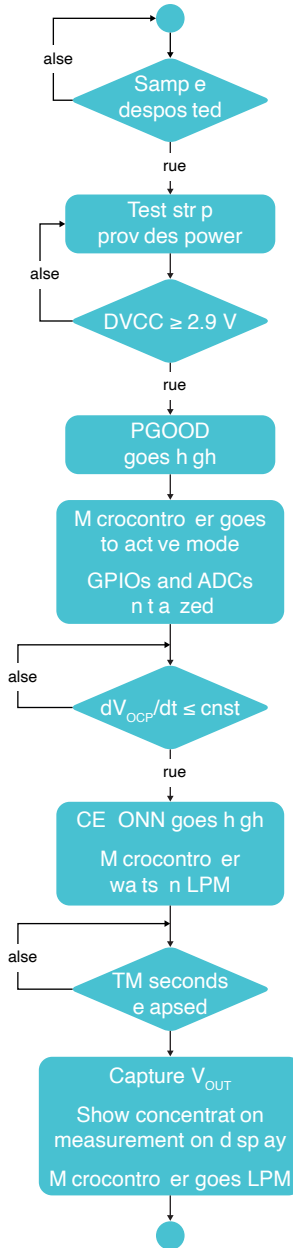


Figure 3.6: Application flow diagram of the 'plug and power' prototype. Image: "Self Powered Portable Electronic Reader for Point of Care Amperometric Measurements" by Yaiza Montes Cebrián *et al.* is licensed under CC BY 4.0.

### 3.3 Results and Discussion

#### 3.3.1 Test strip characterization

Fig. 3.7 shows the results for the embedded paper based battery in the disposable test strip with serum samples. The battery, as can be seen in Fig. 3.7(a), exhibits an OCP of 1.6 V and a short circuit current of 17.345 mA. From Fig. 3.7(b), a maximum power peak of 7.639 mW can be observed for a polarization voltage  $V_{P_{MAX}}$  of 0.710 V. Thus, the voltage reference  $V_{REF}$  that must be set in the PMU of the electronic reader in order to extract power from the battery with maximum efficiency is 0.710 V.

The start up transient when the test strip is connected to the PMU and the sample is deposited is shown in Fig. 3.8. In contrast to other power restricted scenarios where high impedance power sources are available to harvest energy, the great performance of the paper based battery is able to provide a fast response as soon as the sample is deposited. As can be seen in Fig. 3.8(b), the PMU only needs 4.4 ms to provide 1.8 V as  $V_{DVCC}$ , the minimum operative voltage supply of the MCU. At 20 ms, the PMU provides a regulated voltage supply  $V_{DVCC}$  of 3.0 V. Due to the fast initial power peak delivered by the battery, the BQ25504 DC/DC converter is not able to regulate  $V_{DVCC}$  to 3.0 V and an over voltage level of 3.568 V appears at 40 ms. At 103 ms, the LDO is enabled and the 1.8 V voltage supply  $V_{AVCC}$  is available. Thus, the minimum

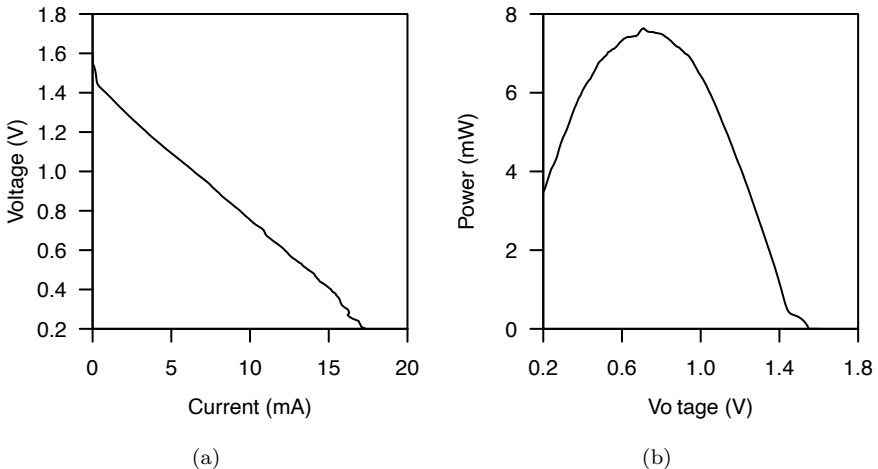
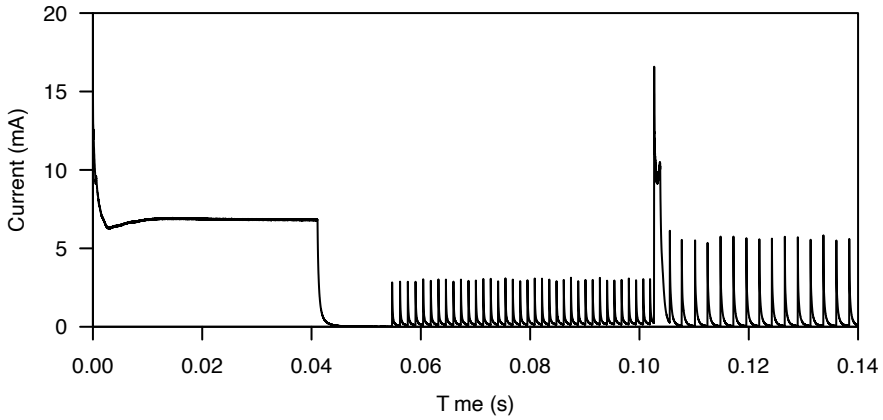
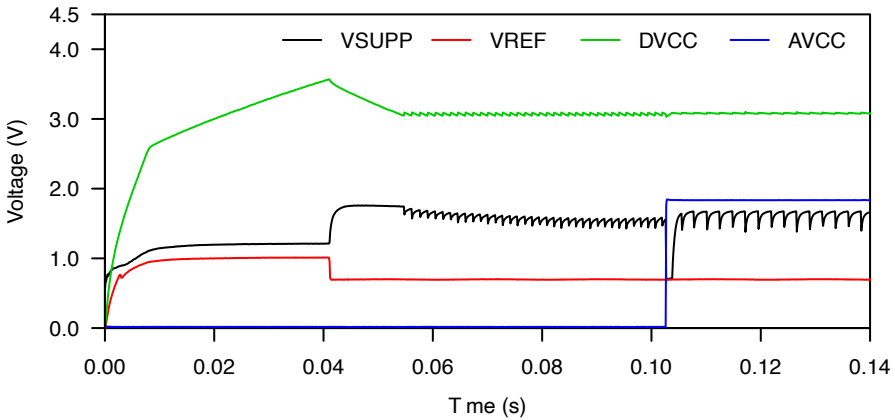


Figure 3.7: Test strip performance as a power source with serum: (a) polarization and (b) power curves. Data from [13].





(a)



(b)

Figure 3.8: Start up (a) current and (b) voltage waveforms for the test strip with serum.

time required by the device to have all the electronic modules powered to start a measurement is 103 ms.

Fig. 3.9 and 3.10 show the different regulated voltage supplies  $V_{ADCC}$  and  $V_{DVCC}$ , used to power the front end and the back end modules, against different current steps load. Fig. 3.9 show the response for a current step load of 1.5 mA at  $V_{AVCC}$ . The LDO is able to regulate 1.8 V while the current step load is applied. However, the paper based battery is not able to provide enough power and  $V_{DVCC}$  starts to decrease. Once  $V_{DVCC}$  drops below 2.4 V, the LDO is disabled and  $V_{DVCC}$  recovers. Thus, the PMU guaranties always

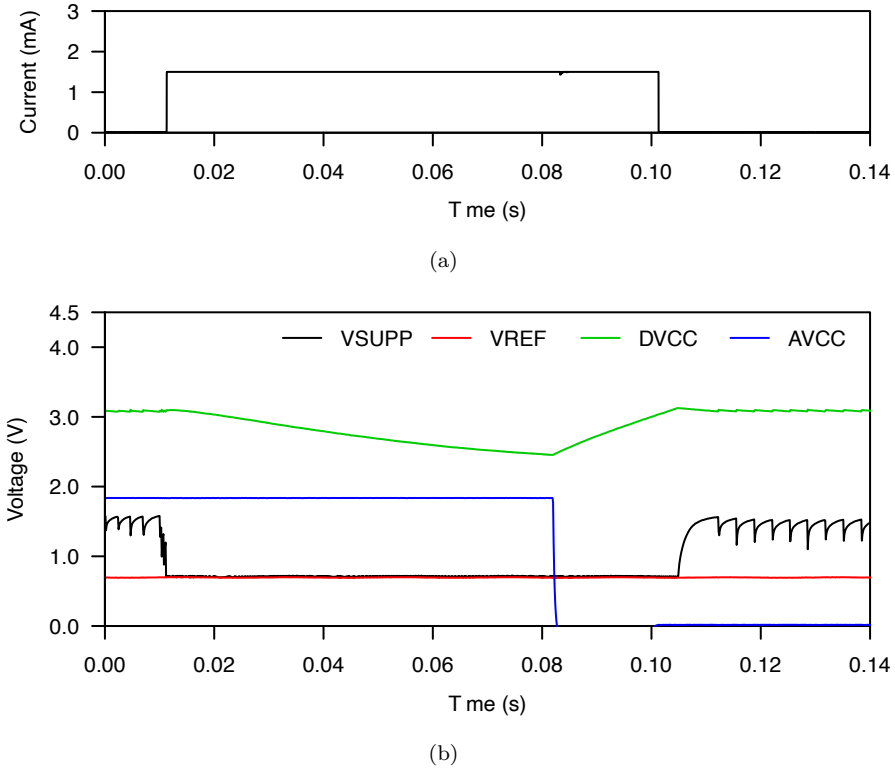


Figure 3.9: (a) Current and (b) voltage waveforms for a current step load at the LDO regulator's output.

that an analog high power requirement of the system does not compromise the power availability for the MCU, which controls the overall system. It can also be observed how the PMU sets the battery's polarization voltage  $V_{SUPP}$  equal to  $V_{REF}$ , which is 0.7 V. Thus, the power is extracted from the paper based battery with maximum efficiency.

In Fig. 3.10, the response for a current step load of 2.5 mA at  $V_{DVCC}$  is shown. The regulation of  $V_{AVCC}$  is not affected by the current step load until, again,  $V_{DVCC}$  drops below 2.4 V. Then, because the current step load is directly applied to  $V_{DVCC}$ , it continued decreasing until the PMU is not able to regulate  $V_{DVCC}$ . Again, it can be seen how, until the PMU is not able to regulate  $V_{DVCC}$ , power is extracted from the battery efficiently. Once the current step load is finished, the system recovers and the PMU starts its normal operation.

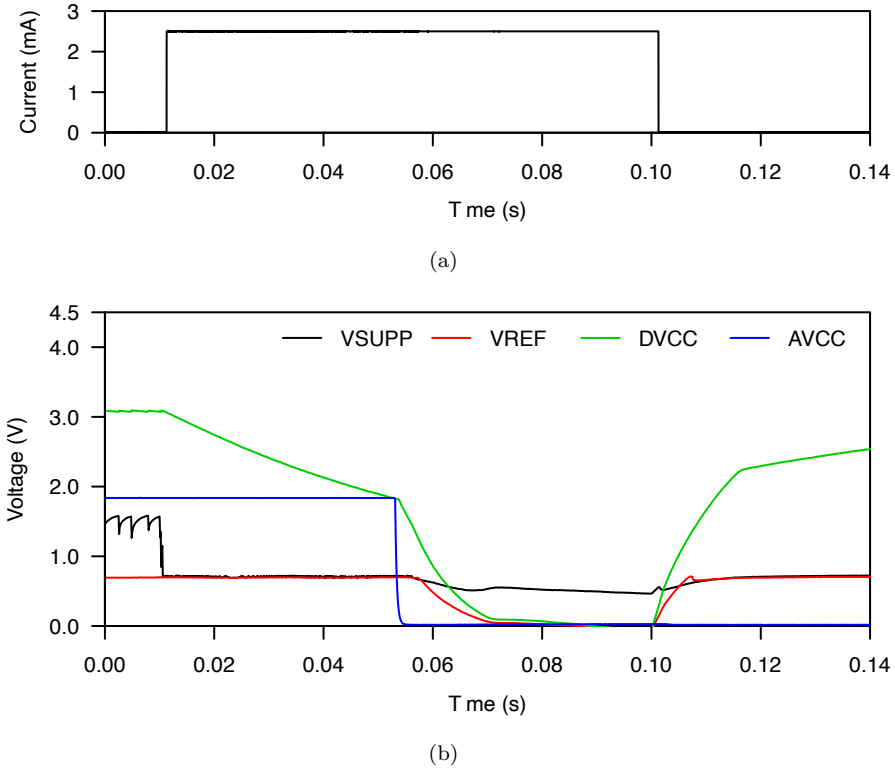


Figure 3.10: (a) Current and (b) voltage waveforms for a current step load at the DC/DC converter's output.

### 3.3.2 Electronic reader characterization

The power consumption of the device during the full measurement process is shown in Fig. 3.11 [13]. Four phases can be observed:

- **Phase I:** In this phase, the sample is not added yet and no power is extracted from the battery. The electronic reader remains unpowered.
- **Phase II:** The sample has been added and the electronic reader has been powered. The MCU remains in LPM while the OCP of the fuel cell is stabilized. Once stabilized, the MCU wakes up, starts the measurement, enters LPM again and the system enters Phase III. The awakening of the MCU can be noticed as a peak power consumption in the transition between Phase II and III.
- **Phase III:** During this phase, the chronoamperometry takes place while the

MCU remains in LPM. Once the desired measurement time has been elapsed, the MCU wakes up, converts the current readout to a glucose concentration, display the result to the user in the display and enters LPM. Then, the system enters Phase IV. Again, a peak power consumption can be observed in the transition from Phase III to IV due to the awakening of the MCU.

- **Phase IV:** In this phase, the measurement has finished and the result is displayed to the user through the LCD while the MCU remains in LPM.

The overall average power consumption of the device until the result is displayed to the user is 0.912 mW.

The characterization of the device as a glucose concentration measurement instrument is shown in Fig. 3.12. Fig. 3.12(a) shows the waveforms of the current provided by the fuel cell during a chronoamperometry for different glucose concentrations and a polarization voltage  $V_{SENSOR}$  of 0.45 V. The current readout, as discussed in [13, 14], is taken for a measurement time of 12 s. Taken the different current readouts at the given measurement time of 12 s for the different glucose concentrations provides the transfer function shown in Fig. 3.12(b), evidencing the measurement capability of this self powered device to measure glucose concentration in a serum sample.

Table 3.1 shows a summary of the results obtained for the 'plug and power' prototype.

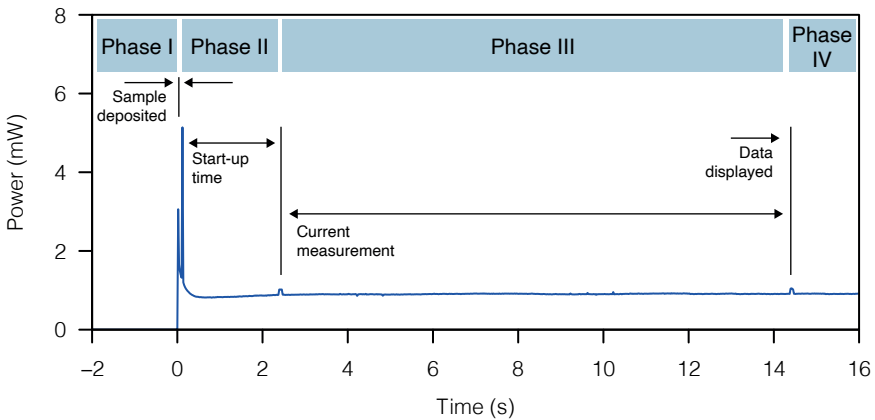


Figure 3.11: 'Plug and power' prototype's power consumption.

Image derived: "'Plug and Power' Point of Care Diagnostics: A Novel Approach for Self Powered Electronic Reader based Portable Analytical Devices" by Yaiza Montes Cebrián *et al.* © 2018 Elsevier, with permission.

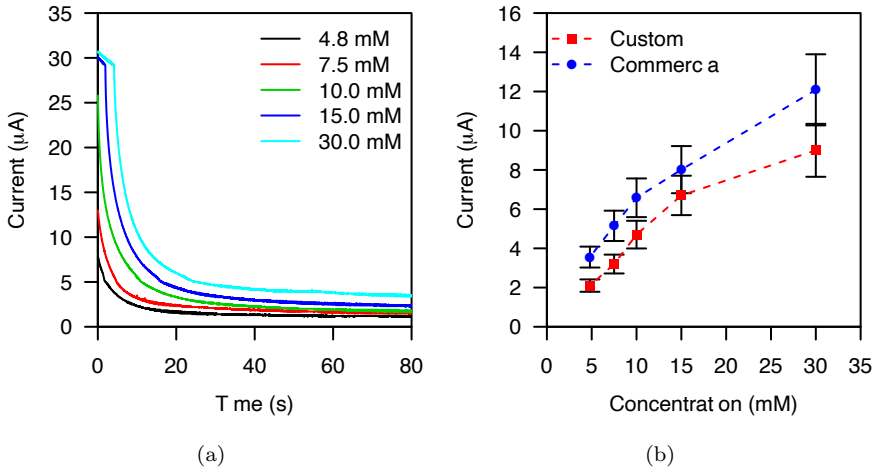


Figure 3.12: (a) Chronoamperometries and (b) transfer function of the 'plug and power' reader.

Images (a) and (b): "Plug and Power" Point of Care Diagnostics: A Novel Approach for Self Powered Electronic Reader based Portable Analytical Devices" by Yaiza Montes Cebrián *et al.* © 2018 Elsevier, with permission.

---

### 3.4 Chapter Conclusions

In this chapter, we have seen what are PoC devices, their benefits and how they face a challenge: to ensure that they meet the ASSURED criteria when following a self powered approach.

Table 3.1: 'Plug and power' prototype's characterization results.

Parameter	Value
Battery OCP	1.6 V
Battery short circuit current	17.345 mA
Battery max. output power	7.639 mW
Battery $V_{P_{MAX}}$	0.710 V
Fuel cell glucose concentration range	max. 30.0 mM min. 4.8 mM
Fuel cell pol. voltage $V_{SENSOR}$	0.45 V
Fuel cell transfer function current range	max. 12.1 µA min. 3.6 µA
Measurement time	12 s
Power consumption	0.912 mW

A PoC device for blood glucose concentration measurement was presented. The solution uses two galvanic cells integrated in a single test strip to operate. The first one is a battery, which can deliver up to 7.639 mW, that power the electronic reader while the second one is a glucose fuel cell used to perform the measurement. Both use the same biological sample as electrolyte to operate. Also, the power extraction and the measurement take place simultaneously. Furthermore, the power extraction is performed efficiently thank to a PMU that applies a MPPT algorithm to set the polarization voltage of the battery  $V_{P_{MAX}}$  to 0.710 V.

On the other hand, the fuel cell provides a way to measure glucose concentrations from 4.8 mmol dm<sup>-3</sup> to 30.0 mmol dm<sup>-3</sup> using a polarization voltage of 0.45 V. The device takes 12 s to perform the measurement. Furthermore, the result is displayed to the user through an LCD display providing a quantitative and objective result.

All this is achieved with a power consumption of 0.912 mW. The low voltage and low power characteristics of the device, in conjunction with the quantitative and objective result, makes the presented device a suitable solution for the development of true self powered devices that meet the ASSURED criteria. The concept of the device can be extrapolated for the measurement of other analytes. However, the design concept used is based on using two galvanic cells to operate the system. This can lead to a higher cost and to a large volume sample requirement. In Chapter 4 a single galvanic cell approach is presented to overcome this drawback.

---

## Acronyms

<b>ADC</b>	Analog to Digital Converter
<b>ASSURED</b>	Affordable, Sensitive, Specific, User friendly, Rapid and robust, Equipment free, and Deliverable to users
<b>BCD</b>	Binary Coded Decimal
<b>BOX</b>	Bilirubin Oxidase
<b>CA</b>	Control Amplifier
<b>CE</b>	Counter Electrode
<b>COTS</b>	Commercial off the Shelf
<b>GDH</b>	Dehydrogenase
<b>GPIO</b>	General Purpose Input/Output
<b>LCD</b>	Liquid Cristal Display

<b>LDO</b>	Low Dropout
<b>LPM</b>	Low Power Mode
<b>LUT</b>	Look Up Table
<b>OCFV</b>	Open Circuit Fractional Voltage
<b>OP</b>	Operating Point
<b>OpAmp</b>	Operational Amplifier
<b>MCU</b>	Microcontroller Unit
<b>PCB</b>	Printed Circuit Board
<b>PFM</b>	Pulse Frequency Modulation
<b>PMU</b>	Power Management Unit
<b>PoC</b>	Point of Care
<b>PoCT</b>	Point of Care Testing
<b>PWM</b>	Pulse Width Modulation
<b>SHM</b>	Structural Health Monitoring
<b>SMPS</b>	Switched Mode Power Supply
<b>SMU</b>	Source Metere Unit
<b>TIA</b>	Transimpedance Amplifier

---

## References

- [1] G. J. Kost, N. K. Tran, and R. F. Louie, "Point of Care Testing: Principles, Practice, and Critical Emergency Disaster Medicine," in *Encyclopedia of Analytical Chemistry*. Chichester, UK: John Wiley & Sons, Ltd, sep 2008.
- [2] J. Vidal Alaball, R. Acosta Roja, N. Pastor Hernández, U. Sanchez Luque, D. Morrison, S. Narejos Pérez, J. Perez Llano, F. López Seguí, and A. Salvador Vèrges, "Telemedicine in the face of the COVID 19 pandemic," 2020.
- [3] P. K. Drain, E. P. Hyle, F. Noubary, K. A. Freedberg, D. Wilson, W. R. Bishai, W. Rodriguez, and I. V. Bassett, "Diagnostic point of care tests in resource limited settings," pp. 239–249, mar 2014.
- [4] E. Fu, P. Yager, P. N. Floriano, N. Christodoulides, and J. T. McDevitt, "Perspective on diagnostics for global health," pp. 40–50, nov 2011.
- [5] L. Gervais, N. De Rooij, and E. Delamarche, "Microfluidic chips for point of care immunodiagnosics," pp. H151–H176, jun 2011.
- [6] C. D. Chin, V. Linder, and S. K. Sia, "Commercialization of microfluidic point of care diagnostic devices," pp. 2118–2134, jun 2012.
- [7] S. Choi, "Powering point of care diagnostic devices," *Biotechnology Advances*, vol. 34, no. 3, pp. 321–330, may 2016.
- [8] A. K. Yetisen, M. S. Akram, and C. R. Lowe, "Paper based microfluidic point of care diagnostic devices," pp. 2210–2251, jun 2013.
- [9] M. A. Pellitero, A. Guimerà, M. Kitsara, R. Villa, C. Rubio, B. Lakard, M. L. Doche, J. Y. Hihn, and F. Javier del Campo, "Quantitative self powered electrochromic biosensors," *Chemical Science*, vol. 8, no. 3, pp. 1995–2002, feb 2017.
- [10] G. Slaughter and T. Kulkarni, "A self powered glucose biosensing system," *Biosensors and Bioelectronics*, vol. 78, pp. 45–50, 2016.
- [11] A. Baingane and G. Slaughter, "Self powered electrochemical lactate biosensing," *Energies*, vol. 10, no. 10, oct 2017.
- [12] G. Slaughter and T. Kulkarni, "Highly Selective and Sensitive Self Powered Glucose Sensor Based on Capacitor Circuit," *Scientific Reports*, vol. 7, no. 1, 2017.



- [13] Y. Montes Cebrián, L. del Torno de Román, A. Álvarez Carulla, J. Colomer Farrarons, S. D. Minter, N. Sabaté, P. L. Miribel Català, and J. P. Esquivel, “Plug and Power’ Point of Care diagnostics: A novel approach for self powered electronic reader based portable analytical devices,” *Biosensors and Bioelectronics*, vol. 118, pp. 88–96, 2018.
- [14] Y. Montes Cebrián, “Sin título,” Ph.D. dissertation, Universitat de Barcelona, 2020.
- [15] Y. Montes Cebrián, A. Álvarez Carulla, J. Colomer Farrarons, M. Puig Vidal, and P. L. Miribel Català, “Self Powered Portable Electronic Reader for Point of Care Amperometric Measurements,” *Sensors*, vol. 19, no. 17, p. 3715, aug 2019.
- [16] “Fuelium Paper based batteries.”
- [17] P. C. Noordzij, “Comparison of blood and breath testing under field conditions,” *Alcohol, Drugs and Traffic Safety*, pp. 553–560, 1975.
- [18] R. J. Leonard, “Evaluation of the Analytical Performance of a Fuel Cell Breath Alcohol Testing Instrument: A Seven Year Comprehensive Study,” *Journal of Forensic Sciences*, vol. 57, no. 6, pp. 1614–1620, nov 2012.
- [19] “UK Drug & Alcohol Safety Experts Dräger Channel Partner AlcoDigital.”
- [20] “Andatech: Breathalysers and Drug Test Kits Australia.”
- [21] “Why Choose Fuel Cell Sensor Technology?”
- [22] “AT8030 Fuel Cell Alcohol Tester Hanwei Electronics.”
- [23] J. Colomer Farrarons and P. L. Miribel Català, *A CMOS self powered front end architecture for subcutaneous event detector devices : three electrodes amperometric biosensor approach*. Springer, 2011.
- [24] J. Punter, J. Colomer Farrarons, and P. Ll., “Bioelectronics for Amperometric Biosensors,” in *State of the Art in Biosensors General Aspects*. InTech, mar 2013.
- [25] J. Punter Villagrasa, J. Colomer Farrarons, F. J. del Campo, and P. Miribel, *Amperometric and Impedance Monitoring Systems for Biomedical Applications*. Springer International Publishing, 2017, vol. 1.
- [26] Texas Instruments, “BQ25504 Ultra Low Power Boost Converter With Battery Management for Energy (Datasheet),” [Online]. Available: <http://ti.com/lit/ds/symlink/bq25504.pdf>. [Accessed September 12, 2019].

- [27] Texas Instruments, “LP5910 300 mA low noise low IQ low dropout (LDO) linear regulator (Datasheet),” [Online]. Available: <http://www.ti.com/lit/ds/symlink/lp5910.pdf>. [Accessed October 18, 2019].
- [28] A. Álvarez Carulla, J. Colomer Farrarons, J. Lopez Sanchez, and P. Miribel Catala, “Piezoelectric Harvester based structural health monitoring that uses a self powered adaptive circuit,” in *2nd IEEE International Workshop on Metrology for Aerospace*. Institute of Electrical and Electronics Engineers Inc., aug 2015, pp. 531–535.
- [29] A. Álvarez Carulla, J. Colomer Farrarons, J. López Sánchez, and P. Miribel Català, “An adaptative self powered energy harvester strain sensing device based of mechanical vibrations for structural health monitoring applications,” in *2016 IEEE 25th International Symposium on Industrial Electronics (ISIE)*, vol. 2016 Novem. IEEE, nov 2016, pp. 638–644.
- [30] A. Álvarez Carulla, J. Colomer Farrarons, and P. L. Miribel, “Low Power Energy Harvesting Solutions for Smart Self Powered Sensors,” in *Sensors for Diagnostics and Monitoring*. CRC Press, 2018, pp. 217–250.
- [31] A. Álvarez Carulla, J. Colomer Farrarons, J. Lopez Sanchez, P. Miribel Catala, A. Alvarez Carulla, J. Colomer Farrarons, J. Lopez Sanchez, and P. Miribel Catala, “PiezoElectric Harvester Based Self Powered Adaptive Circuit with Wireless Data Transmission Capability for Structural Health Monitoring,” in *2015 Conference on Design of Circuits and Integrated Systems, DCIS 2015*. Institute of Electrical and Electronics Engineers Inc., jan 2016.
- [32] Texas Instruments, “REF1004 1.2 Micropower Voltage Reference (Data sheet),” [Online]. Available: <http://www.ti.com/lit/ds/symlink/ref1004.1.2.pdf>. [Accessed October 18, 2019].
- [33] Texas Instruments, “LPV521 NanoPower, 1.8 V, RRIO, CMOS Input, Operational Amplifier (Datasheet),” [Online]. Available: <http://www.ti.com/lit/ds/symlink/lpv521.pdf>. [Accessed September 13, 2019].
- [34] Texas Instruments, “SN74AUC1G66 Single Bilateral Analog Switch,” [Online]. Available: <http://www.ti.com/lit/ds/symlink/sn74auc1g66.pdf>. [Accessed October 18, 2019].
- [35] Texas Instruments, “MSP430FR5969 16 MHz Ultra Low Power Microcontroller featuring 64 KB FRAM, 2 KB SRAM, 40 IO (Datasheet),” [Online]. Available: <http://www.ti.com/lit/ds/symlink/msp430fr5969.pdf>. [Accessed October 18, 2019].

- [36] L. E. Bengtsson, "Lookup Table Optimization for Sensor Linearization in Small Embedded Systems," *Journal of Sensor Technology*, vol. 02, no. 04, pp. 177–184, 2012.
- [37] Texas Instruments, "CD4055B CMOS BCD to 7 Segment LCD Decoder/Driver with Display Frequency Output (Datasheet)," [Online]. Available: <http://www.ti.com/lit/ds/symlink/cd4055b.pdf>. [Accessed October 18, 2019].



## 4.1

One usual method to show the capability of a galvanic cell as sensor is by means of its polarization curves for different analyte concentrations in a sample used as electrolyte [1–5]. The polarization curves are extracted performing a Linear Sweep Voltammetry (LSV) from Open Circuit Potential (OCP) to 0 V. The LSV is a voltammetric electroanalytical method that consists in polarizing an electrochemical cell; in this case, a galvanic cell, to a given polarization voltage  $V_P$  and to sweep it linearly in time. Meanwhile, the current outputted by the cell is logged in order to generate a voltage vs. current curve later on. The polarization voltage variation in time is known as scan rate, which is constant during a LSV. Furthermore, the scan rate must be as low as the polarization curves are independent of it [6]. Common polarization curves for a general purpose galvanic cell and different analyte concentrations are shown in Fig. 4.1.

Once the galvanic cell is characterized for different analyte concentrations, then a voltage level  $V_{SENSOR}$  is selected as a polarization voltage to generate the current vs. concentration transfer function of the cell as a sensor. The optimal voltage is selected in terms of cell's characteristics related to its role as a sensor [7]; i.e, sensitivity, linearity, accuracy, repeatability, among others.

While this approach is widely used in laboratories due to the accurate and precise measurements provided by bench top equipment, like potentiostats; it is an approach hard to be implemented in self powered devices. Common

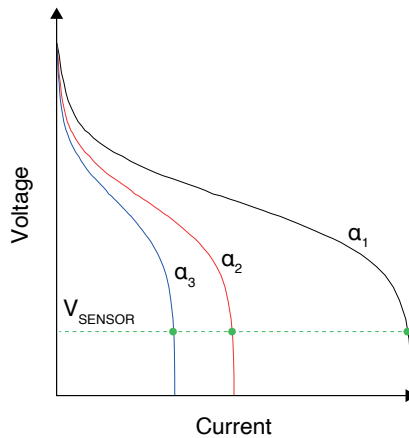


Figure 4.1: Polarization curves for a general purpose galvanic cell for concentrations  $\alpha_1$ ,  $\alpha_2$  and  $\alpha_3$ , being  $\alpha_1 > \alpha_2 > \alpha_3$ .

galvanic cells used in biomedical applications for self powered PoC devices provide low power and low voltage levels usually not enough to power all the electronics involved in a potentiostat. Due to this, basic electronic solutions are implemented with galvanic cells in self powered PoC devices, like resistors [8, 9] or capacitors [4] as loads to transduce the analyte concentration to an electrical signal. These approximations offer a way to monitor the analyte concentration through a continuous cell's output characteristic transduction. However, they do not provide a way to output a one off measurement neither a criterion in when a measurement has finished. Furthermore, due to their simplicity, these approaches usually need for external non self powered devices, like an oscilloscope or a Digital Multimeter (DMM) [8, 9], to visualize the measurement or to display the result to the user. This collides with the very definition of a self powered device.

Other approaches make use of chronoamperometry, a voltammetric electroanalytical method, that consist in polarizing the cell to  $V_{SENSOR}$  while the output current is logged over time [3, 10]. However, these approaches use a dual galvanic cell based implementation, discussed in Chapter 3; or add a Power Management Unit (PMU) to first extract power from the cell and then perform the measurement, discussed in Chapter 5.

[REDACTED]

$$[REDACTED] \tag{4.1}$$

[REDACTED]

[REDACTED] The solution is under a process of intellectual property protection to patent it and a publication [11] is under strict embargo until the resolution of the process.

---

## 4.2

The scheme of the intended application of

The implementation of the device is described in Section 4.2.1 and 4.2.2. Nevertheless, the implementation strongly depends on the application scenario where it is operated. As a demonstrator, a sodium chloride (NaCl) concentration in sample measurement is implemented as a solution for screening cystic fibrosis disease [15].

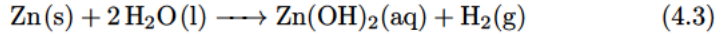
### 4.2.1 The Galvanic Cell

For the intended application, we have implemented a NaCl based galvanic cell. In this case, a NaCl based battery. Different NaCl concentrations in sample used as electrolyte serve to emulate different conductivities in a biological sample used to screening cystic fibrosis disease. The NaCl concentrations used are those with an equivalent conductivity in the range of interest for cystic fibrosis screening defined by Diagnostic Sweat Testing Guidelines from the Cystic Fibrosis Foundation [16, 17]. I.e., NaCl concentrations from 5 to

160 mM. We have implemented a NaCl based battery stacking in series two galvanic cells of which cell diagram is

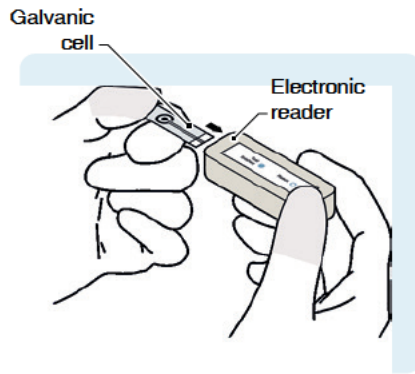


where the following electrochemical reaction takes place



The Cu(s) electrode is inert, while the cell exhibits an OCP of 0.761 V due to the electromotive force potential of the Zn(s) oxidation and H<sup>+</sup> reduction [18]. This OCP can vary as a result of the electrodes polarisation [19]. The active area of each electrode was 2.5 cm x 2.5 cm separated by 2.2 cm.

We have purchased Zn(s) and Cu(s) electrode strips from Pidiscat. For



(a)



(b)

Figure 4.2: (a) Application scheme and (b) [redacted].



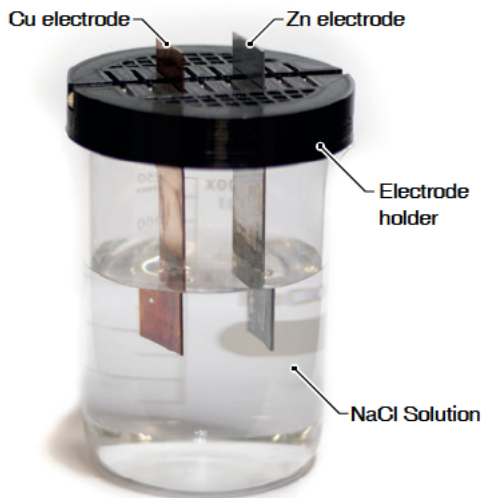


Figure 4.3: Picture of the NaCl galvanic cell. Cu and Zn electrodes with an active area of 2.5 x 2.5 cm.

sample preparation, we have used NaCl solutions with different concentrations using sodium chloride (NaCl, ACS grade, 99.5 %) purchased from ITW Reagents and used as received. We have used deionized water obtained from a Milli Q<sup>®</sup> Advantage A10 water purification system for all experiments. To control the separation and immersion distance of the electrodes, a full custom electrode holder was 3D printed. Fig. 4.3 shows a picture of one of the implemented stacked cells used for the NaCl based battery.

We have validated the galvanic cell using two different methods. The first method consists in validating the battery performing a LSV to the cell from its OCP to 0 V with a scan rate of 10 mV s<sup>-1</sup> for NaCl concentrations of 5, 30, 60 and 160 mM. This initial characterization is intended to validate the construction of the battery using a well known method like LSV. [REDACTED]

[REDACTED]

The cell characterization for the LSV method is shown in Fig. 4.4. The cell exhibits an OCP of 1.715 V and a maximum sensitivity to the analyte concentration at 0.9 V. At this voltage and for a concentration range from 5 to 160 mM, the cell provides an output current from 0.261 to 1.235 mA. The transfer function current vs. concentration of the cell for a polarization voltage

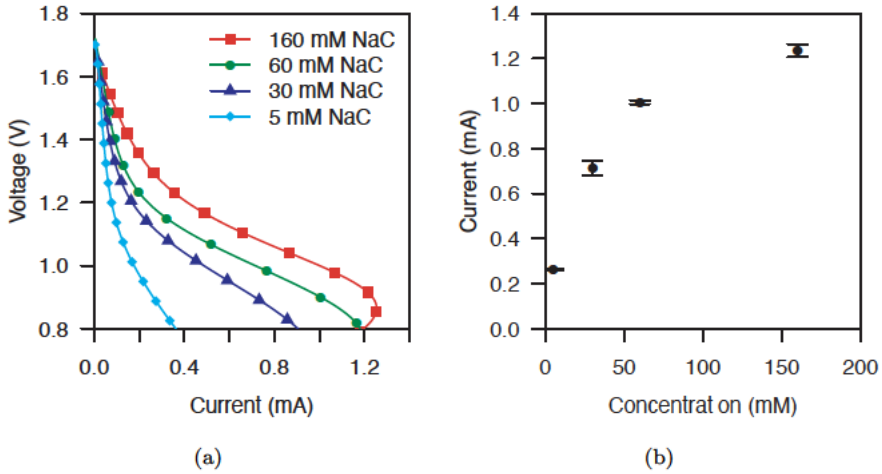
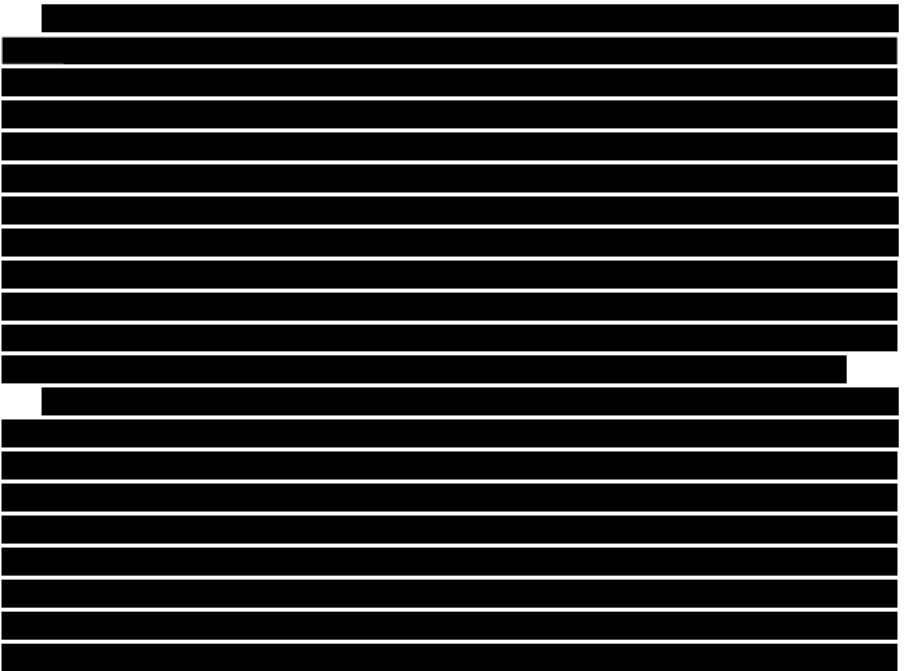


Figure 4.4: (a) Polarisation curves and (b) transfer function at a polarisation voltage of 0.9 V of the NaCl galvanic cell.

of 0.9 V with the LSV method is shown in Fig. 4.4(b). The transfer functions exhibits a maximum standard deviation of 31.035  $\mu$ A at 30 mM and a maximum coefficient of variation of 4.3% for the same concentration.



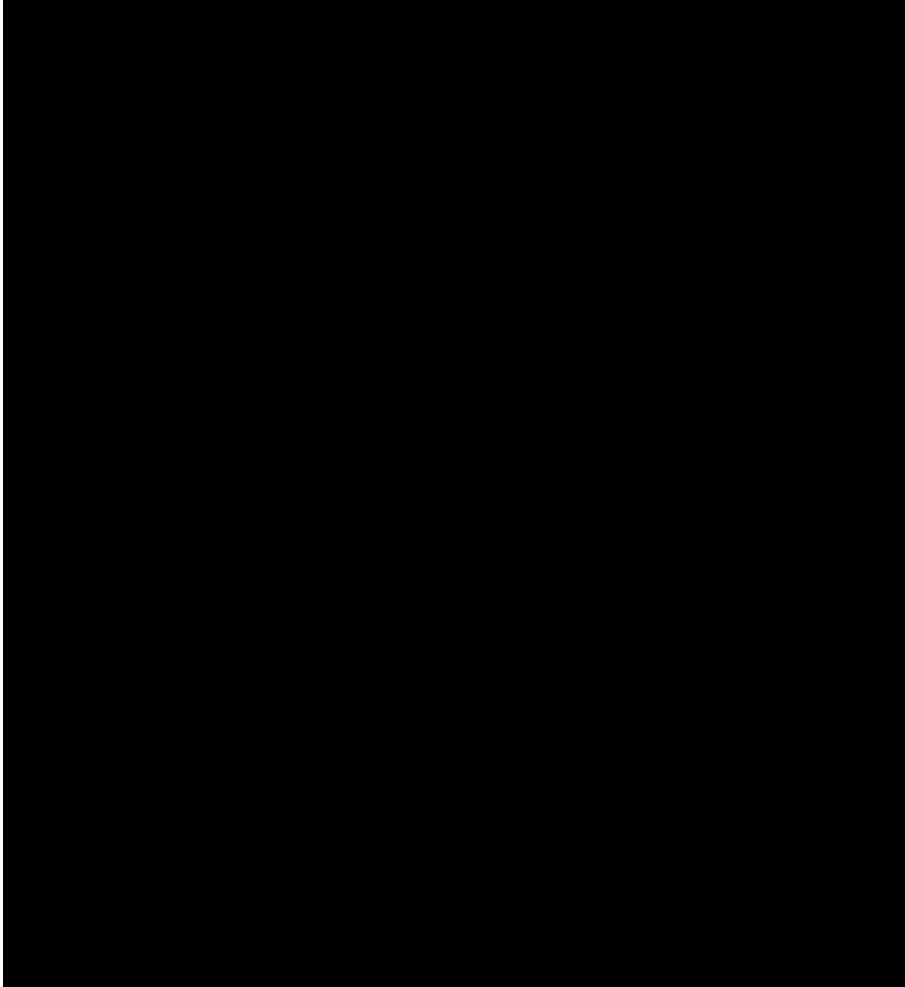


Figure 4.5: [Redacted text]

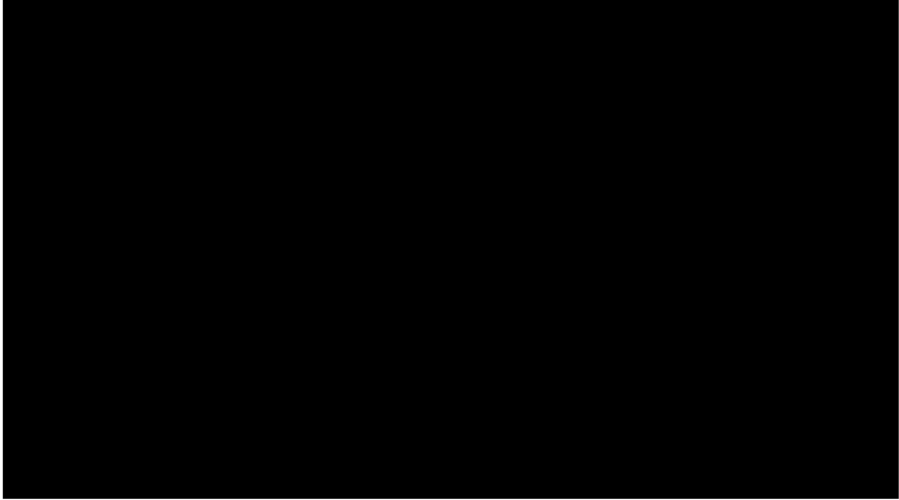
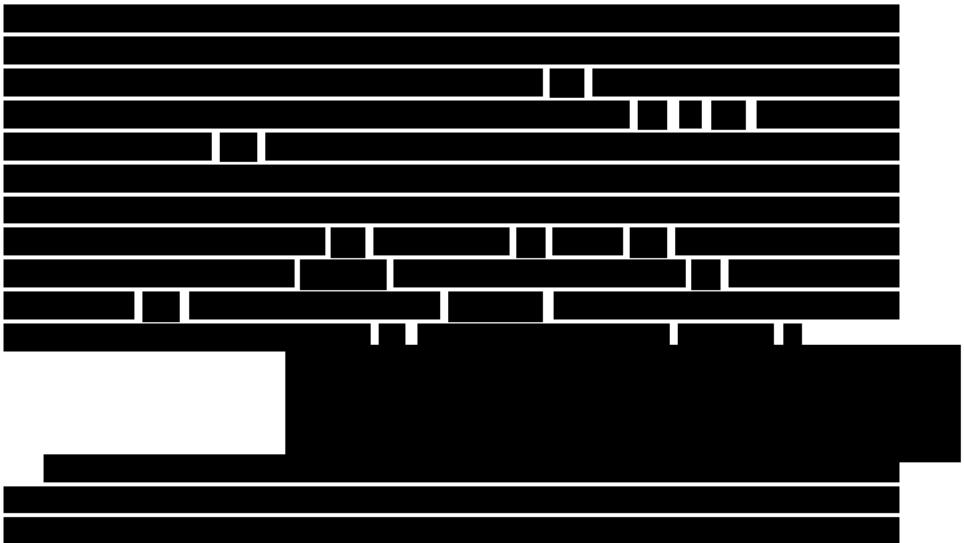


Figure 4.6: [Redacted]

### 4.2.2 The Electronic Reader

The schematic and a picture of the implemented electronic reader prototype are shown in Fig. 4.7. We have implemented the prototype on a 46 mm x 18 mm double sided Printed Circuit Board (PCB) using COTS parts.

#### 4.2.2.1 [Redacted]



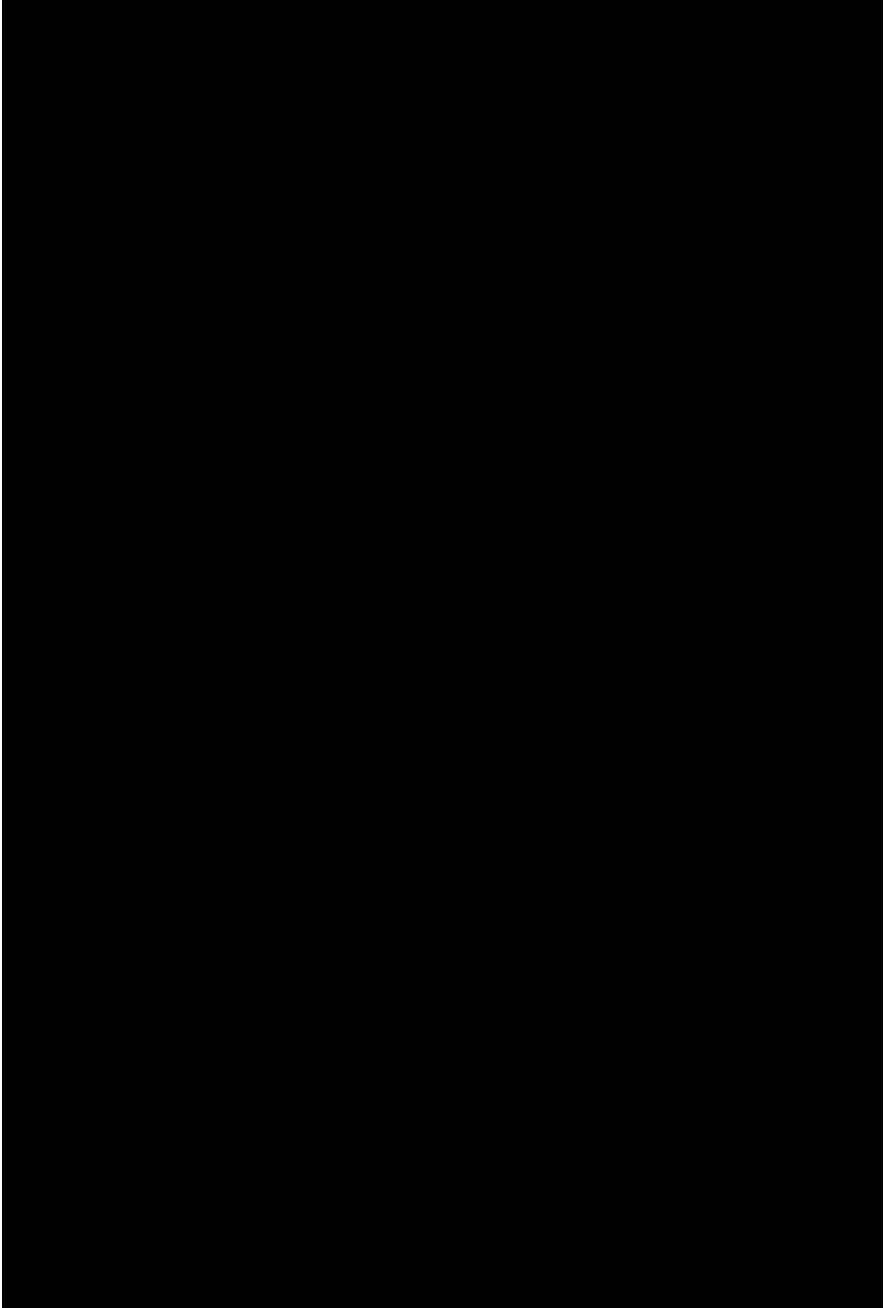


Figure 4.7:

[REDACTED]

4.2.2.2 Ana [REDACTED]

[REDACTED]

4.2.2.3 [REDACTED]

[REDACTED]

[REDACTED]

### 4.2.3 Results and Discussion

[REDACTED]

[REDACTED]

[REDACTED]

[REDACTED]

[REDACTED]

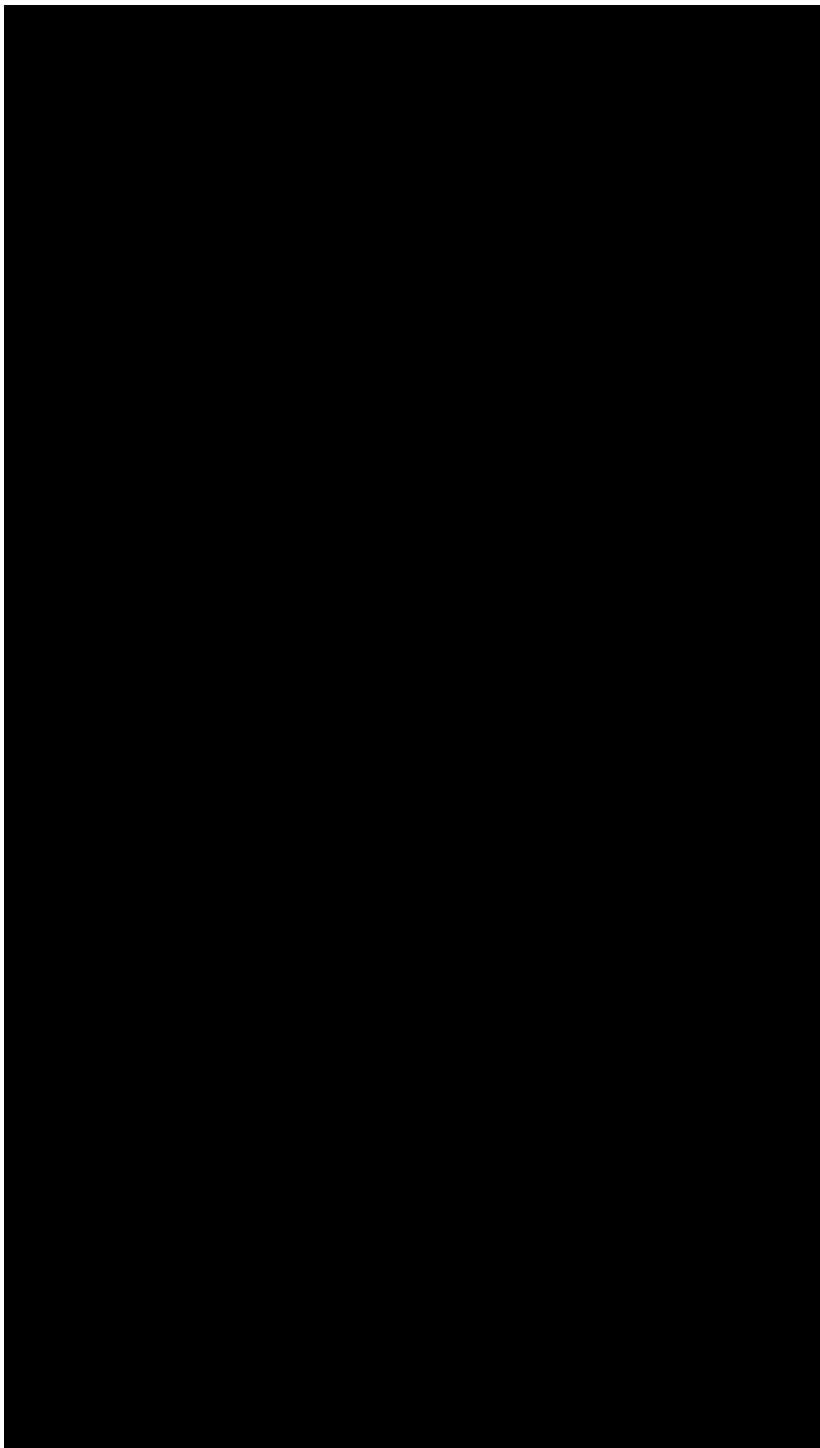


Figure 4.8:





Figure 4.9:

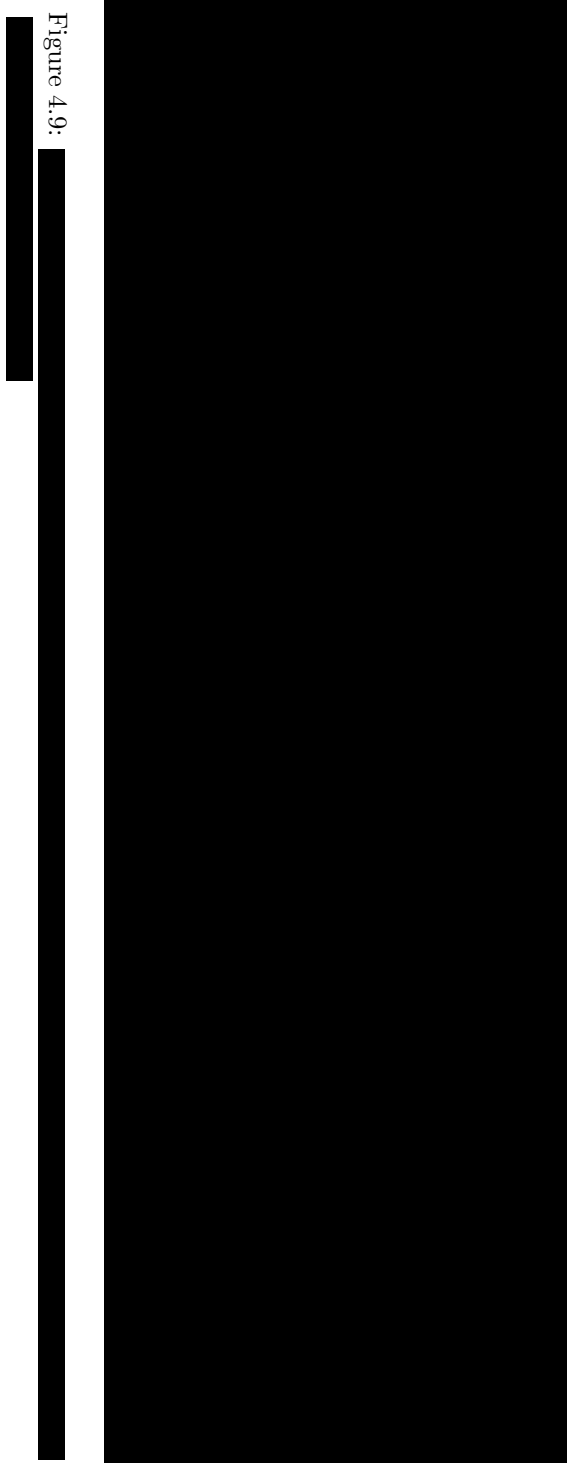
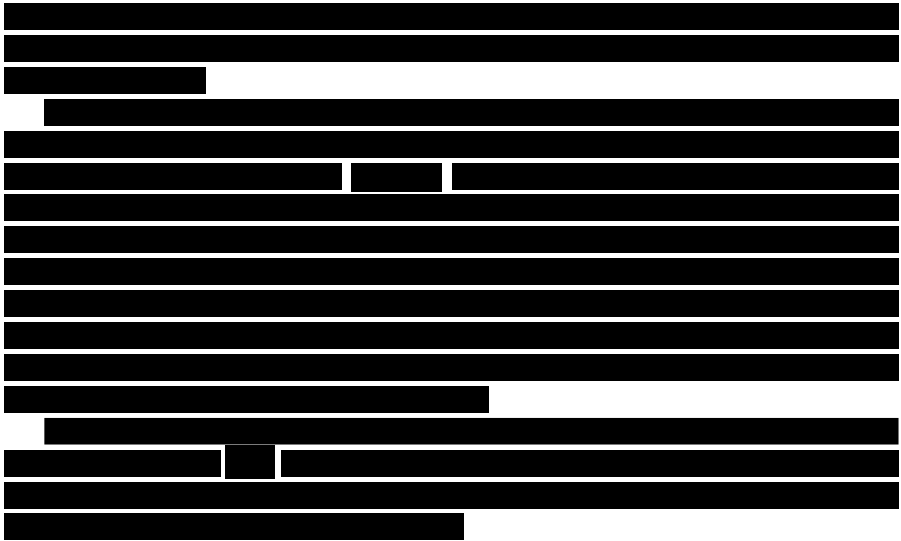
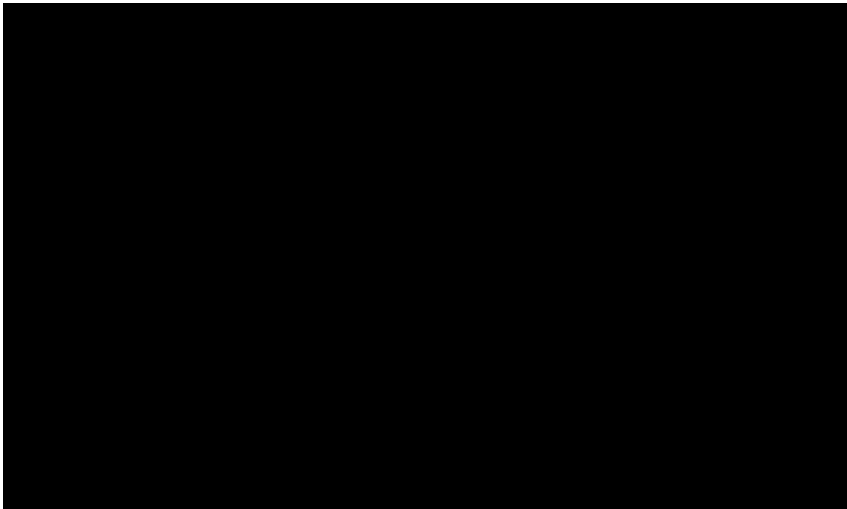




Table 4.1: Prototype’s characterization results.



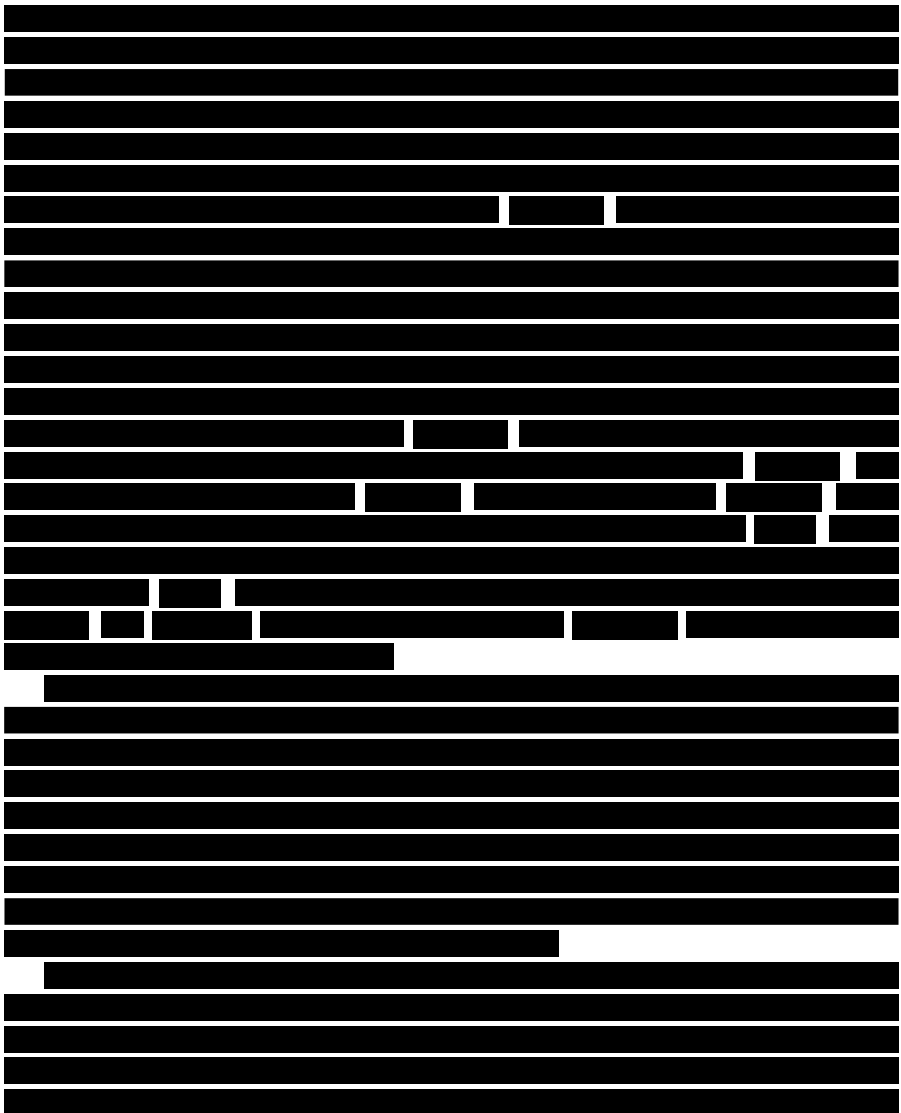
---

### 4.3 Chapter Conclusions

In this chapter, the state of the art regarding single galvanic cell based self powered PoC devices is presented. The presented devices are framed into biomedical applications. Due to the usual hard constrains of low voltage and low power levels provided by the galvanic cells used in these applications, the

state of the art applies basic electronic solutions to transduce the analyte concentration in the sample used as electrolyte in the cell, like a resistor or a capacitor as output transducers. These kind of approximations result in two major drawbacks: 1) the device does not provide a way to display an unequivocal quantitative user readable result without needing an external non self powered device, and 2) the measurement is performed continuously without a criteria in when the result must be taken from the measurement and display it to the user.

To overcome these drawbacks, we present an architecture solution, presented in [11].





The non complex implementation of the proposed solution and its low power consumption make suitable the paper based implementation of the solution following the current trend in biomedical research to develop eco friendly, cost effective and self powered PoC devices.



### Acronyms

- ADC**      Analog to Digital Converter
- COTS**    Commercial off the Shelf
- DMM**     Digital Multimeter
- EHS**     Energy Harvesting Source
- LDO**     Low Dropout
- LSV**     Linear Sweep Voltammetry
- █**        █
- OCP**     Open Circuit Potential
- OpAmp**   Operational Amplifier
- PCB**     Printed Circuit Board
- PMOS**   P channel Metal Oxide Semiconductor
- PMU**     Power Management Unit
- PoC**     Point of Care



---

## References

- [1] Y. Montes Cebrián, A. Álvarez Carulla, J. Colomer Farrarons, M. Puig Vidal, and P. L. Miribel Català, “Self Powered Portable Electronic Reader for Point of Care Amperometric Measurements,” *Sensors*, vol. 19, no. 17, p. 3715, aug 2019.
- [2] Y. Montes Cebrian, A. Álvarez Carulla, J. Colomer Farrarons, M. Puig Vidal, J. Lopez Sanchez, and P. Miribel Catala, “A Fuel Cell based ad aptable Self Powered Event Detection platform enhanced for biosampling applications,” in *2018 Conference on Design of Circuits and Integrated Systems (DCIS)*. IEEE, nov 2018, pp. 1–6.
- [3] Y. Montes Cebrián, L. del Torno de Román, A. Álvarez Carulla, J. Colomer Farrarons, S. D. Minter, N. Sabaté, P. L. Miribel Català, and J. P. Esquivel, “‘Plug and Power’ Point of Care diagnostics: A novel approach for self powered electronic reader based portable analytical devices,” *Biosensors and Bioelectronics*, vol. 118, pp. 88–96, 2018.
- [4] G. Slaughter and T. Kulkarni, “A self powered glucose biosensing system,” *Biosensors and Bioelectronics*, vol. 78, pp. 45–50, 2016.
- [5] A. Baingane and G. Slaughter, “Self powered electrochemical lactate biosensing,” *Energies*, vol. 10, no. 10, oct 2017.
- [6] R. P. O’Hayre, S. W. Cha, W. G. Colella, and F. B. Prinz, *Fuel cell fundamentals*. John Wiley & Sons, Inc., 2016.
- [7] A. H. Jalal, Y. Umasankar, M. A. Ahmed, E. A. Pretto, and S. Bhansali, “Towards a wearable fuel cell sensor for transdermal monitoring of isoflurane an anesthetic,” *Analytical Methods*, vol. 11, no. 15, pp. 2007–2012, apr 2019.
- [8] C. Fischer, A. Fraiwan, and S. Choi, “A 3D paper based enzymatic fuel cell for self powered, low cost glucose monitoring,” *Biosensors and Bioelectronics*, vol. 79, pp. 193–197, may 2016.
- [9] D. Yu, L. Bai, J. Zhai, Y. Wang, and S. Dong, “Toxicity detection in water containing heavy metal ions with a self powered microbial fuel cell based biosensor,” *Talanta*, vol. 168, pp. 210–216, jun 2017.
- [10] D. Majdecka, S. Draminska, D. Janusek, P. Krysinski, and R. Bilewicz, “A self powered biosensing device with an integrated hybrid biofuel cell for intermittent monitoring of analytes,” *Biosensors and Bioelectronics*, vol. 102, pp. 383–388, apr 2018.

- [11] A. Álvarez Carulla, Y. Montes Cebrián, M. Puig Vidal, J. Colomer Farrarons, and P. L. Miribel Català, "Self Powered Point of Care Device for Galvanic Cell based Sample Concentration Measurement," *IEEE Transactions on Biomedical Circuits and Systems*, under embargo.
- [12] Y. Uchida, E. Kätelhön, and R. G. Compton, "Linear sweep voltammetry with non triangular waveforms at a microdisc electrode," *Journal of Electroanalytical Chemistry*, vol. 823, pp. 465–473, aug 2018.
- [13] E. Kätelhön and R. G. Compton, "Non linear sweep voltammetry of adsorbed species: Theory and a method to determine formal potentials," *Physical Chemistry Chemical Physics*, vol. 19, no. 42, pp. 28 820–28 823, 2017.
- [14] H. M. Amin, Y. Uchida, C. Batchelor McAuley, E. Kätelhön, and R. G. Compton, "Non triangular potential sweep cyclic voltammetry of reversible electron transfer: Experiment meets theory," *Journal of Electroanalytical Chemistry*, vol. 815, pp. 24–29, apr 2018.
- [15] L. Ortega, A. Llorella, J. P. Esquivel, and N. Sabaté, "Self powered smart patch for sweat conductivity monitoring," *Microsystems & Nanoengineering*, vol. 5, no. 1, p. 3, dec 2019.
- [16] V. A. LeGrys, J. R. Yankaskas, L. M. Quittell, B. C. Marshall, P. J. Mogayzel, and Cystic Fibrosis Foundation, "Diagnostic sweat testing: the Cystic Fibrosis Foundation guidelines." *The Journal of pediatrics*, vol. 151, no. 1, pp. 85–9, jul 2007.
- [17] P. M. Farrell, B. J. Rosenstein, T. B. White, F. J. Accurso, C. Castellani, G. R. Cutting, P. R. Durie, V. A. Legrys, J. Massie, R. B. Parad, M. J. Rock, P. W. Campbell, and Cystic Fibrosis Foundation, "Guidelines for diagnosis of cystic fibrosis in newborns through older adults: Cystic Fibrosis Foundation consensus report." *The Journal of pediatrics*, vol. 153, no. 2, pp. S4–S14, aug 2008.
- [18] W. M. Haynes, *CRC handbook of chemistry and physics : a ready reference book of chemical and physical data*. CRC, 2012.
- [19] Y. W. on corrosion) Huang and J. W. on corrosion) Zhang, *Materials corrosion and protection*. De Gruyter, 2018.
- [20] Silicon Labs, "TS12011/TS12012 A 0.8V/1.5uA Nanopower Op Amp, Comparator and Reference," [Online]. Available: [https://www.silabs.com/documents/public/data\\_sheets/TS12011\\_12.pdf](https://www.silabs.com/documents/public/data_sheets/TS12011_12.pdf). [Accessed September 23, 2019].
- [21] Nexperia, "PMN70XP 20 V, P channel Trench MOSFET," [Online]. Available: [https://assets.nexperia.com/documents/data\\_sheet/PMN70XP.pdf](https://assets.nexperia.com/documents/data_sheet/PMN70XP.pdf). [Accessed September 23, 2019].

- [22] Silicon Labs, “TS12001 A 0.65V/1uA Nanopower Voltage Detector with Dual Outputs,” [Online]. Available: [https://www.silabs.com/documents/public/data\\_sheets/TS12001.pdf](https://www.silabs.com/documents/public/data_sheets/TS12001.pdf). [Accessed September 23, 2019].
- [23] AVX, “AVX BestCap Ultra low ESR High Power Pulse Supercapacitors,” [Online]. Available: <http://datasheets.avx.com/BestCap.pdf>. [Accessed September 23, 2019].





# 5

---

## *Ubiquitous Self-Powered Architecture for Galvanic Cell-based Applications*

---

### CONTENTS

5.1	Exploiting the Galvanic Cell's Role as Sensor and Power Source Simultaneously .....	109
5.2	The Galvanic Cell as a Sensor .....	112
5.3	The Galvanic Cell as a Power Source .....	113
5.4	Ubiquitous Self Powered Architecture .....	113
5.4.1	Architecture Concept and Operation .....	115
5.4.2	Prototype Implementation .....	116
5.4.2.1	Galvanic cell selection and characterization .	116
5.4.2.2	Architecture implementation .....	119
5.4.3	Results and Discussion .....	123
5.5	Chapter Conclusions .....	126
	Acronyms .....	130
	References .....	132

In Chapter 3, the implementation of self powered devices using multiple galvanic cells has been presented. As has been discussed, this implementation presents some drawbacks in terms of complexity, consumption, cost and, in case of biomedical applications, volume of sample needed by the device to operate. While those drawbacks have been overcome in the single galvanic cell approach presented in Chapter 4, one major benefit is missed: the power efficiency. This chapter presents state of the art single galvanic cell implementations using the cell as a sensor and as a power source, and a novel patented [1] ubiquitous architecture intended to provide an efficient way to perform power extraction from the cell while it is used as a sensor simultaneously.

---

## 5.1 Exploiting the Galvanic Cell's Role as Sensor and Power Source Simultaneously

Nowadays, development of self powered devices based on a single galvanic cell is a trend in energy harvesting and Point of Care (PoC) devices development research fields [2, 3]. The research is focused on solving three critical downsides of current PoC devices: their cost [4], environmental impact and autonomy. While state of the art research is making great progressions to face those downsides (development of eco friendly manufacturing materials [5] and increase of galvanic cell's power density), there is still a gap between the laboratory [6] to the real world industrial scenario [1, 7]

Two critical aspects of state of the art PoC devices need a technological proposal to overcome the gap. The first one is a procedural aspect related to the measurement *per se*. In [8] different approaches are reviewed. One of these follows a colorimetric approach using a paper based sensor [9] or a screen printed biosensor [8]. Those approaches provide a qualitative or semi quantitative readout that makes of the user's perception an unwanted actor during the result readout. Due to this, it is usually needed an external non self powered device to provide an unequivocal quantitative result [10]. The most common way to implement these colorimetric approaches is using paper based readout systems or chromatic Micropaper based Analytical Devices ( $\mu$ PADs) [11]. Although some challenges and difficulties are faced in these paper based approximations [12], some interesting approaches, like the presented in [13] based on [14], are developed. The proposed solutions expose as benefits its capability to provide a quantitative readout and its lower cost compared with silicon based solutions. Actually, the solution, that uses a chromatic  $\mu$ PAD, does not provide a quantitative readout itself. The  $\mu$ PAD needs an external non self powered device, like a camera or smartphone, and an image analysis software to provide a quantitative result. This not only constrains the scenario where the solution can be used [15]; furthermore, this increases notably the cost of the device due to the indirect cost associated to the need of additional external devices. It is very usual to see compared paper based and silicon based devices in terms of their cost omitting the different functionalities and performance that both approximations can offer (repeatability, reproducibility, reliability, etc.).

The second aspect is related to the autonomy of the device [16]. The common approach to power a PoC device is to use standard batteries or external devices, like a smartphone [17]. Different approaches are being presented based on Thermoelectric Generators (TEGs) [18], Triboelectric Nanogenerators (TENGs) [19] or Photovoltaic (PV) cells [20]. In paper based implementations exist several proposes like based on enzymatic [21] or bacteria powered [22] solutions. These approaches offer powering solutions with low power densities in the range from  $\mu\text{W cm}^{-2}$  to few  $\text{mW cm}^{-2}$  with Open Circuit Poten

tials (OCPs) in the range of mV [23]. Some OCPs and power densities for state of the art fuel cells are indicated in Table 5.1. Due to the low power and low voltage levels provided by the fuel cells usually used in biomedical applications, the common approach to develop a self powered device is the introduced in Chapter 4, where non complex electronic circuits are attached to the cell without power management. As discussed in Chapter 4, this results in poor performance as a PoC device because non quantitative result is provided, external non self powered device is need in some approaches and, usually, a continuous measurement is performed without a criteria in when the result must be read. Due to this, some researchers are adding power management functionalities to their solutions in order to overcome these drawbacks.

Table 5.1: OCPs and power densities provided by state of the art fuel cells.

Parameter	Ethanol [24]	Lactate [25]	Glucose [26]
OCP	0.93 V	0.5 V	302.1 mV
Maximum power density	1.237 mW cm <sup>-2</sup>	1.2 mW cm <sup>-2</sup>	15.96 $\mu$ W cm <sup>-2</sup>

The solution presented in [27] uses a charge pump DC/DC converter in order to extract power from a lactate based fuel cell and generate a signal related to the lactate concentration in the sample used as fuel. The approach presents two major drawbacks. Firstly, the power provided by the fuel cell is extracted without taking into consideration the efficiency of the extracted power. The second drawback is that the signal used to indicate the fuel concentration corresponds to frequency (dis)charge of an output capacitor in the charge pump. This approach requires of an external non self powered device, an oscilloscope in this case, to measure the frequency and get a result. The same approach with the same drawbacks is presented in [28] for a glucose based fuel cell. Another approaches, like the presented in [29] or [30], use Maximum Power Point Tracking (MPPT) algorithms to maximise the power extracted from the fuel cell. But these approaches only exploit the role of the fuel cell as a power source; not for sensing. When both roles are exploited, the common approach is to use more than one galvanic cell; or one that is used as a sensor or as power source alternatively, i.e., the role of the galvanic cell is time multiplexed.

As we have seen, nowadays two types of galvanic cell based self powered PoC devices are present in state of the art. The first ones perform a basic electrochemical method to measure a parameter related to the galvanic cell. In biomedical applications, usually, this parameter is the sample's concentration. They experience two major drawbacks: 1) they need an external non self powered device to provide an unequivocal quantitative result, and 2) they do not provide an indicator or a criteria in when the result must be taken during a continuous measurement. These drawbacks are overcome in the solution proposed in Chapter 4. The other type of devices adds a power management

to the system in order to increase its performance and functionalities. However, these solutions lack of a power management taking into account the efficiency with which the power is extracted. When the efficiency is taking into account, the solutions presented applies a time multiplexed approach where the fuel cell is used firstly to extract power and, once enough power is extracted, the fuel cell is used as a sensor. Thus, the role of the fuel cell as a power source and as a sensor is multiplexed. Sections 5.2 and 5.3 introduce a brief description about how a fuel cell is treated as a sensor and as a power source. Section 5.4 presents a novel ubiquitous architecture [1, 7], resulting from the strategy approaches used in Chapters 3 and 4, which provide a solution to exploit the fuel cell as a sensor and a power source simultaneously with maximum efficiency.

---

## 5.2 The Galvanic Cell as a Sensor

Fig. 5.1(a) show common polarization curves for a general purpose galvanic cell. The polarization characteristic of a cell depends on the cell's intrinsic characteristics, like materials used for its construction or its dimensions, and non intrinsic characteristics, like environmental conditions or the concentration of the sample used as electrolyte [31]. This last case is where current research is taking great efforts in order to develop new PoC devices based on galvanic cells that provide an output characteristic dependant on the concentration of a biological sample used as electrolyte.

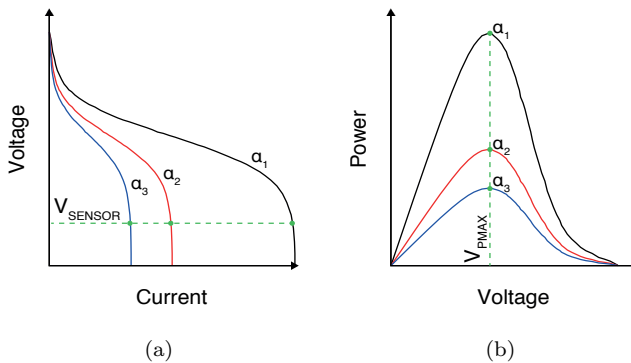


Figure 5.1: Polarization curves for a general purpose galvanic cell for concentrations  $\alpha$ ,  $\alpha_2$  and  $\alpha_3$ , being  $\alpha > \alpha_2 > \alpha_3$ . Images (a) and (b): submitted and under review for publication.

The polarization curves are normally measured carrying out a Linear Sweep Voltammetry (LSV) from cell's OCP to 0V using a slow scan rate to ensure that cell's output characteristic remains independent of the scan rate used [32]. This is repeated for several sample concentrations in order to extract the cell's transfer function. The transfer function is ideally extracted for a given Operating Point (OP) defined by a fixed polarization voltage  $V_P$ . The polarization voltage  $V_P$  is set to an optimal voltage  $V_{SENSOR}$  in terms of cell characteristics related to its role as a sensor, like sensitivity, linearity, accuracy, repeatability, etc.

---

### 5.3 The Galvanic Cell as a Power Source

In order to evaluate the performance of a galvanic cell, usually a power versus current or voltage curve is generated from the polarization curve. Again, this power versus current or voltage curve, from now on indicated as power curve, is measured for several sample concentrations in order to extract the power delivered by the cell as a function of the sample's concentration. Fig. 5.1(b) shows common power curves for a general purpose galvanic cell.

As can be seen in Fig. 5.1(b), a maximum power peak is provided by a cell for a common to all concentrations polarization voltage  $V_{P_{MAX}}$  which sets an optimal OP. Thus, to extract power with maximum efficiency from the galvanic cell's point of view, the strategy is to set the cell's OP by means of its polarization voltage  $V_P$  setting it to  $V_{P_{MAX}}$ . The efficiency from the galvanic cell's point of view  $\eta_{CELL}$  is defined as

$$\eta_{CELL} = \frac{P_P}{P_{P_{MAX}}} \quad (5.1)$$

where  $P_P$  is the power outputted by the galvanic cell at given OP and  $P_{P_{MAX}}$  the maximum power that the galvanic cell can provide in optimal OP.

---

### 5.4 Ubiquitous Self-Powered Architecture

When a galvanic cell is operated as a sensor at the laboratory, the potentiostat is the preferred instrument to carry out the pertinent electrochemical me

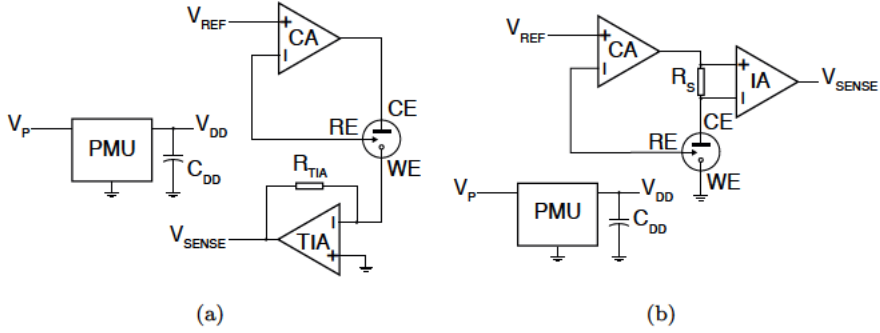


Figure 5.2: Common potentiostat architectures used for fuel cell characterization: (a) Transimpedance Amplifier and (b) Instrumentation Amplifier based current sensing. Images (a) and (b): submitted and under review for publication.

thods. The potentiostat fixes the polarization voltage of the cell to  $V_{SENSOR}$  or sweeps it using a Control Amplifier (CA), while a current sensing stage monitors the current through the cell. Multiple approaches exist to perform this last task. Two of the most used are shown in Fig. 5.2. Fig. 5.2(a) shows a potentiostat based on a Transimpedance Amplifier (TIA), basing its implementation on the virtual ground established at the Working Electrode (WE); and Fig. 5.2(b) shows a potentiostat based on Instrumentation Amplifier (IA) implementation, which measures the current outputted by the CA by means of a shunt resistor.

On the other hand, when the cell is used to extract power, a DC/DC converter is usually used. Multiple types of DC/DC converters are available which are classified firstly by their operating mode: linear or switched. Linear DC/DC converters or regulators, as their name suggest, use a linear element to set a regulator's resistance that varies according to the load in order to provide at the output a regulated voltage always lower than the input voltage. Meanwhile, switched DC/DC converters base their operation on a switching element to transform the input power to an output regulated voltage. This output voltage can be lower (buck converter), higher (boost converter) or alternatively lower/higher (buck boost converter) than the input voltage. While linear regulators provide low noise output regulated voltage at the expense of lower efficiency, switched DC/DC converters provide a more noisy output regulated voltage with high efficiency. In laboratory equipment, where power availability is not critical, a common architecture for a Power Management Unit (PMU) is a switched DC/DC converter with a linear regulator in series. This way a first huge voltage reduction is achieved with maximum efficiency while a low noise output regulated voltage is obtained from the linear regulator penalising slightly the overall PMU's efficiency.

The low power and the low voltage usually provided by a single stack cell in PoC applications are the main constrains in the design of the device. Research focused into galvanic cells solve these constrains stacking multiple cells in series (greater output voltage) or/and in parallel (greater output current). This approach presents three major drawbacks: 1) the volume of sample needed increases; 2) the polarization curve, i.e., the transfer function is devir tualized; and 3) the cost of the cell is significantly higher [33 35]. Another approach consists in designing a PMU that boosts the low voltage provided by the cell to an output regulated voltage level higher enough to power the device. Furthermore, the PMU needs to do it with a very low power consumption and maximum efficiency. Due to linear regulators are less efficient than switched converters and they provide an output regulated voltage always lower than input voltage, switched DC/DC converters are the first candidate to implement a PMU for power extraction of a galvanic cell due to its high efficiency and its capability to boost the input voltage provided by the cell to a voltage level able to power the PoC device.

Finally, in order to extract the power from the cell with maximum efficiency  $\eta_{CELL}$ , the PMU must set the polarization voltage of the cel  $V_P$  to  $V_{P_{MAX}}$  in order to set the cell's OP where maximum power is delivered.

### 5.4.1 Architecture Concept and Operation

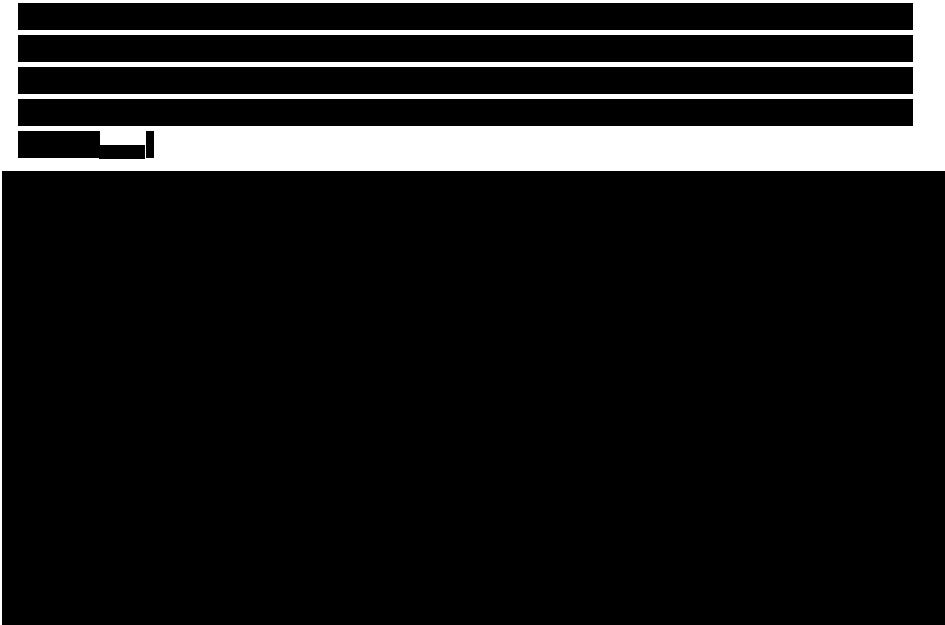


Figure 5.3: [Redacted]

[Redacted]



[REDACTED]

### 5.4.2 Prototype Implementation

#### 5.4.2.1 Galvanic cell selection and characterization

While the ubiquitous characteristic of the architecture allows it to operate with different galvanic cells, in order to select the proper implementation of each module, an application scenario must be set to know the type of galvanic cell used and its performance as a sensor and as a power source. We have



Figure 5.4: Direct Methanol Fuel Cell used to validate the ubiquitous self powered architecture. Dimensions (width x height x depth) of 65 x 85 x 34 mm. Image: from heliocentrisacademia.com.

used state of the art fuel cells in order to validate the prototype. It is a fact that is not possible to get access in a laboratory to all state of the art fuel cells to validate the ubiquity characteristic of the architecture. Due to this, we have emulated state of the art fuel cells using a Keysight B2962A Source Meter Unit (SMU). The SMU permits the precise emulation of the polarization curves available in literature. The prototype is intended to operate with galvanic cells for biomedical and industrial applications. Thus, the cells used for prototype's validation are based on ethanol, lactate and methanol. All are fuel cells. The first two are intended for biomedical applications while the methanol based fuel cell is intended for industrial applications. During validation, we have emulated the ethanol and lactate based fuel cells using the polarization curves from [24] and [25], respectively. In contrast, we have used a non emulated commercial Direct Methanol Fuel Cell (DMFC), shown in Fig. 5.4, from Heliocentris Academia purchased from Fuel Cell Store that can operate with methanol solutions with concentrations up to 1 M. Methanol (ACS grade) was purchased from ITW Reagents and used as received without further purification for sample preparation with different methanol concentrations. De ionized water obtained from a Milli Q<sup>®</sup> Advantage A10 water purification system was used for all experiments. Also, to validate the emulation based validation methodology, we have extracted the polarization curves of the DMFC using the SMU and we have emulated the DMFC to compare the data obtained with emulated and non emulated methodology. Fig. 5.5 shows the polarization and power curves extracted from literature for the emulation of the fuel cells based on ethanol [24] and lactate [25]. Fig. 5.6 shows the measured and later emulated polarization and power curves of the DMFC.

In Fig. 5.5(a) and Fig. 5.5(b), the ethanol based fuel cell exhibits an OCP of 0.900 V and a power peak for OPs where the polarization voltage  $V_P$  is

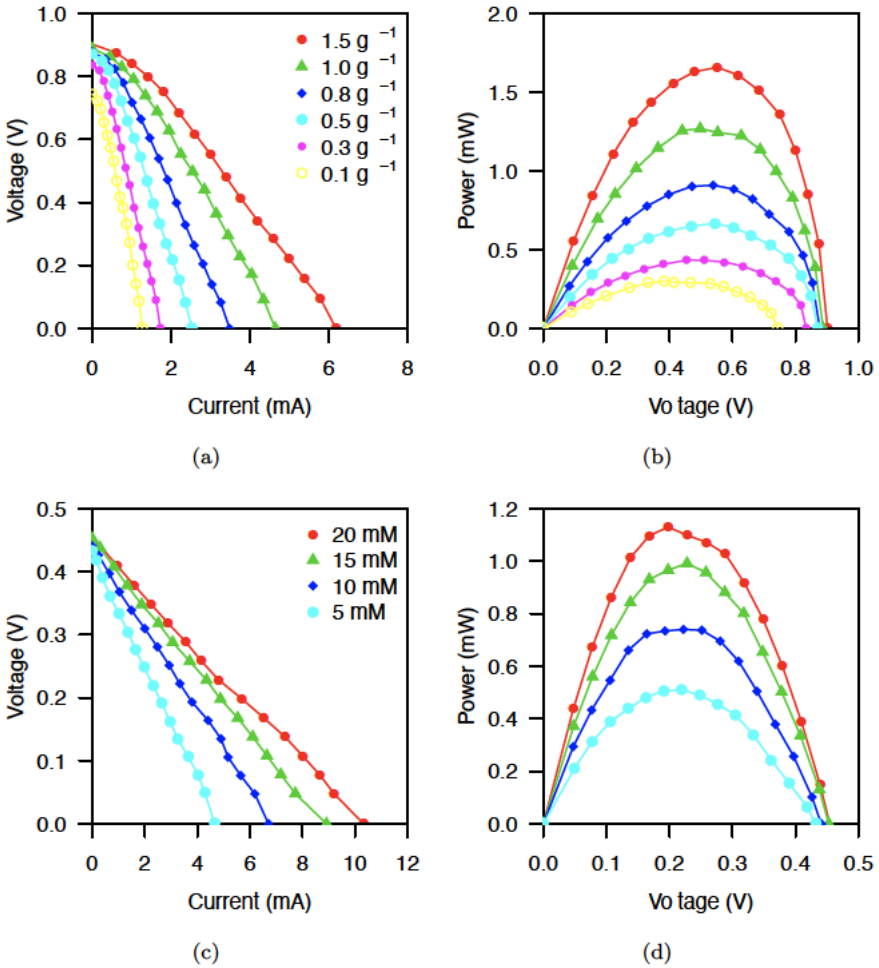


Figure 5.5: Ethanol based fuel cell's emulated (a) polarization and (b) power curves for different ethanol concentrations, and lactate based fuel cell's emulated (c) polarization and (d) power curves for different lactate concentrations. Ethanol and lactate based fuel cell's data extracted from [24] and [25], respectively.

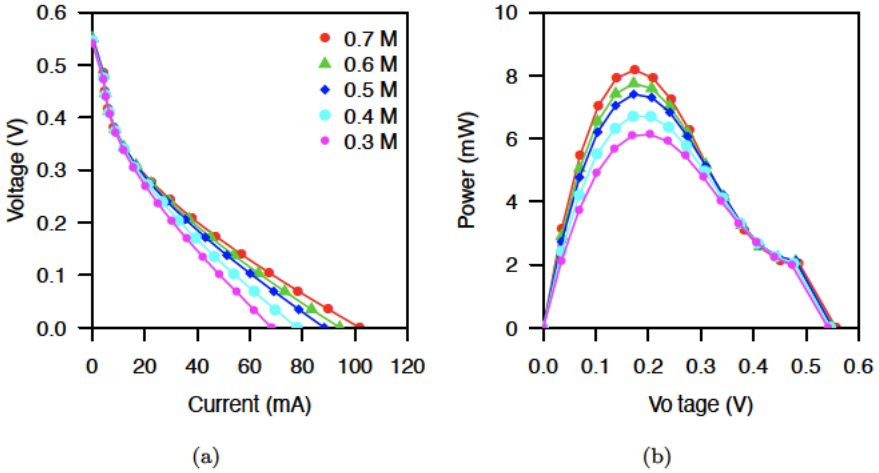


Figure 5.6: Methanol based fuel cell's measured and later emulated (a) polarization and (b) power curves for different methanol concentrations. Images (a) and (b): submitted and under review for publication.

500 mV along all concentrations. If this polarization voltage is used to extract the transfer function from the polarization curves in Fig. 5.5(a) for a concentration range from 0.1 to 1.5 g/l, a current range from 0.579 to 3.285 mA is outputted by the cell. Meanwhile, in Fig. 5.5(c) and Fig. 5.5(d), the lactate based fuel cell exhibits an OCP of 0.454 V and a power peak for OPs where the polarization voltage  $V_P$  is 225 mV along all concentrations. If this polarization voltage is used to extract the transfer function of from the polarization curves in Fig. 5.5(c) for a concentration range from 5 to 20 mM, a current range from 2.253 to 4.908 mA is outputted by the cell.

Fig. 5.6 shows the polarization and power curves of the DMFC for a concentration range from 0.3 to 0.7 M with concentration steps of 0.1 M. We can see an OCP of 0.557 V and a power peak for a polarization voltage of 200 mV along all concentrations. For this polarization voltage, the DMFC's transfer function exhibits a current range from 30.7 to 40.2 mA. The measurements were carried out, for a given concentration, waiting for the OCP stabilisation above the expected OCP of 500 mV and then performing a LSV from OCP to 0 V with a scan rate of 1 mV s<sup>-1</sup>.

#### 5.4.2.2 Architecture implementation



[REDACTED]

[REDACTED]

[REDACTED]

[REDACTED]

[REDACTED]

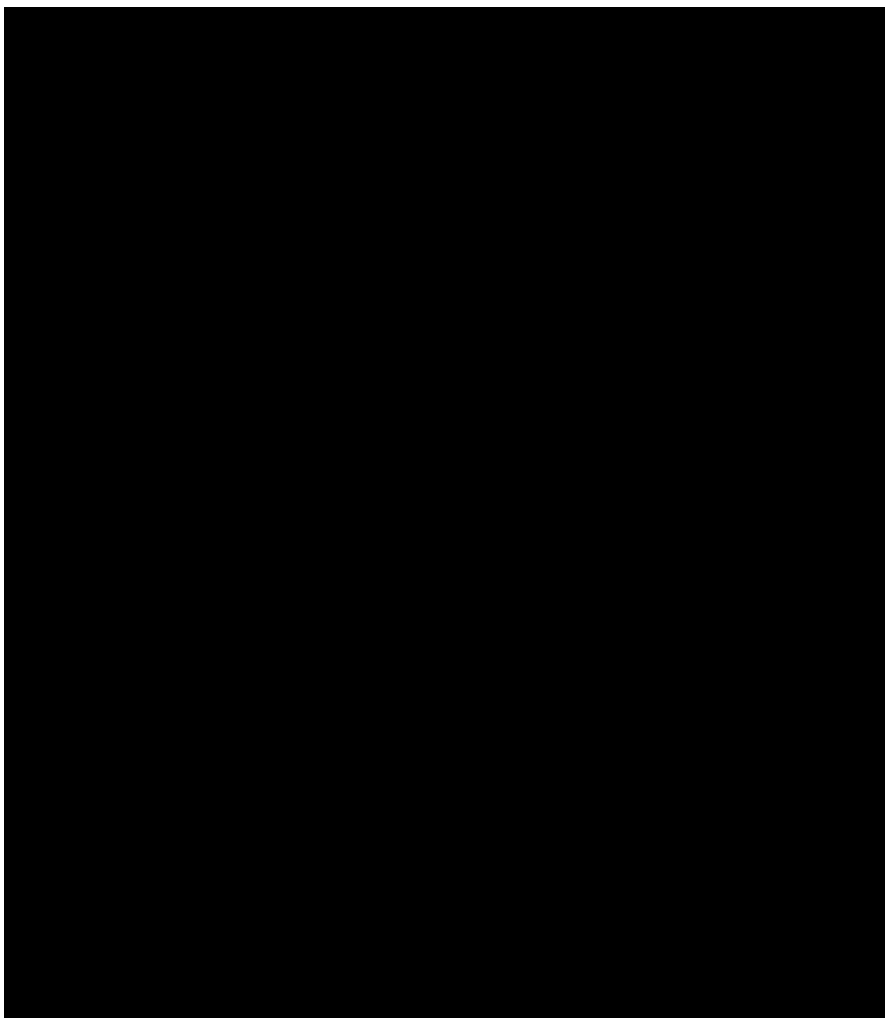


Figure 5.7: [Redacted]  
[Redacted]

[REDACTED]

[REDACTED]

[REDACTED]

[REDACTED]

[REDACTED]

[REDACTED]

[REDACTED]

[REDACTED]

[REDACTED]

[REDACTED]

[REDACTED]

[REDACTED]

[REDACTED]

[REDACTED]



[REDACTED]

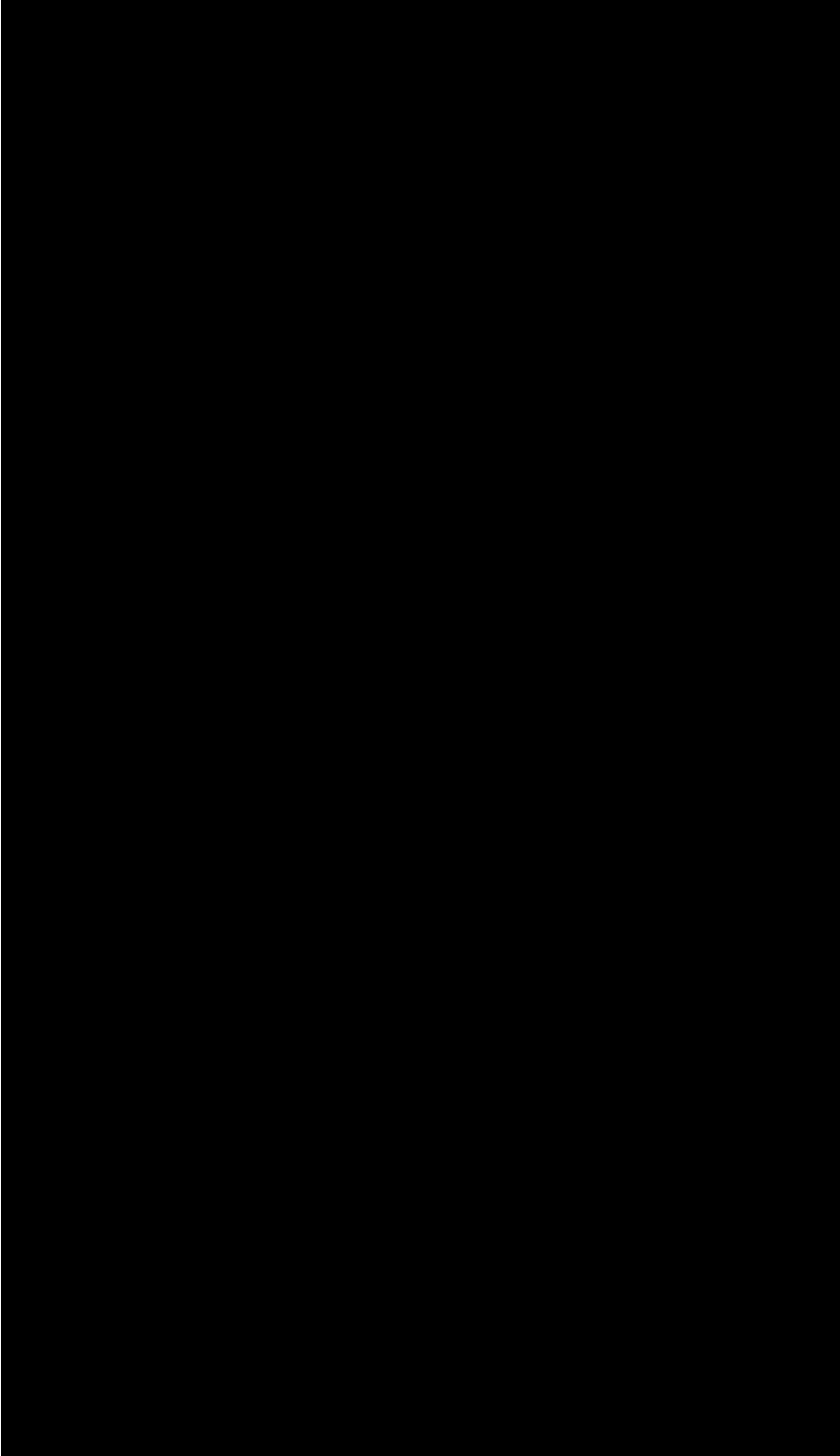


Figure 5.8:

[REDACTED]

Table 5.2: [REDACTED]

[REDACTED]

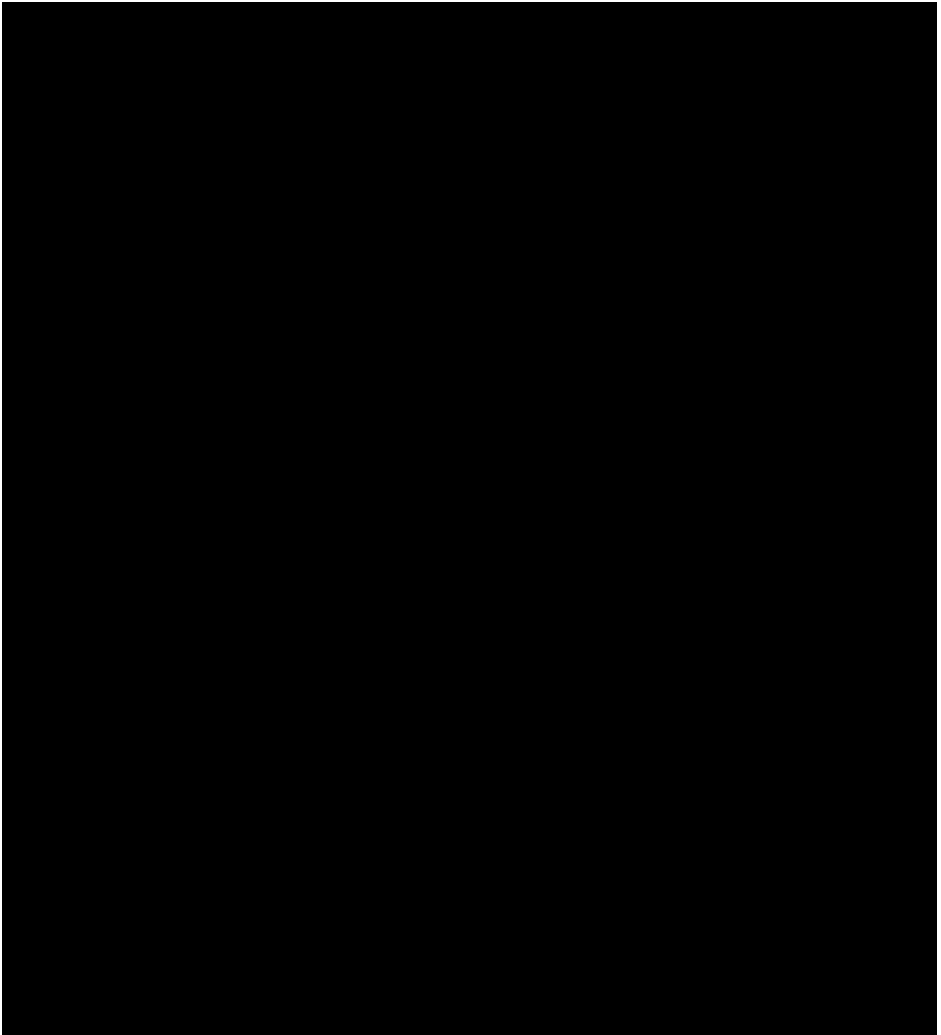


Figure 5.9: [Redacted]  
[Redacted]  
[Redacted]

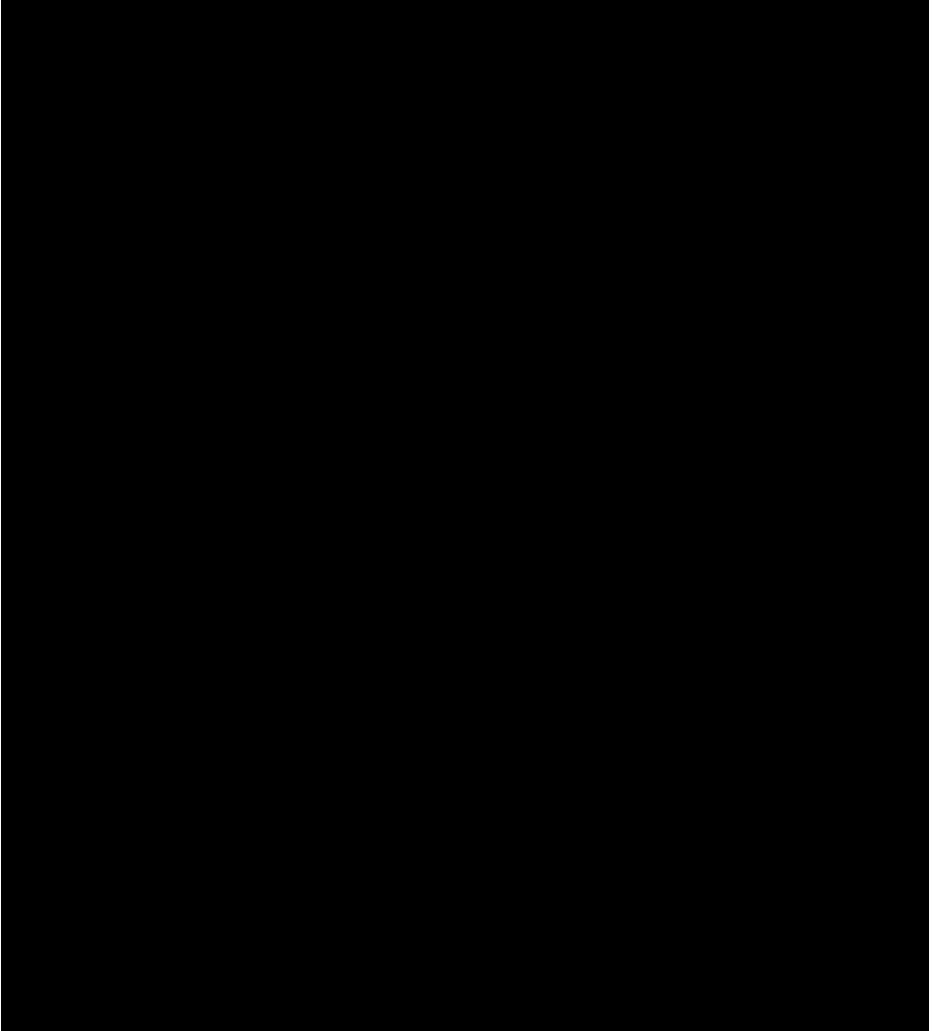


Figure 5.10: [Redacted]  
[Redacted]  
[Redacted]

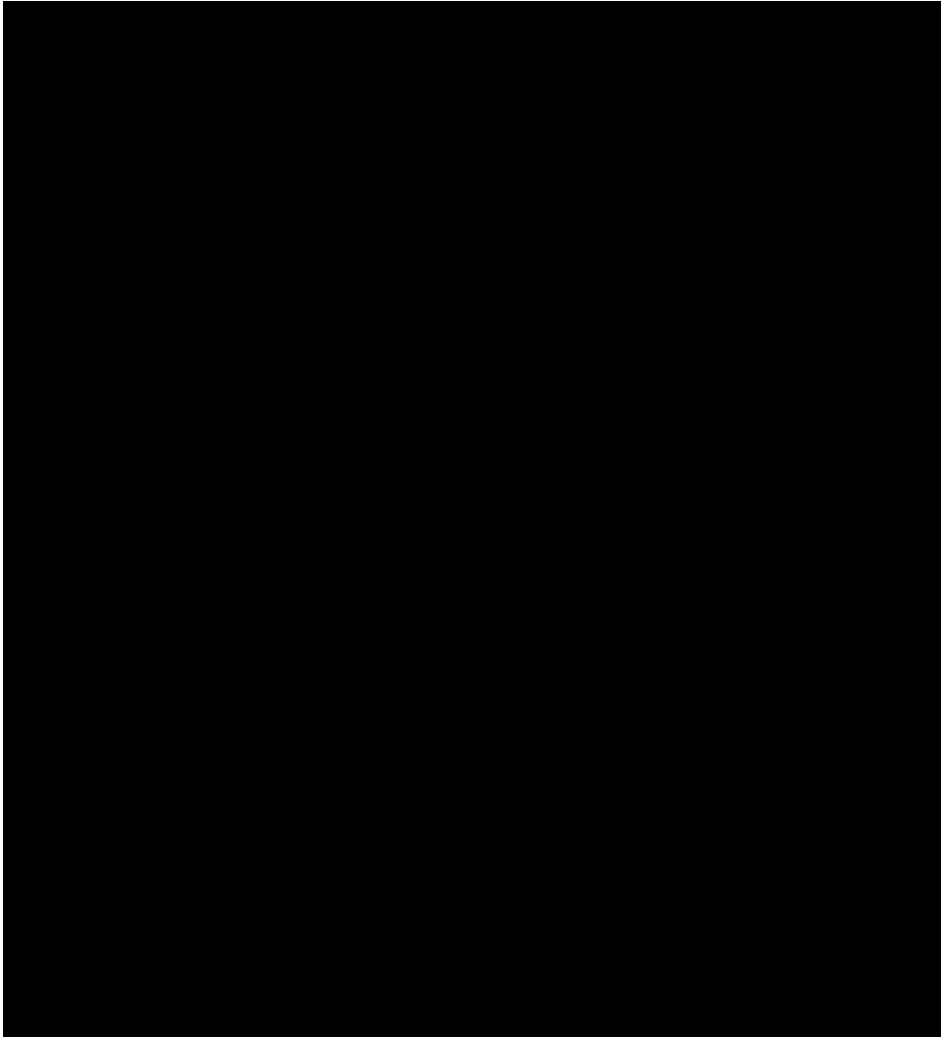


Figure 5.11: [Redacted]  
[Redacted]  
[Redacted]

## 5.5 Chapter Conclusions

This chapter presents some of the most notable state of the art developments based on a single galvanic cell. These developments use a galvanic cell as a sensor and as a power source in order to implement self powered devices.

[REDACTED]

The presented novel patent protected [1] architecture is a firm candidate to enable the development of novel galvanic cell based self powered devices.

## Acronyms

<b>CA</b>	Control Amplifier
<b>CE</b>	Counter Electrode
<b>COTS</b>	Commercial off the Shelf
<b>[REDACTED]</b>	<b>[REDACTED]</b>
<b>LCD</b>	Liquid Cristal Display
<b>LSV</b>	Linear Sweep Voltammetry
<b>IA</b>	Instrumentation Amplifier
<b>DMFC</b>	Direct Methanol Fuel Cell
<b>μPAD</b>	Micropaper based Analytical Device
<b>[REDACTED]</b>	<b>[REDACTED]</b>
<b>[REDACTED]</b>	<b>[REDACTED]</b>
<b>OCP</b>	Open Circuit Potential
<b>OP</b>	Operating Point
<b>OpAmp</b>	Operational Amplifier
<b>PMOS</b>	P channel Metal Oxide Semiconductor Field Effect Transistor
<b>PMU</b>	Power Management Unit
<b>PoC</b>	Point of Care
<b>PV</b>	Photovoltaic
<b>RE</b>	Reference Electrode
<b>SMU</b>	Source Meter Unit
<b>TEG</b>	Thermoelectric Generator
<b>TENG</b>	Triboelectric Nanogenerator
<b>TIA</b>	Transimpedance Amplifier
<b>WE</b>	Working Electrode



---

## References

- [1] A. Álvarez Carulla, P. L. Miribel Català, Y. Montes Cebrián, and J. Colomer Farrarons, “Self Powered System and Method for Power Extraction and Measurement of Energy Generator Units,” European Patent Office Patent Request EP19382604.7, July 17, 2019.
- [2] I. V. Jani and T. F. Peter, “How Point of Care Testing Could Drive Innovation in Global Health,” *The New England journal of medicine*, vol. 368, no. 24, pp. 2319–2324, 2013.
- [3] P. L. Huang, P. H. Kuo, Y. J. Huang, H. H. Liao, Y. J. J. Yang, T. Wang, Y. H. Wang, and S. S. Lu, “A Controlled Release Drug Delivery System on a Chip Using Electrolysis,” *IEEE Transactions on Industrial Electronics*, vol. 59, no. 3, pp. 1578–1587, mar 2012.
- [4] C. M. Cheng, C. M. Kuan, and C. F. Chen, “Low cost In Vitro Diagnostic Technologies,” in *In Vitro Diagnostic Devices*. Cham: Springer International Publishing, 2016, pp. 59–91.
- [5] K. Mahato, A. Srivastava, and P. Chandra, “Paper based diagnostics for personalized health care: Emerging technologies and commercial aspects,” *Biosensors and Bioelectronics*, vol. 96, pp. 246–259, oct 2017.
- [6] S. K. Vashist, P. B. Luppa, L. Y. Yeo, A. Ozcan, and J. H. T. Luong, “Emerging Technologies for Next Generation Point of Care Testing,” pp. 692–705, 2015.
- [7] A. Álvarez Carulla, Y. Montes Cebrián, M. Puig Vidal, J. Colomer Farrarons, and P. L. Miribel Català, “Ubiquitous Self Powered Architecture for FuelCell based Point of Care Applications,” *IEEE Transactions on Industrial Electronics*, submitted for publication.
- [8] L. Syedmoradi, M. Daneshpour, M. Alvandipour, F. A. Gomez, H. Hajghassem, and K. Omidfar, “Point of care testing: The impact of nanotechnology,” 2017.
- [9] Y. Xia, J. Si, and Z. Li, “Fabrication techniques for microfluidic paper based analytical devices and their applications for biological testing: A review,” pp. 774–789, 2016.
- [10] G. G. Morbioli, T. Mazzu Nascimento, A. M. Stockton, and E. Carrilho, “Technical aspects and challenges of colorimetric detection with microfluidic paper based analytical devices ( $\mu$ PADs) A review,” pp. 1–22, jun 2017.

- [11] D. D. Liana, B. Raguse, J. J. Gooding, and E. Chow, "Toward Paper Based Sensors: Turning Electrical Signals into an Optical Readout System," *ACS Applied Materials & Interfaces*, vol. 7, no. 34, pp. 19201–19209, sep 2015.
- [12] T. Akyazi, L. Basabe Desmonts, and F. Benito Lopez, "Review on microfluidic paper based analytical devices towards commercialisation," pp. 1–17, feb 2018.
- [13] M. Aller Pellitero, A. Guimerà, R. Villa, and F. J. del Campo, "iR Drop Effects in Self Powered and Electrochromic Biosensors," *The Journal of Physical Chemistry C*, vol. 122, no. 5, pp. 2596–2607, feb 2018.
- [14] M. A. Pellitero, A. Guimerà, M. Kitsara, R. Villa, C. Rubio, B. Lakard, M. L. Doche, J. Y. Hihn, and F. Javier del Campo, "Quantitative self powered electrochromic biosensors," *Chemical Science*, vol. 8, no. 3, pp. 1995–2002, feb 2017.
- [15] N. P. Pai, C. Vadnais, C. Denkinger, N. Engel, and M. Pai, "Point of care testing for infectious diseases: diversity, complexity, and barriers in low and middle income countries." *PLoS medicine*, vol. 9, no. 9, p. e1001306, 2012.
- [16] S. Choi, "Powering point of care diagnostic devices," *Biotechnology Advances*, vol. 34, no. 3, pp. 321–330, may 2016.
- [17] V. Turbé, E. R. Gray, V. E. Lawson, E. Nastouli, J. C. Brookes, R. A. Weiss, D. Pillay, V. C. Emery, C. T. Verrips, H. Yatsuda, D. Athey, and R. A. McKendry, "Towards an ultra rapid smartphone connected test for infectious diseases," *Scientific Reports*, 2017.
- [18] V. Leonov, "Thermoelectric energy harvesting of human body heat for wearable sensors," in *IEEE Sensors Journal*, vol. 13, no. 6, jun 2013, pp. 2284–2291.
- [19] H. Zhang, Y. Yang, T. C. Hou, Y. Su, C. Hu, and Z. L. Wang, "Triboelectric nanogenerator built inside clothes for self powered glucose biosensors," *Nano Energy*, vol. 2, no. 5, pp. 1019–1024, sep 2013.
- [20] S. Zhang and F. Cicoira, "Flexible self powered biosensors," *Nature*, 2018.
- [21] J. P. Esquivel, J. R. Buser, C. W. Lim, C. Domínguez, S. Rojas, P. Yager, and N. Sabaté, "Single use paper based hydrogen fuel cells for point of care diagnostic applications," *Journal of Power Sources*, vol. 342, pp. 442–451, feb 2017.
- [22] H. Lee and S. Choi, "An origami paper based bacteria powered battery with an air cathod," in *2015 Transducers 2015 18th International Conference on Solid State Sensors, Actuators and Microsystems, TRANSDUCERS 2015*. IEEE, jun 2015, pp. 1009–1012.

- [23] C. Gonzalez Solino and M. Di Lorenzo, "Enzymatic fuel cells: Towards self powered implantable and wearable diagnostics," p. 11, jan 2018.
- [24] J. Galindo de la Rosa, N. Arjona, A. Moreno Zuria, E. Ortiz Ortega, M. Guerra Balcázar, J. Ledesma García, and L. Arriaga, "Evaluation of single and stack membraneless enzymatic fuel cells based on ethanol in simulated body fluids," *Biosensors and Bioelectronics*, vol. 92, pp. 117 124, jun 2017.
- [25] A. J. Bandodkar, J. M. You, N. H. Kim, Y. Gu, R. Kumar, A. M. V. Mohan, J. Kurniawan, S. Imani, T. Nakagawa, B. Parish, M. Parthasarathy, P. P. Mercier, S. Xu, and J. Wang, "Soft, stretchable, high power density electronic skin based biofuel cells for scavenging energy from human sweat," *Energy & Environmental Science*, vol. 10, no. 7, pp. 1581 1589, jul 2017.
- [26] G. Slaughter and T. Kulkarni, "A self powered glucose biosensing system," *Biosensors and Bioelectronics*, vol. 78, pp. 45 50, 2016.
- [27] A. Baingane and G. Slaughter, "Self powered electrochemical lactate biosensing," *Energies*, vol. 10, no. 10, oct 2017.
- [28] G. Slaughter and T. Kulkarni, "Highly Selective and Sensitive Self Powered Glucose Sensor Based on Capacitor Circuit," *Scientific Reports*, vol. 7, no. 1, 2017.
- [29] M. Alaraj and J. D. Park, "Net power positive maximum power point tracking energy harvesting system for microbial fuel cell," *Journal of Power Sources*, pp. 225 232, apr 2019.
- [30] T. Yamashita, T. Hayashi, H. Iwasaki, M. Awatsu, and H. Yokoyama, "Ultra low power energy harvester for microbial fuel cells and its application to environmental sensing and long range wireless data transmission," *Journal of Power Sources*, pp. 1 11, aug 2019.
- [31] D. Shekhawat, J. J. Spivey, and D. A. Berry, *Fuel cells: technologies for fuel processing*. Elsevier, 2011.
- [32] R. P. O'Hayre, S. W. Cha, W. G. Colella, and F. B. Prinz, *Fuel cell fundamentals*. John Wiley & Sons, Inc., 2016.
- [33] L. Wang, M. He, Y. Hu, Y. Zhang, X. Liu, and G. Wang, "A "4 cell" modular passive DMFC (direct methanol fuel cell) stack for portable applications," *Energy*, vol. 82, pp. 229 235, mar 2015.
- [34] D. Fadzillah, S. Kamarudin, M. Zainoodin, and M. Masdar, "Critical challenges in the system development of direct alcohol fuel cells as portable power supplies: An overview," *International Journal of Hydrogen Energy*, vol. 44, no. 5, pp. 3031 3054, jan 2019.

- [35] R. A. Escalona Villalpando, K. Hasan, R. D. Milton, A. Moreno Zuria, L. Arriaga, S. D. Minter, and J. Ledesma García, "Performance comparison of different configurations of Glucose/O<sub>2</sub> microfluidic biofuel cell stack," *Journal of Power Sources*, vol. 414, pp. 150–157, feb 2019.
- [36] L. García Carmona, M. C. González, and A. Escarpa, "On line coupling of millimeter size motors and chronoamperometry for real time biosensing of branched chain amino acids in maple syrup urine disease clinical samples," *Sensors and Actuators, B: Chemical*, vol. 281, pp. 239–244, feb 2019.
- [37] Texas Instruments, "BQ25504 Ultra Low Power Boost Converter With Battery Management for Energy (Datasheet)," [Online]. Available: <http://ti.com/lit/ds/symlink/bq25504.pdf>. [Accessed September 12, 2019].
- [38] A. Álvarez Carulla, J. Colomer Farrarons, and P. L. Miribel, "Low Power Energy Harvesting Solutions for Smart Self Powered Sensors," in *Sensors for Diagnostics and Monitoring*. CRC Press, 2018, pp. 217–250.
- [39] A. Álvarez, M. Baffleur, J. M. M. Dilhac, J. Colomer, D. Dragomirescu, J. Lopez, M. Zhu, and P. Miribel, "Self Powered energy harvester strain sensing device for structural health monitoring," dec 2016.
- [40] A. Álvarez Carulla, J. Colomer Farrarons, J. Lopez Sanchez, P. Miribel Catala, A. Alvarez Carulla, J. Colomer Farrarons, J. Lopez Sanchez, and P. Miribel Catala, "Piezoelectric Harvester Based Self Powered Adaptive Circuit with Wireless Data Transmission Capability for Structural Health Monitoring," in *2015 Conference on Design of Circuits and Integrated Systems, DCIS 2015*. Institute of Electrical and Electronics Engineers Inc., jan 2016.
- [41] A. Álvarez Carulla, J. Colomer Farrarons, J. Lopez Sanchez, and P. Miribel Catala, "Piezoelectric Harvester based structural health monitoring that uses a self powered adaptive circuit," in *2nd IEEE International Workshop on Metrology for Aerospace*. Institute of Electrical and Electronics Engineers Inc., aug 2015, pp. 531–535.
- [42] A. Álvarez Carulla, J. Colomer Farrarons, J. López Sánchez, and P. Miribel Català, "An adaptive self powered energy harvester strain sensing device based of mechanical vibrations for structural health monitoring applications," in *2016 IEEE 25th International Symposium on Industrial Electronics (ISIE)*, vol. 2016 Novem. IEEE, nov 2016, pp. 638–644.
- [43] S. Ziegler, R. C. Woodward, H. H. C. Iu, and L. J. Borle, "Current sensing techniques: A review," *IEEE Sensors Journal*, vol. 9, no. 4, pp. 354–376, apr 2009.

- [44] Texas Instruments, “LPV521 NanoPower, 1.8 V, RRIO, CMOS Input, Operational Amplifier (Datasheet),” [Online]. Available: <http://www.ti.com/lit/ds/symlink/lpv521.pdf>. [Accessed September 13, 2019].
- [45] Linear Technology Corporation, “LT6656 Precision Series Voltage Reference (Datasheet),” [Online]. Available: [https://www.analog.com/media/en/technical\\_documentation/data\\_sheets/6656fc.pdf](https://www.analog.com/media/en/technical_documentation/data_sheets/6656fc.pdf). [Accessed September 13, 2019].
- [46] Texas Instruments, “MSP430F5529 Mixed Signal Microcontroller (Datasheet),” [Online]. Available: <http://www.ti.com/lit/ds/symlink/msp430f5529.pdf>. [Accessed September 13, 2019].
- [47] Varitronix, “VI 301 DP RC S (Datasheet),” [Online]. Available: [https://media.digikey.com/pdf/Data%20Sheets/Varitronix%20PDFs/VI\\_301.pdf](https://media.digikey.com/pdf/Data%20Sheets/Varitronix%20PDFs/VI_301.pdf). [Accessed September 13, 2019].
- [48] Texas Instruments, “CD4055B CMOS BCD to 7 Segment LCD Decoder/Driver with Display Frequency Output (Datasheet),” [Online]. Available: <http://www.ti.com/lit/ds/symlink/cd4055b.pdf>. [Accessed October 18, 2019].

# 6

---

## *Conclusions and Future Work*

---

### CONTENTS

6.1	Conclusions .....	137
6.2	Future Work .....	139
	Acronyms .....	140
	References .....	142

This last chapter summarizes the different solutions developed in this thesis, as well as their characteristics, benefits and drawbacks. In addition, the future lines of work derived from this research are described.

---

### 6.1 Conclusions

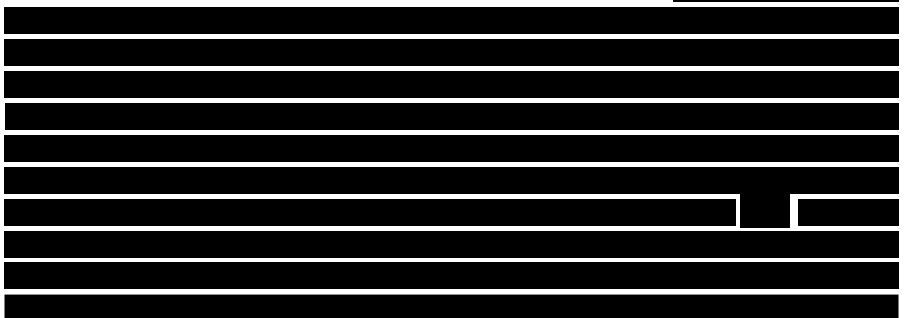
A first self powered device based on a single Piezoelectric Generator (PEG) has been presented in Chapter 2. The device, intended for Wireless Sensor Network (WSN) in Structural Health Monitoring (SHM) applications, is capable of harvesting energy and measuring the mechanical strain with the same single PEG. The solution consists of an Analog Control Unit (ACU) that fulfills two functions: 1) periodically disconnect the PEG in order to measure its Open Circuit Potential (OCP), and 2) regulate the polarization voltage of the PEG to one half of its OCP. With the OCP measurement we have an indicator of the mechanical strain suffered by the structure where it is attached. On the other hand, by regulating the polarization voltage of the PEG to one half of its OCP, we apply an Maximum Power Point Tracking (MPPT) algorithm that allows us to extract energy from the PEG with maximum efficiency. All this is achieved with a consumption of  $150\mu\text{W}$ . In addition, a back end module has been added to the device for the conversion and wireless transmission of the measurement. The transmission has a peak consumption of  $45.6\text{mW}$ . To meet these specific power requirements, the node has been provided with an adaptive super capacitor based energy storage system. The super capacitors form a configurable matrix that, modifying its total equivalent capacity, facilitates the system start up by configuring a minimum capacity, which allows a 94% shorter start up time than in the worst case, and extends its autonomy

by configuring a maximum capacity, which allows a autonomy time 2000% longer than in the worst case. The control system used to configure the matrix based on the stored energy consumes not more than 9.5  $\mu$ A. The solution has also been integrated into a monolithic solution in an Application Specific Integrated Circuit (ASIC). The correspondence between the discrete components and the components integrated in the ASIC is direct except for the need to incorporate an Analog to Digital Converter (ADC). The ADC is a 6 bit Successive Approximation Register (SAR) type with a maximum consumption of 20  $\mu$ W. This solution has been presented in [1 7].

Among the advantages of the device are the use of a single PEG as transducer both to collect energy and to perform a strain measurement, and the use of an MPPT algorithm that allows energy to be extracted from the PEG with maximum efficiency. On the other hand, it has as a disadvantage the need to disconnect the PEG to be able to measure its OCP and thus be able to measure mechanical strain and apply the MPPT algorithm. Thus, we cannot extract energy from the piezoelectric continuously.

In the third chapter, a self powered Point of Care (PoC) device for measuring blood glucose concentration has been presented. For this, two galvanic cells are used: 1) a battery to supply the system, and 2) a fuel cell to carry out the measurement. Both galvanic cells share the same biological sample as electrolyte. Thus, it is possible to overcome the disadvantage of the previous solution and the extraction of energy takes place continuously. However, this is costly due to the integration of two galvanic cells in a single test strip, and a larger sample volume required to fill both cells. This solution also has a MPPT algorithm to set the battery voltage to a fixed value and thus extract energy with maximum efficiency. The extracted energy is used to power a potentiostat intended to perform an amperometric measurement with the fuel cell. Then, the result is offered to the user through an Liquid Cristal Display (LCD). The PoC device is capable of measuring glucose concentrations from 4.8 to 30.0 mmol dm<sup>-3</sup> with a consumption of 0.912 mW. This solution has been presented in [8, 9].

A solution to reduce the number of galvanic cells to implement a self powered PoC device is presented in Chapter 4. Thought for scenarios with an extremely low available power level, the solution uses a single galvanic cell to perform both energy extraction and measurement



[REDACTED]  
[REDACTED] [REDACTED]  
[REDACTED]  
[REDACTED]  
The solution is under a process of intellectual property protection to patent it and a publication [12] is under strict embargo until the resolution of the process.

Finally, in Chapter 5, [REDACTED]  
[REDACTED]  
[REDACTED]  
[REDACTED]  
[REDACTED]  
[REDACTED]  
[REDACTED]  
[REDACTED]  
[REDACTED]  
[REDACTED]  
[REDACTED]  
[REDACTED]  
[REDACTED]  
[REDACTED]

[REDACTED] The result of the measurement is indicated to the user by means of an LCD. The device operates with a maximum consumption of 36  $\mu$ W. The solution is patent protected [13] and a publication is submitted and under review [14].

---

## 6.2 Future Work

The research carried out offers different ways to implement truly self powered devices. Each of them with its advantages and disadvantages. The use of one or other solution will be conditioned by its application and usage scenario. There are three future well defined lines of research. The first of them is to continue with the integration of the solutions developed into monolithic solutions. This seeks to improve the specifications and requirements of the devices so that they can operate with lower voltages and power consumptions. Similarly, its integration into an ASIC would facilitate its implementation in scenarios where the form factor is a critical factor. This line of work would have as its first task the validation and testing of the ASICs presented in Chapter 2 and which have already been manufactured.

The second line of work will be aimed at expanding the repertoire of EHSs types with which the solutions presented can operate, as well as different types



of galvanic cells. The first task of this line of work is focused on studying the feasibility of a device based on microbial fuel cells.

Finally, the third and most ambitious line of work would be focused on migrating these solutions outside the laboratory. For this objective, the role of companies and the industrial and private sectors is crucial. For this reason, development has been protected by patents with the intention of possessing a competitive advantage that encourages the participation of the private sector. Motivated by this ambitious objective, by the potential of the research carried out and by the acceptance received during its presentation in the Science+Partners Edition of the Fundació Bosch i Gimpera [15], this research has been presented to three calls that offer grants to the transfer of knowledge: MAQA Monitorització Autònoma de la Qualitat de l'Aigua (Llabor i Producte 2019 [16]), Monitorització Autònoma de la Qualitat de l'Aigua i la seva Comunicació (Fons per a l'Impuls de la Innovació F2I [17]) i Viabilitat Comercial de la Tecnologia (Innovadors 2019 [18]). The three projects have been awarded achieving a total financing of 209,000.00 € to work in this line and to continue with the development of the technology born in this thesis. The great acceptance of the solutions proposed by specialists from the business world and investors during the Science+Partners Edition, the patents carried out and the obtaining of grants for up to three different calls aimed at the transfer of knowledge, recognize the research of this thesis and its results as highly sophisticated and high impact technologies focused on the great social and environmental challenges of humanity.

---

## Acronyms

<b>ACU</b>	Analog Control Unit
<b>ADC</b>	Analog to Digital Converter
<b>ASIC</b>	Application Specific Integrated Circuit
<b>EHS</b>	Energy Harvesting Source
<b>LCD</b>	Liquid Cristal Display
<b>MPPT</b>	Maximum Power Point Tracking
<b>OCP</b>	Open Circuit Potential
<b>PEG</b>	Piezoelectric Generator
<b>PMU</b>	Power Management Unit

<b>PoC</b>	Point of Care
<b>SAR</b>	Successive Approximation Register
<b>SHM</b>	Structural Health Monitoring
<b>TEG</b>	Thermoelectric Generator
<b>WSN</b>	Wireless Sensor Network

---

## References

- [1] A. Álvarez Carulla, J. Colomer Farrarons, J. Lopez Sanchez, and P. Miribel Catala, "Piezoelectric Harvester based structural health monitoring that uses a self powered adaptive circuit," in *2nd IEEE International Workshop on Metrology for Aerospace*. Institute of Electrical and Electronics Engineers Inc., aug 2015, pp. 531–535.
- [2] A. Álvarez Carulla, J. Colomer Farrarons, J. López Sánchez, and P. Miribel Català, "An adaptative self powered energy harvester strain sensing device based of mechanical vibrations for structural health monitoring applications," in *2016 IEEE 25th International Symposium on Industrial Electronics (ISIE)*, vol. 2016 Novem. IEEE, nov 2016, pp. 638–644.
- [3] A. Álvarez Carulla, J. Colomer Farrarons, and P. L. Miribel, "Low Power Energy Harvesting Solutions for Smart Self Powered Sensors," in *Sensors for Diagnostics and Monitoring*. CRC Press, 2018, pp. 217–250.
- [4] A. Álvarez Carulla, J. Colomer Farrarons, J. Lopez Sanchez, P. Miribel Catala, A. Alvarez Carulla, J. Colomer Farrarons, J. Lopez Sanchez, and P. Miribel Catala, "Piezoelectric Harvester Based Self Powered Adaptive Circuit with Wireless Data Transmission Capability for Structural Health Monitoring," in *2015 Conference on Design of Circuits and Integrated Systems, DCIS 2015*. Institute of Electrical and Electronics Engineers Inc., jan 2016.
- [5] A. Álvarez, M. Baffleur, J. M. M. Dilhac, J. Colomer, D. Dragomirescu, J. Lopez, M. Zhu, and P. Miribel, "Self Powered energy harvester strain sensing device for structural health monitoring," dec 2016.
- [6] A. Alvarez Carulla, Y. Montes Cebrian, M. Puig Vidal, J. Lopez Sanchez, J. Colomer Farrarons, and P. Miribel Catala, "Energy Aware Adaptive Supercapacitor Storage System for Multi Harvesting Solutions," in *Proceedings 33rd Conference on Design of Circuits and Integrated Systems, DCIS 2018*. Institute of Electrical and Electronics Engineers Inc., apr 2019.
- [7] F. E. Mahboubi, M. Baffleur, V. Boitier, A. Alvarez, J. Colomer, P. Miribel, and J. M. Dilhac, "Self Powered Adaptive Switched Architecture Storage," in *Journal of Physics: Conference Series*, vol. 773, no. 1. Institute of Physics Publishing, dec 2016.
- [8] Y. Montes Cebrián, L. del Torno de Román, A. Álvarez Carulla, J. Colomer Farrarons, S. D. Minter, N. Sabaté, P. L. Miribel Català, and J. P. Esquivel, "Plug and Power' Point of Care diagnostics: A novel

- approach for self powered electronic reader based portable analytical devices,” *Biosensors and Bioelectronics*, vol. 118, pp. 88–96, 2018.
- [9] Y. Montes Cebrián, A. Álvarez Carulla, J. Colomer Farrarons, M. Puig Vidal, and P. L. Miribel Català, “Self Powered Portable Electronic Reader for Point of Care Amperometric Measurements,” *Sensors*, vol. 19, no. 17, p. 3715, aug 2019.
- [10] V. A. LeGrys, J. R. Yankaskas, L. M. Quittell, B. C. Marshall, P. J. Mogayzel, and Cystic Fibrosis Foundation, “Diagnostic sweat testing: the Cystic Fibrosis Foundation guidelines.” *The Journal of pediatrics*, vol. 151, no. 1, pp. 85–9, jul 2007.
- [11] P. M. Farrell, B. J. Rosenstein, T. B. White, F. J. Accurso, C. Castellani, G. R. Cutting, P. R. Durie, V. A. Legrys, J. Massie, R. B. Parad, M. J. Rock, P. W. Campbell, and Cystic Fibrosis Foundation, “Guidelines for diagnosis of cystic fibrosis in newborns through older adults: Cystic Fibrosis Foundation consensus report.” *The Journal of pediatrics*, vol. 153, no. 2, pp. S4–S14, aug 2008.
- [12] A. Álvarez Carulla, Y. Montes Cebrián, M. Puig Vidal, J. Colomer Farrarons, and P. L. Miribel Català, “Self Powered Point of Care Device for Galvanic Cell based Sample Concentration Measurement,” *IEEE Transactions on Biomedical Circuits and Systems*, under embargo.
- [13] A. Álvarez Carulla, P. L. Miribel Català, Y. Montes Cebrián, and J. Colomer Farrarons, “Self Powered System and Method for Power Extraction and Measurement of Energy Generator Units,” European Patent Office Patent Request EP19382604.7, July 17, 2019.
- [14] A. Álvarez Carulla, Y. Montes Cebrián, M. Puig Vidal, J. Colomer Farrarons, and P. L. Miribel Català, “Ubiquitous Self Powered Architecture for FuelCell based Point of Care Applications,” *IEEE Transactions on Industrial Electronics*, submitted for publication.
- [15] “La FBG vuelve a reunir a investigadores de la UB y a inversores en la quinta edición del Science + Partners Fundació Bosch i Gimpera,” [Online]. Available: <http://www.fbg.ub.edu/es/actualidad/fbg-vuelve-reunir-investigadores-ub-y-inversores-quinta-edicion-science-partners>. [Accessed July 1, 2020].
- [16] “Proposta resolució provisional en el marc de la convocatòria Llabor i Producte 2019 e TAULER Generalitat de Catalunya,” [Online]. Available: <https://tauler.seu.cat/pagDetall.do?idEdicte=243132&idens=1>. [Accessed July 1, 2020].
- [17] “Ayudas y financiación Fundació Bosch i Gimpera,” [Online]. Available: <http://www.fbg.ub.edu/es/que-hacemos/ayudas-y-financiacion>. [Accessed July 1, 2020].

- [18] “Proposta resolució provisional INNOVADORS 2019 e TAULER Generalitat de Catalunya,” [Online]. Available: <https://tauler.seu.cat/pagDetall.do?idEdicte=250117&idens=1>. [Accessed July 1, 2020].

# A

---

## Resum

---

L'autonomia energètica és una de les funcionalitats més sol·licitades en l'explosió de les aplicacions *off grid* que l'evolució digital, mitjançant paradigmes com *Internet of Things* (IoT), xarxes de nodes sensors sense fils (*Wireless Sensor Nodes* (WSN)) o *Trillion Sensors* (TSensors), comporta. La solució més socorreguda sol ser l'ús de bateries. Tanmateix, hi ha escenaris on l'ús de bateries no es pràctic, com pot ser en emplaçaments remots o entorns perillosos. A més, entre els desavantatges de fer ús de bateries, cal sumar hi l'impacte econòmic que comporta la seva substitució i manteniment a causa dels costos directes, el cost logístic i el mediambiental que passaran a ser inasumibles si realment el nombre de nodes sensors es multiplica exponencialment com apunten les revisions. És oportú, per tant, investigar i desenvolupar altres alternatives a la autonomia energètica, tant per aplicacions que la requereixin durant poc temps com per un temps prolongat.

Aquestes alternatives s'emmarquen dins del camp de recerca de la recollida d'energia o *Energy Harvesting* (EH). En aquest camp, es fa ús de transductors que converteixen en energia elèctrica l'energia disponible en el medi en diferents formes com són les energies de font tèrmica, mecànica, radio freqüència, llum o combustibles. Tot i poder extreure energia del medi mitjançant diferents transductors, actualment s'afronta el repte d'extreure aquesta energia de la manera més eficient possible per a poder extreure el màxim de potència i energia (de tal manera que es pugui incrementar ja sigui o bé la complexitat de l'electrònica o bé la seva autonomia) sota unes condicions d'operació extremes (com són tensions d'operació per sota del volt i potències que poden anar des de mil·liwatts fins a microwatts).

Aquesta tesi té com objectiu el desenvolupament de dispositius veritablement auto alimentats que no necessitin d'alimentació externa ni dispositius addicionals per a poder realitzar una mesura puntual o contínua i oferir el resultat al usuari o *host*. Les solucions presentades van desde l'àmbit del *Structural Health Monitoring* (SHM) o monitorització de la salut estructural, fins a dispositius *Point of Care* (PoC) per aplicacions biomèdiques, sent extrapolables a altres tipus d'aplicacions industrials, com la monitorització de la qualitat de l'aigua.

Es presenta un primer prototip basat en un piezoelèctric per aplicacions SHM en l'àmbit aeroespacial. Aquest primer prototip mostra una primera aproximació on es fa servir un mateix transductor per a recollir i monitoritzar energia del medi i per monitorar la deformació a la que està sotmesa l'ala d'una aeronau.

L'energia és recol·lectada de les vibracions mecàniques de l'ala. Aquest prototip, a més, utilitza una unitat de control analògica de baix consum per extraure energia de manera eficient mitjançant un algoritme de monitoratge del punt de potència màxima o *Maximum Power Point Tracking* (MPPT). La solució també incorpora un sistema d'emmagatzament d'energia basat en super capacitats per atendre els pics de consum puntuals del transmissor sense fils, utilitzat per donar sortida a la mesura, i per dotar de major autonomia al node. Per últim, també s'ha dissenyat un convertidor analògic digital (ADC) tipus SAR per a poder integrar tot el sistema en una solució monolítica.

Els següents desenvolupaments es centren en solucions basades en cel·les galvàniques tant per aplicacions biomèdiques (dispositius PoC) com per aplicacions industrials. Tres prototips neixen d'aquests desenvolupaments. El primer d'ells utilitza dos cel·les galvàniques per a implementar un dispositiu PoC auto alimentat per a la mesura de la concentració de glucosa en sang. Una primera cel·la es fa servir per alimentar l'electrònica del sistema i una segona cel·la per a realitzar la mesura *per se*. La mostra de sang s'utilitza com a electrolit comú per ambdues cel·les. L'extracció d'energia es realitza de manera eficient mitjançant l'ús d'un algoritme MPPT.

El segon i tercer prototips es basen en l'ús d'una sola cel·la galvànica per a que pugui operar el sistema. El primer d'ells no utilitza algorismes MPPT i està pensat per escenaris amb nivells d'energia disponibles extremadament baixos. El segon, a més, incorpora l'ús d'un algoritme MPPT per extreure l'energia amb màxima eficiència. Ambdues solucions es troben protegides per processos de protecció intel·lectual, per lo que no es pot descriure la seva implementació en aquest resum. Les solucions es van presentar, sota acord de confidencialitat, a la 5<sup>a</sup> Edició Science+Partners organitzat per la Fundació Bosch i Gimpera on personalitats del món de l'empresa i inversors van mostrar el seu interès per la tecnologia presentada. Fruit d'aquesta recerca, han estat concedits tres projectes dedicats a la transferència de coneixement per a continuar amb el desenvolupament d'aquestes tecnologies.

# B

## Certificat de Procés de Protecció



**Bosch i Gimpera**  
UNIVERSITAT DE BARCELONA

Barcelona, 25 de juny de 2020

Maria Carme Verdaguer Montanyà amb DNI 77288064Z, com a directora general de la Fundació Bosch i Gimpera (FBG), Centre de Transferència de Coneixement, Tecnologia i Innovació de la Universitat de Barcelona (UB), amb domicili social en Barcelona, carrer Baldri Reixac, 4-8 i NIF G08906653

### CERTIFICA

Que l'Àrea de Valorització i Llicències de l'FBG ha rebut les següents propostes de nova invenció per ser avaluades en col·laboració amb el Centre de Patents de la UB:

- Proposta 2018-48, "*Self-powered system and method for power extraction and measurement of energy generator units*", que han estat objecte de protecció a través d'una sol·licitud de patent europea (número de sol·licitud EP19382604.7, data de presentació 17-07-2019) amb la UB com a únic sol·licitant i amb Albert Álvarez Carulla, Pedro Luis Miribel Català, Yaiza Montes Cebrián i Jordi Colomer Farrarons com a inventors. [Codi intern UBTT0363]

- Proposta 2019-42, "*Self-Powered Event-Detector System for self-polarization of the Energy Unit Cell, and determination of the moment of measurement*", amb Albert Álvarez Carulla, Pedro Luis Miribel Català, Yaiza Montes Cebrián, Jordi Colomer Farrarons i Manel Puig Vidal com a inventors.

Que la patentabilitat i el potencial comercial dels referits resultats estan essent analitzats actualment per part d'un equip de treball creat a tal efecte per a la seva valorització i transferència a la Indústria.

Que els referits resultats formen part de la tesi doctoral anomenada "Energy Harvesting Solutions for Self-Powered Devices: From Structural Health Monitoring to Biomedical Applications" desenvolupada per Albert Álvarez Carulla sota la direcció del Dr. Pedro Luis Miribel Català i del Dr. Jordi Colomer Farrarons.

Que, amb l'objectiu que la protecció i transferència d'aquests resultats no es vegin afectats pel dipòsit, defensa i publicació de la mencionada tesi doctoral, es recomana seguir els procediments descrits a l'article 38 de la Normativa Reguladora del Doctorat a la Universitat de Barcelona (aprovada pel Consell de Govern en sessió de 16 de març de 2012 i modificada pel Consell de Govern de data 22 de juliol de 2019).

I perquè així consti als efectes oportuns, signo aquest certificat a petició de l'interessat.

77288064Z M. Firmado digitalmente  
por 77288064Z M.  
CARME  
VERDAGUER (R: G08906653)  
Fecha: 2020.06.25  
(R: G08906653) 16:16:32 +02'00'

M. Carme Verdaguer Montanyà  
Directora general Fundació Bosch i Gimpera





# C

---

## List of Patents & Publications

---

### CONTENTS

C.1	Patents .....	149
C.2	Journals .....	149
C.3	Books Chapters .....	152
C.4	Conferences proceedings .....	152

---

### C.1 Patents

<b>Authors</b>	<u>A. Álvarez Carulla</u> , P. L. Miribel Català, Y. Montes Cebrián, J. Colomer Farrarons
<b>Title</b>	Self Powered System and Method for Power Extrac- tion and Measurement of Energy Generator Units
<b>Patent country</b>	European Patent Office
<b>Patent number</b>	EP19382604.7
<b>Registration date</b>	July 17, 2019
<b>State</b>	Patent Request

---

<b>Authors</b>	<u>A. Álvarez Carulla</u> , P. L. Miribel Català, Y. Montes Cebrián, and J. Colomer Farrarons, and M. Puig Vidal
<b>Title</b>	Self Powered Event Detector System for Self Polar- ization of the Energy Unit Cell, and Determination of the Moment of Measurement (provisional)
<b>Patent country</b>	European Patent Office
<b>State</b>	Writing in progress

## C.2 Journals

**Authors** Albert Álvarez Carulla, Yaiza Montes Cebrián,  
Manel Puig Vidal, Jordi Colomer Farrarons,  
and Pere Ll. Miribel Català

**Title** Ubiquitous Self Powered Architecture for Fuel Cell based Point of Care Applications

**Journal** IEEE Transactions on Industrial Electronics

**Year** 2020 **State** Submitted

**Authors** Albert Álvarez Carulla, Yaiza Montes Cebrián,  
Manel Puig Vidal, Jordi Colomer Farrarons,  
and Pere Ll. Miribel Català

**Title** Self Powered Point of Care Device for Galvanic Cell based Sample Concentration Measurement

**Journal** IEEE Transactions on Biomedical Circuits and Systems

**Year** 2020 **State** Under embargo until patent request

**Authors** Yaiza Montes Cebrián, Albert Álvarez Carulla,  
Jordi Colomer Farrarons, Manel Puig Vidal,  
and Pere Ll. Miribel Català

**Title** Self Powered Portable Electronic Reader for Point of Care Amperometric Measurements

**Journal** Sensors

**Volume** 19 **Number** 17 **Year** 2019 **ISSN** 1424 8220

**Authors** Yaiza Montes Cebrián, Lorena del Torno de Román,  
Albert Álvarez Carulla, Jordi Colomer Farrarons,  
Shelley D. Minter, Neus Sabaté, Pere Ll. Miribel Català,  
and Juan Pablo Esquivel

**Title** 'Plug and Power' Point of Care diagnostics: A Novel Approach  
for Self Powered Electronic Reader based Portable Analytical  
Devices

**Journal** Biosensors and Bioelectronics

**Volume** 118 **Year** 2018 **Pages** 88-96 **ISSN** 0956-5663

---

**Authors** Albert Álvarez Carulla, M. Baffleur, J. M. Dilhac,  
Jordi Colomer Farrarons, D. Dragomirescu, Jaime López Sánchez,  
M.Zhu, and Pere Ll. Miribel Català

**Title** Self Powered Energy Harvester Strain Sensing Device for Struc-  
tural Health Monitoring

**Journal** IOP Publishing Journal of Physics: Conference Series

**Volume** 773 **Number** 1 **Year** 2016 **DOI** 10.1088/1742-6596/773/1/012070

---

**Authors** F. ElMahboubi, M. Baffleur, V. Boitier, Albert Álvarez Carulla,  
Jordi Colomer Farrarons, Pere Ll. Miribel Català,  
and J. M. Dilhac

**Title** Self Powered Adaptive Switched Architecture Storage

**Journal** IOP Publishing Journal of Physics: Conference Series

**Volume** 773 **Number** 1 **Year** 2016 **DOI** 10.1088/1742-6596/773/1/012103

### C.3 Books Chapters

**Authors** Albert Álvarez Carulla, Jordi Colomer Farrarons,  
and Pere Ll. Miribel Català

**Title** Low Power Energy Harvesting Solutions for Smart Self Powered  
Sensors

**Book title** Sensors for Diagnostics and Monitoring

**Publisher** CRC Press

**Pages** 217-250 **Year** 2018 **ISBN** 9780815370208

---

### C.4 Conferences proceedings

**Authors** Albert Álvarez Carulla, Yaiza Montes Cebrián,  
Manel Puig Vidal, Jaime López Sánchez,  
Jordi Colomer Farrarons, and Pere Ll. Miribel Català

**Title** Energy Aware Adaptive Supercapacitor Storage System for  
Multi Harvesting Solutions

**Conference** IEEE Design of Circuits and Integrated Systems (DCIS)

**Location** Lyon, France **Date** Nov. 14-16, 2018 **ISSN** 2640-5563  
**ISBN** 978-1-7281-0171-2

---

**Authors** Yaiza Montes Cebrián, Albert Álvarez Carulla,  
Jordi Colomer Farrarons, Manel Puig Vidal,  
Jaime López Sánchez, and Pere Ll. Miribel Català

**Title** A Fuel Cell based Adaptable Self Powered Event Detection  
Platform Enhanced for Biosampling applications

**Conference** IEEE Design of Circuits and Integrated Systems (DCIS)

**Location** Lyon, France **Date** Nov. 14-16, 2018 **ISSN** 2640-5563  
**ISBN** 978-1-7281-0171-2

**Authors** F. El Mahboubi, M. Baffleur, V. Boitier, A. Álvarez, J. Colomer, P. Miribel, and J M. Dilhac

**Title** Self Powered Adaptive Switched Architecture Storage

**Conference** International Conference on Micro and Nanotechnology for Power Generation and Energy Conversion Applications (PowerMEMS)

**Journal** IOP Publishing Journal of Physics: Conference Series

**Location** Paris, France **Date** Sep. 12, 2016 **Volume** 773

**DOI** 10.1088/1742 6596/773/1/012103

---

**Authors** A. Álvarez, M. Baffleur, J M. Dilhac, J. Colomer, D. Dragomirescu, J. López, M. Zhu, and P. Miribel

**Title** Self Powered Energy Harvester Strain Sensing Device for Structural Health Monitoring

**Conference** International Conference on Micro and Nanotechnology for Power Generation and Energy Conversion Applications (PowerMEMS)

**Journal** IOP Publishing Journal of Physics: Conference Series

**Location** Paris, France **Date** Sep. 12, 2016 **Volume** 773

**DOI** 10.1088/1742 6596/773/1/012070

---

**Authors** Albert Álvarez Carulla, Jordi Colomer Farrarons, Jaime López Sánchez, and Pere Ll. Miribel Català

**Title** An Adaptive Self Powered Energy Harvester Strain Sensing Device based of Mechanical Vibrations for Structural Health Monitoring Applications

**Conference** IEEE International Symposium on Industrial Electronics (ISIE)

**Location** Santa Clara, CA, USA **Date** Jun. 8 10, 2016 **ISSN** 2163 5145

**ISBN** 978 1 5090 0873 5

**Authors** Albert Álvarez Carulla, Jordi Colomer Farrarons,  
Jaime López Sánchez, and Pere Ll. Miribel Català

**Title** Piezoelectric Harvester based Self Powered Adaptive Circuit  
with Wireless Data Transmission Capability for Structural  
Health Monitoring

**Conference** IEEE Design of Circuits and Integrated Systems (DCIS)

**Location** Estoril, Portugal **Date** Nov. 25 27, 2015  
**ISBN** 978 1 4673 7228 2

---

**Authors** Albert Álvarez Carulla, Jordi Colomer Farrarons,  
Jaime López Sánchez, and Pere Ll. Miribel Català

**Title** Piezoelectric Harvester based Structural Health Monitoring  
that Uses a Self Powered Adaptive Circuit

**Conference** IEEE Metrology for Aerospace (MetroAeroSpace)

**Location** Benevento, Italy **Date** Jun. 4 5, 2015 **ISBN** 978 1 4799 7569 3

# D

---

## *Patent & Journal Publications*

---

### CONTENTS

European Patent Office: Self Powered System and Method for Power Extraction and Measurement of Eenergy Generator Units .....	156
Ubiquitous Self Powered Architecture for Fuel Cell based Point of Care Applications .....	184
Self Powered Point of Care Device for Galvanic Cell based Sample Concentration Measurement .....	194
Biosensors & Bioelectronics: 'Plug and Power' Point of Care Diagnostics: A Novel Approach for Self Powered Electronic Reader based Portable Analytical Devices .....	202
Sensors: Self Powered Portable Electronic Reader for Point of Care Amperometric Measurements .....	212
IOPscience (PowerMEMS): Self Powered Adaptive Switched Architecture Storage .....	228
IOPscience (PowerMEMS): Self Powered Energy Harvester Strain Sensing Device for Structural Health Monitoring .....	232













































































































## 'Plug-and-Power' Point-of-Care diagnostics: A novel approach for self-powered electronic reader-based portable analytical devices

Yaiza Montes Cebrián<sup>a,\*</sup>, Lorena del Torno de Román<sup>b</sup>, Albert Álvarez Carulla<sup>a</sup>, Jordi Colomer Farrarons<sup>a</sup>, Shelley D. Minter<sup>c</sup>, Neus Sabatè<sup>b,d,e</sup>, Pere Ll. Miribel Català<sup>a</sup>, Juan Pablo Esquivel<sup>b</sup>

<sup>a</sup>Discrete to Integrated (D2I) Research Group, Department of Electronic and Biomedical Engineering, Faculty of Physics, University of Barcelona (UB), 1st Marí i Franqués St., 08028 Barcelona, Spain

<sup>b</sup>Instituto de Microelectrónica de Barcelona IMB CNM (CSIC), C/ del Tíllers, Campus Universitat Autònoma de Barcelona (UAB), 08193 Bellaterra, Barcelona, Spain

<sup>c</sup>Department of Chemistry, University of Utah, 315 S 1400 E Room 2020, Salt Lake City, UT 84112, USA

<sup>d</sup>Catalan Institution for Research and Advanced Studies (ICREA), Passeig Lluís Companys 23, 08010 Barcelona, Spain

<sup>e</sup>Fuelium, Av. De Can Domenech Edifici Eureka, Campus de la UAB, 08193 Bellaterra, Barcelona, Spain



### ARTICLE INFO

#### Keywords:

Plug and Power  
Self powered  
Paper based  
Glucometer  
Low power electronics

### ABSTRACT

This paper presents an innovative approach in the portable Point-of-Care diagnostics field, the Plug-and-Power concept. In this new disposable sensor and plug-and-play reader paradigm, the energy required to perform a measurement is always available within the disposable test component. The reader unit contains all the required electronic modules to run the test, process data and display the result, but does not include any battery or power source. Instead, the disposable part acts as both the sensor and the power source. Additionally, this approach provides environmental benefits related to battery usage and disposal, as the paper-based power source has non-toxic redox chemistry that makes it eco-friendly and safe to follow the same waste stream as disposable test strips. The feasibility of this Plug-and-Power approach is demonstrated in this work with the development of a self-powered portable glucometer consisting of two parts: a test strip including a paper-based power source and a paper-based biofuel cell as a glucose sensor; and an application-specific battery-less electronic reader designed to extract the energy from the test strip, process the signal provided and show the glucose concentration on a display. The device was tested with human serum samples with glucose concentrations between 5 and 30 mM, providing quantitative results in good agreement with commercial measuring instruments. The advantages of the present approach can be extended to any kind of biosensors measuring different analytes and biological matrices, and in this way, strengthen the goals of Point-of-Care diagnostics towards laboratory decentralization, personalized medicine and improving patient compliance.

### 1. Introduction

Point of Care (POC) diagnostics have been proving their benefits in public global health over centralized laboratory diagnostics as they remove the constraints of requiring large healthcare infrastructures, complex medical equipment and well-trained technicians. POC devices allow monitoring of health conditions, reducing medical costs, as well as controlling infectious outbreaks, without the need of dedicated laboratory equipment. In addition, these devices offer the advantages of rapid results and patient proximity (Chan et al., 2017; Choi, 2016;

Drain et al., 2014; Wang et al., 2016a; Zarei, 2017; Yager et al., 2006). The development of portable POC diagnostics pursues the characteristics defined by the World Health Organization in the acronym AS-SURED (affordable, sensitive, specific, user-friendly, rapid and robust, equipment free, and deliverable to users) to provide suitable solutions to even the lowest-resource global health settings (Fu et al., 2011). Despite the many advances in the field, equipment-free POC diagnostic devices still face important challenges related to reliability. The use of an electronic reader allows overcoming this aspect, as it provides an unambiguous qualitative/quantitative result of an assay and can

\* Corresponding author.

E-mail addresses: [ymontes@ub.edu](mailto:ymontes@ub.edu) (Y. Montes-Cebrián), [lorena.deltorno@imb-cnm.csic.es](mailto:lorena.deltorno@imb-cnm.csic.es) (L. del Torno-de Román), [albertalvarez@ub.edu](mailto:albertalvarez@ub.edu) (A. Álvarez-Carulla), [jcolomer@ub.edu](mailto:jcolomer@ub.edu) (J. Colomer-Farrarons), [minter@chem.utah.edu](mailto:minter@chem.utah.edu) (S.D. Minter), [nsabat@fuelium.tech](mailto:nsabat@fuelium.tech) (N. Sabatè), [peremirbelcatala@ub.edu](mailto:peremirbelcatala@ub.edu) (P.L. Miribel-Català), [juanpablo.esquivel@csic.es](mailto:juanpablo.esquivel@csic.es) (J.P. Esquivel).

<https://doi.org/10.1016/j.bios.2018.07.034>

Received 3 May 2018; Received in revised form 13 July 2018; Accepted 16 July 2018

Available online 18 July 2018

0956-5663/© 2018 Elsevier B.V. All rights reserved.



improve the sensitivity and the limit of detection.

The reader-disposable approach is predominantly used in the POC devices commercially available, and it is still the one mostly followed by initiatives undergoing research and development phases (Chin et al., 2012; Gervais et al., 2011; Zarei, 2017). These devices consist on a reusable electronic reader unit and a disposable part in the form of a strip, cartridge or card. The disposable test strip is used to collect the sample and transport it to the biosensor where the measurement is performed. After a single use, this strip is discarded avoiding cross-contamination. Depending on the detection principle and sample matrix to be detected, portable readers may also perform a variety of functions including for example sample pretreatment, hydraulic controls, heating, timing, light sources, photodetectors, electrochemical instrumentation, Radio frequency communications and, in most cases, displays as the interface between the device and the user to set up the test and show the result.

An example is the system presented by (Cruz et al., 2014). The authors present an approach capable of performing cyclic voltammetry for electrochemical immunosensing of cortisol. In contrast to the device presented here, the reported approach is not self-powered and, moreover, it does not have a custom-made design for the application since it uses a commercial miniaturized potentiostat on an evaluation board. However, the developed prototype is low-cost, portable and the analog front-end is based on a transimpedance amplifier (TIA).

To perform these functions, portable readers require a source of electrical power. This need has been fulfilled with either primary or secondary batteries. Regardless of their autonomy, batteries must be replaced or recharged periodically to maintain the device operation. This may seem a simple task in developed regions with reliable electric power grids and ubiquitous battery supplies. However, it can be quite challenging in low-resource settings, which is precisely where this kind of portable diagnostic devices are needed the most. Additionally, uncontrolled disposal of used batteries is becoming a severe problem in such regions of the world, as there is not only a lack of environmental regulations but also proper recycling facilities (Widmer et al., 2005; Larcher and Tarascon, 2015; Ongondo et al., 2011).

This paper presents a novel solution to the power requirements in the portable diagnostics field, the Plug-and-Power concept. We propose a plug-and-play reader-disposable device in which the energy required to perform a single test is always available within the disposable test component. In this case, the reader unit contains all the required electronic systems to run the test, including a display to visualize the result, but does not include any battery or power source. Instead, the disposable part acts as both the sensor and the power source. Additionally, this approach provides environmental benefits related to battery usage and disposal. The paper-based power source used for this approach has non-toxic redox chemistry that makes it eco-friendly and safe to follow the same waste stream as the disposable test strip or cartridge, including incineration, a typical outcome of those components that have been in contact with biological samples. The operation of this device, from the user perspective, is the same as for a conventional device, with the added advantage of not worrying about recharging it or where to recycle the used batteries. This approach strengthens the goals of Point-of-Care diagnostics towards laboratory decentralization, personalized medicine and improving patient compliance.

The applicability of this novel approach is demonstrated with the development of a self-powered portable blood glucometer, one of the Point-Of-Care applications that is already well-established in the market. Although many methods of glucose monitoring have been proposed (Fischer et al., 2016; Kulkarni and Slaughter, 2017; Lee et al., 2017; Narvaez Villarrubia et al., 2016; Slaughter and Kulkarni, 2016), the most widely used by both patients and healthcare professionals are the portable blood glucometers, as they are small, inexpensive, rapid and user-friendly (Wang et al., 2016a; Wang et al., 2016b; Zarei, 2017). These advantages are maintained in the presented Plug-and-Power

prototype, which consists of two parts: a test strip including a paper-based power source and a paper-based bio-fuel cell as the glucose sensor; and an application-specific battery-less electronic reader designed to extract the energy from the test strip, sample and process the signal provided by it and display the glucose concentration in the sample on a digital display.

## 2. Device concept and operation

The design and operation of the presented device resembles that of a typical commercial handheld glucometer, consisting of two parts: a disposable test strip and an electronic reader. However, this device introduces a new approach based on two main features: 1) the disposable test strip generates the electrical power used by the electronic reader to perform a measurement, and 2) the glucose concentration is measured by the reader from the output signal of a bio fuel cell, rather than using a classical solution based on a three-electrode configuration electrochemical cell.

The whole system is compact, lightweight and portable. The battery-less electronic reader has a size of  $85.0 \times 42.0 \times 21.0$  mm, while the disposable test strip has a size of  $20.0 \times 25.0 \times 1.8$  mm. From a user point of view, the device is easy to operate, as shown in Fig. 1. First, the strip is introduced in the reader. Then, the user adds the sample to the inlet of the test strip. Finally, the user can read the result of the test in the display of the smart electronic reader. After the measurement, the test strip can be safely discarded, while the electronic reader can be reused indefinitely for subsequent measurements.

The internal operation of the device can also be seen in Fig. 1. Once the liquid sample is added to the test strip, it flows by capillary action through a piece of paper. The sample diverges towards both ends of the paper, reaching on one side the power source, and on the other side, the sensor. The liquid activates the power source and the produced energy wakes up the electronic circuit in the reader. Then, the electronics regulate the power to a suitable working voltage of up to 3 V for the instrumentation. Afterwards, the circuit performs an amperometric glucose measurement using the sensor. The signal measured from the sensor is converted and processed to, finally, show on a display the quantitative result of glucose concentration contained in the sample.

### 2.1. Paper-based test strip

The disposable test strip is composed by two main components, a paper-based power source and a paper-based bio fuel cell acting as a glucose sensor. The components share a single paper strip of  $5 \times 20$  mm that receives the sample in its middle zone and diverges it towards both ends. Fig. 2a shows a picture of the disposable test strip and Fig. 2b depicts an exploded view of its main components.

The paper-based power source has been customized by Fuelium Company for this application based on one of their batteries models LF55. This paper-based power source is composed of a paper membrane placed in contact with two electrodes. The proprietary electrode technology contains no heavy metals nor other toxic components, so it does not require special disposal considerations after its use. The batteries are only activated upon addition of an aqueous sample and provide a steady power output after being activated by either deionized water (D.I.) water or any physiological fluid such as plasma, serum, saliva, sweat or urine. Since these batteries only start their operation after activation with the liquid sample, they do not suffer from self-discharge during storage so their shelf life complies with the requirements of diagnostics test kits. For this application, the electrodes have been placed on top and bottom sides of a paper strip and the power source has been adjusted to provide an output voltage of 1.5 V and a minimum power of 10 mW for at least 20 min after being activated with a serum sample with a minimum volume of 12.5  $\mu$ L.

Instead of using a sensor based on a typical three-electrode configuration electrochemical cell, the glucose concentration is measured

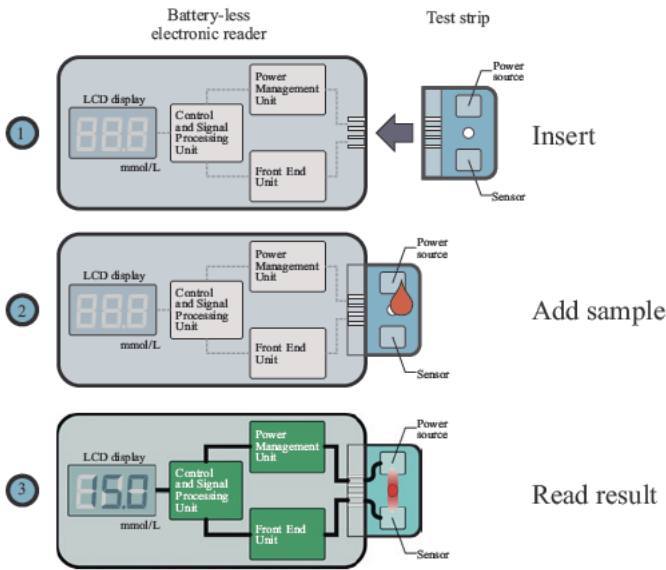


Fig. 1. Operation of Plug-and-Power Point-of-Care diagnostics device.

from the output signal of a paper-based enzymatic fuel cell. The device is composed of a glucose dehydrogenase (GDH) anode and a bilirubin oxidase (BOX) cathode placed on both sides of the paper strip. The fuel cell provides a response in power output that is proportional to the glucose concentration in the sample. This sensing method based in fuel cells response is used, for example, in many commercial breath alcoholmeters, known as breathalysers. It is a well-established and proven technique that is endorsed by industry and law-enforcement agencies worldwide (Leonard, 2012; Noordzij, 1975). In this case, the device performs a chronoamperometric measurement, subjecting the fuel cell to a fixed voltage while recording the produced current. All the electrodes are connected to silver tracks ink-jet printed on a plastic film.

The disposable strip components are assembled on top of an acrylic substrate to provide mechanical robustness.

2.2. Battery-less electronic reader

The electronic reader was conceived considering the particular features of this application. It was designed to operate with the voltage and power ranges provided by the paper-based power source and ensures robustness and portability. The block diagram of the electronic reader is depicted in Fig. 3. The disposable test strip provides the power that must be managed by the reader, and the signal to generate the glucose measurement.

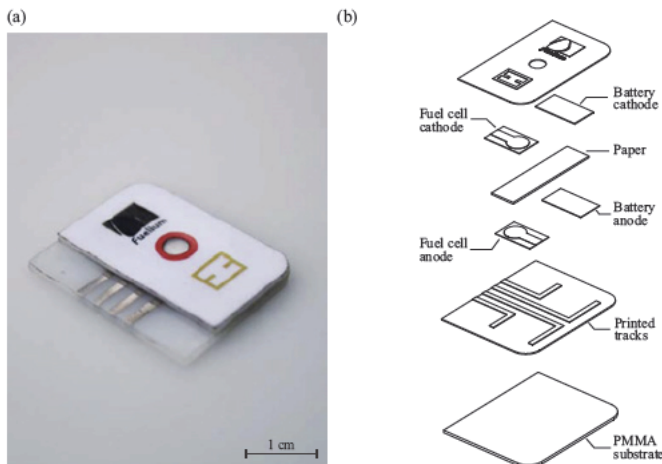


Fig. 2. a) Picture of paper-based test strip. b) Exploded view of its main components.

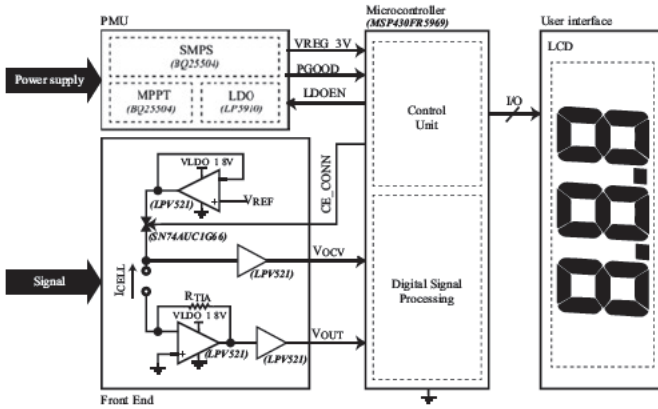


Fig. 3. Circuit of the battery-less electronic reader system.

The power supplied by the test strip goes to the Power Management Unit (PMU), where it is managed, and the control signals and voltage supplies of the system are generated. Meanwhile, the measurement signal, proportional to the concentration of glucose, is sent to the Front-End (FE) where the measurement is performed. Finally, the Control and Processing Unit (CPU), converts and processes the received information and sends it to a display, where the measurement result is shown.

2.2.1. Power management unit

The PMU is responsible for extracting and managing the available energy from the power source and offering a regulated output voltage in order to supply the different modules in the system. The PMU has been designed to work with the power provided by the disposable paper-based power source. In order to provide the necessary voltage to supply the components, a boost DC/DC converter in a cascade with a Low-Dropout (LDO) linear regulator are used. The first one boosts the voltage provided by the power source to 3.0V (VREG 3V) to supply power to both the control and processing unit and the screen used to display the result. Meanwhile, the LDO provides a very stable 1.8V (VLD0 1.8V) regulated voltage with high noise rejection (Fig. 3). The 1.8V is used to supply the analog block composed by the front-end module, which needs a very stable and well-regulated voltage supply with high noise rejection to avoid the effect of the inherent switching noise at the output of the boost converter and the effect of transient voltage variations at the power supply. The regulated voltage levels were selected in order to be able to supply common Components off-the-shelf (COTS) parts, where 3.0V is a typical voltage supply for digital parts (as microcontrollers or Analog-to-Digital Converters (ADC)) and 1.8 V, for low-voltage analog COTS parts (as Operational Amplifiers (OpAmp) or bandgap references).

Furthermore, the PMU has a Maximum Power Point Tracking (MPPT) module, which ensures that the energy is extracted efficiently from the power source, i.e. when the system demands energy from the power source, it extracts the maximum power that the power source is able to deliver at that moment. Thus, the solution can attend punctual high-power requirements coming from the different modules and shorten the required start-up time. To achieve that, the MPPT modulates the input impedance of the boost converter and sets the power source operating point to that with output voltage of 0.7V, where the power source is able to provide the maximum power.

This module also provides some additional features that enable the system to perform a smart power management carried out by the microcontroller. The boost converter outputs a signal called PGOOD. This is a low-level signal by default that changes to a high voltage level, as a

flag, when the voltage outputted by the boost converter reaches a voltage of 2.9 V. When regulated voltage drops under 2.4 V, the signal goes to low voltage level. This way, the microcontroller, able to operate with a minimum voltage supply of 1.8V, can (dis)enable the LDO through a LDOEN signal or manage its different Ultra-Low-Power Modes (LPMs) to adapt the system operation to the available energy.

2.2.2. Front-end

In order to measure the current provided by the sensor, which is proportional to the glucose concentration, a potentiostat amplifier has been implemented. The potentiostat circuit can be divided into two stages. The first stage is responsible for setting the working voltage of the sensor. Based on the fuel cell characterization, it was obtained the working voltage where the sensor has the highest sensitivity to discriminate between glucose concentrations. During operation, this working voltage is generated using a voltage divider and a buffer amplifier. The second stage performs the current readout and translates this current into voltage using a transimpedance amplifier (TIA) stage. The TIA translates the current signal provided by the sensor (I\_CELL) into a voltage signal by means of a resistor (R\_TIA). The output signal (V\_OUT) obtained at the output of the amplifier is proportional to the current provided by the strip. The equation that relates the output voltage and the current proportional to the glucose concentration is shown in the following equation:

$$V_{OUT} = R_{TIA} \cdot I_{CELL} \tag{1}$$

2.2.3. Control and Processing Unit

The system is managed through the CPU. It has been chosen an ultra-low-power microcontroller that needs only 1.8V as minimum voltage to operate. This device has different operating modes: one active mode and seven software-selectable low-power modes. An interruption event wakes up the microcontroller from low-power mode. Then, the relevant tasks or operations are performed, and finally the microcontroller restores back to the low-power mode on return from the interrupt program. The microcontroller has been selected, because it presents an ultra-low-power system architecture that increases performance at lowered energy budgets, and an ultra-low-power 16-bit control processing unit and intelligent peripherals to extend the autonomy of the system.

For this application two ADC have been used to capture two analog signals. One is the open-circuit voltage of the fuel cell (OCV), which allows to know if the sensor is ready to perform the measurement. The other one is the measurement signal (V\_OUT) related to the current across

the fuel cell ( $I_{\text{CELL}}$ ), which is proportional to the glucose concentration. Some General Purpose Input/Output (GPIO) pins have been used in order to manage and control the PMU module and the display interface.

The conversion of the measured current to a glucose concentration has been carried out by means of a Lookup Table (LUT) (Bengtsson, 2012).

To manage the system, the microcontroller has been programmed to perform the next tasks. Initially, when the voltage supply provided by the boost converter reaches the 1.8 V needed to start its operation, it configures a GPIO pin connected to *PGOOD*. This pin will monitor the state of the regulated voltage supply. Meanwhile, the LDO is disabled using the *LDOEN* signal and the microcontroller goes to LPM to minimize power consumption. When *PGOOD* goes high, meaning that the regulated voltage supply has reached the 2.9 V, and enough energy is harvested to start the application operation, the microcontroller exits the Low-Power Mode (LPM) and starts to configure the different peripherals that are used.

Once the system is initialized, the microcontroller monitors the OCV of the fuel cell to check if the sample is available and start the measurement. If that is the case, it enables the LDO and starts the chronoamperometry, connecting the counter electrode through the *CE\_CONN* signal. During this time, the microcontroller remains in LPM. After the selected time, the microcontroller exits the LPM, outputs the concentration measurement to the display and returns to LPM.

#### 2.2.4. Display output

A commercial 7-Segments Liquid Crystal Display (LCD) has been used to show glucose concentration result due to its low power consumption. The numeric LCD used can display up to 3 digits. In order to facilitate connection and control of the LCD, an integrated circuit has been used, which reduces the number of control signals needed to control the display. The total consumption of this module is 0.33  $\mu\text{A}$  at 3 V.

### 2.3. System integration and assembly

A scheme and picture of the whole system are shown in Fig. 4. The exploded view shows the placement of the different electronic blocks comprising the system, the connector for the disposable test strip, and the 3D printed casing. A Printed Circuit Board (PCB) with dimensions of 77 mm  $\times$  32 mm was designed and implemented.

## 3. Material and methods

### 3.1. Chemicals and materials

All chemicals and biochemicals were, unless otherwise stated, purchased from Sigma-Aldrich. Human serum (H4522, Lot # SLBQ9160V) from human male AB plasma, USA origin, sterile-filtered, was used to validate the operation of the device. Phosphate buffer at pH 7.4 was utilized in preliminary validation studies. It was prepared by the combination of sodium phosphate monobasic dihydrate ( $\text{NaH}_2\text{PO}_4 \cdot 2\text{H}_2\text{O}$ ), sodium phosphate dibasic dihydrate ( $\text{Na}_2\text{HPO}_4 \cdot 2\text{H}_2\text{O}$ ) and potassium chloride (KCl) for a final 100 mM concentration. Glucose solutions were allowed to mutarotate for 24 h and were kept refrigerated at 4 °C until use. Tetrabutylammonium bromide (TBAB)-modified Nafion was prepared as previously reported. (Klotzbach et al., 2006) Flavin adenine dinucleotide-dependent glucose dehydrogenase (FAD-GDH, E.C. 1.1.99.10, GLDE-70-1192, *Aspergillus* sp.) was purchased from Sekisui Diagnostics (Lexington, MA, USA) and used as received. Bilirubin oxidase (BOX, E.C. 1.3.3.5, *Myrothecium* sp., BO-3) was obtained from Amano Enzyme Inc. (Japan) and used as received. Glucose oxidase from *Aspergillus niger* (EC 1.1.3.4, Type X-S, 175 units/mg of solid, 75% protein) and 5% by wt. Nafion EW1100 suspension were purchased from Sigma-Aldrich and used as received. Carboxylated MWCNT and hydroxylated MWCNTs were purchased

from cheaptubes.com.

Standard 14 papers were purchased from GE Healthcare, Pittsburgh, PA, USA. The main structure of the test strip was constructed from pressure sensitive adhesives (PSA) (Adhesives Research) and poly(methylmethacrylate) (PMMA) (Plexiglas, Evonik Performance Materials GmbH, Harmstadt, Germany).

Silver ink (LOCTITE ECI 1011, Henkel, Dusseldorf, Germany) and carbon ink (C2030519P4, Gwent Electronic Materials Ltd., Pontypool, Wales) were used to print the base electrodes for the fuel cell onto a polyethylene terephthalate (PET) substrate. The test strip conducting tracks were ink-jet printed using silver ink (PE410, DuPont, Bristol, UK) on a 125  $\mu\text{m}$  polyethylene naphthalate (PEN) sheet (Teonex, DuPont, Chester, VA, USA). Paper-based power source electrodes were provided by Fuelium (Barcelona, Spain). All electronics components used for the electronic reader were purchased from Farnell (Madrid, Spain).

### 3.2. Device fabrication

The test strip structural components were designed with CorelDraw software (Corel, Ottawa, ON, Canada). Paper, PSA sheets and PMMA were cut with a CO<sub>2</sub> laser cutter (Mini 24, Epilog Laser, Golden, CO, USA).

The fuel cell configuration was adapted from the one reported in (del Torno-de Román et al., 2018). The fuel cell base electrodes were prepared by screen-printing onto a PET substrate. Initially, a track of silver ink was printed to improve conductivity. Following this, a carbon ink was screen printed on top of the silver layer in order to produce a rounded working electrode surface of 4-mm diameter. The screen-printed substrate was cut in segments of 5 mm  $\times$  9 mm, each containing a single electrode. The active area of the screen-printed electrodes was then functionalized with the corresponding enzymatic ink for anode and cathode. The fuel cell anodes were prepared by adding 1.5 mg of FAD-GDH (30 mg mL<sup>-1</sup>) enzyme to 75  $\mu\text{L}$  of a 0.2 M citrate/phosphate buffer in ultrapure water. The crosslinker ethylene glycol diglycidyl ether (EGDGE) is diluted in ultrapure water to a concentration of 10% v/v. COOH-MWCNTs are added to isopropanol at a concentration of 5 mg mL<sup>-1</sup> and sonicated for 1 h. Naphthoquinone-Linear poly(ethyleneimine) (NQ-LPEI) was prepared as described in (Milton, 2017) and diluted at a concentration of 10 mg mL<sup>-1</sup> in ultrapure water. In an Eppendorf tube, 67% v/v of the NQ-LPEI solution, 30% v/v of the enzyme and 3% v/v of the cross-linker solution (EGDGE) are combined. 8.5  $\mu\text{L}$  of the combined mixture is deposited on the surface of the electrode and left to dry overnight at room temperature. The fuel cell cathodes were modified by suspending 1.5 mg of BOX in 75  $\mu\text{L}$  of 0.2 M citrate/phosphate buffer. 75  $\mu\text{L}$  of the solution is added to 7.5 mg of Ac-MWCNTs as described in (Meredith et al., 2011; Milton et al., 2015). The solution is vortex mixed for 1 min, followed by 15 s of sonication: this procedure is repeated a total of 4 times. To this mixture, 25  $\mu\text{L}$  of TBAB-Nafion suspension is added, followed by another vortex/sonication step. 33  $\mu\text{L}$  of the mixture is then drop coated onto the surface of the screen-printed electrode and left to dry under a fan for 1.5–2 h. Both anodes and cathodes are stored at 4 °C when not in use.

A modified version of LF55 paper-based power source from Fuelium was adapted to the test strip. The anode and cathode power source electrodes were customized for this application considering the sample type, volume and power requirements. Each electrode had dimensions of 5 mm  $\times$  9 mm, with a projected electroactive surface of 5 mm  $\times$  5 mm. The conducting tracks of the test strip were ink-jet printed using Ag ink on a PEN sheet with a Cera Printer X-serie (CeraDrap, Limoges, France). Silver conducting paste was used for interconnection of fuel cell and power source electrodes to the conducting tracks. All the test strip components were manually assembled layer by layer using an acrylic alignment holder.

The electronic circuit of the battery-less reader was first simulated using Multisim software (National Instruments, Austin, Texas, United States). Ultiboard program (National Instruments, Austin, Texas, United

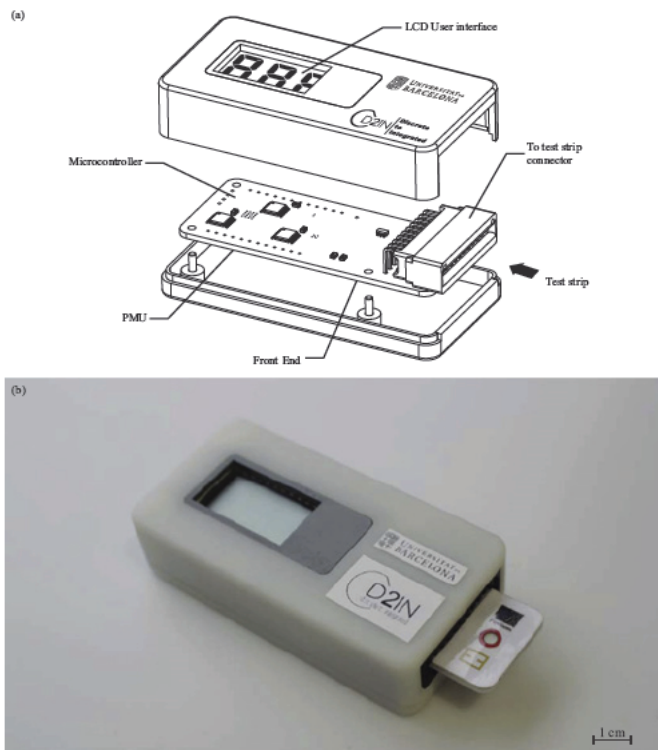


Fig. 4. a) Schematic of the system assembly. b) Photograph of the system.

States) was used to design the printed circuit board. The reader casing was designed using DesignSpark Mechanical.

### 3.3. Electronic and electrochemical characterization and validation

All electrochemical experiments were carried out with an Autolab PGSTAT204 (Metrohm, NL). For fuel cell and power source characterization, the open-circuit voltage of the fuel cell (OCV) of each cell was measured before polarization. Polarization curves were performed in potentiodynamic mode at a scan rate of  $5 \text{ mV s}^{-1}$ . Chronoamperometric curves of fuel cells were measured at  $0.45 \text{ V}$  for each glucose concentration.

The electronic validation and characterization were performed with a Source Measurement Unit (SMU) B2962A by Keysight Technology (USA) and an Agilent Technologies oscilloscope MSO-X 3034A (USA). Initial electronic characterization was carried out simulating the electrical behavior of the test strip via the SMU. The output voltage of the potentiostat was captured for different current curves corresponding to different glucose concentrations.

## 4. Results and discussion

### 4.1. Test strip characterization

The power source polarization curve was obtained after depositing  $50 \mu\text{L}$  of serum at the inlet pad of the consumable test strip. In order to see its performance in time, discharge curves at 1 and  $10 \text{ mA}$  were also recorded. Fig. 5a and b show the obtained results. The power source

shows its capability of delivering  $1 \text{ mA}$  for at least 40 min (far beyond the typical operating time of point-of-care devices) whereas at  $10 \text{ mA}$  it sustained a voltage above  $1.25 \text{ V}$  for at least 5 min.

Bioelectrocatalysis of fuel cell electrodes was validated with half-cell voltammetric characterization. Figs. S1, S2 show representative voltammograms of bioanode and biocathode, respectively. Next, the glucose fuel cell of the test strip was characterized with human serum at different glucose concentrations. Serum as-purchased had a glucose concentration of  $4.8 \text{ mM}$ . A solution of  $1 \text{ M}$  glucose in  $100 \text{ mM}$  PBS buffer was prepared and spiked into the serum sample in order to increase glucose concentration while minimizing dilution of the original biological sample. Fig. 5c shows the polarization curves obtained at different glucose concentrations. From these I-V curves, it could be seen that the highest sensitivity is obtained between  $0.35$  and  $0.50 \text{ V}$ . Therefore, it was decided to polarize the fuel cell at  $0.45 \text{ V}$  to obtain the chronoamperometry curves of the fuel cell and sense glucose concentration. The currents generated by the fuel cell biased at  $0.45 \text{ V}$  were measured for  $80 \text{ s}$ , recording a variability below  $15\%$  for each of the glucose concentrations in serum. Mean chronoamperometric curves are depicted in Fig. 5d.

### 4.2. Battery-less electronic reader validation and characterization

All electronic modules introduced in Section 2.2 were fully characterized and validated individually as a prior step to the total integration of the system shown in Fig. 4. This individual characterization of the full-custom electronics was carried out following a two-phase testing procedure: Phase 1) an initial step using a SMU (section 3.3) to

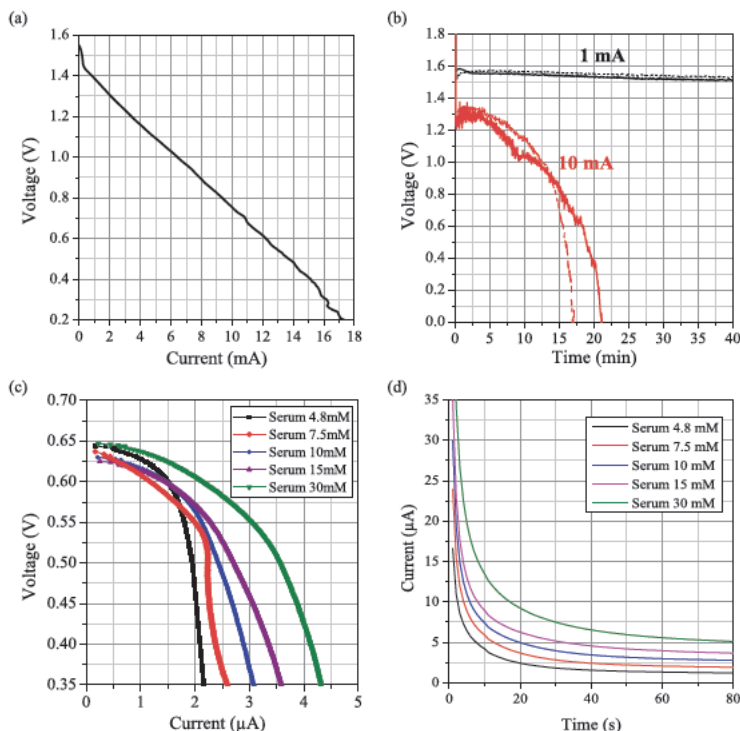


Fig. 5. Characterization of the Fuelium LF55 paper-based power source activated with serum samples. a) I-V paper-based power source characteristic. b) Paper-based fuel cell polarization curves at 1 and 10 mA. Characterization of glucose fuel cell integrated in the test strip with different glucose concentrations in serum. c) Fuel cell polarization curves. d) Fuel cell chronoamperometry curves at 0.45 V.

simulate the electrical response/behavior of the test strip; and Phase 2) a second phase using real test strips. Upon successful completion of these two phases, the implementation, integration and validation of the full system (Fig. 4) was done. In such a way, the final assembly was programmed, calibrated to work with the given sensor and validated with real test strips in the final test procedure (Phase 3).

It is important to underline the accurate design of the front-end module to reduce the deviation error of the measurement through it. This error was derived as the difference between the injected current and the current measured through the full-custom electronic module. The electronic system was validated and a final error lower than 1% was verified in test phase 1 with a test strip simulated current produced by the SMU unit and in phase 2 using test strips.

From calibration phase (Phase 3), it was obtained that the electronic reader is able to measure currents up to 30 μA with a resolution of 13 nA. Fig. 6a shows the accuracy of the electronic reader. The electronic reader error is lower than 1.8%. This error depends on the ADC quantification error and the passive component tolerances.

The main effort was to settle the appropriate time to extract the measurement. This point was defined in terms of device resolution and the uncertainty related to the electronics. In this sense, the reader was programmed to measure the current corresponding to a given glucose concentration. In order to characterize the whole system and determine the precise time to extract the measurement, the consumable test strip was connected to the reader and fed with 50 μL of serum at different glucose concentrations between 5 and 30 mmol/L (same considerations as section 4.1).

The currents generated by the glucose fuel cell biased at 0.45 V were measured and recorded by the reader for 80 s. As seen in Fig. 6b, the current measured by the reader ( $I_{CELL}$ ) virtually match with the chronoamperometry curves presented in Fig. 5d obtained with a commercial potentiostat (Autolab PGSTAT2014). These results allow to validate the operation of the reader and disposable strip system. As expected, the main difference between the curves measured by both instruments was identified for currents larger than 30 μA where the full-custom reader presents a maximum current detection limit, saturating for any higher value.

The chronoamperometric curves shown in Fig. 6b were used to define three operation regions (A, B and C) based on two criteria: the device resolution and the uncertainty in the time of measurement. These regions were used to determine the time to perform the measurement of current after submitting the fuel cell to the bias voltage.

The first criterion, device resolution, depends mainly on the sensor sensitivity and the electronic reader resolution. Based on the data from Fig. 6b, the sensor presents a higher sensitivity in region A whereas the lowest sensitivity is obtained in region C due to its decrease rate over time. On the other side, the electronic reader resolution is defined by the ADC resolution with a time-invariant value of 13 nA, negligible compared to the sensor sensitivity. According to this analysis, region C was ruled out to settle the time to extract the measurement.

The next step was the study of the measurement uncertainty to accurately define the time of the measurement. As it is shown in Fig. 6b, the chronoamperometry has a decreasing exponential response. This response excludes region A to carry out the measurement. In this

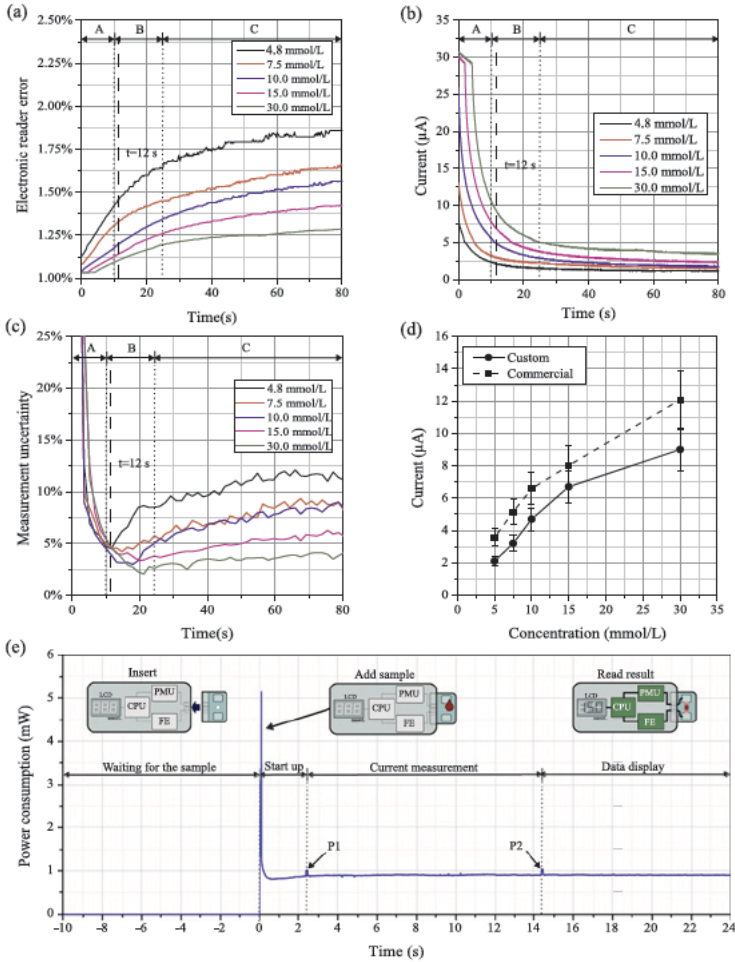


Fig. 6. a) Electronic reader current error. b) Chronoamperometry curves done with the battery-less electronic reader. c) Uncertainty in current measurement produced by the electronic reader. d) Transfer function that relates the current captured by the electronic reader with the glucose concentration and comparison against a commercial potentiostat (Autolab PGSTAT204). e) Temporal evolution of the electronic reader power consumption.

region, a small instability in the measurement time instant causes an important uncertainty in current measurement. Therefore, region B is the best region to perform the measurement. At this point, the current uncertainty in time was calculated (Fig. 6c) to establish the best time to extract the measurement within region B. The uncertainty is based on a 0.5 s range defined by the measurement sampling period of the processing unit. It was obtained that the best time to carry out the measurement is at 12 s, because it presents an electronics' uncertainty lower than 5% for the lowest glucose concentration.

A Lookup Table (LUT) (Bengtsson, 2012) based technique was used to translate the current value into the glucose concentration. Fig. 6d shows the transfer function that relates the current captured by the electronic reader with the glucose concentration and compares it against the one measured with the commercial potentiostat (Autolab PGSTAT204). Error bars in both curves account for the variability of the glucose sensor. As it can be seen, the data are proportional and only a

slight shift between the curves is presented. This is caused by the initial current saturation peak but, due to its systematic behavior, it is adjusted by a LUT in the postprocessing at the control unit.

Finally, Fig. 6e shows the operation phases of the system and the temporal evolution of the power consumption. The electronic reader is switched on when the serum sample is introduced into the disposable test strip, defining the start-up of the system. At this moment ( $t = 0$  s), the typical inrush current peak takes place, reaching a value of up to 5 mW. Then, the reader enters into a low power mode, consuming just 900  $\mu$ W. It should be noted that the total electronics power consumption is much lower than the maximum power that the paper-based power source is able to supply, above the 10 mW. During this phase, the system waits in the low power mode of operation until the voltage provided by the disposable is stable. Then, the front-end module is switched on, the measurement is started and maintained during 12 s, which is labeled as the Current measurement phase. Finally, in the Data

display phase, the reader returns to the low power mode and the numerical result is displayed. Two small current peaks take place during the device operation. The first peak (P1) occurs when the front-end module is activated and the second (P2) when the measurement data is acquired and displayed. The result of the glucose concentration measurement is displayed on the screen until the disposable component is removed or it runs out of power after a few hours.

Significant research efforts have been made to develop systems which generate energy while monitor the glucose of a sample (Lee et al., 2017; Slaughter and Kulkarni, 2017). Nevertheless, the proposed systems do not have any electronics module to display the result, and it is necessary an external system to show it. Furthermore, accurate commercial glucometers are available, which just need a small sample volume to perform the measurement (Rajendran and Rayman, 2014). However, they require batteries which become hazardous waste and pose threats to health and the environment if improperly disposed. The novel battery-less system presented in this paper provides quantitative data, besides having a reusable reader and a disposable test-strip, acting as sensor and a power source, which does not contain any toxic material, so it can be safely disposed of after its use without the need of recycling.

## 5. Conclusions

This work presents the Plug-and-Power concept, a novel approach of powering portable Point-Of-Care devices that offers several advantages. In this case, the disposable test strip provides the energy needed to run an electronic reader and perform the test, defining a self-powered plug-and-play POC.

In this case, the developed system is able to monitor glucose and process and display the data without the need to either recharge or replace the batteries, as the energy to run a measurement is always available within the test strip. Additionally, this approach provides environmental benefits related to battery usage and disposal, as uncontrolled battery disposal leads to severe environmental pollution. The paper-based power source used for the present approach does not contain any toxic material, so it can be safely disposed of after its use without the need of recycling. Therefore, this eco-friendly power source can follow the same waste stream as a test strip that has been in contact with biological samples.

The results show that the battery-less reader is able to operate and manage the power provided by the paper-based power source integrated in the consumable test strip. In addition, the electronic reader performs an electrochemical detection, process the output signal of the sensor and express the result on a display. The electronic reader designed is able to measure currents up to 30  $\mu$ A with a resolution of 13 nA and an error below 1.8%. Due to the low power design of the reader that consumes only 900  $\mu$ W in low power mode, it is possible to perform the measurement with the power provided by the test strip, which is above the 10 mW. This shows that the self-powered device could be further improved to include additional functionalities for sample preparation or a wireless communications module to visualize the results on a laptop or even on a smartphone. A big challenge would be to integrate the electronic system into a single chip, making possible develop a flexible and totally disposable system.

The advantages of this approach were here demonstrated with the development of a portable glucometer, but this concept can be extended to other kinds of electrochemical sensors measuring other analytes and/or other biological matrices (Chin et al., 2012; da Silva et al., 2017; Kaushik et al., 2018; Wan et al., 2013). Moreover, this can also benefit

portable electronic analytical devices beyond clinical diagnostics, as for example the veterinary or environmental fields.

## Acknowledgements

We would like to acknowledge I. Gonzalez-Valls from Fuelium, S.L. for guidance in paper-battery handling and operation. Also, the authors would like to thank the support of the MINAUTO Project (TEC2016-78284-C3-3-R and TEC2016-78284-C3-1-R), Ministerio de Economa, Industria y Competitividad – Agencia Estatal de Investigacion, and Fondo Europeo de Desarrollo Regional (AEI/FEDER, UE). N. Sabate would like to thank the financial support received from ERC Consolidator Grant (SUPERCELL - GA.648518). S.D. Minter would like to thank the financial support of the United States Department of Agriculture NIFA program (11322204).

## Appendix A. Supporting information

Supplementary data associated with this article can be found in the online version at doi:10.1016/j.bios.2018.07.034.

## References

- Bengtsson, L.E., 2012. *J. Sens. Technol.* 02, 177–184.
- Chan, H.N., Tan, M.J.A., Wu, H., 2017. *Lab Chip* 17, 2713–2739.
- Chin, C.D., Linder, V., Sia, S.K., 2012. *Lab Chip* 12, 2118.
- Choi, S., 2016. *Biotechnol. Adv.* 34, 321–330.
- Cruz, A.F.D., Norena, N., Kaushik, A., Bhansali, S., 2014. *Biosens. Bioelectron.* 62, 249–254.
- Drain, P.K., Hyle, E.P., Noubary, F., Freedberg, K.A., Wilson, D., Bishai, W.R., Rodriguez, W., Bassett, I.V., 2014. *Lancet Infect. Dis.* 14, 239–249.
- Fischer, C., Frawlan, A., Choi, S., 2016. *Biosens. Bioelectron.* 79, 193–197.
- Fu, E., Yager, P., Floriano, P.N., Christodoulides, N., McDevitt, J.T., 2011. *IEEE Pulse* 2, 40–50.
- Gervais, L., de Rooij, N., Delamarche, E., 2011. *Adv. Mater.* 23, H151–H176.
- Kaushik, A., Yndart, A., Kumar, S., Jayant, R.D., Vashist, A., Brown, A.N., Li, C.Z., Nair, M., 2018. *Sci. Rep.* 8, 9700.
- Klotzbach, T., Watt, M., Ansari, Y., Minter, S.D., 2006. *J. Membr. Sci.* 282, 276–283.
- Kulkarni, T., Slaughter, G., 2017. *Proc. IEEE Sens.*
- Larcher, D., Tarascon, J.M., 2015. *Nat. Chem.* 7, 19–29.
- Lee, L., Sode, T., Loew, N., Tsugawa, W., Lowe, C.R., Sode, K., 2017. *Biosens. Bioelectron.* 93, 335–339.
- Leonard, R.J., 2012. *J. Forensic Sci.* 57, 1614–1620.
- Meredith, M.T., Minson, M., Hickey, D., Artyushkova, K., Klutzhofer, D.T., Minter, S.D., 2011. *ACS Catal.* 1, 1683–1690.
- Milton, R.D., Lim, K., Hickey, D.P., Minter, S.D., 2015. *Bioelectrochemistry* 106, 56–63.
- Milton, R.D., 2015. FAD Dependent glucose dehydrogenase immobilization and media tion within a naphthoquinone redox polymer. In: Minter, S. (Ed.), *Enzyme stabilization and immobilization. Methods in molecular biology* 1504 Humana Press, New York, NY. <https://doi.org/10.1007/978-1-4939-6499-4-15>.
- Narvaez Villarrubia, C.W., Soavi, F., Santoro, C., Arbizzani, C., Serov, A., Rojas Carbonell, S., Gupta, G., Atanassov, P., 2016. *Biosens. Bioelectron.* 86, 459–465.
- Noordzij, P.C., 1975. *Alcohol Drugs Traffic Saf.* 553–560.
- Ongondo, F.O., Williams, I.D., Cherrett, T.J., 2011. *Waste Manag.* 31, 714–730.
- Rajendran, R., Rayman, G., 2014. *J. Diabetes Sci. Technol.* 8, 1081–1090.
- da Silva, E.T.S.G., Souto, D.E.P., Barragan, J.T.C., de F. Giarola, J., de Moraes, A.C.M., Kubota, L.T., 2017. *ChemElectroChem* 4, 778–794.
- Slaughter, G., Kulkarni, T., 2016. *Biosens. Bioelectron.* 78, 45–50.
- Slaughter, G., Kulkarni, T., 2017. *Sci. Rep.* 7, 1471.
- del Torno de Roman, L., Navarro, M., Hughes, G., Esquivel, J.P., Milton, R.D., Minter, S.D., Sabate, N., 2018. *Electrochim. Acta* 282, 336–342.
- Wan, Y., Su, Y., Zhu, X., Liu, G., Fan, C., 2013. *Biosens. Bioelectron.* 47, 1–11.
- Wang, S., Lifson, M.A., Inci, F., Liang, L.G., Sheng, Y.F., Demirci, U., 2016a. *Expert Rev. Mol. Diagn.* 16, 449–459.
- Wang, S.Q., Chinnaasamy, T., Lifson, M.A., Inci, F., Demirci, U., 2016b. *Trends Biotechnol.*
- Widmer, R., Osswald Krapf, H., Sinha Khetriwal, D., Schnellmann, M., Boni, H., 2005. *Environ. Impact Assess. Rev.* 25, 436–458.
- Yager, P., Edwards, T., Fu, E., Helton, K., Nelson, K., Tam, M.R., Weigl, B.H., 2006. *Nature Lond.* 442, 412.
- Zarei, M., 2017. *TrAC Trends Anal. Chem.*







## Article

# Self-Powered Portable Electronic Reader for Point-of-Care Amperometric Measurements

Yaiza Montes-Cebrián <sup>\*</sup>, Albert Álvarez-Carulla , Jordi Colomer-Farrarons, Manel Puig-Vidal and Pere LL. Miribel-Català

Department of Electronics and Biomedical Engineering, Faculty of Physics, University of Barcelona, Martí i Franquès 1, 08028 Barcelona, Spain

\* Correspondence: ymontes@ub.edu; Tel.: +34-93-4020-876

Received: 1 August 2019; Accepted: 25 August 2019; Published: 27 August 2019



**Abstract:** In this work, we present a self-powered electronic reader (e-reader) for point-of-care diagnostics based on the use of a fuel cell (FC) which works as a power source and as a sensor. The self-powered e-reader extracts the energy from the FC to supply the electronic components concomitantly, while performing the detection of the fuel concentration. The designed electronics rely on straightforward standards for low power consumption, resulting in a robust and low power device without needing an external power source. Besides, the custom electronic instrumentation platform can process and display fuel concentration without requiring any type of laboratory equipment. In this study, we present the electronics system in detail and describe all modules that make up the system. Furthermore, we validate the device's operation with different emulated FCs and sensors presented in the literature. The e-reader can be adjusted to numerous current ranges up to 3 mA, with a 13 nA resolution and an uncertainty of 1.8%. Besides, it only consumes 900  $\mu$ W in the low power mode of operation, and it can operate with a minimum voltage of 330 mV. This concept can be extended to a wide range of fields, from biomedical to environmental applications.

**Keywords:** self-powered; point-of-care diagnostics; low power electronics; smart electronics; portable; amperometric measurements

## 1. Introduction

The use of a fuel cell (FC) to replace conventional batteries in portable systems is of great interest [1–3]. FCs open up new opportunities, mainly in the field of consumer and industrial portable devices. There is a particular interest in the field of diagnostic tools based on biofuel cells, notably in the frame of point-of-care (POC) devices and biosensors for environmental monitoring [4]. In such systems, a big challenge is to implement self-powered sensing devices [5].

The general architecture of such devices is defined mainly by three modules. On the one hand the sensor and the power source, which can be a conventional battery, sensor or a FC, and on the other hand, the electronic reader (e-reader), which is the center of interest in the present work.

Particularly, portable and wearable devices are of interest due to their applications in health monitoring, diagnostics, prevention, among others [6,7]. In most cases, these systems use batteries as power sources. Generally, developed countries have a good electricity grid and batteries are inexpensive. The problem arises if we focus on the developing world, where they are in most need of these kind of portable diagnostic devices [8]. Furthermore, batteries are limited by their reduced lifetime, negative environmental impact, large size, and weight. Different approaches are looking for the best way to power a POC solution [9]. An example is paper-based assays (PBAs), wherein sample manipulation, pre-treatment, and electronics are not required [5] since they usually use colorimetric systems to read the results [10]. Promising alternative solutions are emerging whereby the energy

from the environment is used by energy harvesters to produce power, which can be used to supply portable and wearable devices. There are many approaches to harvest energy based on biofuel cells (BFCs) [11,12], thermo-electric generators (TEG) [13], piezoelectric generators (PZT) [14], among others.

FCs are electrochemical devices that harvest electrical energy from chemical reactions. They can work as a power source and as a sensor because they produce electricity for as long as there is available fuel. Their output current is directly correlated with the concentration of fuel. Two sub-categories of FCs are enzymatic fuel cells (EFCs) and microbial fuel cells (MFCs) [15,16]. Both have similar operational principles for energy production. EFCs produce electrical power using enzymes as a catalyst to oxidize their fuel, while MFCs use bacteria as the catalysts to oxidize organic and inorganic matter.

So far, it is only possible to power low-consumption microelectronic systems with these kinds of FCs since their power density output ranges from  $\mu\text{W}$  up to mW. Due to the fact that EFCs have higher power density and a more compact size, they are suitable to power portable and wearable electronic solutions [11,16]. Nevertheless, MFCs are an eco-friendly way of producing electrical energy from waste, since the electricity can come from waste material. This waste material becomes cleaner after the break-down process and can be directly discharged to the environment [17]. Moreover, MFCs may be employed as long-term power generating systems for online environment quality monitoring [18].

An ideal scenario is based on an FC which uses the same sample to power electronics and sense the concentration. However, the FC can be replaced by other power sources like standard batteries, printed batteries, energy-harvesting resources or a combination of such solutions. For instance, a possible scenario is a FC that supplies the electronics and a sensor that measures the analyte concentration. The sensor can be an amperometric biosensor to monitor oxygen and catechol [19] or glucose [20]. Furthermore, there are examples of amperometric systems based on the detection of the inhibition of glucose oxidase enzyme [21] or horseradish peroxidase activity [22]. Another interesting case is the air/water quality monitoring using FCs as a power source along with amperometric or potentiometric sensors [23,24]. In [25], a degradable battery was proposed fabricated using organic materials. It was able to operate up to 100 min with an adaptable output voltage from 1.5 to 3.0 V. The battery could be combined with amperometric biosensors to power a commercial water quality POC and detect heavy metals. Moreover, the device can be powered from polluted air generated during the treatment of wastewater [26], or in space missions [27,28] where FCs generate electrical power from hydrogen and oxygen.

Systems based on commercial off-the-shelf (COTS) integrated circuits (IC) are an affordable way to develop biomedical biosensing systems. Some examples of COTS-based systems have been reported in the literature. In this context, Baingane et al. developed a self-powered biosensor system for real-time sensing of lactic acid [29]. The system was comprised of an enzymatic biofuel cell and a simple capacitor circuit operating as a transducer. The fuel cell-based sensor generated an electrical power proportional to the lactic acid concentration, which was deduced by measuring the charging/discharging frequency of the capacitor circuit. The system did not rely on external power sources, although it required external equipment, like an oscilloscope, to monitor the capacitor frequency. Some works proposed the use of FC to monitor lactate in sweat. An example is a non-invasive system designed by Garcia et al. [30]. The device was composed of an enzymatic sensor, a biological FC as a power source and an electronic system. The electronic circuit consisted of an energy harvester, which boosted the FC voltage, and a potentiostat that performed a chronoamperometric detection. However, the system needed an external multimeter to perform the readout. In this context, an electronic-skin-based biofuel cell was developed by Bandodkar et al. [31]. The device harvested lactate present in human sweat to power a light-emitting diode and a bluetooth low energy radio. Other authors also proposed wireless systems [32], in which an operation using an organic biofuel cell was demonstrated. The full-custom circuit was able to operate with a voltage supply of 0.23 V. Besides, the authors designed and validated a receiver and off-chip inductor to transmit the data.

In the particular case of glucometers, recent innovative concepts have been proposed, which are capable of generating electrical power from the biochemical energy stored in glucose [33,34]. An example

is the self-powered fuel cell-based system for glucose monitoring developed by Fischer et al. [35]. The low-cost device operated with a single drop of 20  $\mu\text{L}$  and lacked external power sources with the capacity to generate rapid results, although it required a digital multi-meter for signal readout. These monitoring approaches have a simple electronic system capable of extracting the glucose level from the sample. However, most of them are subjective because they cannot store and process the information [12,36].

The motivation of the batteryless e-reader derives from the needs of POC devices in different scenarios [8,37,38]. The e-reader is an equipment with a quantitative output reading that seeks to achieve the requirements defined by the World Health Organization with the ASSURED criteria (Affordable, Sensitive, Specific, User-friendly, Rapid and Robust, Equipment-free, and Deliverable to users [39]).

In this work, we present in detail, the electronic modules that build up an e-reader based on the use of FC, following two approaches: Using the FC as a power element or as a dual power/sensor element. This power/sensor element is an external item that is inserted into the e-reader in which the same sample is used for powering and detecting. The e-reader was previously validated with a custom disposable test strip composed of a glucose battery, which supplied the device, and a glucose FC, which monitored the glucose concentration [20]. However, the e-reader can be adapted to operate in other scenarios, with another kind of FC, as power sources or biosensors. The e-reader was validated with a FC of simulated body fluid with an ionic composition similar to human blood plasma enriched with ethanol [40]. This FC has an open circuit voltage (OCV) of 930 mV with a maximum power density close of  $1.237 \text{ mW}\cdot\text{cm}^{-2}$ . Another example of application is the urine/Cr(VI) FC with an OCV of 1.3 V and a power of  $340 \mu\text{W}\cdot\text{cm}^{-2}$  [41]. In both cases, the e-reader could be supplied from the energy extracted by the fuel. At the same time, the concentration could be obtained from the current provided by the FC. Also, it is possible to perform a combination with another power source, like a direct methanol fuel cell (DMFC) for portable applications [42,43], with a specific amperometric sensor [44,45]. We describe in detail the conception, design, implementation, and characterization of the electronic modules that build-up the electronic reader based on a FC as a power source and a direct reading interface for a FC or an amperometric biosensor. Moreover, the operation of the reader is validated for different scenarios by emulating different FCs and sensors.

## 2. Materials and Methods

### 2.1. Architecture of the Self-Powered Measurement

As it has been pointed out before, the e-reader is conceived to operate with a FC as a power source and as a sensor, taking a direct amperometric reading of the FC current. Also, it is possible to use any amperometric biosensor based on a two-electrode configuration, although configuration can be easily extended to a three-electrode configuration. Using this technique, when a potential is applied to the counter electrode (CE), a current is produced as a consequence of the reaction at the working electrode (WE) surface.

The general architecture of the system is defined mainly by two modules: The power and sensor unit and the e-reader unit. The power source can be based on paper, as was presented in [20], where the device was validated with different glucose concentrations.

The architecture of the e-reader is divided into four modules (Figure 1): A power management unit (PMU), a front-end unit (FEU), a control and signal processing unit (CSPU) and a display unit (DU). The PMU extracts the power from the power source and manages it to generate the control signals and voltage supplies. All the while, the FEU picks up the measurement signal, which is proportional to the concentration of the agent to be detected. Lastly, the output signal is converted and processed by the CSPU and it is sent to the DU, where the measurement result is shown.

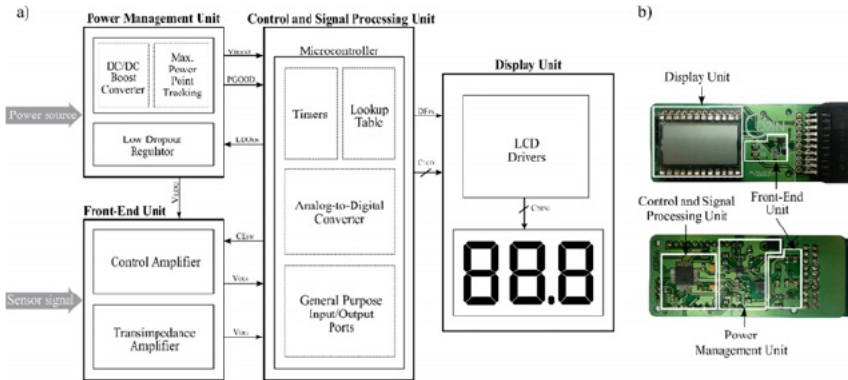


**Figure 1.** (a) Block diagram of the e-reader, and (b) picture of the e-reader, the four principal modules are labeled, derived from [20].

**2.1.1. Power Management Unit**

The PMU extracts the energy from the power source and generates a regulated output voltage to supply the electronic modules that compose the e reader. It is comprised of a DC/DC boost converter in cascade with a low drop out (LDO) linear regulator (Figure 2a). The DC/DC boost converter steps up the voltage provided by the power source to 3.0 V ( $V_{BOOST}$ ) to supply both the CSPU and the DU.

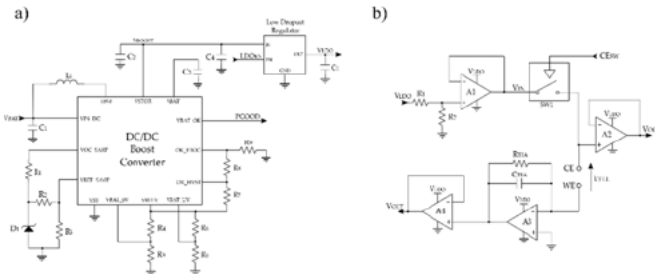


**Figure 2.** Circuits that compose the (a) power management unit, and (b) front-end unit circuit.

The LDO provides a 1.8 V ( $V_{LDO}$ ) regulated voltage with high noise rejection, which is used to supply the analog components that compose the FEU. This electronic module provides a stable and regulated voltage avoiding the switching noise of the boost converter and the voltage variations of the power supply.

Moreover, a maximum power point tracking (MPPT) module is implemented in the PMU. It guarantees an efficient energy extraction from the power source. This module can cope with a punctual high-power demand, such as the system’s start-up. For that purpose, the MPPT module adapts the input impedance of the DC/DC boost converter and changes the operating point of the power source to the voltage at which the power source provides the maximum power. This module allows managing the energy intelligently through the microcontroller. The DC/DC boost converter incorporates the PGOOD (power good) signal (Figure 2a). This signal is at a low level by default but, when the converter ( $V_{BOOST}$ ) reaches 2.9 V, this signal goes high state. However, if the voltage falls below 2.4 V, it returns to a low level. In this way, the microcontroller, which operates at 1.8 V, can enable/disable the LDO through the LDO<sub>EN</sub> signal. Moreover, as it will be explained in the next

sections, the microcontroller has different ultra-low-power modes (LPMs) in order to adapt the system operation to the available energy.

The PMU module is based on the BQ25504 and the LP5910 LDO (Texas Instruments; Dallas, TX, USA). Both devices have a very marked low power character with a typical quiescent current of 330 nA for the first one and 12  $\mu$ A for the second one in shutdown mode. The total consumption of this PMU module is 21  $\mu$ A.

### 2.1.2. Front-End Unit

The current measurement was performed by a potentiostat amplifier (Figure 2b). The main tasks of this module are: (a) To apply a stable voltage difference between the electrodes of the electrochemical cell, and (b) to readout and process the output signal.

In order to control the potential applied to the cell, an operational amplifier (Op-Amp) is used as a control amplifier (A1). A1 provides the optimal bias voltage to the sensor ( $V_{IN}$ ), which is the voltage that enables the best sensor's performance. The e-reader is designed to adjust the voltage  $V_{IN}$ , adapting the system to a wide range of applications. The voltage  $V_{IN}$  is generated through the low-dropout regulator ( $V_{LDO}$ ), and a voltage divider resistor network ( $R_1$  and  $R_2$ ). Because the resistor network modifies the measure, a unity gain buffer amplifier (A1) is introduced between the network and the sensor to isolate both parts.

As stated above, it is possible that the power source needs some time to reach the voltage to supply the electronic components (1.8 V). Therefore, when the PGOOD signal is at a high-level voltage, the microcontroller sends a high-level signal ( $LDO_{EN}$ ) to turn on the LDO ensuring the e-reader measures when enough energy is harvested to start the application operation.

For the best performance, the open circuit voltage ( $V_{OCV}$ ) applied to the counter electrode (CE) is monitored by an analog to digital converter (ADC) pin of the microcontroller. The ADC controls the  $V_{OCV}$  applied to the sensor and when the sample is available, it starts the measurement turning on the analog switch (SW1) through the  $CE_{SW}$  signal, depicted in Figure 2b. Since the microcontroller's port impedance can affect the measurement, a unity gain buffer amplifier (A2) is connected between the CE and the microcontroller.

The Transimpedance Amplifier circuit (TIA) (A3), connected to the working electrode (WE), provides the output voltage ( $V_{OUT}$ ) that is proportional to the cell current ( $I_{CELL}$ ). It translates the current signal into a voltage signal by means of transimpedance gain resistor ( $R_{TIA}$ ). The expression that relates both magnitudes is shown in Equation (1). In this configuration, the working electrode is kept to the virtual ground by the TIA. As before, a unity gain buffer amplifier (A4) is connected between the TIA and the microcontroller so as not to affect the measurement value.

$$V_{OUT} = R_{TIA} \cdot I_{CELL} \quad (1)$$

The current generated by the sensor is amplified by the TIA and translated to an output voltage through the  $R_{TIA}$ . Ideally, this current flows through  $R_{TIA}$ , but in fact, the op-amp takes some of this current (called input bias current). A similar error is derived from the input offset voltage, which is caused by a mismatch in the input terminals of the op-amp. It specifies the voltage across the terminals that must be applied in order to get an output voltage of zero. This input bias current and input offset voltage results in an error voltage at the output and limits the dynamic range of the FEU circuit. Therefore, it is important to select an op-amp with low input bias current and low input offset voltage, to achieve the required dynamic range and overall accuracy. The selected op-amp in the FEU is the LPV521 (Texas Instruments; Dallas, TX, USA). It is a nano-power amplifier which is able to operate from 1.6 V up to 5.5 V with typically 345 nA of supply current. It also presents a very low offset voltage (0.1 mV, typically at 1.8 V) and an ultra-low bias current (0.01 pA, typically at 1.8 V). The maximum output current is 3 mA, which is the maximum current that the e-reader can read.

The analog switch used is the SN74AUC1G66 (Texas Instruments; Dallas, TX, USA) It presents a low power character since it is able to operate at 0.8 V to 2.7 V with only 10  $\mu\text{A}$  of typical quiescent current. In addition the design is made up of accurate resistors with 1% tolerance. The total consumption of the front-end unit circuit is 7.5  $\mu\text{A}$ .

### 2.1.3. Control and Signal Processing Unit

This unit is based on a low power microcontroller, which has three main tasks: a) Generate the signals that control the modules of the system; b) process the data and; c) show it on the display.

Figure 3 shows the flow diagram of the application. Initially, the device is switched off, waiting for the introduction of the power and sensor module (“Disconnected phase”) into the reader. As soon as it is inserted and the sample deposited, the “start-up phase” begins.

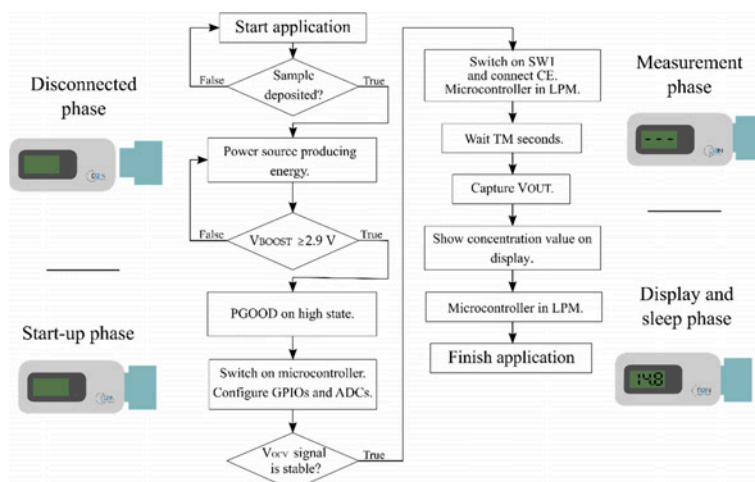


Figure 3. Diagram of the application's flow.

Thereafter, the FC-based power source starts to deliver energy to the system, and when the output voltage of the boost converter ( $V_{\text{BOOST}}$ ) reaches 1.8 V (the minimum voltage to turn on the microcontroller) the microcontroller is switched on. It configures and initializes general-purpose input/output (GPIO) pins as well as the ADCs to monitor the sample and control the power delivered by the FC.

The PGOOD signal (Figure 2b) monitors the state of the regulated voltage supply ( $V_{\text{BOOST}}$ ). It ensures that the e-reader performs the measurement when enough energy is harvested to start the application operation. In order to minimize power consumption, meanwhile there is not enough energy to start the measurement (PGOOD signal in a low state), the LDO remains disabled and the microcontroller stays in the low power mode (LPM). When the boost converter ( $V_{\text{BOOST}}$ ) reaches 2.9 V, the PGOOD changes to the high state. Afterwards, an interruption event wakes up the microcontroller from LPM, and it enables the LDO, which supplies the FEU's components.

Then, the ADC pin ( $V_{\text{OCV}}$ ) begins to monitor the state of the sensor's voltage. The “measurement phase” starts as soon as the signal provided by the sensor is stable.

Afterwards, the microcontroller turns on the analog switch (SW1), which connects the CE, and applies a DC bias voltage ( $V_{\text{IN}}$ ) to the sensor as is depicted in Figure 2b. Then, a timer starts to count until the moment in which the measurement takes place, TM. TM is the time that elapses between the CE's connection and the measurement takes place, fixed for each particular biosensor.

During this time, the microcontroller remains in LPM. The criteria for determining the TM time is described in Section 3.2.

After the TM, the microcontroller exits the LPM state and the ADC captures the measurement signal ( $V_{OUT}$ ), which is proportional to the current provided by the sensor ( $I_{CELL}$ ).  $I_{CELL}$  can be obtained by Equation (1), as the input bias voltage ( $V_{IN}$ ), the TIA resistor ( $R_{TIA}$ ) and the output voltage ( $V_{OUT}$ ) are known.

In most situations, the relationship between the magnitude to measure and the voltage obtained is not linear. For this reason, we implemented a lookup table (LUT) [46–48] in the microcontroller to translate the data obtained to a current or concentration. A LUT is an array of data that allows linking input values to output values, replacing the runtime computation with a simple array indexing operation. It maps inputs to an output value by looking up or interpolating in a defined table of values.

Later, following Figure 3, the “display and sleep phase” takes place. In this phase, the microcontroller manages the drivers that control the display and shows the concentration value on the display. Finally, the microcontroller returns back to the LPM and remains in this state permanently.

The CSPU module is based on the MSP430FR5969 microcontroller (Texas Instruments; Dallas, Texas, USA). This microcontroller has been selected because of its good characteristics in terms of voltage, quiescent current and operating power consumption. It has a supply voltage that ranges from 1.8 V up to 3.6 V with one operating active mode and seven software-selectable low power modes. Furthermore, it consumes only 0.4  $\mu\text{A}/\text{MHz}$  in standby mode and 100  $\mu\text{A}/\text{MHz}$  in active mode. The microcontroller has an ultra-low-power 16-bit architecture that allows controlling the intelligent peripherals to extend the autonomy of the system.

#### 2.1.4. Display Unit

Different low power solutions could be used to show the detection result, like printed and flexible electrochromic displays [49,50]. In this study, a 3-digit 7-segments numerical liquid crystal display (LCD) has been used to show the result, due to its simple operation and low power consumption, it also operates at 3 V with a typical quiescent current of 0.33  $\mu\text{A}$ .

This kind of LCD uses many interconnects, to facilitate connection and control of the LCD, the CD4055B integrated circuit (IC) (Texas Instruments; Dallas, Texas, USA) has been used. It reduces the number of control signals needed to control the display and typically consumes 5  $\mu\text{A}$ . This IC is a single-digit BCD-to-7-segment decoder that allows controlling the 7-segments of each digit with only four pins. The display is controlled by the display-frequency input signal, which is a square-wave signal. The IC provides a square-wave signal to the selected segments that is 180 degrees out-of-phase with the common-signal, making these segments visible. The segments which are not selected have the square-wave signal and are in phase with the common-signal, so they are not visible. The consumption of the DU module is 16  $\mu\text{A}$ .

#### 2.2. Fuel Cells and Sensors

In order to validate the operation of the e-reader, we emulated different FCs and sensors reported in the literature (Figure 4). We emulated FCs and sensors based on urine/Cr(VI) [41] and methanol [51,52] by using a source measurement unit (SMU). Moreover, we carried out experimental tests with an emulated ethanol FC as a sensor [40] and a commercial ethanol FC as a power source.

These approaches fully validated the e-reader implementation. For each case, key design parameters are indicated, like the open-circuit voltage (OCV), and the related concentrations of the involved sample.



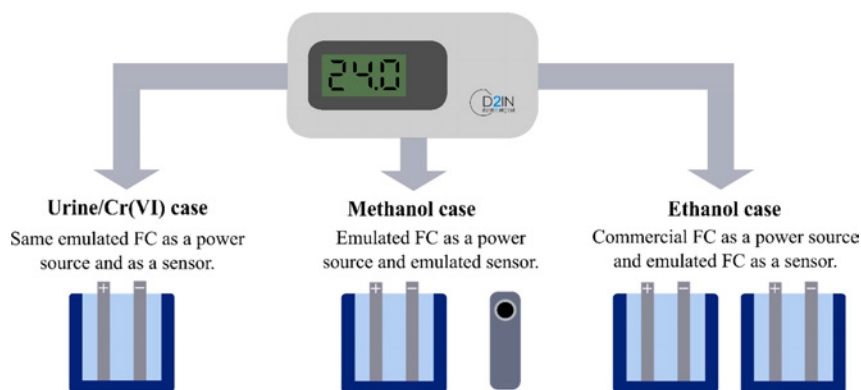


**Figure 4.** Summary diagram of the validation tests performed.

### 2.2.1. Urine/Cr(VI) Fuel Cell Case

The urine/Cr(VI)'s FC presented by [41] is able to generate electrical power from processing human urine and heavy metal, in this case, Cr(VI). This FC reduces Cr(VI) in human urine, using urine as fuel and Cr(VI) as oxidant. The open-circuit voltage (OCV) ranges from 1.11 V at 13 mg·L<sup>-1</sup> to 1.26 V at 50 mg·L<sup>-1</sup>. In addition, this FC provides a maximum power density going from 3.4 W·m<sup>-2</sup> at 50 mg·L<sup>-1</sup> of Cr(VI) to 2.2 W·m<sup>-2</sup> at 13 mg·L<sup>-1</sup> of Cr(VI). To validate the operation of the proposed system, we used the same urine/Cr(VI) FC as a sensor and as a power source.

### 2.2.2. Methanol Fuel Cell and Sensor Case

In this case, we used a methanol FC as a power source and as a sensor to detect methanol. We emulated and employed a passive direct methanol fuel cell (DMFC) as a power source for portable electronic devices [51]. In the study, the authors used six dual DMFC connected in series to produce energy. In order to validate the e-reader operation, we considered a single FC of 1 cm<sup>2</sup> with a 1 M of methanol concentration. It was only necessary to use a single FC because the developed e-reader was a low power device and operated with a minimum voltage of 330 mV. A single DMFC with a 1 M of methanol concentration provides a maximum power density of 5 mW·cm<sup>-2</sup>, a maximum current density of 22 mA·cm<sup>-2</sup> and an OCV of 0.6 V.

The emulated sensor is reported in [52]. It is a wearable vapor/liquid amphibious electrochemical sensor for monitoring methanol. The sensor exhibits high selectivity, good repeatability, and reliable stability for both vapor and liquid methanol. It was tested with methanol concentrations that go from 0% to 6%, providing current densities that go from 90 to 3.5 μA·mm<sup>-2</sup>. We validated the e-reader considering a methanol sensor of 1 mm<sup>2</sup>.

### 2.2.3. Ethanol Fuel Cell Case

After emulating different approaches based on fuel cells and sensors, we carried on experimental verification working with a commercial FC. To perform the experimental test with the e-reader, we used as a power source the commercial FCJ-42 ethanol fuel cell science kit (Horizon Fuel Cell Technologies; Singapore). Due to the fact that the characteristics of this FC are not described, we characterized it, obtaining the I-V curves for different ethanol concentrations that go from 3% to 9%. This ethanol FC provides a maximum power going from 0.23 W at 9% to 0.186 W at 3%. The maximum current given is 700 mA at 9% and 540 mA at 3%. All concentrations tested presented an OCV close to 1 V. To validate the system, we used the commercial ethanol FC with 3% of concentration as a power source.

The chosen FC used to sense ethanol was presented in [40]. It is a single-cell membraneless microfluidic FC that operates in the presence of simulated body fluids, human serum, and blood enriched with ethanol as the fuel. It provides current densities up to  $6.5 \text{ mA}\cdot\text{cm}^{-2}$ .

### 2.3. Experimental Set-Up

The electronics validation and characterization were carried out with a source measurement unit (SMU) B2962A by Keysight Technology (Santa Rosa, CA, USA) and an Agilent Technologies oscilloscope MSO-X 3034A (Santa Clara, CA, USA).

In order to emulate the FCs and sensors previously presented, we introduced their I–V polarization curves into the SMU and performed a piecewise linear (PWL) interpolation. The PWL interpolation is a technique used in engineering to approximate a complex function by a simple linear function, which allows expressing the non-linear I–V characteristics that present FCs. Next, we analyzed the start-up of the power management unit (PMU) and emulated the current ( $I_{\text{CELL}}$ ) provided by the sensors and FCs.

Furthermore, we obtained the I–V curves in potentiodynamic mode at a scan rate of  $2 \text{ mV}\cdot\text{s}^{-1}$  to characterize the ethanol FC. We performed the ethanol concentrations with deionized water obtained from a Milli-Q® Advantage A10 water purification system and absolute ethanol for analysis (ACS grade) at a concentration of 99.8% (Panreac, Barcelona, Spain).

## 3. Results and Discussion

### 3.1. Electronic Reader Manufacturing

We developed a printed circuit board (PCB) and an outer case, both items build up the e-reader (Figure 5). The PCB is a double-sided printed circuit made in glass-reinforced epoxy laminate material (FR4) with silver-finish. The total size of the board was  $77.5 \text{ mm} \times 32.5 \text{ mm} \times 2 \text{ mm}$ . The case of the device had a size of  $85 \text{ mm} \times 42 \text{ mm} \times 21 \text{ mm}$  and was developed using three-dimensional (3D) printing. The case was made of a photosensitive epoxy resin called Accura® 25 and it was created with the solid-state stereolithography (SLA®) printing technology.

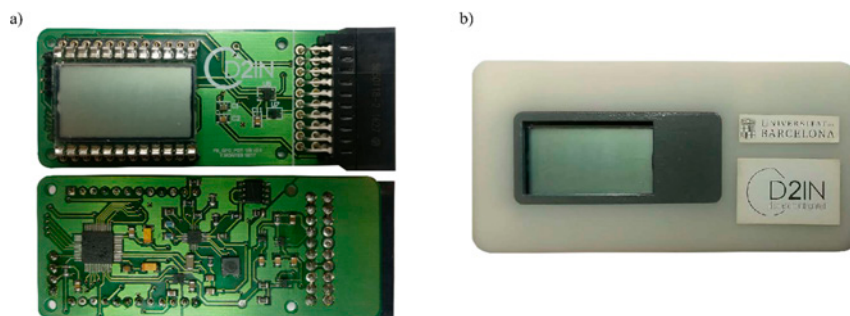


**Figure 5.** (a) Picture of the e-reader's printed circuit board (PCB). (b) Picture of the whole self-powered electronic reader: PCB and outer case.

### 3.2. Characterization and Calibration of the Self-Powered Electronic Reader

We characterized the e-reader in order to analyze its performance and uncertainty translating the cell current ( $I_{\text{CELL}}$ ) into a voltage ( $V_{\text{OUT}}$ ). The procedure followed was previously explained, in which the SMU and the oscilloscope were used.

First, we connected the SMU to the e-reader and we applied a current ramp ( $I_{\text{G}}$ ) from  $13 \mu\text{A}$  to  $0 \mu\text{A}$  with a change rate of  $1.85 \mu\text{A}/\text{s}$ . Then, we captured the potentiostat output voltage ( $V_{\text{OUT}}$ ) by the oscilloscope. We translated  $V_{\text{OUT}}$  into the measurement current ( $I_{\text{M}}$ ) with Equation (1). As is

shown in Figure 6, we compared the current measured by the e-reader ( $I_M$ ) with those applied by the SMU ( $I_G$ ). This test allowed us to obtain the uncertainty between the current generated ( $I_G$ ) and the current measured by the e-reader ( $I_M$ ). Analyzing these data, we obtained that the maximum relative uncertainty between  $I_G$  and  $I_M$  is 1.8%, which is the uncertainty associated with the FEU module. This maximum uncertainty was obtained at a nominal current value of 12.91  $\mu\text{A}$ , and it had an absolute uncertainty value of 0.24  $\mu\text{A}$ .

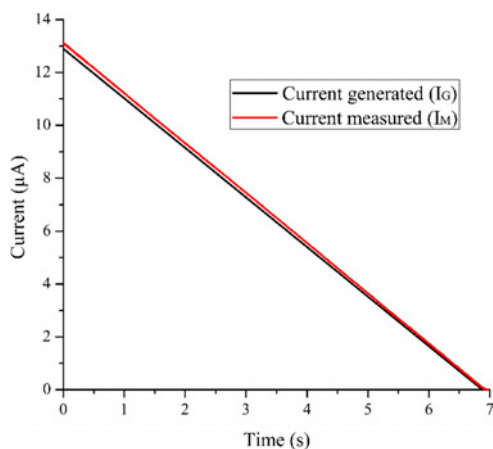


**Figure 6.** Uncertainty between the current generated by the SMU ( $I_G$ ) and the current measured by the front-end unit ( $I_M$ ).

As it is stated in Section 2.1.3., the definition of the moment in which the measurement takes place,  $T_M$ , is the key point. It depends mainly on two aspects: (a) The device resolution, which is constrained by the electronics' resolution, and (b) the measurement uncertainty. This depends on the change rate of the current because a slight deviation in the measurement time can affect the current value, since initially the current decreased quickly. In order to obtain the ideal moment to perform the measurement, the e-reader was calibrated for each sensor.

First, we established the polarization voltage ( $V_{IN}$ ) from the sensor's characterization, and we programmed the e-reader to drive the sensor to  $V_{IN}$ . Then, we connected the sensor to the e-reader and polarized it. After that, we captured the chronoamperometry curves with the SMU and analyzed the device resolution and the measurement.

The e-reader resolution is defined by the ADC resolution, which is time-invariant and has a value of 13 nA.

In a chronoamperometry, a redox reaction occurs when a potential step is applied to the electrode. The current decays  $t^{1/2}$ , obeying the Cottrell equation for reactions that are under diffusion control [53]. Consequently, the initial and the final region cannot afford to extract a measurement. During the initial time, a small deviation in the moment to extract the measurement is translated into a large current uncertainty. While in the final region, it is difficult to distinguish between concentrations because they are too close.

Considering these facts, we found the measurement uncertainty for different concentrations. As a result, we were able to establish the best moment to extract the measurement ( $T_M$ ). The time chosen in each case was the one which presented the lower uncertainty value for the worst case of detection, which was the detection of the lowest level of concentration.

### 3.3. Start-Up and Power Consumption of the E-Reader

Figure 7a shows the startup curve graph of the e-reader when it is powered by a commercial ethanol FC as an example case. The upper graph shows the voltage provided by the ethanol FC ( $V_{FC}$ ). While, the middle graph shows the boost converter voltage ( $V_{BOOST}$ ), which is used to supply both CSPU and the DU. In the end, the bottom graph displays the voltage provided by the low-dropout voltage regulator ( $V_{LDO}$ ), which supplies the analog components that comprise the FEU.

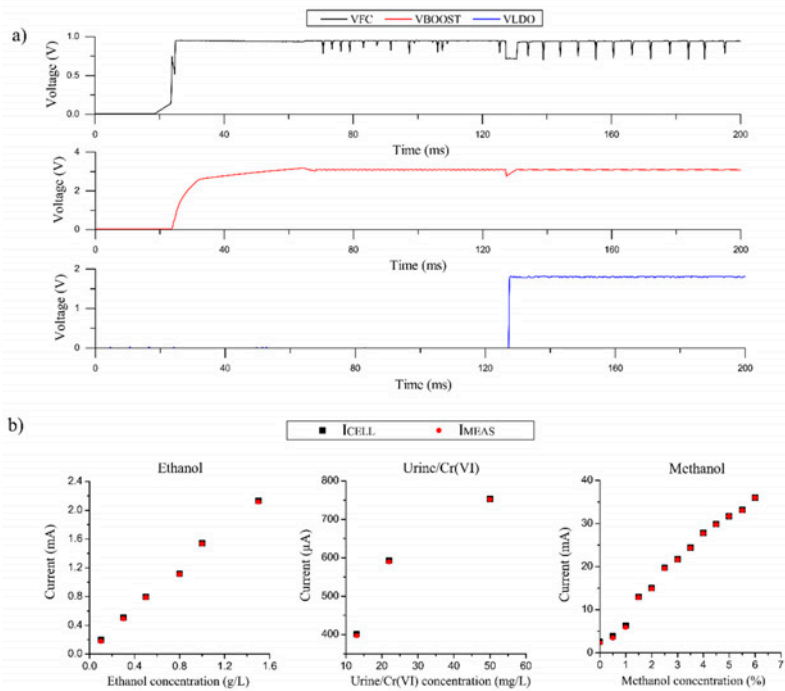


**Figure 7.** (a) Start-up curves of the e-reader powered by an ethanol FC. (b) Transfer function that relates the measured current by the e-reader with different emulated sensors and fuel cell concentrations (ethanol, urine and methanol), and the comparison against the current produced by the sensor ( $I_{CELL}$ ).

When the FC is connected to the e-reader, the PMU is enabled. It starts collecting energy and the  $V_{BOOST}$  signal increases. During 100 ms the  $V_{LDO}$  signal remains in a low state since there is not enough energy to start the whole system. When the PMU has harvested enough energy, the  $V_{LDO}$  signal changes to a high state and the system begins to operate. The peaks that appear in the  $V_{FC}$  signal correspond to the MPPT sampling system that optimizes the energy extraction from the power source. As it is shown in Figure 7a,  $V_{FC}$  is a noisy signal. For this reason,  $V_{FC}$  did not power any electronic components directly. The periodical peaks of  $V_{FC}$  were reduced by DC/DC boost converter ( $V_{BOOST}$ ), which supplies both CSPU and the DU. The FEU was the most sensitive circuit because it is the circuit that carried out the measurement. Thus, the voltage which supplied the FEU circuit ( $V_{LDO}$ ) was stabilized and regulated by a low-dropout voltage regulator (LDO).

We also obtained the e-reader's power consumption. When the power source was connected to the e-reader, it had a typical inrush current peak of 5 mW. At this moment, the e-reader enters into a low power operation mode, and consumes only 900 µW. The system waits in this low power mode

until the voltage provided by the power source is stable. Then, the FEU module is switched on and the measurement is performed. Lastly, the numerical data is processed and displayed, and the e-reader returns to the low power mode. During the device's operation, the power consumption presents two peaks that increase the consumption instantly to 1 mW. These peaks occur when the FEU module is activated and when the data is processed and displayed.

### 3.4. Validation of the E-Reader

The system has been validated in different conditions and cases, with FCs of urine/Cr(VI), methanol and ethanol, and the methanol sensor.

We verified the efficient extraction of energy from the sample in different cases, enabling the operation of both the DC/DC boost converter and the LDO, components that supply the FEU and the CPSU. The transitory performance of the commercial FC was obtained, extracting the curves shown in Figure 7a. This figure shows the behavior of the power signals in the "disconnected phase" and the "start-up phase", explained in Figure 3. Moreover, we validated the stationary behavior of the device with the emulated FCs of methanol and urine. These tests confirmed the self-powered performance of the system, which can power the e-reader circuits with the same monitored sample.

Furthermore, we validated the FEU's module operation, measuring different current ranges produced by the FCs of urine/Cr(VI) and ethanol, and the methanol sensor. For all these experiments, we followed the same procedure. Firstly, we connected the sensor to the e-reader, and we polarized it to the proper bias voltage ( $V_{IN}$ ). When the sensor is polarized, it produces a current proportional to the concentration of the analyte ( $I_{CELL}$ ).  $I_{CELL}$  flows through the potentiostat circuit, which translates it into the voltage ( $V_{OUT}$ ). The microcontroller's ADC reads  $V_{OUT}$  and translates it to current ( $I_{MEAS}$ ) by a LUT, as stated in Section 2.1.3.

Figure 7b shows the comparison between the current produced by the emulated FC/sensor ( $I_{CELL}$ ) and the current measured by the e-reader ( $I_{MEAS}$ ). The figure depicts that the current measured by the e-reader is practically the same as the nominal current injected by the emulated FC. The results show that the maximum difference between  $I_{CELL}$  and  $I_{MEAS}$  is 1.8%, validating the operation of the FEU module of the e-reader with different ranges of current and demonstrating the accuracy of the e-reader.

These tests validated the operation of the system, demonstrating the ability of the device to power the whole system while measuring the concentration of the sample and displaying the numerical result on the e-reader's display. The validation has been carried out with three different FCs, although it can be adapted to operate with other FCs, measuring a wide range of analytes.

## 4. Conclusions

In this work, we presented and described, in detail, the full implementation of an electronic reader for self-powered POC solutions based on the use of FCs as a power source or as a power source and as a sensor. The operation of the e-reader was validated in different cases, using a commercial ethanol FC, three emulated FCs (urine, ethanol, and methanol) and a sensor (methanol), showing its capability of adaptation to different scenarios.

Due to its low power design, the platform can operate with a minimum voltage of 330 mV, consuming only 900  $\mu$ W in the low power mode. The device has been proven to exhibit reliable, robust, and effective results. It has a measurement uncertainty below 1.8%, a minimum resolution of 13 nA and a maximum measurement current of 3 mA. Furthermore, the plug-and-play device performs amperometric measurements automatically, in only a few seconds. The device presented in this work could be the first step towards the future of point-of-care since the system provides quantitative data, showing the numerical result on the display. Some advantages of the proposed device include: (i) No need for external power sources, since the same sample is used to power and sense; (ii) the ease of use; (ii) compactness and portability; (iii) the possibility of showing the data on a display, without the need for external laboratory equipment; (iv) adaptability to wide range of cases; and (v) the rapidity and accuracy of results. The portable device can operate with conventional lithium

batteries or biodegradable batteries [25] or with the sensing sample. It is a valuable characteristic in disadvantaged regions without a good electricity grid and batteries.

As future work, we propose to introduce a wireless communication system to show the resulting data on a smartphone or a laptop, a module to set the polarization voltage (VIN) externally, or an adjustable signal generator to perform cyclic voltammetry. A big challenge would be to integrate the device in a single chip, developing the system in a flexible substrate.

**Author Contributions:** Y.M.-C. developed, implemented and tested the point-of-care (POC) electronic device and acquisition software, performed the experimental study and analyzed and interpreted the acquired data. She wrote the manuscript and approved the final version of the manuscript. A.Á.-C. designed the power management unit and the outer case of the device as well as developed acquisition software. Besides, P.L.M.-C., M.P.-V. and J.C.-F. supervised the development of the POC device. P.L.M.-C., J.C.-F., M.P.-V. and A.Á.-C. have discussed the resultant data, contributed in the manuscript and approved the final version for its publication.

**Funding:** This research was funded by the Spanish Ministry of Economy, Agencia Estatal de Investigación, and Fondo Europeo de Desarrollo Regional (AEI/FEDER, UE), through the project Circuits for Energy Harvesting Management for Low-Voltage Low-Power Applications (MINAUTO) – grant number TEC2016-78284-C3-3-R).

**Conflicts of Interest:** The authors declare no conflict of interest.

## References

1. Dyer, C.K. Fuel cells and portable electronics. In Proceedings of the 2004 Symposium on VLSI Circuits. Digest of Technical Papers (IEEE Cat. No.04CH37525), Honolulu, HI, USA, 17–19 June 2004; pp. 124–127.
2. Stone, C. Fuel cell technologies powering portable electronic devices. *Fuel Cells Bull.* **2007**, *2007*, 12–15. [[CrossRef](#)]
3. Safdar, M.; Jänis, J.; Sánchez, S. Microfluidic fuel cells for energy generation. *Lab Chip* **2016**, *16*, 2754–2758. [[CrossRef](#)] [[PubMed](#)]
4. Justino, C.I.L.; Duarte, A.C.; Rocha-Santos, T.A.P. Recent progress in biosensors for environmental monitoring: A review. *Sensors* **2017**, *19*, 2918. [[CrossRef](#)] [[PubMed](#)]
5. Grattieri, M.; Minter, S.D. Self-Powered Biosensors. *ACS Sens.* **2018**, *3*, 44–53. [[CrossRef](#)] [[PubMed](#)]
6. Kim, J.; Campbell, A.S.; de Ávila, B.E.-F.; Wang, J. Wearable biosensors for healthcare monitoring. *Nat. Biotechnol.* **2019**, *37*, 389–406. [[CrossRef](#)] [[PubMed](#)]
7. Hong, Y.J.; Jeong, H.; Cho, K.W.; Lu, N.; Kim, D. Wearable and Implantable Devices for Cardiovascular Healthcare: From Monitoring to Therapy Based on Flexible and Stretchable Electronics. *Adv. Funct. Mater.* **2019**, *29*, 1808247. [[CrossRef](#)]
8. Zarei, M. Portable biosensing devices for point-of-care diagnostics: Recent developments and applications. *TrAC-Trends Anal. Chem.* **2017**, *91*, 26–41. [[CrossRef](#)]
9. Choi, S. Powering point-of-care diagnostic devices. *Biotechnol. Adv.* **2016**, *34*, 321–330. [[CrossRef](#)]
10. Yetisen, A.K.; Akram, M.S.; Lowe, C.R. Paper-based microfluidic point-of-care diagnostic devices. *Lab Chip* **2013**, *13*, 2210–2251. [[CrossRef](#)]
11. Jia, W.; Wang, X.; Imani, S.; Bandodkar, A.J.; Ramírez, J.; Mercier, P.P.; Wang, J. Wearable textile biofuel cells for powering electronics. *J. Mater. Chem. A* **2014**, *2*, 18184–18189. [[CrossRef](#)]
12. Slaughter, G.; Kulkarni, T. A self-powered glucose biosensing system. *Biosens. Bioelectron.* **2016**, *78*, 45–50. [[CrossRef](#)]
13. Bahk, J.-H.; Fang, H.; Yazawa, K.; Shakouri, A. Flexible thermoelectric materials and device optimization for wearable energy harvesting. *J. Mater. Chem. C* **2015**, *3*, 10362–10374. [[CrossRef](#)]
14. Dagdeviren, C.; Joe, P.; Tuzman, O.L.; Park, K.-I.; Lee, K.J.; Shi, Y.; Huang, Y.; Rogers, J.A. Recent progress in flexible and stretchable piezoelectric devices for mechanical energy harvesting, sensing and actuation. *Extrem. Mech. Lett.* **2016**, *9*, 269–281. [[CrossRef](#)]
15. Slate, A.J.; Whitehead, K.A.; Brownson, D.A.C.; Banks, C.E. Microbial fuel cells: An overview of current technology. *Renew. Sustain. Energy Rev.* **2019**, *101*, 60–81. [[CrossRef](#)]
16. Gonzalez-Solino, C.; Lorenzo, M. Enzymatic Fuel Cells: Towards Self-Powered Implantable and Wearable Diagnostics. *Biosensors* **2018**, *8*, 11. [[CrossRef](#)] [[PubMed](#)]
17. Winfield, J.; Ieropoulos, I.; Greenman, J. Investigating a cascade of seven hydraulically connected microbial fuel cells. *Bioresour. Technol.* **2012**, *110*, 245–250. [[CrossRef](#)]

18. Pasternak, G.; Greenman, J.; Ieropoulos, I. Self-powered, autonomous Biological Oxygen Demand biosensor for online water quality monitoring. *Sens. Actuators B Chem.* **2017**, *244*, 815–822. [[CrossRef](#)]
19. Majdecka, D.; Draminska, S.; Janusek, D.; Krysinski, P.; Bilewicz, R. A self-powered biosensing device with an integrated hybrid biofuel cell for intermittent monitoring of analytes. *Biosens. Bioelectron.* **2018**, *102*, 383–388. [[CrossRef](#)]
20. Montes-Cebrián, Y.; del Torno-de Román, L.; Álvarez-Carulla, A.; Colomer-Farrarons, J.; Minteer, S.D.; Sabaté, N.; Miribel-Català, P.L.; Esquivel, J.P. 'Plug-and-Power' Point-of-Care diagnostics: A novel approach for self-powered electronic reader-based portable analytical devices. *Biosens. Bioelectron.* **2018**, *118*, 88–96. [[CrossRef](#)]
21. Mugheri, A.Q.; Tahira, A.; Sherazi, S.T.H.; Abro, M.I.; Willander, M.; Ibupoto, Z.H. An Amperometric Indirect Determination of Heavy Metal Ions through Inhibition of Glucose Oxidase Immobilized on Cobalt Oxide Nanostructures. *Sens. Lett.* **2016**, *14*, 1178–1186. [[CrossRef](#)]
22. Nomngongo, P.N.; Ngila, J.C.; Nyamori, V.O.; Songa, E.A.; Iwuoha, E.I. Determination of Selected Heavy Metals Using Amperometric Horseradish Peroxidase (HRP) Inhibition Biosensor. *Anal. Lett.* **2011**, *44*, 2031–2046. [[CrossRef](#)]
23. Szulczyński, B.; Gebicki, J. Currently Commercially Available Chemical Sensors Employed for Detection of Volatile Organic Compounds in Outdoor and Indoor Air. *Environments* **2017**, *4*, 21. [[CrossRef](#)]
24. Spinelle, L.; Gerboles, M.; Kok, G.; Persijn, S.; Sauerwald, T. Review of portable and low-cost sensors for the ambient air monitoring of benzene and other volatile organic compounds. *Sensors* **2017**, *17*, 1520. [[CrossRef](#)] [[PubMed](#)]
25. Esquivel, J.P.; Alday, P.; Ibrahim, O.A.; Fernández, B.; Kjeang, E.; Sabaté, N. A Metal-Free and Biotically Degradable Battery for Portable Single-Use Applications. *Adv. Energy Mater.* **2017**, *7*, 1700275. [[CrossRef](#)]
26. Hamoda, M.F. Air pollutants emissions from waste treatment and disposal facilities. *J. Environ. Sci. Heal.—Part A Toxic/Hazard. Subst. Environ. Eng.* **2006**, *41*, 77–85. [[CrossRef](#)] [[PubMed](#)]
27. Brey, J.; Muñoz, D.; Mesa, V.; Guerrero, T. Use of Fuel Cells and Electrolyzers in Space Applications: From Energy Storage to Propulsion/Deorbitation. In Proceedings of the E3S Web of Conferences, Seville, Spain, 3–7 October 2016.
28. Burke, K.A. Fuel Cells for Space Science Applications. In Proceedings of the 1st International Energy Conversion Engineering Conference IECEC, Cleveland, OH, USA, 17–21 August 2003.
29. Baingane, A.; Slaughter, G. Self-Powered Electrochemical Lactate Biosensing. *Energies* **2017**, *10*, 1582. [[CrossRef](#)]
30. Garcia, S.O.; Ulyanova, Y.V.; Figueroa-Teran, R.; Bhatt, K.H.; Singhal, S.; Atanassov, P. Wearable Sensor System Powered by a Biofuel Cell for Detection of Lactate Levels in Sweat. *ECS J. Solid State Sci. Technol.* **2016**, *5*, M3075–M3081. [[CrossRef](#)] [[PubMed](#)]
31. Bandodkar, A.J.; You, J.-M.; Kim, N.-H.; Gu, Y.; Kumar, R.; Mohan, A.M.V.; Kurniawan, J.; Imani, S.; Nakagawa, T.; Parish, B.; et al. Soft, stretchable, high power density electronic skin-based biofuel cells for scavenging energy from human sweat. *Energy Environ. Sci.* **2017**, *10*, 1581–1589. [[CrossRef](#)]
32. Niitsu, K.; Kobayashi, A.; Nishio, Y.; Hayashi, K.; Ikeda, K.; Ando, T.; Ogawa, Y.; Kai, H.; Nishizawa, M.; Nakazato, K. A Self-Powered Supply-Sensing Biosensor Platform Using Bio Fuel Cell and Low-Voltage, Low-Cost CMOS Supply-Controlled Ring Oscillator With Inductive-Coupling Transmitter for Healthcare IoT. *IEEE Trans. Circuits Syst. I Regul. Pap.* **2018**, *65*, 2784–2796. [[CrossRef](#)]
33. Narvaez Villarrubia, C.W.; Soavi, F.; Santoro, C.; Arbizzani, C.; Serov, A.; Rojas-Carbonell, S.; Gupta, G.; Atanassov, P. Self-feeding paper based biofuel cell/self-powered hybrid  $\mu$ -supercapacitor integrated system. *Biosens. Bioelectron.* **2016**, *86*, 459–465. [[CrossRef](#)] [[PubMed](#)]
34. Slaughter, G.; Kulkarni, T. Highly Selective and Sensitive Self-Powered Glucose Sensor Based on Capacitor Circuit. *Sci. Rep.* **2017**, *7*, 1417. [[CrossRef](#)] [[PubMed](#)]
35. Fischer, C.; Fraiwan, A.; Choi, S. A 3D paper-based enzymatic fuel cell for self-powered, low-cost glucose monitoring. *Biosens. Bioelectron.* **2016**, *79*, 193–197. [[CrossRef](#)] [[PubMed](#)]
36. Lee, I.; Sode, T.; Loew, N.; Tsugawa, W.; Lowe, C.R.; Sode, K. Continuous operation of an ultra-low-power microcontroller using glucose as the sole energy source. *Biosens. Bioelectron.* **2017**, *93*, 335–339. [[CrossRef](#)] [[PubMed](#)]
37. Bissonnette, L.; Bergeron, M.G. Portable devices and mobile instruments for infectious diseases point-of-care testing. *Expert Rev. Mol. Diagn.* **2017**, *17*, 471–494. [[CrossRef](#)] [[PubMed](#)]

38. Stoot, L.J.; Cairns, N.A.; Cull, F.; Taylor, J.J.; Jeffrey, J.D.; Morin, F.; Mandelman, J.W.; Clark, T.D.; Cooke, S.J. Use of portable blood physiology point-of-care devices for basic and applied research on vertebrates: A review. *Consero. Physiol.* **2014**, *2*, 1. [[CrossRef](#)] [[PubMed](#)]
39. Vashist, S.K.; Luppia, P.B.; Yeo, L.Y.; Ozcan, A.; Luong, J.H.T. Emerging Technologies for Next-Generation Point-of-Care Testing. *Trends Biotechnol.* **2015**, *33*, 692–705. [[CrossRef](#)]
40. Galindo-de-la-Rosa, J.; Arjona, N.; Moreno-Zuria, A.; Ortiz-Ortega, E.; Guerra-Balcázar, M.; Ledesma-García, J.; Arriaga, L.G. Evaluation of single and stack membraneless enzymatic fuel cells based on ethanol in simulated body fluids. *Biosens. Bioelectron.* **2017**, *92*, 117–124. [[CrossRef](#)]
41. Xu, W.; Zhang, H.; Li, G.; Wu, Z. A urine/Cr(VI) fuel cell—Electrical power from processing heavy metal and human urine. *J. Electroanal. Chem.* **2016**, *764*, 38–44. [[CrossRef](#)]
42. Wang, L.; He, M.; Hu, Y.; Zhang, Y.; Liu, X.; Wang, G. A “4-cell” modular passive DMFC (direct methanol fuel cell) stack for portable applications. *Energy* **2015**, *82*, 229–235. [[CrossRef](#)]
43. Kamarudin, S.K.; Achmad, F.; Daud, W.R.W. Overview on the application of direct methanol fuel cell (DMFC) for portable electronic devices. *Int. J. Hydrog. Energy* **2009**, *34*, 6902–6916. [[CrossRef](#)]
44. Rashid, M.; Jun, T.-S.; Jung, Y.; Kim, Y.S. Bimetallic core-shell Ag@Pt nanoparticle-decorated MWNT electrodes for amperometric H<sub>2</sub> sensors and direct methanol fuel cells. *Sens. Actuators B Chem.* **2015**, *208*, 7–13. [[CrossRef](#)]
45. Sales, M.G.F.; Brandão, L. Autonomous electrochemical biosensors: A new vision to direct methanol fuel cells. *Biosens. Bioelectron.* **2017**, *98*, 428–436. [[CrossRef](#)] [[PubMed](#)]
46. Liang, K.-F.; Chen, J.-H.; Chen, Y.-J.E. A Quadratic-Interpolated LUT-Based Digital Predistortion Technique for Cellular Power Amplifiers. *IEEE Trans. Circuits Syst. II Express Briefs* **2014**, *61*, 133–137. [[CrossRef](#)]
47. Bandyopadhyay, S.; Das, A.; Mukherjee, A.; Dey, D.; Bhattacharyya, B.; Munshi, S. A Linearization Scheme for Thermistor-Based Sensing in Biomedical Studies. *IEEE Sens. J.* **2016**, *16*, 603–609. [[CrossRef](#)]
48. Shyu, L.-H.; Wang, Y.-C.; Chang, C.-P.; Shih, H.-T.; Manske, E. A signal interpolation method for Fabry–Perot interferometer utilized in mechanical vibration measurement. *Measurement* **2016**, *92*, 83–88. [[CrossRef](#)]
49. Andersson Ersman, P.; Kawahara, J.; Berggren, M. Printed passive matrix addressed electrochromic displays. *Org. Electron.* **2013**, *14*, 3371–3378. [[CrossRef](#)]
50. Cao, X.; Lau, C.; Liu, Y.; Wu, F.; Gui, H.; Liu, Q.; Ma, Y.; Wan, H.; Amer, M.R.; Zhou, C. Fully Screen-Printed, Large-Area, and Flexible Active-Matrix Electrochromic Displays Using Carbon Nanotube Thin-Film Transistors. *ACS Nano* **2016**, *10*, 9816–9822. [[CrossRef](#)] [[PubMed](#)]
51. Achmad, F.; Kamarudin, S.K.; Daud, W.R.W.; Majlan, E.H. Passive direct methanol fuel cells for portable electronic devices. *Appl. Energy* **2011**, *88*, 1681–1689. [[CrossRef](#)]
52. Jiang, Y.; Ma, J.; Lv, J.; Ma, H.; Xia, H.; Wang, J.; Yang, C.; Xue, M.; Li, G.; Zhu, N. Facile Wearable Vapor/Liquid Amphibious Methanol Sensor. *ACS Sens.* **2019**, *7*, 56. [[CrossRef](#)]
53. Bard, A.J.; Faulkner, L.R. *Electrochemical Methods: Fundamentals and Applications*; Wiley: New York, NY, USA, 2001; ISBN 0471043729.







## Self-Powered Adaptive Switched Architecture Storage

F. El Mahboubi<sup>1</sup>, M. Bafleur<sup>1</sup>, V. Boitier<sup>1</sup>, A. Alvarez<sup>2</sup>, J. Colomer<sup>2</sup>, P. Miribel<sup>2</sup> and J.-M. Dillhaç<sup>1</sup>

<sup>1</sup>LAAS-CNRS, Université de Toulouse, CNRS, INSA, UPS, Toulouse, France

<sup>2</sup>University of Barcelona, Barcelona, Spain

E-mail: felmahbo@laas.fr

**Abstract.** Ambient energy harvesting coupled to storage is a way to improve the autonomy of wireless sensors networks. Moreover, in some applications with harsh environment or when a long service lifetime is required, the use of batteries is prohibited. Ultra-capacitors provide in this case a good alternative for energy storage. Such storage must comply with the following requirements: a sufficient voltage during the initial charge must be rapidly reached, a significant amount of energy should be stored and the unemployed residual energy must be minimised at discharge. To answer these apparently contradictory criteria, we propose a self-adaptive switched architecture consisting of a matrix of switched ultra-capacitors. We present the results of a self-powered adaptive prototype that shows the improvement in terms of charge time constant, energy utilization rate and then energy autonomy.

### 1. Introduction

Energy harvesting is necessary to ensure energy autonomy of networked wireless sensors. Generally, this type of system incorporates a device to store energy, in order to cope with ambient energy intermittency. The device used for storage, is either a battery or an ultra-capacitor. In some cases the ultra-capacitor is an interesting alternative to batteries: on the one hand, to benefit from an almost infinite lifetime compared to battery and on the other, in the case of extreme temperatures (in an aircraft, for ex.), to get rid of safety issues. Moreover, ultra-capacitors can deliver much larger power peaks than batteries. However, ultra-capacitors have three major disadvantages. Firstly, the output voltage varies with the amount of stored energy, preventing the direct supply of a load and therefore requiring a DC-DC regulator. The second disadvantage is relative to start-up with empty ultra-capacitors: enough energy has to be stored to reach a sufficient voltage to operate the associated electronics. If storage of a large amount of energy is needed, the capacitance should be high, and so will be the charge time constant. If a fast start-up is required, the value of the capacitance could be too small for efficient storage. A compromise must be found between these two constraints. The third disadvantage is that the DC-DC converter stops working below a certain voltage threshold. Thus, during the discharge, part of the stored energy in the ultra-capacitors is lost. To partially solve these problems, we propose in this paper a self-adaptive architecture of energy storage.

### 2. Self-adaptive switched architecture and prototype

The self-adaptive structure consists of four identical ultra-capacitors (with a capacitance of  $C=100\text{mF}$ ). The cells are judiciously interconnected by switches, thus allowing for three configurations. The first one is a configuration « all-series » (S) which allows a fast start-up by having an equivalent capacitance four times smaller than the final one. Then, when sufficient voltage is reached for proper operation, the architecture moves to a « series-parallel » (SP) configuration, and



finally to an « all-parallel » (P) configuration to maximize energy storage. The process is reversed towards the SP step and finally the S configuration when discharging the ultra-capacitor to use as much as possible the stored energy.

The use of adaptive storage topologies is not new. There are many solutions: one using DC-DC converters [1], another requiring many ultra-capacitors [2], and a third one exhibiting heavy losses due to the number of used switches [3]. This study is carried out within the European project SMARTER [4], dedicated to the development of adaptive storage architecture for a wireless sensor node that is self-powered by piezoelectric energy harvesting. In this project, the whole node will be implemented on a flexible substrate and ultra capacitors integrated onto silicon [4].

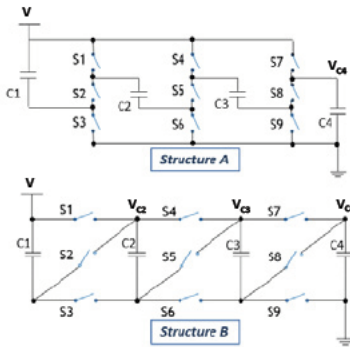


Figure 1. Configuration of the two studied self-adaptive switched architectures.

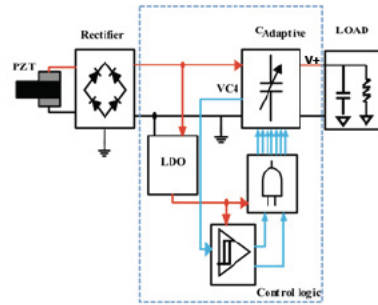


Figure 2. Block diagram of the self-powered adaptive storage architecture.

Two different architectures (Figure 1) have been studied [6][7] and compared with regard to losses to assess if a balancing circuitry is needed. Table 1 summarizes the simulation results, for both structures A and B: it provides the losses related to the variability of the capacitance value for a tolerance range of  $\pm 20\%$ . We found out that to minimize losses, a judicious placement of the capacitors allows limiting them to an acceptable level and balancing circuitry is then useless. This information is quite important since ultra-capacitors integrated onto silicon could exhibit such large variability. For the implementation of a self-powered adaptive storage prototype, we then used structure B that is slightly more efficient. In addition, this structure has an advantage regarding the associated control circuitry. Instead of monitoring the voltage  $V+$  that is applied to the load (see Fig. 1 and 2), the control circuitry only monitors the voltage across the ultracapacitor  $C4$  that is connected to ground, assuming that it provides a good image of  $V+$  voltage. Compared to the approach of [6] that uses a complex sequential logic, for this latter architecture, a simpler combinational logic can be used that is beneficial in terms of energy consumption.

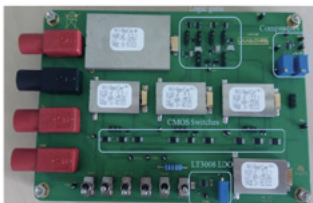


Figure 3. Prototype of the self-powered adaptive storage.

Tolerance range $\pm 20\%$	$E_{max}$ loss (%)	C1 (F)	C2 (F)	C3 (F)	C4 (F)
Structure A	2.08	0.12	0.08	0.08	0.12
Structure B	2.16	0.08	0.08	0.12	0.12

Table 1. Impact of the dispersion in capacitance values on losses (worst case capacitor placement).

A preliminary validation of this concept was already presented [6] but it was not autonomous, i.e. an external power supply was used for the control circuitry. The schematic architecture of the self-powered adaptive storage architecture is given in Figure 2 and was validated using commercial components (Figure 3). The matrix of ultracapacitors is made up of four AVX-BestCap supercapacitors of 100mF that are interconnected by nine ADG801 normally-off CMOS switches. An LT3008 LDO allows powering the control circuitry that is composed of two comparators and four logical gates driving the switches.

The comparison of the charge voltage of the structure (or of a cell) to predetermined voltage thresholds ( $V_{high}$  and  $V_{low}$ ) allows switching from one configuration to another. During the charge, when the measured charging voltage exceeds  $V_{high}$ , the control circuitry changes the topology of the structure towards a higher capacitance value. Similarly, during the discharge, when the measured voltage reaches  $V_{low}$ , the configuration switches to a lower capacitance value. The choice of the threshold depends on the desired goal (maximizing harvested power [6], high voltage...). For an optimized behavior,  $V_{high}$  and  $V_{low}$  should respect:

$$2V_{min} < V_{high} < V_{max} \quad \text{and} \quad V_{min} < V_{low} \tag{1}$$

where  $V_{min}$  and  $V_{max}$  are the minimum and maximum operating voltages of the electronics to supply, respectively.

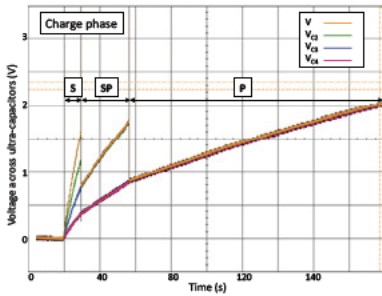


Figure 4. Measurement of the self-adaptive storage prototype in the charge phase. S, SP and P indicate ultra-capacitor configuration: all series, series/parallel and all parallel.

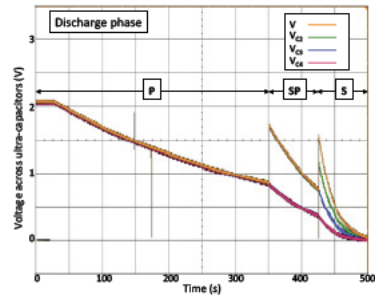


Figure 5. Measurement of the self-adaptive storage prototype in the discharge phase. S, SP and P indicate ultra-capacitor configuration: all series, series/parallel and all parallel.

### 3. Experimental results

We have tested the proposed architecture. For the charging phase, we used a Thevenin generator made up of 1kΩ resistor and 4.5V voltage source to simulate an energy harvester source. For the discharge phase, we connected a resistive load of 1kΩ between  $V+$  and ground to simulate a constant power load. During these two phases, in addition to  $V+$ , we monitored the voltages at each intermediate node ( $VC_4$ ,  $VC_3$  and  $VC_2$ ) with reference to ground.

#### 3.1. Charge phase

Figure 4 presents the experimental waveforms obtained during the charging phase. At starting, the ultra-capacitors are empty and they are configured in series (S). This allows reaching very rapidly, in 5 s, the voltage threshold (0.8V) required for operating the electronics. This has to be compared with a configuration with a single storage capacitor that requires a starting time of 55 s. We can notice that voltage  $V_{C4}$  used to monitor the switching to another configuration is exactly proportional to one fourth (400 mV) of  $V+$  voltage when switching from S to SP configuration. Then the adaptive storage switches to a series-parallel (SP) configuration and finally to an all parallel (P) one.

We have measured the total energy stored in the adaptive storage and compared it to a single capacitor architecture when the storage element is fully charged up to 4.5V. The losses related to the required control electronics result in 91% energy storage efficiency.

### 3.2. Discharge phase

Figure 5 depicts the voltage evolution across the self-adaptive matrix during the discharge phase. In this case, the system stops operating at a minimum voltage corresponding to the one required to operate the electronics, while a significant portion of the energy is still stored in the capacitors. Using the adaptive configuration that switches back to SP and finally to S configurations, it is possible to minimize this residual energy. Compared to single storage capacitor architecture, the adaptive approach allows saving 5% of this residual energy, which is in this case, does not completely compensate the energy required to power the control electronics. However, this performance should be greatly improved by moving to a dedicated power-management integrated circuit.

## 4. Conclusion

We have validated the concept of an adaptive storage for improving the dynamic behaviour of a battery-free storage architecture based on ultra-capacitors. It allows significantly boosting the start-up time and the energy management requires some more optimization to get the full benefits of this approach in terms of energy usage efficiency that an integrated solution should provide.

## 5. References

- [1] M. Uno, K. Tanaka, Single-Switch Cell Voltage Equalizer Using Multistacked Buck-Boost Converters Operating in Discontinuous Conduction Mode for Series-Connected Energy Storage Cells, *IEEE Trans. Veh. Technol.*, vol. 60, no 8, p. 3635-3645, oct. 2011
- [2] J.-F. Nie, X. Xiao, Z. Nie, P. Tian, and R. Ding, A novel three-level changeover circuit of super-capacitor bank for energy storage systems, in *IECON 2012 - 38th Annual Conference on IEEE Industrial Electronics Society*, 2012, p. 144-149.
- [3] M. Uno, H. Toyota, Equalization technique utilizing series-parallel connected supercapacitors for energy storage system, in *IEEE International Conference on Sustainable Energy Technologies*, 2008. ICSET 2008, 2008, p. 893-897
- [4] M. Bafleur, J.M. Dilhac, Towards Energy Autonomy of Wireless Sensors in Aeronautics Applications: SMARTER Collaborative Project, *Proc. IEEE International Conference on Green Computing and Communications and IEEE Internet of Things and IEEE Cyber, Physical and Social Computing*, 2013, pp.1668-1672.
- [5] T.M. Dinh, A. Achour, S. Vizireanu, G. Dinescu, L. Nistor, K. Armstrong, D. Guay, D. Pech, Hydrous RuO<sub>2</sub>/carbon nanowalls hierarchical structures for all-solid-state ultrahigh-energy-density micro-supercapacitors, *Nano Energy*, vol. 10 (2014) p. 288-294.
- [6] R. Monthéard, M. Bafleur, V. Boitier, J.-M. Dilhac and X. Lafontan, Self-adaptive switched ultra-capacitors: a new concept for efficient energy harvesting and storage, in *PowerMEMS Proceedings*, 2012, pp. 283-286.
- [7] P. Miribel-Català, J. Colomer-Fararons, J. Lafuente Brinquis, J. López-Sánchez, Self-Powered Adaptive Circuit Sampling for a Piezoelectric Harvester, *2014 DCIS Conference on Design of Circuits and Integrated Systems*, 26-29 Nov. 2014, Madrid, Spain.

## Acknowledgments

This work is carried out within the framework of the European project SMARTER funded by the CHIST-ERA program, "Green ICT, towards Zero Power ICT".

## Self-Powered energy harvester strain sensing device for structural health monitoring

A. Álvarez<sup>1</sup>, M. Baffleur<sup>2</sup>, J.-M. Dilhac<sup>2</sup>, J. Colomer<sup>1</sup>, D. Dragomirescu<sup>2</sup>, J. Lopez<sup>1</sup>, M. Zhu<sup>3</sup> and P. Miribel<sup>1</sup>

<sup>1</sup>Engineering Department: Electronics, Physics Faculty, Martí i Franqués, 1, 08028 Barcelona, Spain

<sup>2</sup>LAAS-CNRS, Université de Toulouse, CNRS, INSA, Toulouse, France

<sup>3</sup>College of Engineering, Mathematics and Physical Sciences, Harrison Building, University of Exeter, Exeter, EX4, 4QF, UK

[aalvarez@el.ub.edu](mailto:aalvarez@el.ub.edu)

**Abstract** This paper presents an envisaged autonomous strain sensor device, which is dedicated to structural health monitoring applications. The paper introduces the ASIC approach that replaces the discrete approach of some of the main modules.

### 1. Introduction

The proposed device is developed in the frame of the SMARTER (Smart Multifunctional Architecture & Technology for Energy-Aware wireless sensor) Project [1].

The device is self-powered, based on a piezoelectric transducer as an energy-harvesting source, enabling a battery-free solution. The system would be capable to sense the mechanical strain, which is an interesting topic in structural health monitoring applications, particularly in the aerospace field, which is the present field of application, defining the frequencies available for the transducer, harvesting the energy provided by the in-flight vibration of the aircraft's wing [2].

The nice approach of the device, which defines its Multifunctional concept, is that the same transducer used to harvest energy also allows extracting the mechanical strain. On the one hand, based on a piezoelectric transducer, the mechanical vibrations are harvested to generate electrical energy, in order to start-up and supply the system, but on the other hand, the system is capable to extract the open voltage (VOC) of the piezoelectric harvester, which has a relationship with the mechanical strain [3]. Then, based on the open circuit voltage concept to adapt the maximum power transferred condition between the piezoelectric mechanical to electrical energy [4,5,6], a detection of the open voltage of the piezoelectric transducer is derived. Based on these approaches, initial fully discrete electronic solutions have been implemented [7][8] as a proof of concept.

The system is based on four main modules, figure 1: a) the energy transducer as a multifunctional device (MFC) based on a piezoelectric generator (PZT); b) the Power Management, Control and Sensing Circuitry Unit, to be implemented in an ASIC solution (ASIC1); c) the Dynamic Storage Module to store the generated energy (SCap), and d) the Communication (RF) and Data Processing Unit (ASIC2). Full electronics that define the Smarter Device would be placed on a flexible PCB.

In this paper we focus the work regarding the design of ASIC1. This implementation has the role to manage the power harvested, the measurements and the management of the other modules.



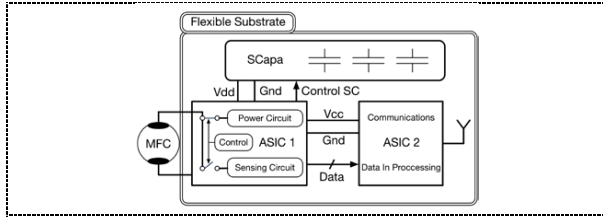


**Figure 1.** Main blocs for the Smarter Device.

In section 2 is introduced the ASIC1 approach. The initial discrete solutions [7][8] are translated to a microelectronic one, for a more compact solution.

Finally in section 3 are derived some conclusions and future perspectives.

**2. Integrated approach**

Thanks to the discrete approaches [7,8], the contemplate architecture is validated and with the gained experience we proceeded with the ASIC integration. A first ASIC is going to be implemented based on an AMS 0.35 technology. In figure 2 is depicted the ASIC1 at the functional block level and its layout design in figure 3, in an AMS 0.35µm technology, that will be placed in a QFN32 package.

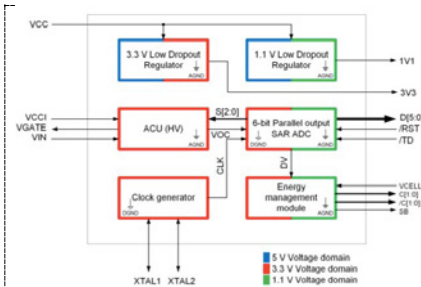


**Figure 2.** ASIC1's block diagram conception.

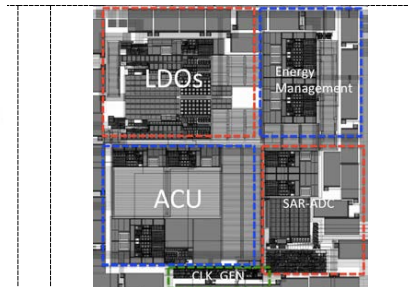


**Figure 3.** ASIC1 layout implementation.

To interface ASIC1 and ASIC2, figure 1,a communication protocol has been implemented, working with 8 bits: Two bits of control, and 6-bits of data. This protocol is implemented in [8] and validated. In t1 data is available on ASIC1. In t2 ASIC activates Start Bit (SB) when data is ready of transmitting. In ta SB is activated during all operation. In t3 ASIC2 is ready to operate. In tb, the bit Transmission Done (TD) is activated during UR-UWB transmission. In t4 TD is grounded when the transmission is completed. In t5 SB is turned off after communication is done. Finally, in t6 the system waits till new data is available on ASIC1.

The system is focused into the extraction of the strain through VOC, and the validation of the architecture that will combine the electronics envisaged in ASIC1 with those of ASIC2. The wireless solution implemented in [7] will be replaced by ASIC2 in the future Smarter prototype, and ASIC1 has a Data Processing Unit, based on a 6-bits SAR-ADC converter, which prepares the data to be sent by the RF module (ASIC2) replacing the TI Microcontroller in [8]. The strain is measured and related with the open circuit voltage, and the measurement is outputted by 6- parallel bit ADC, which

translates the measurement to the Communication. The main blocs are defined by the Power Circuit Unit, which combines linear regulators and the Energy Management module. The system needs a 1.1V regulated voltage source and a 3.3V regulated voltage source. From the AC/DC rectifier two LDOs will generate these voltages. The 1.1V LDO is designed to bias ASIC2, and the 3.3V LDO to bias the rest of the electronics. Then, the Energy Management module has the role to control the Dynamic Storage Element or SCap [9]. Finally, the ACU module and the 6-bit SAR ADC Converter define the Control Circuit and Sensing Circuitry.

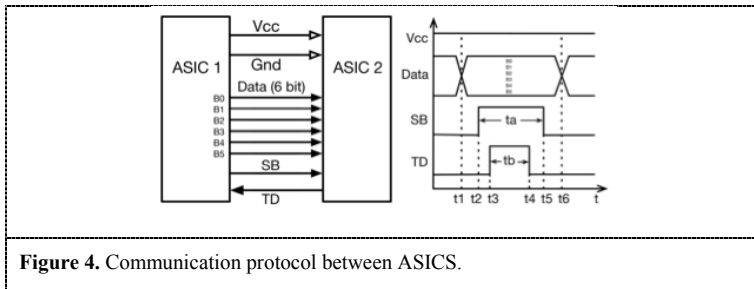


Figure 4. Communication protocol between ASICs.

The Power Circuit Unit is described more in detail. A specific low-power bandgap reference and current reference circuit has been designed; with a current consumption lower than  $9\mu\text{A}$ , nominally and a nominal power consumption of  $30\mu\text{W}$ . It has the capability to work from a lower voltage of 2V till 5V, the maximum operating voltage, with an output voltage of 1.23V with a Temperature Coefficient (TC) lower than 60ppm. The current reference is  $105\text{nA}$  with a TC lower than 250ppm, in the temperature range of  $-40\text{ C}$  to  $125\text{ C}$ .

Then, based on the architectures presented in [5], the LDO circuits have been designed. The 3.3V LDO is designed to work with a current up to 1mA, and the 1.1V LDO with a maximum DC current of 10mA. The main parameters for the LDO are introduced. In the case of the 3.3V LDO the Linear Regulation is  $68.7 \cdot 10^{-3} \text{ (V/V)}$ . In the case of the 1.1V LDO is  $665 \cdot 10^{-9} \text{ (V/V)}$ . The ability to maintain the output voltage with variations of the input voltage is reasonable for both designs. The measurement of the capability of the circuitry to keep the regulated output voltage to the desired value against changes of the load, that is, between light and high load conditions (in our case between few  $\mu\text{A}$  that define the quiescent operating point of the electronics and the load condition of 1mA for the 3.3V LDO and 10mA for the 1.1V LDO), is the load regulation, which is  $81.6 \cdot 10^{-3} \text{ (V/A)}$  in the case of the 3.3V LDO and  $99 \cdot 3 \cdot 10^{-6} \text{ (V/A)}$  for the 1.1V LDO regulator.

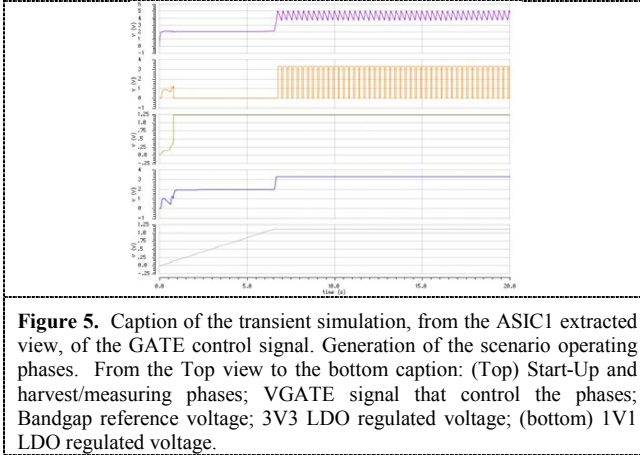
Full Monte Carlo analyses have been carried out for the bandgap reference circuit and LDOs. In the particular case of the Linear Dropout Regulators, it is the 1.1V LDO that has the greater limitation, with an accepted range between 1.05 and 1.18V, with 200 samples. The average regulated voltage is 1.12V with a standard deviation of 34,19 mV (Yield of 95%).

The ACU module, which is quite complex, and the Energy management module, are out of the scope of the present work. In figure 5 is depicted the caption of the simulation, at the extracted ASIC view level, of the performance of the ACU control stage through the GATE signal (VGATE) [7][8].

### 3. Conclusions

This paper presents the ASIC approach for the power management, control and sensing for the SMARTER project. Future full test and characterization will be carried out before its implementation in the final prototype on flexible substrate and reported in future publications.





### References

- [1] Bafleur M and Dillac J.M 2013 *Proc. IEEE International Conference on Green Computing and Communications and IEEE Internet of Things and IEEE Cyber, Physical and Social Computing (Beijing)* (Los Alamitos, California/Washington/Tokio Conference Publishing Services IEEE Computer Society) p 1668-72
- [2] Giuliano A Marsic V and Zhu M 2013 *Proc. IEEE International Conference on Green Computing and Communications and IEEE Internet of Things and IEEE Cyber, Physical and Social Computing (Beijing)* (Los Alamitos, California/Washington/Tokio Conference Publishing Services IEEE Computer Society) p 681-684
- [3] Chen X, Xu S, Yao N and Shi Y 2010 *Nanoletters* **10** 2133-37
- [4] Ottman G.K, Hofmann H.F, and Lesieutre G.A 2003 *IEEE Tran. On Power Electronics* **18** 696-703.
- [5] Colomer-Farrarons J, Miribel-Català P, Saiz-Vela A, Puig-Vidal M and Samitier J 2008 *IEEE Tran. On. Industrial Electronics* **55** 3249-57
- [6] Lafuente Brinquis J 2008 Final Project Degree, (Barcelona: Electronics Department, University of Barcelona).
- [7] Álvarez-Carulla A Colomer-Farrarons J López-Sánchez J Miribel-Català P 2015 *Proc. Conference on Design Circuits and Integrated Systems (Estoril)* (IEEE Conference Publications)
- [8] Álvarez-Carulla A Colomer-Farrarons J López-Sánchez J Miribel-Català P 2016 *Proc. IEEE International Symposium on Industrial Electronics (Santa Clara)* (IEEE Conference Publications)
- [9] El Mahboubi F 2016 *Proc. Powermems 2016 (Paris)*. (To be published Journal of Physics Conferene Series. JPCS)

### Acknowledgements

The SMARTER project is supported by European Union under the ERA-Net funding scheme of the FP7 (CHIST-ERA), and in the case of the spaniard partner through MINECO, reference PCIN-2013-069.